NASA CONTRACTOR REPORT

NASA CR-313

MAGNETIC ATTITUDE CONTROL OF RIGID, AXIALLY SYMMETRIC, SPINNING SATELLITES IN CIRCULAR EARTH ORBITS

by Phillip C. Wheeler

Prepared under Grant No. NsG 133-61 *by*
STANFORD UNIVERSITY
Stanford, Calif.
for

NATIONAL AERONAUTICS AND SPACE ADMINISTRATION • WASHINGTON, D. C. • OCTOBER 1965

NASA CR-313

MAGNETIC ATTITUDE CONTROL OF RIGID, AXIALLY SYMMETRIC, SPINNING SATELLITES IN CIRCULAR EARTH ORBITS

By Phillip C. Wheeler

Prepared under Grant No. NsG 133-61 by
STANFORD UNIVERSITY
Stanford, Calif.

for

NATIONAL AERONAUTICS AND SPACE ADMINISTRATION

For sale by the Clearinghouse for Federal Scientific and Technical Information
Springfield, Virginia 22151 – Price $6.00

ACKNOWLEDGMENT

The author is pleased to express his gratitude to Professor Robert H. Cannon, Jr. for his encouragement and guidance during this research, and to Professors David G. Luenberger and John V. Breakwell for their comments and suggestions. He also extends his appreciation to Robert Dressler and John Schaefer for many enjoyable and useful discussions.

The conscientious efforts of Cheryl Sampson and Kathy Omura during preparation of this manuscript were indispensable.

The contribution of the National Aeronautics and Space Administration is gratefully acknowledged; the author was supported by a NASA Training Grant, and the computational aspects of this study were financed under NASA Contract NsG 133-61.

ABSTRACT

34606

This dissertation reports a study of the attitude control of spinning satellites in circular earth orbits by means of passing current through a single coil on board the vehicle. The interaction between this current and the earth's magnetic field produces control torques. A new and practical magnetic control law is presented and shown to produce (in the absence of disturbances) asymptotic stability, from arbitrarily large initial attitude errors and vehicle angular velocities, for any circular orbit and any desired spin-axis direction.

Accurate estimates of the performance of this control system are obtained by using a combination of Krylov-Bogoliubov averaging and other heuristic techniques, supported by simulation studies. These estimates place in evidence the influence of control system parameters, orbital parameters, and the desired spin-axis direction upon system performance.

The usefulness of this magnetic control law is demonstrated by general discussions of its mechanization and, finally, by its application to a representative mission.

Author

TABLE OF CONTENTS

LIST OF ILLUSTRATIONS

LIST OF SYMBOLS*

Chapter I

$\bar{B}$	environmental magnetic induction measured at the satellite
$\bar{m}$	magnetic moment of the satellite
$\bar{N}$	torque applied to satellite
$\bar{J}$	current density
$\bar{r}$	radius vector from satellite center of mass to the differential volume
dv	differential volume
A_c	coil area
i	coil current
N_c	number of turns on the coil
$\bar{e}_n$	unit vector normal to a surface
$\bar{H}_E$	excess angular momentum
$\bar{H}_\perp$	component of $\bar{H}_E$ which is perpendicular to $\bar{B}$
$\bar{e}$	see expression (1.4)
m_x, m_y, m_z	components of $\bar{m}$ along control axes
N_x, N_y, N_z	components of $\bar{N}$ along control axes
B_x, B_y, B_z	components of $\bar{B}$ along control axes
ω_s	vehicle spin speed (component of angular velocity along the z_b axis)
N_s	total torque along the spin axis

---

* Symbols are listed in the chapter of their first appearance and in their order of appearance.

Chapter II

θ_i	orbital inclination
β	line of nodes displacement--see Fig. 2-1
α	satellite orbit position--see Fig. 2-1
ω_o	orbital angular velocity
r_o	radius of orbit
R_e	radius of the earth
P, Q, R	angles defining the desired spin-axis direction relative to the equatorial plane--see Fig. 2-2
ϕ, δ, ξ'	angles defining the desired spin-axis direction relative to the orbit plane--see Fig. 2-3
x_R, y_R, z_R	reference coordinate axes--see Figs. 2-1, 2-2, and 2-3 for definition of coordinate frames
A	rotation matrix from reference coordinate frame to body coordinate frame, with elements a_{ij} --see expression (2.3)
$\bar{e}_{xR}$, $\bar{e}_{yR}$, $\bar{e}_{zR}$	unit vectors defining the (x_R, y_R, z_R) coordinate frame (typical)
γ	spin angle $(\gamma = \omega_s t+\gamma_o)$
C	rotation matrix from reference coordinate frame to "despun" (x_1, y_1, z_1) coordinate frame, with elements c_{ij} --see expression (2.5)
I_x, I_y, I_z	satellite moments of inertia
N_{xb}, N_{yb}, N_{zb}	components of external torque in body coordinates
ω_x, ω_y, ω_z	components of the total inertial angular velocity of the (x_b, y_b, z_b) coordinate frame resolved in the (x_b, y_b, z_b) coordinate frame
n_x, n_y	normalized applied torque in the transverse body axes
k	inertia parameter; $k = (I_z-I_x)/I_x$
m_c	control magnetic moment
B_{xb}, B_{yb}, B_{zb}	components of the earth's magnetic field in (x_b, y_b, z_b) coordinates (typical)

u	control--see expression (2.9)
ω_1, ω_2	components of the total inertial angular velocity of the (x_1, y_1, z_1) coordinate frame resolved in the (x_1, y_1, z_1) coordinate frame
n_1, n_2	normalized applied torque in the transverse "despun" axes
p, q, r	components in vehicle coordinates of the angular velocity of the body coordinate frame relative to the reference frame
$\bar{\Omega}^R$	inertial angular velocity of the reference coordinate frame with components Ω_x, Ω_y, and Ω_z in reference coordinates
E_1, E_2, E_3, E_4	Euler parameters defining the transformation from (x_R, y_R, z_R) to (x_b, y_b, z_b) --see expression (2.19)
$\bar{H}$	total satellite angular momentum
H_s	component of angular momentum along the spin axis
$\bar{h}$	normalized momentum vector with components h_x, h_y, and h_z in reference coordinates: $h_\alpha = H_\alpha/I_\alpha$

Chapter III

σ_h	error function for control of simplified equations of motion
u_h	feedback control for simplified equations of motion; $u_h = \eta(\sigma_h)$
$\eta(\sigma)$	general control function--see Fig. 3-1
σ_p	position error function
σ_R	rate error function
σ	total error function
K_R	rate gain in the total error function
e	emf induced in shorted loop
Φ	total magnetic flux linking shorted loop
ρ	resistance per unit length of the wire comprising the coil

ℓ	length of one turn of the shorted loop
T_K	total kinetic energy of satellite

Chapter IV

V	Lyapunov function
$\bar{x}$	general state vector
$\bar{f}(\bar{x},t)$	right-hand side of vector differential equation
$\mathcal{R}_\Sigma$	open region of the origin in state space--see expression (4.2)
$\dot{V}$	time rate of change of V along trajectories of the equations of motion
$\mathcal{L}$	subspace of $(\bar{x},t)$ space defined by $\dot{V} = 0$
$\Upsilon(\bar{x},t)$	scalar function defining $\mathcal{L}$ --see expression (4.3)
ω_e	spin rate of the earth
$\alpha_1, \alpha_2, \alpha_3$	parameters in the uncontrolled solution to the simplified equations of motion--see expressions (4.15) and (4.16)
M_e/r_o^3	coefficient in magnetic field model--see Appendix A
d_1, d_3, d_5, d_7, d_8	coefficients in tilted dipole model of the earth's magnetic field--see Appendix A
μ	see Appendix A
a	amplitude of the transverse angular velocity
ϕ', ψ', θ'	Euler angles--see Fig. 4-1
ω	time rate of change of ϕ'
X_b	column matrix composed of the unit vectors $\bar{e}_{xb}$, $\bar{e}_{yb}$, and $\bar{e}_{zb}$ (typical)
B	constant rotation matrix defined by expression (4.32)
D	rotation matrix, with elements d_{ij}, defined by expression (4.33)
S°	constant orthogonal matrix, with elements s_{ij}, defining initial values of the a_{ij}, as in expression (4.40)

v_{ij} — element of transformation from (x_n, y_n, z_n) coordinates to (x_R, y_R, z_R) coordinates

p_{ij} $(i,j = 1,2,3)$ — constants defined in expression (4.43)

F_1, F_2, F_3 — see expression (4.46)

G_1, G_2 — see expression (4.54)

Chapter V

K — control gain in linear region of saturating proportional control function

σ_s — error saturation level for saturating proportional control function

U_o — control saturation level for saturating proportional (or signum) control function

ψ, λ — polar variables for simplified equations of motion--see Fig. 5-3

ψ_{AV} — estimate of the average (in time) variation of ψ on the average (in λ)

G_{AV} — average gain factor for signum control function--see expression (5.7)

F_{AV} — average gain factor for proportional control function --see expression (5.8)

β_{xR}, β_{yR} — normalized magnetic field components along the x_R and y_R axes

ω_n — nutation frequency $[\omega_n = (1+k)\omega_s]$

χ_1, χ_2 — slowly varying attitude components in the small-error exact equations of motion--see expression (5.14)

ψ^a, λ_a — $\psi^a = \sqrt{\chi_1^2+\chi_2^2}; \quad \chi_1 = \psi^a \cos \lambda_a; \quad \chi_2 = \psi^a \sin \lambda_a$

ξ — see expression (5.15)

a_{AV} — estimate of average (in time) variation of a

ψ^a_{AV} — estimate of average (in time) variation of ψ^a on the average (in λ_a)

Chapter VI

Ω	class of admissible controls
J	cost of control--see expression (6.2)
$\bar{\lambda}$	adjoint vector
$\mathcal{H}$	Hamiltonian function--see expression (6.3)
$\bar{u}^*$, $\bar{x}^*$, $\bar{\lambda}^*$	optimal control, and corresponding state and adjoint vectors
$\mathcal{H}'$	augmented Hamiltonian function
$\bar{p}$	reduced adjoint vector with components $p_1 = \lambda_1$, $p_2 = \lambda_2$, and $p_3 = \lambda_3$
$\bar{y}$	auxiliary vector for determination of the optimal control--see expression (6.11)
Θ_f	angle defining the terminal state of $\bar{y}$; $y_1(t_f) = \cos \Theta_f$, $y_2(t_f) = \sin \Theta_f$, $y_3(t_f) = 0$
τ	reverse time; $\tau = t_f - t$

Chapter VII

p_a	aerodynamic pressure
τ_a	aerodynamic shear
ρ_a	atmospheric density
v	magnitude of vehicle velocity
f_t	tangential accommodation coefficient
f_n	normal accommodation coefficient
q^*	dynamic pressure
$\bar{\ell}$	vector from the vehicle center of mass to the geometric centroid, with components ℓ_x, ℓ_y, and ℓ_z in (x_b, y_b, z_b) coordinates
$\bar{N}_a$	aerodynamic torque
R_b	radius of the (spherical) vehicle

C_D	aerodynamic drag coefficient
n_{a1}, n_{a2}	components of normalized external torque in the x_1 and y_1 axes due to aerodynamic pressure
n_{s1}, n_{s2}	same as above for solar radiation pressure
n_{g1}, n_{g2}	same as above for gravity gradient
n_{m1}, n_{m2}	same as above for residual magnetic moments
D_a	aerodynamic acceleration coefficient--see expression (7.8)
V_s	solar radiation pressure constant
ν	solar reflectivity
D_s	solar radiation acceleration coefficient--see expression (7.10)
$\bar{e}_{xs}$	unit vector from the earth to the sun
S	angle defining the time of year--see Fig. 7-3
ζ	inclination of the ecliptic plane to the equatorial plane (-23.45 deg)
D_g	gravity gradient acceleration coefficient--see expression (7.14)
D_m	residual magnetic acceleration coefficient--see expression (7.17)
m_x, m_y, m_z	components of residual magnetic moment in (x_b, y_b, z_b) coordinates
$n_{10}, n_{20}, n_{11}, n_{12}$	see expression (7.20)
a_o	disturbed motion of a given by the unrefined first approximation of Krylov and Bogoliubov--see expressions (7.22) and (7.25)
A_1, A_2, A_3, A_4	see expression (7.24)

Chapter VIII

v_m	maximum available coil voltage
m_m	maximum required magnetic moment

R_c	control coil radius
P	power consumed by control coil
P_m	maximum power consumed by control coil
W	coil weight
w	mass per unit length of the coil wire
K_s	solar cell gain
θ_1, θ_2, θ_3	angles used (nonuniquely) to define attitude sensor outputs--see Figs. 8-4 and 8-6

Chapter IX

No new symbols.

Chapter X

No new symbols.

I. INTRODUCTION

The generation of attitude control torques by causing an interaction between the vehicle and its environment has received considerable attention. The primary appeal of these techniques is that they eliminate the need for control propellant which would otherwise be required to counteract the effect of secular disturbance torques. An additional potential advantage is increased reliability attained through the elimination of mechanical components (e.g., pneumatic valves).

The environmental sources most commonly considered for attitude control are the earth's gravitational field and the earth's magnetic field. Gravity gradient control has been studied extensively and satellites utilizing this concept have been placed in orbit [Ref. 1-1]. Perhaps the most attractive feature of gravity gradient control is that it is passive; the vehicle automatically aligns itself with its minimum axis of inertia toward the earth's center. The only attitude sensors required are those associated with the energy-removal system used for damping and, in many instances, these can be eliminated by the use of a passive energy-removal mechanism.

However, gravity gradient control has limitations which for some applications are prohibitive. The nominal attitude of the vehicle is constrained to be earth referenced. Consequently, gravitational torques cannot be used to orient a vehicle in orbit around the earth toward the sun, for example. Furthermore, the magnitude of the torques available, and thus the speed of response of the system, is severely limited by the mass distribution of the vehicle.

The limitations and advantages associated with magnetic attitude control are rather different from those which relate to gravity gradient control. Foremost of these is the ability to control the torque level (within limits), thus removing the necessity to align with the environmental field. This, on the other hand, implies the need for attitude sensors. As will be shown, the direction as well as the magnitude of the earth's magnetic field can vary significantly during the satellite orbit. It is generally conceded, therefore, that magnetic control

systems must either be operated by ground command, or be equipped with means for on-board measurement of the magnetic field.

Despite these considerable disadvantages several magnetic control schemes have been advanced, and the method has been used in a limited way in the TIROS and TRAAC satellites [Refs. 1-1, 1-2]. The future of magnetic control depends largely upon the solution of several outstanding unresolved problems and in particular upon the development of simply implemented control laws.

A. PRELIMINARY CONCEPTS

The basic physical effect which makes possible magnetic generation of control moments is the Lorentz force experienced by a moving charge in a magnetic field, $\bar{B}$. The cumulative effect of a moving distribution of charge in a magnetic field is a torque, $\bar{N}$. It is particularly convenient to express this torque in terms of the magnetic dipole moment, $\bar{m}$, of the current distribution [Ref. 1-3].

$$\bar{N} = \bar{m} \times \bar{B} \tag{1.1}$$

where $\bar{N}$ is expressed in newton-meters, $\bar{m}$ in amp-m^2 and $\bar{B}$ in webers/m^2 For a completely general charge distribution

$$\bar{m} = \frac{1}{2} \int_v \bar{r} \times \bar{J} \, dv \tag{1.2}$$

where v is the volume over which the current density $\bar{J}$ is distributed. In the case of an N_c-turn planar current loop of area A_c carrying a current i

$$\bar{m} = N_c A_c i \, \bar{e}_n \tag{1.3}$$

where $\bar{e}_n$ is a unit vector normal to the plane of the coil in the usual right-hand sense relative to the direction of current flow. Thus a well-calibrated magnetic moment can be developed simply by passing a current through a planar coil. This is, indeed, a simple and reliable actuator.

Expression (1.1) demonstrates elegantly the basic limitation associated with magnetic control: the torque developed is always normal to both $\bar{B}$ and $\bar{m}$. Thus at each instant there is a direction, defined by the magnetic field vector, along which no component of torque can be generated with any $\bar{m}$.

The function of any momentum removal system is to produce a torque which will tend to remove the excess angular momentum stored in the system. This momentum may be stored in the vehicle itself or in an auxiliary storage mechanism (e.g., a set of reaction wheels). Figure 1-1

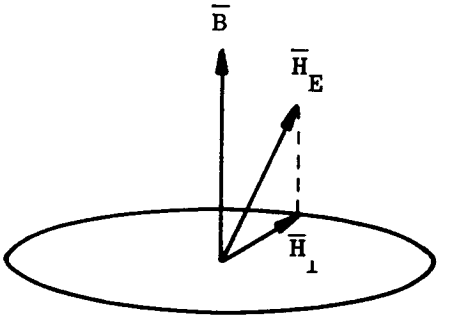

FIG. 1-1. MOMENTUM REMOVAL GEOMETRY.

indicates a typical geometrical situation. Note that the excess angular momentum, $\bar{H}_E$, can be resolved into a component parallel to $\bar{B}$ and a component, $\bar{H}_\perp$, normal to $\bar{B}$. It is clear that at any instant the ideal policy for any magnetic control scheme is to generate a torque opposing $\bar{H}_\perp$. Any component of momentum parallel to $\bar{B}$ will be unaffected.

If the relative orientation of $\bar{B}$ and $\bar{H}_E$ were fixed there would always be a direction along which momentum could accumulate without bound. Fortunately, in almost all cases $\bar{B}$ varies widely in direction relative to both the satellite axes and, more importantly, in inertial coordinates as the vehicle traverses its orbit.* The precise nature of

---

*It is important to recognize that $\bar{B}$ is a vector function defined on a vector field. Thus we are concerned with the magnetic field measured at the point in space occupied by the vehicle.

this variation is a key factor in determining the feasibility of magnetic control. Appendix A presents a development of the dipole model of the earth's magnetic field in several coordinate frames defined in the next chapter. It is worth noting here that, owing to the tilt of the magnetic dipole relative to the earth's spin axis (approximately 11 deg), the components of the magnetic field depend to some extent upon the rotation of the earth and nodal regression.

Considered in inertial coordinates, the dominant variation of the components of $\overline{B}$ is at twice orbital frequency, while the total stored momentum of the system (vehicle plus any momentum storage mechanism) will generally vary negligibly over an orbit. Thus $\overline{B}$ and $\overline{H}_E$ (Fig. 1-1) are in constant relative motion, so that a component of momentum not removable at one point in orbit may very well be eliminated at some later position in orbit. This phenomenon is essential to magnetic control; its nonoccurrence in some orbits, notably in synchronous equatorial orbits where the satellite is fixed in the magnetic field, represents a fundamental limitation of magnetic control techniques.

As indicated in Appendix A the magnitude of the magnetic field decreases as the cube of the orbital radius. Estimates of the altitude at which the earth's field becomes ineffective as a control torque source vary. It appears reasonable to consider magnetic control of vehicles at altitudes as great as 10,000 to 20,000 nautical miles.

B. PREVIOUS CONTRIBUTIONS

Automatic control of vehicle attitude by magnetic techniques has received considerable attention in the literature. The majority of the contributions to date deal with control of fully stabilized vehicles, while the most successful application of the concept has been in the spinning TIROS satellites.

1. Fully Stabilized Vehicles

Magnetic control systems suggested for fully stabilized vehicles are of two types, continuous and intermittent. The earliest implementations suggested were of the former type. Thus far, only one

basic continuous scheme has been presented in the literature [Refs. 1-4, 1-5, 1-6, 1-7]. Consider Fig. 1-2, which is seen to be an evolution of Fig. 1-1. As suggested above, it is desired that the torque generated oppose $\bar{H}_\perp$, as shown in the figure. Since $\bar{N}$ is normal to both $\bar{B}$

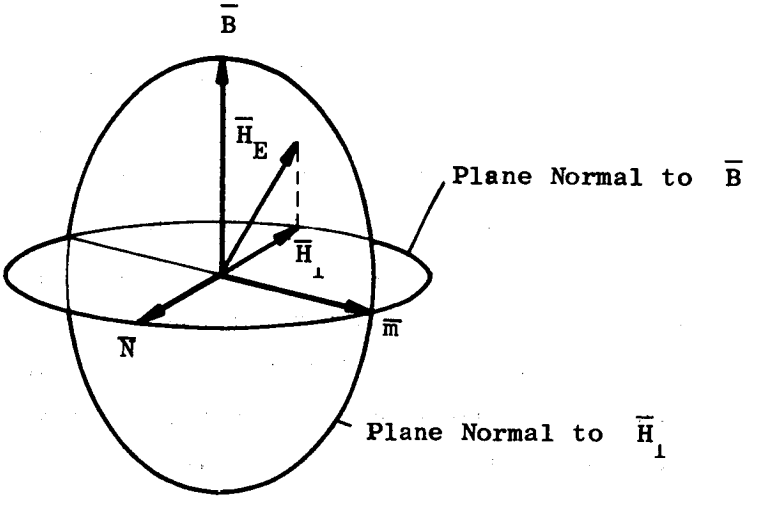

FIG. 1-2. CONTINUOUS CONTROL GEOMETRY.

and $\bar{m}$, $\bar{m}$ must be in the plane normal to $\bar{H}_\perp$ to achieve this result. Furthermore, since for given magnitudes of $\bar{m}$ and $\bar{B}$ the magnitude of $\bar{N}$ will be greatest when $\bar{m}\cdot\bar{B} = 0$, we arrive finally at the requirement that $\bar{m}$ be in the direction of $\bar{H}_E \times \bar{B}$.

The actual gain factor required by this procedure can be arrived at by a least-square approach. Assume that the ideal control torque would be a solution to the equation $\bar{N} = -K\bar{H}_E$. Clearly, from the geometry of Fig. 1-2, this equation will generally have no solution. Consider then solving the normal equations

$$\bar{N} + K\,\bar{H}_E = \bar{e} \tag{1.4}$$

in such a way that the squared-error, $\bar{e}\cdot\bar{e}$, is minimized. This technique yields:

$$-B^2\bar{m} + (\bar{m}\cdot\bar{B})\bar{B} = K(\bar{B}\times\bar{H}_E) \tag{1.5}$$

Examination of (1.5) reveals that the solution vector $\bar{m}$ will always lie in the plane normal to $\bar{H}_{\perp}$, but is otherwise unspecified. Imposing the efficiency constraint mentioned above $(\bar{m}\cdot\bar{B} = 0)$, a unique result is obtained.

$$\bar{m} = - \frac{K(\bar{B} \times \bar{H}_E)}{B^2} . \qquad (1.6)$$

Notice that, as mentioned previously, B^2 will vary in magnitude to a degree depending upon the orbit, but usually by no more than a factor of 4:1. It is reasonable then to consider a slightly less ideal control system in which the B^2 term is replaced by a constant, thus reducing the arithmetic requirements of the control law [Ref. 1-4].

It is clear that a magnetic moment $\bar{m}$ satisfying expression (1.6) can always be generated given, for example, three orthogonal coils with equal areas and turns. However, it is still necessary to establish for any mission whether, in the light of kinematical considerations, this system will prevent the unbounded accumulation of momentum along some inertial direction. Intuitively, at least, this control law should be effective if any type of magnetic control is feasible, because it is at each instant doing its best to reduce $\bar{H}_E$.

The continuous control law of (1.6), while rather simple conceptually, is not so simple to implement. In its pure form it requires at least six multiplications (to form the cross product) and one division. From the point of view of sensing it is rather displeasing, because continuous measurements of all three components of both $\bar{B}$ and $\bar{H}_E$ are required.

These disadvantages can for the most part be avoided by noting that if the vehicle possesses a momentum storage system (e.g., reaction wheels), and the sole purpose of the magnetic torquing loop is the transference of the excess stored momentum into the external environment, then continuous control will generally not be required. It is sufficient in this case to provide a system which bounds the total vehicle momentum by intermittent torque application.

Intermittent magnetic attitude control of a fully stabilized earth satellite has been mentioned briefly in Ref. 1-5 and discussed in more detail in Ref. 1-7. One of the schemes in the latter reference possesses similarities with the simple and elegant mechanization presented in Ref. 1-8. This system utilizes logic devices and threshold-measuring sensors to obtain (nonsimultaneously) decoupled torques about three orthogonal vehicle axes. These torques are used to desaturate three orthogonal reaction wheels mounted parallel to the same axes.

The overall block diagram of a control system such as that presented in Ref. 1-8 is shown in Fig. 1-3. The logic for this system is based upon the observation that in order to obtain a decoupled torque about, for example, the z axis the components of both $\overline{B}$ and $\overline{m}$ along this axis must be zero. This is seen by examining the expanded torque equations below.

$$\begin{aligned} N_x &= m_y B_z - m_z B_y \\ N_y &= m_z B_x - m_x B_z \\ N_z &= m_x B_y - m_y B_x \end{aligned} \qquad (1.7)$$

This requirement places two constraints upon the torquing logic. Additional requirements must be imposed in order to (a) produce a correction only when needed to desaturate a wheel and (b) produce a correction in the proper direction. Requirement (a) is accommodated by using a threshold element with hysteresis to monitor the speed of each of the reaction wheels; whenever the output of this element is nonzero a correction will be made if the proper magnetic field conditions (above) exist.* The correction will continue until the magnetic field availability conditions are violated, or until the wheel is sufficiently desaturated (as determined by the hysteresis level of the speed detection element), whichever event occurs first.

*Again, it is a tacit assumption, in most cases justified, that the proper conditions will occur sufficiently often.

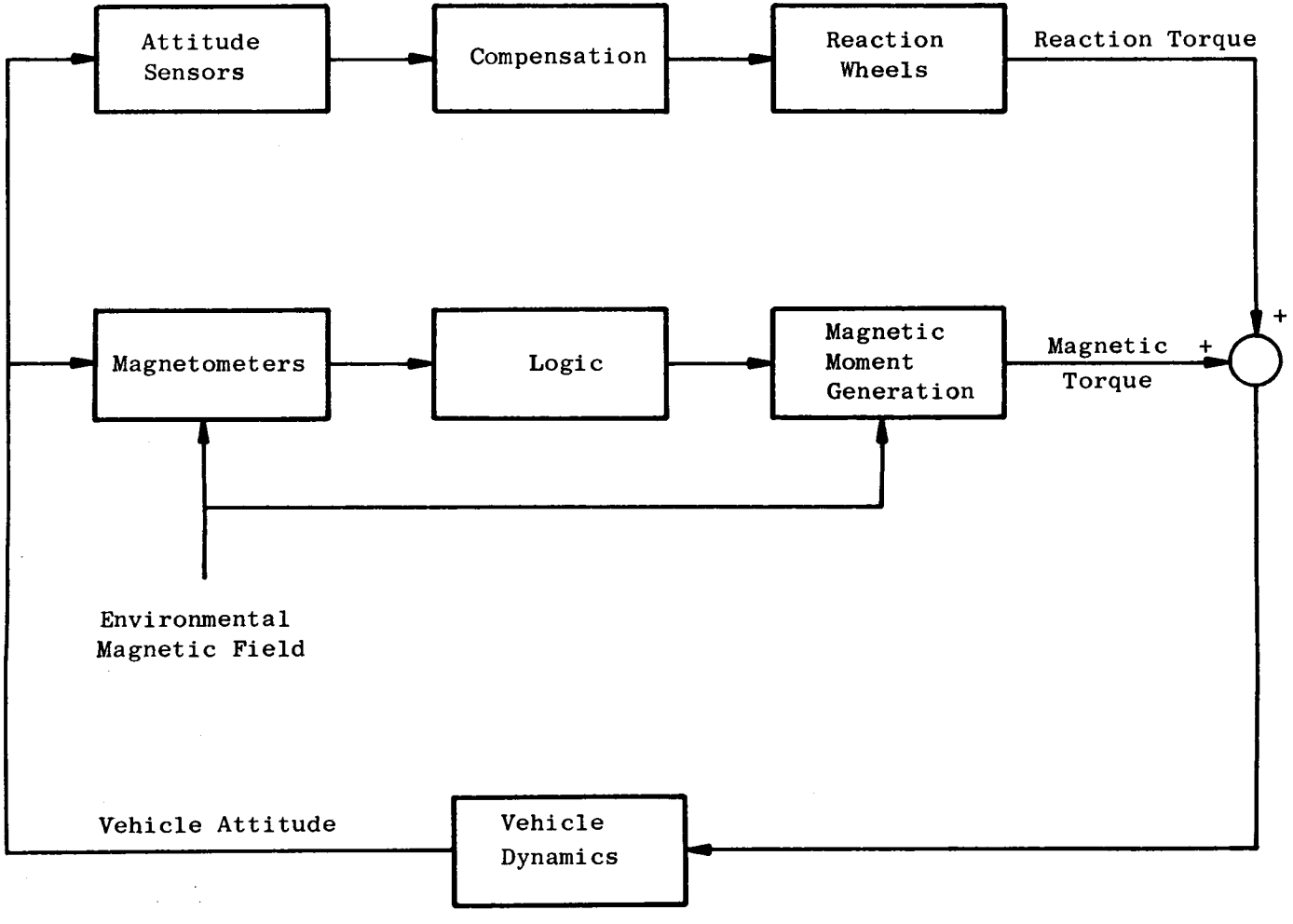

FIG. 1-3. BLOCK DIAGRAM OF INTERMITTENT MAGNETIC MOMENTUM REMOVAL SYSTEM.

The magnetic field sensors utilized in this system are also threshold devices. Their outputs are used to indicate when the component along any single axis is sufficiently near zero for a decoupled torque to be produced and, at this time, how the magnetic field vector is oriented in the plane of the other two axes. The latter information is used to produce a torque of the desired sign. For example, consider the production of a torque to desaturate the z-axis reaction wheel. The torque is desired to oppose the stored wheel momentum and at the time of torquing $B_z \approx 0$, $m_z = 0$ for the reasons mentioned above. The torque produced is

$$N_z = m_x B_y - m_y B_x \tag{1.8}$$

where m_y, for example, is restricted to the discrete values $-m_{cy}$, 0 and $+m_{cy}$. Selection of the signs of m_x and m_y is based upon consideration of where the $\bar{B}$ vector lies; for example if B_x exceeds its threshold while B_y does not, application of a magnetic moment with the y-axis coil is indicated. The direction of the current in the coil will be determined by the sign of B_x and the sign of the z-axis wheel speed.

Figure 1-4 presents the logic for using a y-axis magnetic moment to desaturate the z-axis wheel. The torquing logic for using an x-axis coil to desaturate the z-axis wheel would be similar, and the complete system is a collection of three such logic systems. Notice that three magnetometers suffice for such a system, because the magnetometers for threshold detection (e.g., the B_x magnetometer of the figure) will also indicate when the magnetic field is primarily along the other two axes.

With an intermittent control scheme, such as the one described above, it is reasonable to consider using fewer than three coils. With two coils, for example, there will be one axis of the vehicle along which no magnetic moment can be generated. If a sizable component of the magnetic field were always along this axis, such a scheme might make a great deal of sense.

A single coil system would be tolerable only if there were some axis of the vehicle along which magnetic torques were never required.

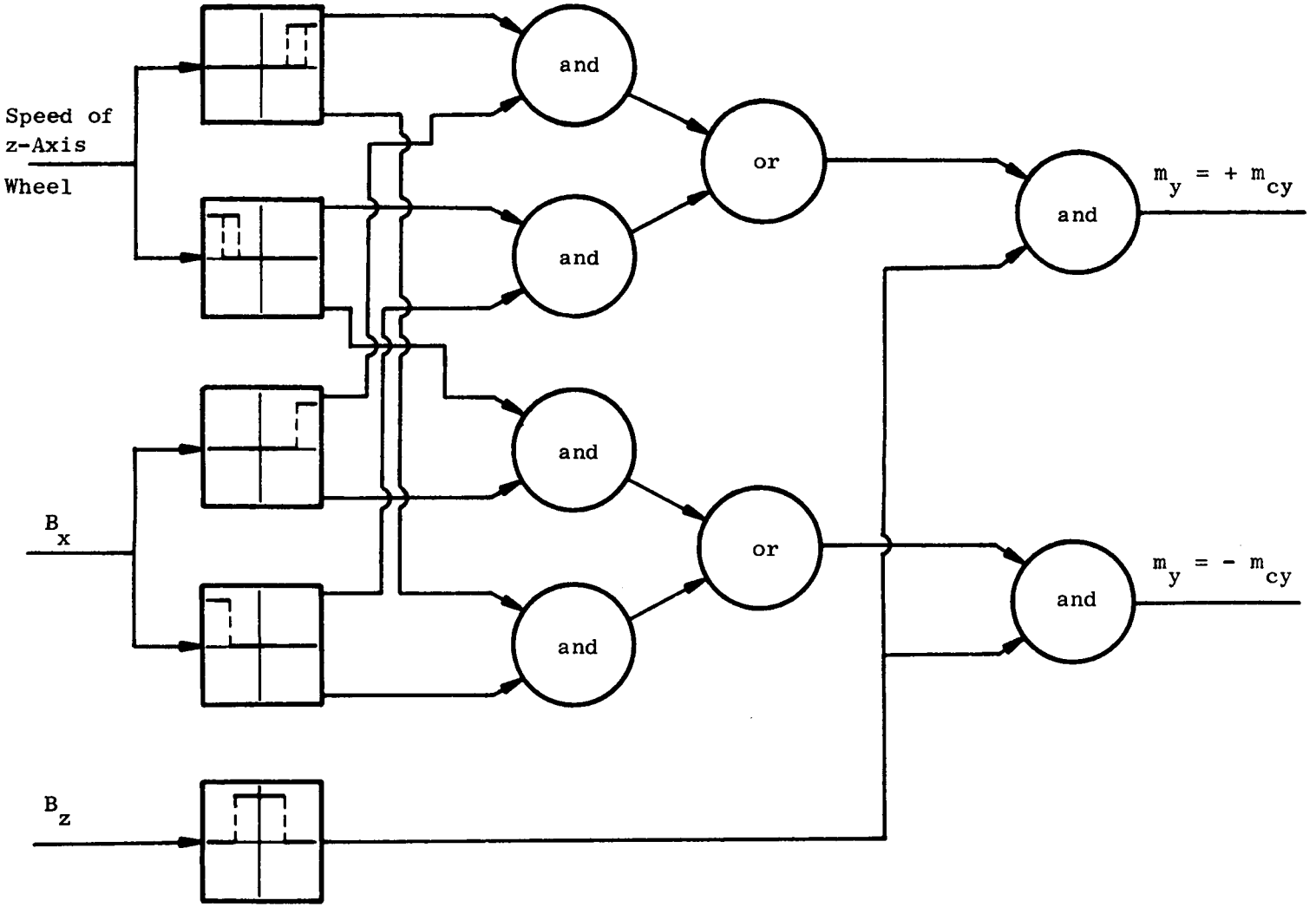

FIG. 1-4. LOGIC FOR GENERATION OF z-AXIS TORQUES USING A COIL NORMAL TO THE y-AXIS ($m_x = m_z = 0$).

This situation is particularly pertinent to the attitude control of spinning vehicles.

2. Spinning Vehicles

Magnetic attitude control techniques are particularly well adapted to the problem of precessing the spin axis of a spinning vehicle [Ref. 1-2, 1-9]. A single coil normal to the spin axis is sufficient for this purpose, since only torques normal to the spin axis are required. In contrast to mass-expulsion systems which must be pulsed, thus exciting wobble in the motion, the magnetic torque can be applied continuously for relatively long intervals.

Again, the magnetic control systems for spinning vehicles can be classified as: (a) those in which control effort is being applied continuously, and, (b) those in which the control is intermittent. Only the latter have been treated in the literature [Ref. 1-2, 1-9]. This is not surprising since all contributions to date (for both spinning and fully stabilized vehicles) have treated only the small-error case for which intermittent schemes, which depend upon the momentum storage of the spinning vehicle (and a passive damper) to maintain short-term accuracy, are adequate. A discussion of intermittent magnetic control for spinning vehicles is presented in Appendix B.

C. CONTROL CONFIGURATIONS FOR SPINNING VEHICLES

The simplest control system for a spinning vehicle is no control system at all; that is, sufficient control accuracy may be provided by the stored momentum and, perhaps, a passive damper to maintain the alignment of the stored momentum with the spin axis [Ref. 1-10]. The applicability of this scheme is limited to missions of short duration having modest accuracy requirements.

Generally, due to the action of disturbance torques and motion of the desired spin-axis orientation, it is necessary to provide an auxiliary system capable of altering both the magnitude of the stored momentum (spin-speed control) and the direction (attitude control) of the spin axis. The former problem, spin-speed control, is straightforward because, for a vehicle possessing symmetry with respect to the

spin axis, the spin-speed differential equation is simply:

$$\dot{\omega}_s = N_s \tag{1.9}$$

where ω_s is the spin speed and N_s is the total torque (control and disturbance) along the spin axis. For all practical purposes, ω_s can be considered constant because it will vary only minutely from its nominal value, again due to the relatively large stored momentum which is a characteristic of spinning vehicles. Thus, it is possible to consider the attitude control problem as independent of the spin-speed control and, moreover, to assume the spin speed to be constant. In this dissertation, only the problem of attitude control is considered.

The most versatile method of altering the spin-axis direction is by means of a mass-expulsion system. Such a system is self-contained and is not affected by the environment of the satellite. Changes in attitude are accomplished by torque pulses applied normal to the spin axis and timed with the spin of the satellite so that the required inertial change in the total momentum is achieved. This pulsing excites significant transverse angular velocities in the vehicle which in turn cause the spin axis to wobble following the correction. Most of this wobble can be avoided by applying two pulses so that the wobble produced by the second pulse exactly cancels that caused by the first pulse [Ref. 1-11].

Magnetic torquing is another technique which may be used to alter the spin-axis attitude. This method is particularly appealing because a single coil in a plane normal to the spin axis can be used to produce torques normal to the spin axis. Damping can be achieved by passive techniques (a mechanical damper) or by active (magnetic) techniques. The latter approach is developed in a subsequent chapter.

The major advantages offered by magnetic control in relation to mass-expulsion techniques are increased reliability (by eliminating mechanical actuators) and reduced system weight (because system weight is independent of mission duration).

D. CONTRIBUTIONS

As mentioned above, previous investigations of magnetic control of spinning vehicles have dealt only with the problem of removing, or reducing, small attitude errors. Furthermore, only specific applications have been examined--for example, alignment of the spin axis normal to the plane of the vehicle's orbit. It is important, therefore, to extend the understanding of the problem, both in the direction of considering large attitude errors and by examining general applications. However, it is not enough just to demonstrate feasibility; it is necessary also to develop a practical, simply mechanized control law which has general applicability.

This dissertation deals specifically with the attitude control of an axially symmetric, rigid, spinning space vehicle in a circular earth orbit by means of passing current (on a continuous, rather than intermittent, basis) through a single coil so aligned as to produce a magnetic moment along the spin axis of the vehicle.

The following are the principal contributions of this dissertation:

1. A new control law is developed for magnetic attitude control of spinning vehicles. This control law includes provisions for both position control and active magnetic wobble damping (Chapter III).

2. The theoretical feasibility of magnetic attitude control of spinning vehicles is demonstrated by showing that the above control law produces asymptotic stability in-the-large for a satellite in a circular earth orbit of any inclination with the desired spin-axis direction inertially fixed, but otherwise arbitrary (Chapter IV).

3. The performance of the undisturbed system with this control law is evaluated by deriving estimates for the solutions to the equations of motion (which are time varying and, for large errors, nonlinear). These results indicate the influence of the altitude, the orbital inclination and the desired spin-axis direction upon the response of the undisturbed system (Chapter V).

4. The large-error response of the feedback control law developed in this study is shown, for signum control of the coil current, to compare very favorably with the response using minimal-time control programs derived by applying Pontryagin's maximum principle (Chapter VI).

5. The feedback control law is shown to be practical by general discussions of the relationship between the mechanization problem (e.g., measurement of the variables required in the control law) and the mission of the satellite (Chapter VIII), and finally, by its

application to a specific representative mission with disturbances taken into account (Chapter IX). The evaluation of the response of the system to disturbances (which requires machine solution of the equations of motion) is greatly facilitated by applying the techniques of Krylov and Bogoliubov to obtain averaged equations of motion which can be solved much more efficiently than the exact equations of motion (Chapter VII).

II. PRELIMINARY DEVELOPMENTS

In this chapter coordinate frames are defined, and the general equations of motion required in subsequent chapters are developed.

A. COORDINATE SYSTEMS

Coordinate geometry plays a major role in any study involving the earth's magnetic field, as will be seen. It is necessary, therefore, to define at the outset a complete system of coordinate frames which will be employed consistently in the following developments.

The fundamental coordinate sets required are shown in the following three figures. Figure 2-1 defines the orbit and orbital position of the vehicle relative to the inertially stationary (x_e, y_e, z_e) coordinate frame, where the z_e axis is along the spin axis of the earth, and the

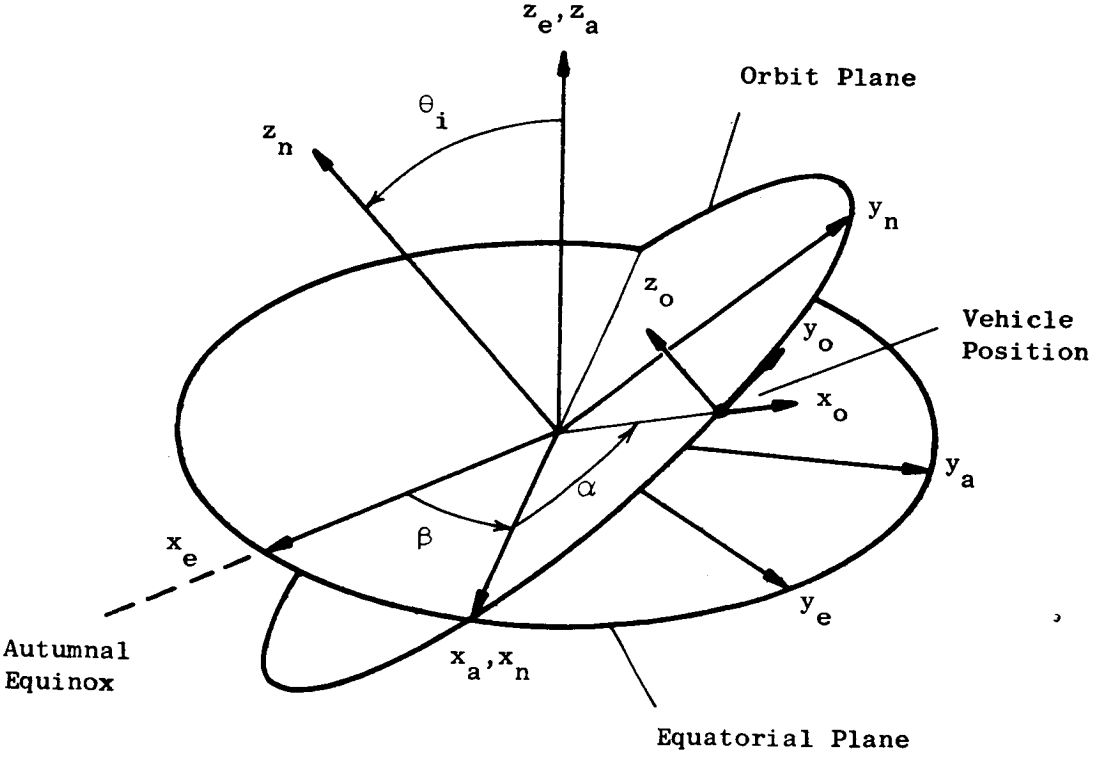

FIG. 2-1. ORBITAL-EQUATORIAL COORDINATE FRAMES.

x_e axis is aligned with the Autumnal Equinox. The three angles so defined are θ_i (the orbital inclination), β (the position of the ascending line of nodes), and α (the orbit position). For any particular circular orbit θ_i is constant, $\dot{\alpha}$ is equal to ω_o, and the rate of change of β is given by

$$\dot{\beta} = - J \left(\frac{R_e}{r_o}\right)^2 \omega_o \cos \theta_i \quad \text{rad/sec} \tag{2.1}$$

where J is approximately 1.64×10^{-3} [Refs. 1-11, 2-1], r_o is the radius of the orbit and R_e is the radius of the earth. The orbital rate is, of course,

$$\omega_o = \sqrt{\frac{GM}{r_o^3}} \quad \text{rad/sec} \tag{2.2}$$

where G is the universal gravitational constant and M is the mass of the earth. Notice that $\dot{\beta}$ is, at its maximum, approximately three orders of magnitude less than the orbital rate.

Figure 2-2 defines the desired spin-axis attitude relative to the inertially fixed (x_e, y_e, z_e) coordinate frame. Notice that the angle R can be chosen arbitrarily since x_R and y_R are located arbitrarily (with $y_R \perp x_R$) in the plane normal to z_R. The (x_R, y_R, z_R) coordinate frame will be referred to as the reference coordinate frame.

It will be useful in the following discussion to define (x_R, y_R, z_R) relative to the (x_n, y_n, z_n) coordinate axes. This definition can be made in terms of the three angles δ, ϕ, and ξ' defined in Fig. 2-3. Notice that whenever the (x_R, y_R, z_R) frame is inertially fixed, the angles δ, ϕ, and ξ' will be time varying owing to the time variation of β. This variation can be derived by imposing directly the consistency of Figs. 2-2 and 2-3 with the relationship between (x_n, y_n, z_n) and (x_e, y_e, z_e) as defined in Fig. 2-1. This procedure yields:

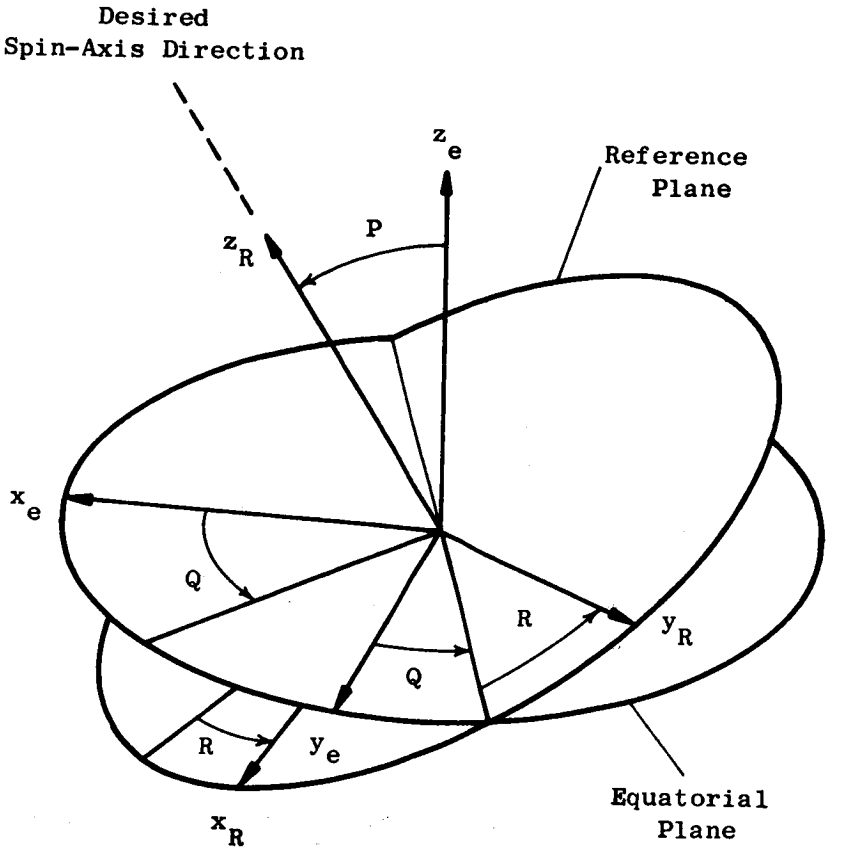

FIG. 2-2. DEFINITION OF THE REFERENCE COORDINATE FRAME RELATIVE TO THE EQUATORIAL PLANE.

$$\cos \phi = \cos \theta_i \cos P + \sin \theta_i \sin P \sin (\beta - Q)$$

$$\frac{\sin \delta}{\cos \delta} = \frac{\sin \theta_i \cos P - \cos \theta_i \sin P \sin (\beta - Q)}{\sin P \cos (\beta - Q)}$$

$$\frac{\sin \xi'}{\cos \xi'} = \frac{\sin P \sin R \cos \theta_i - [\cos P \sin R \sin (\beta - Q) + \cos R \cos (\beta - Q)] \sin \theta_i}{\sin P \cos R \cos \theta_i + [-\cos P \cos R \sin (\beta - Q) + \sin R \cos (\beta - Q)] \sin \theta_i}$$

where ϕ and P are assumed to be always in the range $[0, \pi]$.

In the analyses which follow, time variation of β will be neglected (as a dynamic effect), so that the (x_n, y_n, z_n) axes will be inertially fixed. Justification of this assumption is based upon the extremely slow

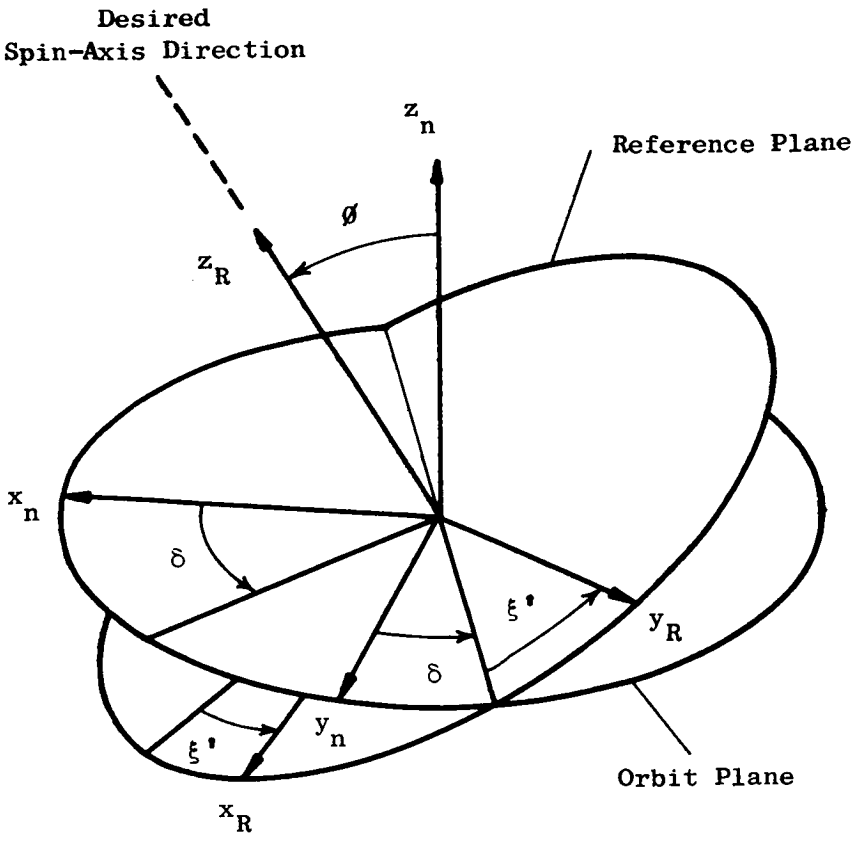

FIG. 2-3. DEFINITION OF THE REFERENCE COORDINATE FRAME RELATIVE TO THE ORBIT PLANE.

variation of β (less than 10 deg per day in the lowest equatorial orbit). Alternately, assuming β to be constant is precisely equivalent to restricting the problem definition to vehicles in orbit around a spherical earth.

With this assumption the angles δ, ϕ, and ξ' will be constant with stationary reference axes. Moreover, ξ' can be made equal to zero by choosing the angle R appropriately, so that only the angles δ and ϕ are necessary to define the relationship between the nodal coordinate set (x_n, y_n, z_n) and the reference coordinates. This scheme will be used throughout.*

---

* This procedure of defining $\xi' = 0$ could also be extended to the general case when β is considered as time varying. If this were done, the x_R and y_R axes would be moving in inertial space even in the important case when z_R, the nominal spin-axis direction, is fixed inertially.

Two additional coordinate frames must be defined. The (x_b, y_b, z_b) axes form an orthogonal set fixed in the spinning vehicle, with the z_b axis as the spin axis. The transformation from the reference frame (x_R, y_R, z_R) to the body frame (x_b, y_b, z_b) is given by a matrix of direction cosines, A:

$$\begin{bmatrix} \bar{e}_{xb} \\ \bar{e}_{yb} \\ \bar{e}_{zb} \end{bmatrix} = \begin{bmatrix} a_{11} & a_{12} & a_{13} \\ a_{21} & a_{22} & a_{23} \\ a_{31} & a_{32} & a_{33} \end{bmatrix} \begin{bmatrix} \bar{e}_{xR} \\ \bar{e}_{yR} \\ \bar{e}_{zR} \end{bmatrix}^* \tag{2.3}$$

The (x_1, y_1, z_1) coordinate frame will be defined by "despinning" the body frame. Thus

$$\begin{bmatrix} \bar{e}_{x1} \\ \bar{e}_{y1} \\ \bar{e}_{z1} \end{bmatrix} = \begin{bmatrix} \cos\gamma & -\sin\gamma & 0 \\ \sin\gamma & \cos\gamma & 0 \\ 0 & 0 & 1 \end{bmatrix} \begin{bmatrix} \bar{e}_{xb} \\ \bar{e}_{yb} \\ \bar{e}_{zb} \end{bmatrix} \tag{2.4}$$

where $\gamma = \omega_s t + \gamma_o$. The orientation of the (x_1, y_1, z_1) set relative to the reference axes is defined by the matrix C:

$$\begin{bmatrix} \bar{e}_{x1} \\ \bar{e}_{y1} \\ \bar{e}_{z1} \end{bmatrix} = \begin{bmatrix} c_{11} & c_{12} & c_{13} \\ c_{21} & c_{22} & c_{23} \\ c_{31} & c_{32} & c_{33} \end{bmatrix} \begin{bmatrix} \bar{e}_{xR} \\ \bar{e}_{yR} \\ \bar{e}_{zR} \end{bmatrix} \tag{2.5}$$

The angle γ_o is defined so that with ideal spin-axis attitude $(\bar{e}_{zb} = \bar{e}_{zR})$ the matrix C is the identity matrix.

---

* The symbol $\bar{e}_{xb}$, for example, denotes the unit vector along the x_b axis.

B. EQUATIONS OF MOTION

1. Dynamical Equations

The dynamical equations describing the motion of a rigid body are Euler's equations [Ref. 2-2]:

$$\begin{aligned} I_x\dot{\omega}_x + (I_z - I_y)\omega_y\omega_z &= N_{xb} \\ I_y\dot{\omega}_y + (I_x - I_z)\omega_x\omega_z &= N_{yb} \\ I_z\dot{\omega}_z + (I_y - I_x)\omega_x\omega_y &= N_{zb} \end{aligned} \tag{2.6}$$

where

I_x, I_y, I_z are the principal axis moments of inertia.

N_{xb}, N_{yb}, N_{zb} are the components of external torque in body coordinates.

ω_x, ω_y, ω_z are the components of the total inertial angular velocity of the (x_b, y_b, z_b) coordinate frame resolved in the (x_b, y_b, z_b) coordinate axes.

For the symmetric spinning vehicle, it is assumed that $I_y = I_x$ and $\omega_z = \omega_s$, a constant. The dynamical equations then become:

$$\begin{aligned} \dot{\omega}_x &= -k\omega_s\omega_y + n_x \\ \dot{\omega}_y &= +k\omega_s\omega_x + n_y \end{aligned} \tag{2.7}$$

where

$$n_x = \frac{N_{xb}}{I_x}, \qquad n_y = \frac{N_{yb}}{I_x}, \qquad k = \frac{I_z - I_x}{I_x}$$

With a single coil normal to the spin axis the magnetic moment $\bar{m}$ is aligned with the spin axis. Thus, from expression (1.1), the components of control torque (in newton-meters) are:

$$\begin{bmatrix} N_{xb} \\ N_{yb} \\ N_{zb} \end{bmatrix} = \begin{bmatrix} 0 & -m_c & 0 \\ m_c & 0 & 0 \\ 0 & 0 & 0 \end{bmatrix} \begin{bmatrix} B_{xb} \\ B_{yb} \\ B_{zb} \end{bmatrix} \tag{2.8}$$

where m_c is the (scalar) magnetic moment produced by current in the torquing coil (in amp-m^2), and B_{xb}, B_{yb}, B_{zb} are the components of the earth's magnetic field in body coordinates in webers/m^2. For purposes of normalization, the control u will be defined as

$$u = \frac{m_c}{I_z \omega_s} = \frac{m_c}{H_s} \tag{2.9}$$

The controlled equations can be written as

$$\boxed{\begin{aligned} \dot{\omega}_x &= -k\omega_s \omega_y - (1 + k)\omega_s B_{yb} u \\ \dot{\omega}_y &= k\omega_s \omega_x + (1 + k)\omega_s B_{xb} u \end{aligned}} \tag{2.10}$$

It is of interest to express the vehicle dynamics in terms of the inertial angular velocity of the (x_1, y_1, z_1) coordinate frame; expressed in the (x_1, y_1, z_1) axes, this angular velocity has components

$$\begin{bmatrix} \omega_1 \\ \omega_2 \end{bmatrix} = \begin{bmatrix} \cos\gamma & -\sin\gamma \\ \sin\gamma & \cos\gamma \end{bmatrix} \begin{bmatrix} \omega_x \\ \omega_y \end{bmatrix} \tag{2.11}$$

where ω_3 is zero because this coordinate frame has been defined as "despun" relative to the vehicle coordinate axes. Define

$$D = \begin{bmatrix} \cos\gamma & -\sin\gamma \\ \sin\gamma & \cos\gamma \end{bmatrix}$$

Then

$$\begin{bmatrix} \dot{\omega}_1 \\ \dot{\omega}_2 \end{bmatrix} = \dot{D} \begin{bmatrix} \omega_x \\ \omega_y \end{bmatrix} + D \begin{bmatrix} \dot{\omega}_x \\ \dot{\omega}_y \end{bmatrix}$$

Pursuing this development yields:

$$\begin{bmatrix} \dot{\omega}_1 \\ \dot{\omega}_2 \end{bmatrix} = (1 + k)\omega_s \begin{bmatrix} -\sin\gamma & -\cos\gamma \\ \cos\gamma & -\sin\gamma \end{bmatrix} \begin{bmatrix} \omega_x \\ \omega_y \end{bmatrix} + \begin{bmatrix} n_1 \\ n_2 \end{bmatrix}$$

or, finally

$$\begin{aligned} \dot{\omega}_1 &= -(1 + k)\omega_s\omega_2 + n_1 \\ \dot{\omega}_2 &= (1 + k)\omega_s\omega_1 + n_2 \end{aligned} \tag{2.12}$$

where n_1, n_2 are the two components of the normalized applied torque in (x_1, y_1, z_1) coordinates as in (2.7). The equations with magnetic control are, from (2.10) and (2.12):

$$\boxed{\begin{aligned} \dot{\omega}_1 &= -(1 + k)\omega_s[\omega_2 + B_{y1}u] \\ \dot{\omega}_2 &= +(1 + k)\omega_s[\omega_1 + B_{x1}u] \end{aligned}} \tag{2.13}$$

2. Kinematical Equations

The kinematical equations (that is, those which give the time-rate-of-change of the attitude variables) are developed using two types of attitude variables, direction cosines and Euler parameters. Direction cosines are particularly convenient in the subsequent analyses because: (1) only three are necessary to define the spin-axis position

in reference coordinates, and (ii) the feedback control law developed is simply expressed in terms of direction cosines. On the other hand, Euler parameters are convenient for numerical integration of the differential equations because they allow the use of four attitude variables instead of the nine direction cosines. It should be noted that three orthogonal rotation angles (such as Euler angles) are unsuitable for a study of this nature because the rate of change of one of the angles will become unbounded for certain attitudes; furthermore, the differential equations with direction cosines and with Euler parameters exhibit a useful symmetry.

a. Direction Cosine Kinematics

Let p, q, and r be the components in vehicle coordinates of the angular velocity of the vehicle coordinate frame relative to the reference coordinate frame. Let Ω_x, Ω_y, and Ω_z be the components in reference coordinates of the angular velocity, $\bar{\Omega}^R$, of the reference coordinate frame relative to inertial space. It is desirable to express the time-rate-of-change of the direction cosines in terms of ω_x, ω_y, ω_z, Ω_x, Ω_y, Ω_z, and the direction cosines.

The kinematical equations in terms of p, q, r, and the direction cosines are well-known [Refs. 2-3, 2-4]. For the matrix A defined in (2.3):

$$\dot{A} = -\begin{bmatrix} 0 & -r & q \\ r & 0 & -p \\ -q & p & 0 \end{bmatrix} A \qquad (2.14)$$

Utilizing the fact that $A^T = A^{-1}$ and $\det A = 1$, it is seen that $a_{ij} = \text{cof}\,(a_{ij})$, the cofactor of the element a_{ij}. This yields nine very useful identities [Ref. 2-4].

$$
\begin{aligned}
a_{11} &\equiv a_{22}a_{33} - a_{23}a_{32} \\
a_{12} &\equiv a_{23}a_{31} - a_{21}a_{33} \\
a_{13} &\equiv a_{21}a_{32} - a_{22}a_{31} \\
a_{21} &\equiv a_{13}a_{32} - a_{12}a_{33} \\
a_{22} &\equiv a_{11}a_{33} - a_{13}a_{31} \\
a_{23} &\equiv a_{12}a_{31} - a_{11}a_{32} \\
a_{31} &\equiv a_{12}a_{23} - a_{13}a_{22} \\
a_{32} &\equiv a_{13}a_{21} - a_{11}a_{23} \\
a_{33} &\equiv a_{11}a_{22} - a_{12}a_{21}
\end{aligned}
\tag{2.15}
$$

Notice that p, q, r are given in terms of ω_x, ω_y, ω_z, Ω_x, Ω_y, and Ω_z by:

$$
\begin{bmatrix} p \\ q \\ r \end{bmatrix} = \begin{bmatrix} \omega_x \\ \omega_y \\ \omega_z \end{bmatrix} - A \begin{bmatrix} \Omega_x \\ \Omega_y \\ \Omega_z \end{bmatrix} \tag{2.16}
$$

Then, combining (2.14), (2.15), and (2.16):

$$
\boxed{\dot{A} = - P(\omega)A + AP(\Omega)} \tag{2.17}
$$

where

$$P(\alpha) = \begin{bmatrix} 0 & -\alpha_z & \alpha_y \\ \alpha_z & 0 & -\alpha_x \\ -\alpha_y & \alpha_x & 0 \end{bmatrix}$$

Similarly, replacing A by C, ω_x by ω_1, ω_y by ω_2 and ω_z by zero, the rate of change of the matrix C can be derived.

b. Euler Parameter Kinematics

In a similar manner, the differential equations for the Euler parameters can be derived. In terms of p, q, and r [Ref. 2-3]:

$$\begin{bmatrix} \dot{E}_1 \\ \dot{E}_2 \\ \dot{E}_3 \\ \dot{E}_4 \end{bmatrix} = \frac{1}{2} \begin{bmatrix} 0 & r & -q & p \\ -r & 0 & p & q \\ q & -p & 0 & r \\ -p & -q & -r & 0 \end{bmatrix} \begin{bmatrix} E_1 \\ E_2 \\ E_3 \\ E_4 \end{bmatrix} \qquad (2.18)$$

The Euler parameters admit to the following identity

$$\sum_{j=1}^{4} E_j \equiv 1$$

Furthermore, the direction cosines may be expressed in terms of the Euler parameters:

$$a_{11} \equiv E_1^2 - E_2^2 - E_3^2 + E_4^2$$

$$a_{12} \equiv 2(E_1E_2 + E_3E_4)$$

$$a_{13} \equiv 2(E_1E_3 - E_2E_4)$$

$$a_{21} \equiv 2(E_1E_2 - E_3E_4)$$

$$a_{22} \equiv -E_1^2 + E_2^2 - E_3^2 + E_4^2 \tag{2.19}$$

$$a_{23} \equiv 2(E_2E_3 + E_1E_4)$$

$$a_{31} \equiv 2(E_1E_3 + E_2E_4)$$

$$a_{32} \equiv 2(E_2E_3 - E_1E_4)$$

$$a_{33} \equiv -E_1^2 - E_2^2 + E_3^2 + E_4^2$$

Utilizing relationships (2.16), (2.18), and (2.19) the following result is obtained:

$$\begin{bmatrix} \dot{E}_1 \\ \dot{E}_2 \\ \dot{E}_3 \\ \dot{E}_4 \end{bmatrix} = \frac{1}{2} \left\{ \begin{bmatrix} 0 & \omega_z & -\omega_y & \omega_x \\ -\omega_z & 0 & \omega_x & \omega_y \\ \omega_y & -\omega_x & 0 & \omega_z \\ -\omega_x & -\omega_y & -\omega_z & 0 \end{bmatrix} + \begin{bmatrix} 0 & \Omega_z & -\Omega_y & -\Omega_x \\ -\Omega_z & 0 & \Omega_x & -\Omega_y \\ \Omega_y & -\Omega_x & 0 & -\Omega_z \\ \Omega_x & \Omega_y & \Omega_z & 0 \end{bmatrix} \right\} \begin{bmatrix} E_1 \\ E_2 \\ E_3 \\ E_4 \end{bmatrix} \tag{2.20}$$

c. The Simplified Model

The "exact" description of the system under consideration can be obtained by combining (2.10) and (2.17). However, this set of equations is not particularly appealing to the intuition. It is possible to derive a simplified model which, though it is less rigorous, will yield valuable insight into the design of a magnetic control system.

The concept of a spinning satellite suggests that the angular velocity about the spin axis is much larger than that about either of the transverse axes--that is, that the total momentum vector is very nearly aligned with the spin axis.* The dynamics described above by Euler's

---

* The terminology "spin axis" refers to the body-fixed z_b axis, not the instantaneous total angular velocity vector.

equations can be described equivalently by Newton's second law in rotational form. That is,

$$\overset{\mathcal{R}}{\bar{H}} + \bar{\Omega}^{R} \times \bar{H} = \bar{N} \tag{2.21}$$

where $\overset{\mathcal{R}}{\bar{H}}$ is the rate of change of the total momentum vector relative to the (x_R, y_R, z_R) coordinate frame, $\bar{N}$ is the external torque (here the control torque) and $\bar{\Omega}^{R}$ is the angular velocity of the reference coordinate frame relative to inertial space, as before. The torque, $\bar{N}$, for magnetic control is

$$\bar{N} = \bar{m} \times \bar{B}$$

where, for the single-coil system under consideration,

$$\bar{m} = m_c \bar{e}_{zb} = H_s u \bar{e}_{zb} \tag{2.22}$$

with u defined in (2.9). Now, assuming that the total momentum vector is <u>exactly</u> aligned with the spin axis (that is, $\bar{H} = H_s \bar{e}_{zb}$), Eq. (2.21) assumes a very interesting form:

$$\overset{\mathcal{R}}{\bar{H}} + \bar{\Omega}^{R} \times \bar{H} = (\bar{H} \times \bar{B})u \tag{2.23}$$

For convenience define the normalized momentum components in reference coordinates as:

$$h_x = \frac{H_{xR}}{H_s} ; \qquad h_y = \frac{H_{yR}}{H_s} ; \qquad h_z = \frac{H_{zR}}{H_s} \tag{2.24}$$

and let $\bar{h}$ be the unit vector with these components in the (x_R, y_R, z_R) frame. Then

$$\boxed{\overset{\mathcal{R}}{\bar{h}} + (\bar{B}u + \bar{\Omega}^{R}) \times \bar{h} = 0} \tag{2.25}$$

These equations will be referred to as the simplified model of the system.

It is of interest to compare these equations with the "exact" model derived earlier.* Notice that the variables defined in (2.24) have meaning in the exact model as well but that they will not generally form a unit vector. The total momentum can be written in (x_1, y_1, z_1) space as:

$$\bar{H} = I_x(\omega_1 \bar{e}_{x1} + \omega_2 \bar{e}_{y1}) + H_s \bar{e}_{z1} \tag{2.26}$$

Then, in (x_R, y_R, z_R) space the normalized momentum components are:

$$\begin{bmatrix} h_x \\ h_y \\ h_z \end{bmatrix} = \begin{bmatrix} c_{11} & c_{21} & c_{31} \\ c_{12} & c_{22} & c_{32} \\ c_{13} & c_{23} & c_{33} \end{bmatrix} \begin{bmatrix} \frac{I_x}{H_s}\omega_1 \\ \frac{I_x}{H_s}\omega_2 \\ 1 \end{bmatrix} \tag{2.27}$$

Notice that with $\omega_1 = \omega_2 = 0$, (2.27) reduces to $h_x = c_{31}$, $h_y = c_{32}$, and $h_z = c_{33}$.

Using expression (2.21) without assuming alignment of $\bar{m}$ and $\bar{H}$, the components in the reference coordinate frame of the time-rate-of-change of the normalized momentum vector relative to this coordinate frame can be derived for the exact equations of motion:

---

* Hereafter the quotation marks on "exact" will be omitted, but their presence is understood.

$$\dot{\bar{h}} \cdot \bar{e}_{xR} = \Omega_z h_y - \Omega_y h_z + (B_{zR} h_y - B_{yR} h_z)u$$

$$+ \frac{I_x}{H_s}\left[B_{yR}(c_{13}\omega_1 + c_{23}\omega_2) - B_{zR}(c_{12}\omega_1 + c_{22}\omega_2)\right]u$$

$$\dot{\bar{h}} \cdot \bar{e}_{yR} = \Omega_x h_z - \Omega_z h_x + (B_{xR} h_z - B_{zR} h_x)u \qquad (2.28)$$

$$+ \frac{I_x}{H_s}\left[B_{zR}(c_{11}\omega_1 + c_{21}\omega_2) - B_{xR}(c_{13}\omega_1 + c_{23}\omega_2)\right]u$$

$$\dot{\bar{h}} \cdot \bar{e}_{zR} = \Omega_y h_x - \Omega_x h_y + (B_{yR} h_x - B_{xR} h_y)u$$

$$+ \frac{I_x}{H_s}\left[B_{xR}(c_{12}\omega_1 + c_{22}\omega_2) - B_{yR}(c_{11}\omega_1 + c_{21}\omega_2)\right]u$$

Upon expanding the equations of the simplified model, we find that they agree precisely with the equations above for $\omega_1 = \omega_2 = 0$. Furthermore, it is natural to ask how much the response of the simplified model (in terms of h_x, h_y, h_z) resembles that of the exact model (in terms of c_{31}, c_{32}, c_{33}). The answer, from digital computer solution of both sets of equations, is that (for the control system developed in the next chapter) the systems respond quite similarly except for small attitude errors. The degree of similarity is dependent upon the magnitude of the transverse angular velocities and, therefore, upon the amount of damping provided.

III. CONTROL LAW DEVELOPMENT

The attitude control system for a spinning vehicle has two basic functions--the reorientation of the total momentum vector (position control) and the alignment of the spin axis with the momentum vector by removal of the transverse components of angular velocity (damping). The former function must be accomplished by an active system which applies external torques to the vehicle; damping, however, since it does not necessarily entail a change in the total momentum, can be accomplished by passive dampers which remove energy from the system whenever excited by transverse angular velocities. Typical passive dampers are a spring-restrained mass moving in a viscous medium (or coupled to a viscous damper), and an annular ring (in a plane normal to the spin axis) which is partially filled with mercury [Refs. 1-10, 3-1].

Typically, then, the position control and the damping device function independently in a spinning vehicle. Furthermore, given any position control system, it is possible to consider combining it with any damping device with sufficient energy removal capability. In this discussion, however, a control law will be developed in which the damping is provided by active techniques. For this scheme, it will be possible to specify precisely the "amount" of damping required to produce asymptotic stability.

A. POSITION CONTROL

The goal of the position control can be regarded, in terms of the third-order simplified model, as bringing the system to the equilibrium state $h_x = h_y = 0$, $h_z = 1$ (hereafter referred to as the origin). Thus, a control policy which always causes h_z to increase at any point away from the origin, or at least never to decrease, would appear to be a good one. With $\bar{\Omega}^R = 0$, that is, an inertially fixed desired spin-axis direction, z_R:

$$\dot{h}_z = (B_{yR}h_x - B_{xR}h_y)u \tag{3.1}$$

Defining

$$\sigma_h = B_{yR} h_x - B_{xR} h_y \tag{3.2}$$

it is clear that a control of the form

$$u_h = \eta(\sigma_h) \tag{3.3}$$

where the function η is of the general form shown in Fig. 3-1, will be very desirable. With this control, $\dot{h}_z > 0$ except at times when $\sigma_h = 0$.

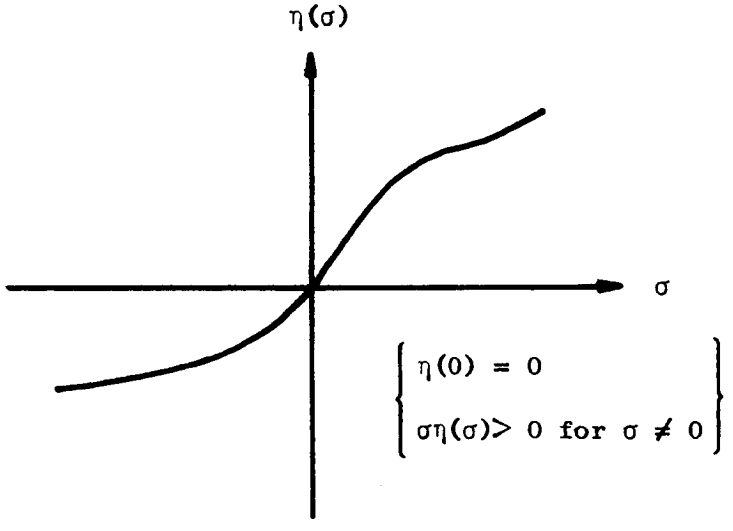

FIG. 3-1. THE CONTROL FUNCTION $u = \eta(\sigma)$.

Translating this control to the exact system model we note that from (2.27):

$$h_x = c_{31} + \frac{I_x}{H_s}(c_{11}\omega_1 + c_{21}\omega_2)$$

$$h_y = c_{32} + \frac{I_x}{H_s}(c_{12}\omega_1 + c_{22}\omega_2)$$

Neglecting the rate-dependent terms (on the premise that the position control should be a function of the position variables only), the position error function becomes:

$$\sigma_p = B_{yR}c_{31} - B_{xR}c_{32} \tag{3.4}$$

This error function can be expressed in terms of magnetic field components measured in (x_1, y_1, z_1) coordinates or in terms of components measured directly in vehicle coordinates as:

$$\sigma_p = B_{x1}c_{23} - B_{y1}c_{13}$$

or (3.5)

$$\sigma_p = B_{xb}a_{23} - B_{yb}a_{13}$$

These forms are convenient both for the analyses which follow and for mechanization considerations.

B. ACTIVE DAMPING

Active magnetic damping (if attainable) is particularly appealing for use in conjunction with a magnetic position control because no additional actuator is required. Assume a total error function of the form:

$$\sigma = \sigma_p + K_R\sigma_R \tag{3.6}$$

The problem is to: (i) find σ_R, and (ii) specify K_R.

One possible mechanism for passive damping is the energy dissipation caused by the eddy currents induced in a circular shorted loop of N_c turns located in a plane normal to the spin axis. An analysis of this effect (which provides only a minute amount of damping in any practical case) will provide insight into the development of an active damping law. Consider, as shown in Fig. 3-2, a shorted loop of N_c turns in the (x_1, y_1) plane as defined in Chapter II. The emf induced in the loop is:

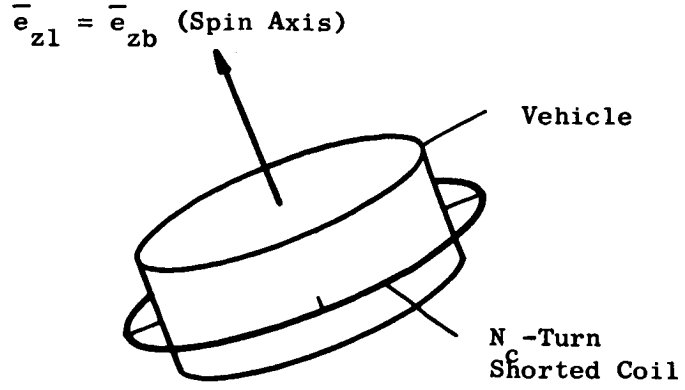

FIG. 3-2. SHORTED LOOP FOR PASSIVE EDDY CURRENT DAMPING.

$$e = - N_c \frac{d\Phi}{dt} \tag{3.7}$$

where Φ is the total magnetic flux linking the coil. In terms of the area of the loop, A_c, and the magnetic field vector:

$$\Phi = (\bar{B} \cdot \bar{e}_{z1})A_c \tag{3.8}$$

Therefore

$$e = - N_c A_c (\dot{\bar{B}} \cdot \bar{e}_{z1} + \bar{B} \cdot \dot{\bar{e}}_{z1}) \tag{3.9}$$

where the overscript "1" denotes time differentiation with respect to the (x_1, y_1, z_1) coordinate frame. Since $\dot{\bar{e}}_{z1}$ is identically zero:

$$e = - N_c A_c \dot{\bar{B}} \cdot \bar{e}_{z1} \tag{3.10}$$

Using the law of Coriolis regarding time differentiation with respect to rotating coordinate frames [Ref. 2-2]:

$$\dot{\bar{B}} = \frac{e}{B} - \bar{\omega}^1 \times \bar{B} \tag{3.11}$$

where the components of $\bar{\omega}^{1}$ in (x_1, y_1, z_1) space are, respectively, ω_1, ω_2, and zero.

As a first approximation, the rate of change of $\bar{B}$ in the inertial (x_e, y_e, z_e) coordinate frame can be neglected, since the frequencies involved are no more than twice orbital frequency. With the term $\dot{\bar{B}}$ neglected, (3.10) can be expanded to yield:

$$e = N_c A_c (B_{y1}\omega_1 - B_{x1}\omega_2) \tag{3.12}$$

If the coil is formed by N_c turns of wire with a resistance per unit length of ρ, and each turn is of length ℓ, the current induced in the coil is, neglecting inductive reactance:

$$i = \frac{A_c}{\rho\ell} (B_{y1}\omega_1 - B_{x1}\omega_2) \tag{3.13}$$

Assuming that all other sources of magnetic moment (e.g. eddy currents in the structure of the vehicle) are negligible, the magnetic moment is

$$\bar{m} = \frac{N_c A_c^2}{\rho\ell} (B_{y1}\omega_1 - B_{x1}\omega_2)\bar{e}_{z1} \tag{3.14}$$

or, transforming into variables referenced to the spinning (x_b, y_b, z_b) body coordinate frame

$$\bar{m} = \frac{N_c A_c^2}{\rho\ell} (B_{yb}\omega_x - B_{xb}\omega_y)\bar{e}_{zb} \tag{3.15}$$

These naturally induced eddy currents have the effect of reducing the kinetic energy of the satellite. For a symmetric spinning vehicle, the total kinetic energy is

$$T_K = \frac{1}{2}\left[I_x(\omega_1^2 + \omega_2^2) + I_z\omega_s^2\right] \tag{3.16}$$

In the parlance of expression (2.13), the control, u, produced by the above effect is

$$u = \frac{N_c A_c^2}{\rho \ell H_s} (B_{y1}\omega_1 - B_{x1}\omega_2) \tag{3.17}$$

Then along the trajectories of the system as defined in (2.13):

$$\dot{T}_K = - H_s (B_{y1}\omega_1 - B_{x1}\omega_2) u \tag{3.18}$$

Thus with u as above

$$\dot{T}_K = - \frac{N_c A_c^2}{\rho \ell} (B_{y1}\omega_1 - B_{x1}\omega_2)^2 \leq 0 \tag{3.19}$$

As mentioned above, the damping available from this passive effect is quite small; in fact, using a circular coil of copper wire with an assumed temperature of 20°C., it has been shown that the lower limit on the damping time constant is approximately one day [Ref. 3-2]. This limiting case assumes that the "vehicle" is made up completely of the coil; additions to this somewhat impractical vehicle increase the vehicle inertias without adding to the damping capability and, therefore, lengthen the time constant.

Although this passive technique is impractical, we can consider an active damping law using as a rate error function

$$\sigma_R = B_{y1}\omega_1 - B_{x1}\omega_2 = B_{yb}\omega_x - B_{xb}\omega_y \tag{3.20}$$

Clearly, in the absence of any other torque (e.g. position control), the kinetic energy will be reduced except at the times when σ_R is zero. Intuitively, this will eventually bring ω_1 and ω_2 to zero, which is the desired state if the (x_R, y_R, z_R) coordinate frame is inertially stationary.

It is of interest to note that with this damping law (in the absence of all other torques) angular momentum is not conserved because, although ω_1 and ω_2 are reduced to zero, the component of angular velocity along the z_1 axis is constant. In contrast, with a passive mechanical damper there are no external torques on the vehicle and the total angular momentum of the vehicle (including the damper) is conserved;

reduction of ω_1 and ω_2 to zero increases the component of angular velocity along the z_1 axis, and the terminal state is reached with the vehicle in pure spin about its axis of maximum inertia (here the z_b axis), which corresponds to the condition of minimum <u>total</u> kinetic energy. It is for this reason that spinning vehicles are generally constrained to be spun about the axis of maximum inertia. Even though the active damping law (since it seeks the condition of minimum <u>transverse</u> kinetic energy) imposes no such constraint, there will usually be a certain amount of internal energy dissipation in any vehicle (e.g., due to flexing of external antennae). With this in mind, this study will assume $I_z > I_x = I_y$ where z_b is the spin axis. In this case the inertia parameter k is always between zero and unity.

C. CONTROL LAW SUMMARY

To summarize, the control to be considered is

$$u = \eta(\sigma)$$

where

$$\sigma = \sigma_p + K_R \sigma_R$$

and

$$\sigma_p \mp B_{x1} c_{23} - B_{y1} c_{13}$$

$$\sigma_R = B_{y1} \omega_1 - B_{x1} \omega_2$$

We have yet to assure that this control will be stable or if it is stable, that it will give acceptable performance, or, granting these two tests are satisfied, that this control can be mechanized in a reasonable fashion. These questions are the topics of subsequent chapters.

IV. STABILITY ANALYSES

The usual approach to stability analysis of spacecraft attitude control systems is, first, to study stability for small errors by linearization and the classical techniques applicable to linear stationary systems (or low-order stationary systems with contactor control), and then to study stability for large errors by analog simulation. This technique is generally acceptable; however, the scope of the analog study must be sufficient to give a high level of confidence in acquisition (that is, convergence from large initial attitude errors and angular velocities).

An alternate approach to the problem is via the second method of Lyapunov [Refs. 4-1, 4-2]. By finding an "energy-like" function (a positive definite function of the state variables) which can be shown never to increase along any solution to the system of differential equations, stability can be verified; by showing that this function, V, goes to zero as $t \to \infty$, asymptotic stability can be concluded.* The difficulty with this powerful method lies in finding a suitable Lyapunov function, V.

Previous application of Lyapunov's second method to attitude control systems has been limited to single axis (rotation about only one axis of the vehicle) cases or to problems in which the motion of the vehicle is unrestricted but the control is constrained (e.g., control of a fully stabilized vehicle using proportional gas jets as opposed to the more realistic case of contactor control [Ref. 4-3]).

The system of equations dealt with in this discussion is nonstationary; thus, even the small-error linearized equations are not amenable to explicit solution. It is natural to attempt to apply the second method of Lyapunov to such a problem. Fortunately, this approach can be readily

---

* A basic familiarity with the fundamental concepts and theorems of the second method of Lyapunov is assumed; thus, terms such as stability and asymptotic stability are presented without explanation. For reference, certain basic definitions and theorems are summarized in Appendix C.

applied, using two theorems of Krasovskii, and will yield definite information regarding the theoretical feasibility of magnetic control for spinning vehicles, and the "amount" of damping required, as specified by the damping gain, K_R.

A. THE APPROACH

The second method of Lyapunov requires the exhibition of a positive-definite function of the system state variables whose time derivative, evaluated along the trajectories of the system, is a negative definite (or negative semidefinite) function of the state variables. The basic theorems (Appendix C) allow the conclusion of asymptotic stability with $\dot{V}$ negative definite, but only of stability with $\dot{V}$ negative semidefinite. However, there are results which will allow the conclusion of asymptotic stability in the latter case, as well, by consideration of the type of motion which can occur with $\dot{V}$ equal to zero. The most general of these results are summarized by two theorems of Krasovskii [Ref. 4-4]; both relate to a system defined in the following manner.

The system is described for all $t \geq t_o$ by the vector ordinary differential equation

$$\dot{\bar{x}} = \bar{f}(\bar{x}, t) \tag{4.1}$$

where the component functions $f_i(\bar{x}, t)$ of $\bar{f}(\bar{x}, t)$ are either explicit periodic functions of time with period T, or have no explicit time dependence. It is further assumed that these functions are defined and continuous on the open region

$$\mathcal{R}_\Sigma = \{(\bar{x}, t): \ \|\bar{x}\| < \Sigma, \ -\infty \leq t \leq \infty\} \tag{4.2}$$

with Σ constant but not necessarily finite, and that the functions f_i satisfy a Lipschitz condition with respect to each of the components of $\bar{x}$ in every region $\|\bar{x}\| < \Sigma_u < \Sigma$. The theorems to be used are:

Stability Theorem (Th. 14.1 of Ref. 4-4)

Suppose the Eqs. (4.1) enjoy the properties that:

1. There exists a function $V(\bar{x}, t)$ which is periodic in time with period T, or does not depend explicitly on time;

2. $V(\bar{x}, t)$ is positive definite;

3. $V(\bar{x}, t)$ admits an infinitely small upper bound in the region $\mathcal{R}_\Sigma$;

4. $\sup(V \text{ in the region } \|\bar{x}\| \leq \Sigma_o, \ 0 \leq t < T) < \inf(V \text{ for } \|\bar{x}\| = \Sigma_1)$, where $\Sigma_o < \Sigma_1 < \Sigma$:

5. $\dot{V} \leq 0$ in $\mathcal{R}_\Sigma$;

6. The set $\mathcal{L}$ of points at which the derivative $\dot{V}$ is zero contains no nontrivial half trajectory

$$\bar{\varphi}(t; \bar{x}_o, t_o) \qquad (t_o \leq t < \infty)$$

of the system (4.1).

Under these conditions, the null solution $\bar{x} = 0$ is asymptotically stable and the region $\|\bar{x}\| \leq \Sigma_o$ lies in the region of attraction of the point $\bar{x} = 0$.

Instability Theorem (Th. 15.1 of Ref. 4-4)

Let $\Sigma_1 < \Sigma$. Suppose that there exists a function $W(\bar{x}, t)$ which is periodic in time or does not depend explicitly on the time, such that

1. W is defined in the region $\mathcal{R}_\Sigma$;

2. W admits an infinitely small upper bound in this region

3. $\dot{W} \geq 0$ in the region $\mathcal{R}_\Sigma$ along a trajectory of (4.1);

4. The set of points $\mathcal{L}$ at which $\dot{W}$ is zero contains no nontrivial half trajectory

$$\bar{\varphi}(t; \bar{x}_o, t_o) \qquad (t_o \leq t < \infty)$$

of the system (4.1).

Suppose further that in every region of the point $\bar{x} = 0$ there is a point $\bar{x}_o$ such that for arbitrary $t_o \geq 0$ we have $W(\bar{x}_o, t_o) > 0$.

Then the null solution $\bar{x} = 0$ is unstable, and the trajectories $\bar{\varphi}(t; \bar{x}_o, t_o)$ for which $W(\bar{x}_o, t_o) > 0$ leave the region $\|\bar{x}\| < \Sigma_1$ as the time increases.

Aside from the discovery of a suitable Lyapunov function, the greatest difficulty in applying these theorems is that of showing that the subspace M contains no nontrivial solution of the system of differential equations. In Ref. 4-4, it is suggested that if $\mathcal{L}$ is a surface defined by the scalar function

$$\Upsilon(\bar{x}, t) = 0 \tag{4.3}$$

the condition on $\mathcal{L}$ will always be satisfied if the inequality

$$\dot{\Upsilon} = \bar{\nabla}_x \Upsilon \cdot \bar{f} + \frac{\partial \Upsilon}{\partial t} \neq 0 \tag{4.4}$$

holds on the surface (4.3) in the region $\|\bar{x}\| < \Sigma_1$. This inequality is sufficient, because $\dot{\Upsilon}$ is assured to be nonzero whenever Υ is equal to zero, but is certainly not necessary.

A more useful approach, at least in the present study, is to attempt a general solution to the system differential equations under the constraint that $\dot{V}$ is zero, and then to show that these solutions are inconsistent with $\dot{V}$ remaining zero for all time. This technique, which deals with a condition which is necessary as well as sufficient for the nonexistence of nontrivial solutions on the set $\mathcal{L}$, will (when it can be applied) yield more definitive results. For the system equations and Lyapunov functions considered here (for both the simplified and exact equations of motion), $\dot{V} = 0$ will occur when the control is zero. Thus, the equations to be solved will be stationary and, as will be seen, can be solved.

In the development to follow, four distinct cases will be solved, considering the simplified and exact equations of motion each with two magnetic field models, the untilted dipole and the tilted dipole. The most rigorous model is, of course, the exact equations of motion combined with the tilted dipole model of the magnetic field. However, consideration of the simpler models will yield valuable insight.

A word must be said about the magnetic field models developed in Appendix A. The untilted dipole model, which assumes coincidence of the magnetic dipole with the spin axis of the earth, yields magnetic

field components in the (x_n, y_n, z_n) coordinate frame which are periodic at twice orbital rate. With the tilted magnetic dipole model, B_{xn}, B_{yn} and B_{zn} are, in general, almost periodic functions of time, containing the frequencies $2\omega_o$, ω_e, $2\omega_o+\omega_e$ and $2\omega_o-\omega_e$, where ω_o is the orbital rate and ω_e is the spin rate of the earth.* In this general case, the theorems of Krasovskii are not applicable. However, if we restrict our attention to those circular orbits for which the ratio of ω_o to ω_e is a rational number, the coefficients will be periodic, and the theorems can be applied. This set of orbits is a set dense in the set of all possible circular orbits; this means that given any circular orbit we can, by changing its altitude by an arbitrarily small amount, transfer to another orbit such that ω_o/ω_e is rational. Intuitively, then, it is conjectured that if stability can be demonstrated for these "rational" orbits, the system will be stable in "irrational" orbits as well.

The alternative to this conjecture would be the extension of the theorems of Krasovskii to the case of almost periodic coefficients. The present proof would not suffice, nor does it appear that it can be readily extended to the more general case. Indeed, although it would appear intuitively that periodic and almost periodic systems are similar, there is no special stability theory for the latter systems similar to that which has been developed for the former. For example, for systems with periodic coefficients (asymptotic) stability implies uniform (asymptotic) stability; but, according to Hahn [Ref. 4-1], this relationship has been neither proved nor disproved for equations with almost periodic coefficients.

In the analyses which follow, there is a stable equilibrium (for example, $h_x = h_y = 0$, $h_z = +1$) as well as an unstable equilibrium ($h_z = -1$ in this case). $\dot{V}$ can remain zero on this trivial solution, as well as at the origin; however, eventually a perturbation would

---

* As mentioned in Chapter II, the (x_n, y_n, z_n) frame is assumed inertially fixed by neglecting nodal regression. Also (x_R, y_R, z_R) will be assumed fixed in inertial space--that is, $\Omega_x = \Omega_y = \Omega_z = 0$.

drive the system away from the unstable equilibrium. This case will be ignored.

In summary, the procedure by which stability will be analyzed is:

1. Find a Lyapunov function satisfying the requirements of the stability theorem. In this study, the Lyapunov functions used will have no explicit time dependence and $\dot{V} = 0$ will correspond to $\sigma = 0$; that is, no control.

2. Solve the uncontrolled equations of motion without small error assumptions.

3. Show that none of these solutions (other than the trivial solution $\bar{x} = 0$) is consistent with the assumption that $\sigma = 0$, thereby showing that no nontrivial solutions can remain for all time in the set of points $\mathcal{L}$ given by $\dot{V}(\bar{x}, t) = 0$.

B. STABILITY OF THE SIMPLIFIED MODEL

For the simplified equations of motion (2.25), the state vector, $\bar{x}$, is

$$\bar{x} = \begin{bmatrix} h_x \\ h_y \\ 1-h_z \end{bmatrix} \tag{4.5}$$

so that $\bar{x} = 0$ corresponds to the desired terminal state $h_x = h_y = 0$, $h_z = 1$. Consider as a Lyapunov function one-half of the square of the Euclidean norm of $\bar{x}$:

$$\boxed{V = \frac{1}{2}\left[h_x^2 + h_y^2 + (1 - h_z)^2\right].} \tag{4.6}$$

Since $\bar{h}$ is a unit vector

$$h_x^2 + h_y^2 + h_z^2 = 1 \tag{4.7}$$

and it is easy to show that

$$V = 1 - h_z \tag{4.8}$$

which is positive definite, since $|h_z| \leq 1$, and since $h_z = 1$ can occur only if $h_x = h_y = 0$. It is readily shown that V admits to an infinitely small upper bound because this requires only the existence of a positive definite continuous function $U(x)$ such that

$$|V(x, t)| \leq U(x) \tag{4.9}$$

In this case, we choose $U(x) = V(x)$.

With the (x_R, y_R, z_R) axes inertially fixed $(\bar{\Omega}^R = 0)$, the simplified equations of motion (2.25) become

$$\dot{\bar{h}} = -(\bar{B} \times \bar{h})u \tag{4.10}$$

The rate of change of V along the trajectories is

$$\dot{V} = -\dot{h}_z = -(B_{yR}h_x - B_{xR}h_y)u \tag{4.11}$$

With $u = u_h = \eta(\sigma_h)$ as defined in Chapter III, we have

$$\dot{V} = -\sigma_h\eta(\sigma_h) \leq 0 \tag{4.12}$$

Note that $\dot{V} = 0$ corresponds to $\sigma_h = 0$.

In this case, solution of the unforced equations is trivial; with $u = 0$, $\dot{\bar{h}}$ is zero, and the solution is of the form

$$h_x = h_{xo}, \qquad h_y = h_{yo}, \qquad h_z = h_{zo} \tag{4.13}$$

the initial conditions.

It remains only to investigate the circumstances under which σ_h can be zero for solutions of this form. It will be convenient to deal with this problem in terms of the field components in (x_n, y_n, z_n) space. Examining Fig. 2-3, we see that (with $\xi' = 0$ as in Chapter II)

$$\begin{bmatrix} B_{xR} \\ B_{yR} \\ B_{zR} \end{bmatrix} = \begin{bmatrix} \cos\phi\cos\delta & \cos\phi\sin\delta & -\sin\phi \\ -\sin\delta & \cos\delta & 0 \\ \sin\phi\cos\delta & \sin\phi\sin\delta & \cos\phi \end{bmatrix} \begin{bmatrix} B_{xn} \\ B_{yn} \\ B_{zn} \end{bmatrix} \tag{4.14}$$

Then, from (3.2), σ_h can be written

$$\sigma_h = \alpha_1 B_{xn} + \alpha_2 B_{yn} + \alpha_3 B_{zn} \tag{4.15}$$

where

$$\begin{aligned} \alpha_1 &= -h_x \sin\delta - h_y \cos\phi \cos\delta \\ \alpha_2 &= h_x \cos\delta - h_y \cos\phi \sin\delta \\ \alpha_3 &= h_y \sin\phi \end{aligned} \tag{4.16}$$

For solutions of the uncontrolled system α_1, α_2, α_3 are constants.

1. Untilted Dipole

The magnetic field of the untilted dipole is (Appendix A)

$$\begin{bmatrix} B_{xn} \\ B_{yn} \\ B_{zn} \end{bmatrix} = -\frac{M_e}{2r_o^3} \begin{bmatrix} 3 \sin 2\alpha \sin\theta_i \\ (1 - 3\cos 2\alpha)\sin\theta_i \\ -2\cos\theta_i \end{bmatrix} \tag{4.17}$$

where α is the orbit position measured from the ascending line of nodes ($\alpha = \omega_o t + \alpha_o$), θ_i is the inclination of the orbit, r_o is the radius of the orbit and M_e is the magnetic dipole moment of the earth. For this magnetic field model

$$\sigma_h = -\frac{M_e}{2r_o^3}(\alpha_2 \sin\theta_i - 2\alpha_3 \cos\theta_i + 3\alpha_1 \sin\theta_i \sin 2\alpha - 3\alpha_2 \sin\theta_i \cos 2\alpha). \tag{4.18}$$

For the solution of (4.13), σ_h can be identically zero only if the following conditions are simultaneously satisfied:

$$\begin{aligned} \alpha_2 \sin\theta_i - 2\alpha_3 \cos\theta_i &= 0 \\ \alpha_1 \sin\theta_i &= 0 \\ \alpha_2 \sin\theta_i &= 0 \end{aligned} \tag{4.19}$$

or, in matrix form:

$$\begin{bmatrix} 0 & \sin\theta_i & -2\cos\theta_i \\ \sin\theta_i & 0 & 0 \\ 0 & \sin\theta_i & 0 \end{bmatrix} \begin{bmatrix} \alpha_1 \\ \alpha_2 \\ \alpha_3 \end{bmatrix} = \begin{bmatrix} 0 \\ 0 \\ 0 \end{bmatrix} . \qquad (4.20)$$

Since $\alpha_1^2+\alpha_2^2+\alpha_3^2 = h_{xo}^2+h_{yo}^2$, any solution of (4.20) such that $\alpha_1 = \alpha_2 = \alpha_3 = 0$ is the trivial solution. For nontrivial solutions to exist the determinant of the coefficient matrix (which is $-2\cos\theta_i \sin^2\theta_i$) must be zero, which implies that the system must be <u>asymptotically stable in-the-large</u> (ASIL) unless $\theta_i = 0°$ or $\theta_i = 90°$. For $\theta_i = 0$, the existence of a nontrivial solution such that $\dot{V} = 0$ requires only that $\alpha_3 = 0$, a condition which is satisfied whenever $h_y = 0$ (or for any value of h_y if $\phi = 0$). Examining the case $\theta_i = 90°$, we find that it is necessary that $\alpha_1 = \alpha_2 = 0$. This condition is satisfied if $\phi = 90°$ and $h_x = 0$.

It is concluded, therefore, that the system is ASIL unless $\theta_i = 0$ or $\theta_i = 90°$ <u>and</u> $\phi = 90°$. The first case is, of course, that of a vehicle in an equatorial orbit, while the latter corresponds to a vehicle in a polar orbit with the desired spin-axis orientation in the orbit plane.

2. <u>Tilted Dipole</u>

The magnetic field of the tilted dipole is

$$B_{xn} = -\frac{M_e}{2r_o^3}\left[(d_1 - d_3)\sin\mu + 3d_1\sin(2\alpha+\mu) + 3d_3\sin(2\alpha-\mu) + 3d_5\sin 2\alpha\right]$$

$$B_{yn} = -\frac{M_e}{2r_o^3}\left[(d_1 + d_3)\cos\mu - 3d_1\cos(2\alpha+\mu) - 3d_3\cos(2\alpha-\mu) + d_5 - 3d_5\cos 2\alpha\right]$$

$$B_{zn} = -\frac{M_e}{2r_o^3}(d_7 + d_8\cos\mu) \qquad (4.21)$$

where

$$d_1 = \sin \epsilon \sin^2 \frac{1}{2} \theta_i$$

$$d_3 = - \sin \epsilon \cos^2 \frac{1}{2} \theta_i$$

$$d_5 = \cos \epsilon \sin \theta_i$$

$$d_7 = - 2 \cos \epsilon \cos \theta_i$$

$$d_8 = - 2 \sin \epsilon \sin \theta_i$$

and

$$\mu = \alpha_e + \Delta + \beta \qquad (\dot{\mu} = \omega_e)$$

$$\epsilon \approx 11 \text{ deg}$$

$$\Delta \approx 20 \text{ deg} .$$

For this magnetic field model, σ_h along solutions of the uncontrolled equations is somewhat more complex:

$$\sigma_h = - \frac{M_e}{2r_o^3} \left\{ \alpha_1 \left[\sin \epsilon \sin \mu + 3 \sin \epsilon \sin^2 \frac{1}{2} \theta_i \sin (2\alpha + \mu) \right.\right.$$

$$\left. - 3 \sin \epsilon \cos^2 \theta_i \sin (2\alpha - \mu) + 3 \cos \epsilon \sin \theta_i \sin 2\alpha \right]$$

$$+ \alpha_2 \left[- \sin \epsilon \cos \theta_i \cos \mu - 3 \sin \epsilon \sin^2 \frac{1}{2} \theta_i \cos (2\alpha + \mu) \right.$$

$$\left. + 3 \sin \epsilon \cos^2 \theta_i \cos (2\alpha - \mu) + \cos \epsilon \sin \theta_i - 3 \cos \epsilon \sin \theta_i \cos 2\alpha \right]$$

$$\left. + \alpha_3 \left[- 2 \cos \epsilon \cos \theta_i - 2 \sin \epsilon \sin \theta_i \cos \mu \right] \right\} \qquad (4.22)$$

Again we exclude $\alpha_1 = \alpha_2 = \alpha_3 = 0$, since this is the trivial solution, and search for conditions under which σ_h can be zero with the α_i constant but not all equal to zero. The synchronous cases

($\omega_o = \omega_e$, $2\omega_o = \omega_e$) will be omitted for convenience; in any event, the lowest altitude where one of these cases occurs is in excess of 19,000 nautical miles, and at these altitudes the magnetic field dipole models are undoubtedly invalidated by the effects of the solar wind, etc. (Appendix A).

The coefficients in σ_h at the various frequencies can be summarized as follows:

constant:

$$\alpha_2 \cos \epsilon \sin \theta_i - 2\alpha_3 \cos \epsilon \cos \theta_i$$

$2\omega_o$:

$$3\alpha_1 \cos \epsilon \sin \theta_i; \qquad -3\alpha_2 \cos \epsilon \sin \theta_i$$

$2\omega_o + \omega_e$:

$$3\alpha_1 \sin \epsilon \sin^2 \frac{1}{2} \theta_i; \qquad -3\alpha_2 \sin \epsilon \sin^2 \frac{1}{2} \theta_i$$

$2\omega_o - \omega_e$:

$$-3\alpha_1 \sin \epsilon \cos^2 \theta_i; \qquad 3\alpha_2 \sin \epsilon \cos^2 \frac{1}{2} \theta_i$$

ω_e:

$$\alpha_1 \sin \epsilon; \qquad -\alpha_2 \sin \epsilon \cos \theta_i - 2\alpha_3 \sin \epsilon \sin \theta_i$$

where all of these coefficients must be zero if σ_h is to be zero for all time. Examining the coefficients at frequencies $2\omega_o$, $2\omega_o + \omega_e$, and $2\omega_o - \omega_e$, it is readily deduced that $\alpha_1 = \alpha_2 = 0$ for $\sigma_h = 0$. Under these circumstances, examination of the remaining constant and ω_e coefficients shows that α_3 must be zero as well. Thus, σ_h can be zero only for the trivial solution of the uncontrolled equations. We conclude that the system is ASIL for all values of ϕ, δ, and θ_i.

C. STABILITY OF THE EXACT MODEL

As might be suspected, demonstration of stability for the exact equations of motion is more involved. With $\Omega_x = \Omega_y = \Omega_z = 0$ the exact equations of motion are, from Chapter II:

$$
\begin{aligned}
\dot{\omega}_x &= -k\omega_s\omega_y - (1+k)\omega_s B_{yb} u \\
\dot{\omega}_y &= k\omega_s\omega_x + (1+k)\omega_s B_{xb} u \\
\dot{a}_{13} &= a_{23}\omega_s - a_{33}\omega_y \\
\dot{a}_{23} &= a_{33}\omega_x - a_{13}\omega_s \\
\dot{a}_{33} &= a_{13}\omega_y - a_{23}\omega_x \\
\dot{a}_{12} &= a_{22}\omega_s - a_{32}\omega_y \\
\dot{a}_{22} &= a_{32}\omega_x - a_{12}\omega_s \\
\dot{a}_{32} &= a_{12}\omega_y - a_{22}\omega_x \\
\dot{a}_{11} &= a_{21}\omega_s - a_{31}\omega_y \\
\dot{a}_{21} &= a_{31}\omega_x - a_{11}\omega_s \\
\dot{a}_{31} &= a_{11}\omega_y - a_{21}\omega_x
\end{aligned}
\tag{4.23}
$$

The control is

$$u = \eta(\sigma) \tag{4.24}$$

where

$$\sigma = B_{xb}(a_{23} - K_R\omega_y) - B_{yb}(a_{13} - K_R\omega_x)$$

The desired steady state is $a_{33} = 1$ and $\omega_x = \omega_y = 0$. With this condition $a_{31} = a_{32} = a_{13} = a_{32} = 0$. It is natural to consider as a state vector in this case

$$\bar{x} = \begin{bmatrix} \omega_x \\ \omega_y \\ a_{13} \\ a_{23} \\ 1-a_{33} \end{bmatrix} \tag{4.25}$$

because these variables are sufficient to describe the desired equilibrium and the control. Furthermore, with this state vector only the first five differential equations of (4.23) need be considered explicitly.

The Lyapunov function to be tested is

$$V = \frac{1}{2}\left\{(a_{13} - K_R\omega_x)^2 + (a_{23} - K_R\omega_y)^2 + [K_R(1+k)\omega_s - 1](a_{13}^2 + a_{23}^2) + K_R(1+k)\omega_s(1-a_{33})^2\right\} \tag{4.26}$$

For $u = \eta(\sigma)$:

$$\dot{V} = -K_R(1+k)\omega_s\sigma\eta(\sigma) \ . \tag{4.27}$$

This Lyapunov function is positive definite if and only if $K_R > 1/(1+k)\omega_s$. Thus, if we can show that there are no nontrivial solutions such that $\dot{V}(\bar{x}, t) = 0$ for all time, the amount of rate gain required for asymptotic stability will be established because, letting $W = -V$ in the instability theorem, all necessary conditions for instability will be satisfied for $K_R < 1/(1+k)\omega_s$. Of course, for K_R equal to this critical value, the system will be stable but not asymptotically stable. As an infinitely small upper bound for both V and W consider the function $U(x)$ given by replacing the coefficient $K_R(1+k)\omega_s - 1$ in V by its absolute value.

As before, the uncontrolled system equations must be solved as the next step. It is necessary to solve the complete set of eleven equations because the expression of B_{xb} and B_{yb} in terms of ϕ, δ, B_{xn}, B_{yn}, and B_{zn} requires knowledge of a_{11}, a_{12}, a_{21}, and a_{22} as well as a_{13} and a_{23}.

Define Euler angles θ', ψ', and ϕ' as in Fig. 4-1. Solution

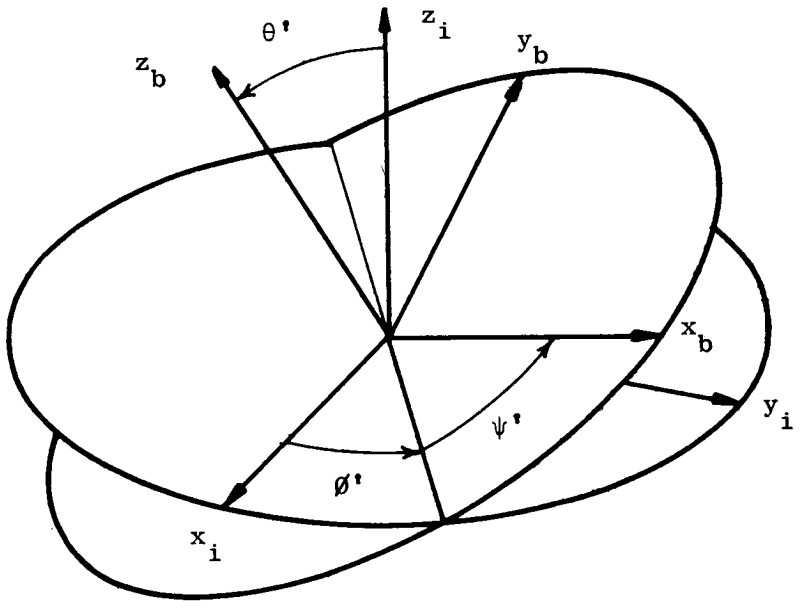

FIG. 4-1. DEFINITION OF THE EULER ANGLES ϕ', θ' AND ψ'.

for the variation of θ', ψ', ϕ', ω_x, and ω_y under torque-free conditions is a classical problem (see, for example, Ref. 4-5). The general solution is:

$$\begin{aligned} \omega_x &= -\, a \sin (k\omega_s t - \psi_o') \\ \omega_y &= \quad a \cos (k\omega_s t - \psi_o') \\ \theta' &= \quad \theta_o' \\ \psi' &= -\, k\omega_s t + \psi_o' \\ \phi' &= \quad \omega t + \phi_o' \end{aligned} \tag{4.28}$$

where

$$a = \sqrt{\omega_{xo}^2 + \omega_{yo}^2}$$

$$\omega = \frac{a}{\sqrt{1 - (H_s/H)^2}} = \sqrt{a^2 + (1 + k)^2\omega_s^2} \tag{4.29}$$

$$H^2 = I_x^2(\omega_x^2 + \omega_y^2) + H_s^2$$

From these results, the time variation of the a_{ij}'s can be determined. For convenience, define

$$X_b = \begin{bmatrix} \bar{e}_{xb} \\ \bar{e}_{yb} \\ \bar{e}_{zb} \end{bmatrix}, \text{ etc.} \tag{4.30}$$

Then expression (2.3) can be written

$$X_b = AX_R \tag{4.31}$$

and

$$X_i = BX_R \tag{4.32}$$

where (x_i, y_i, z_i) is an inertial coordinate frame (Fig. 4-1) defined so that $\bar{e}_{zi}$ corresponds to the direction of the total angular momentum vector. The matrix B is constant. Continuing, we define a matrix D by

$$X_b = DX_i \tag{4.33}$$

where the elements of D can be derived by examination of Fig. 4-1. Then

$$A = DB \ . \tag{4.34}$$

Furthermore:

$$A(0) = D(0)B \tag{4.35}$$

so that

$$B = D^{T}(0)A(0)$$

Hence

$$A(t) = [D(t)D^{T}(0)]\ A(0) = G(t)A(0) \tag{4.36}$$

Letting, for example, the notation $\tilde{\tilde{X}}_{\theta'}$ denote a rotation about an x axis through an angle θ':

$$D = \tilde{\tilde{Z}}_{\psi'}, \tilde{\tilde{X}}_{\theta'}, \tilde{\tilde{Z}}_{\phi'} \ . \tag{4.37}$$

Then

$$G(t) = \tilde{\tilde{Z}}_{\psi'}, \tilde{\tilde{X}}_{\theta'}, \tilde{\tilde{Z}}_{(\phi'-\phi'_o)} \tilde{\tilde{X}}^{T}_{\theta'_o}, \tilde{\tilde{Z}}^{T}_{\psi'_o} \tag{4.38}$$

and, choosing $\phi'_o = 0$ (thus specifying the x_i and y_i axes):

$$A(t) = D(t)\left[\tilde{\tilde{X}}^{T}_{\theta'_o}, \tilde{\tilde{Z}}^{T}_{\psi'_o}, A(0)\right] \tag{4.39}$$

Denote the term of (4.39) in brackets as S°, a constant orthogonal matrix which can be chosen arbitrarily to give arbitrary initial conditions. $A(0)$ gives the initial attitude error, and the terms concerning θ'_o and ψ'_o give the initial location of the total momentum vector in vehicle coordinates. Notice that since $H_{zb} = H \cos \theta' = H_s$, θ' as defined here is always in the range $[0, 90^{\circ})$ and is never, it is important to note, equal to 90°.

Then, in summary:

$$A(t) = D(t)S^{\circ} \tag{4.40}$$

where

$$d_{11} = \cos^2 \frac{1}{2} \theta_o' \cos (\psi' + \phi') + \sin^2 \frac{1}{2} \theta_o' \cos (\psi' - \phi')$$

$$d_{12} = \cos^2 \frac{1}{2} \theta_o' \sin (\psi' + \phi') - \sin^2 \frac{1}{2} \theta_o' \sin (\psi' - \phi')$$

$$d_{13} = \sin \theta_o' \sin \psi'$$

$$d_{21} = -\cos^2 \frac{1}{2} \theta_o' \sin (\psi' + \phi') - \sin^2 \frac{1}{2} \theta_o' \sin (\psi' - \phi')$$

$$d_{22} = \cos^2 \frac{1}{2} \theta_o' \cos (\psi' + \phi') - \sin^2 \frac{1}{2} \theta_o' \cos (\psi' - \phi')$$

$$d_{23} = \sin \theta_o' \cos \psi'$$

$$d_{31} = \sin \theta_o' \sin \phi'$$

$$d_{32} = -\sin \theta_o' \cos \phi'$$

$$d_{33} = \cos \theta_o'$$

and

$$\psi'(t) = -k\omega_s t + \psi_o'$$

$$\phi'(t) = \sqrt{a^2 + (1 + k)^2 \omega_s^2}\, t$$

$$\theta_o' = \cos^{-1} (H_s/H)$$

$$\omega_x = a \sin \psi'$$

$$\omega_y = a \cos \psi'$$

$$H_{xb}(0) = H \sin \theta_o' \sin \psi_o'$$

$$H_{yb}(0) = H \sin \theta_o' \cos \psi_o' .$$

As an additional preliminary step, σ can be expressed in terms of B_{xn}, B_{yn}, B_{zn}, ϕ, δ, a_{31}, a_{32}, $\dot{a}_{31}$, $\dot{a}_{32}$, and $\dot{a}_{33}$. First, using the direction cosine relationships presented in Chapter II, it can be shown that

$$\sigma = B_{yR}a_{31} - B_{xR}a_{32} - K_R(B_{xR}\dot{a}_{31} + B_{yR}\dot{a}_{32} + B_{zR}\dot{a}_{33}). \tag{4.41}$$

Then, using the transformation (4.14):

$$\begin{aligned}\sigma = {} & B_{xn}[v_{21}a_{31} - v_{11}a_{32} - K_R(v_{11}\dot{a}_{31} + v_{21}\dot{a}_{32} + v_{31}\dot{a}_{33})] \\ & + B_{yn}[v_{22}a_{31} - v_{12}a_{32} - K_R(v_{12}\dot{a}_{31} + v_{22}\dot{a}_{32} + v_{32}\dot{a}_{33})] \\ & + B_{zn}[v_{23}a_{31} - v_{13}a_{32} - K_R(v_{13}\dot{a}_{31} + v_{23}\dot{a}_{32} + v_{33}\dot{a}_{33})]\end{aligned} \tag{4.42}$$

where

$$\begin{bmatrix} v_{11} & v_{12} & v_{13} \\ v_{21} & v_{22} & v_{23} \\ v_{31} & v_{32} & v_{33} \end{bmatrix} = \begin{bmatrix} \cos\phi\cos\delta & \cos\phi\sin\delta & -\sin\phi \\ -\sin\delta & \cos\delta & 0 \\ \sin\phi\cos\delta & \sin\phi\sin\delta & \cos\phi \end{bmatrix}.$$

Utilizing the result (4.40) we can write an expression for σ along a general uncontrolled solution.

$$\begin{aligned}\sigma = {} & B_{xn}(p_{11}\sin\phi' + p_{12}\cos\phi' + p_{13}) \\ & + B_{yn}(p_{21}\sin\phi' + p_{22}\cos\phi' + p_{23}) \\ & + B_{zn}(p_{31}\sin\phi' + p_{32}\cos\phi' + p_{33})\end{aligned} \tag{4.43}$$

where

$$p_{11} = (v_{21}s_{11} - v_{11}s_{12}) \sin \theta_o' - K_R a(v_{11}s_{21} + v_{21}s_{22} + v_{31}s_{23})$$

$$p_{12} = (v_{11}s_{22} - v_{21}s_{21}) \sin \theta_o' - K_R a(v_{11}s_{11} + v_{21}s_{12} + v_{31}s_{13})$$

$$p_{13} = (v_{21}s_{31} - v_{11}s_{32}) \cos \theta_o'$$

$$p_{21} = (v_{22}s_{11} - v_{12}s_{12}) \sin \theta_o' - K_R a(v_{12}s_{21} + v_{22}s_{22} + v_{32}s_{23})$$

$$p_{22} = (v_{12}s_{22} - v_{22}s_{21}) \sin \theta_o' - K_R a(v_{12}s_{11} + v_{22}s_{12} + v_{32}s_{13})$$

$$p_{23} = (v_{22}s_{31} - v_{12}s_{32}) \cos \theta_o'$$

$$p_{31} = (v_{23}s_{11} - v_{13}s_{12}) \sin \theta_o' - K_R a(v_{13}s_{21} + v_{23}s_{22} + v_{33}s_{23})$$

$$p_{32} = (v_{13}s_{22} - v_{23}s_{21}) \sin \theta_o' - K_R a(v_{13}s_{11} + v_{23}s_{12} + v_{33}s_{13})$$

$$p_{33} = (v_{23}s_{31} - v_{13}s_{32}) \cos \theta_o' \qquad \{v_{23} \equiv 0\}$$

It is convenient that, because it can be expressed in terms of a_{31}, a_{32}, $\dot{a}_{32}$, and $\dot{a}_{33}$, σ along the unforced solution is independent of the variable ψ'.

As before, we will examine the existence of nontrivial solutions such that σ is zero for all time. One requirement of the trivial solution is that $a = 0$ so that $\omega_x = \omega_y = 0$ for all t. The other requirement is that $a_{33} = 1$ for all time. From (4.40)

$$a_{33} = d_{31}s_{13} + d_{32}s_{23} + d_{33}s_{33}$$

and, with $a = 0$, $\sin \theta_o' = 0$ and $\cos \theta_o' = 1$. Under these circumstances

$$a_{33} = s_{33} .$$

Therefore, the equilibrium will be completely specified by

$$a = 0, \qquad s_{33} = 1 \tag{4.44}$$

and because S° is an orthogonal matrix

$$s_{13} = s_{23} = s_{31} = s_{32} = 0 \tag{4.45}$$

at the equilibrium.

It is clear from (4.43), (4.44), and (4.45), that the equilibrium solution implies that all p_{ij} are equal to zero. But, does the nullity of all p_{ij} imply that the conditions of (4.44) and (4.45) must be satisfied; that is to say, are all p_{ij} equal to zero only for the trivial solution? The answer is yes, for those values of K_R which are of interest, as shown by the following argument.

It will be convenient to consider three new functions:

$$\begin{aligned} F_1 &= p_{11}^2 + p_{21}^2 + p_{31}^2 \\ F_2 &= p_{12}^2 + p_{22}^2 + p_{32}^2 \\ F_3 &= p_{13}^2 + p_{23}^2 + p_{33}^2 \,. \end{aligned} \tag{4.46}$$

Expansion using (4.43) and application of the identities of (2.15)--which apply to any orthogonal transformation matrix--to the matrix S° yields:

$$\begin{aligned} F_1 &= [(1 - s_{13}^2) - 2K_R\omega s_{33} + K_R^2\omega^2] \sin^2 \theta_o' \\ F_2 &= [(1 - s_{23}^2) - 2K_R\omega s_{33} + K_R^2\omega^2] \sin^2 \theta_o' \\ F_3 &= (1 - s_{33}^2) \cos^2 \theta_o' \end{aligned} \tag{4.47}$$

where

$$a = \omega \sin \theta_o' \ . \tag{4.48}$$

Now, if all p_{ij} are zero, then $F_1 = F_2 = F_3 = 0$. $F_3 = 0$ implies that $s_{33} = +1$ (the case $s_{33} = -1$ relates to the unstable equilibrium, and will be omitted, as discussed in Sec. A of this chapter), because $0 \leq \theta_o' < 90°$ as noted in the discussion following expression (4.39). Thus if all $p_{ij} = 0$, $s_{33} = 1$ and it remains only to show that a (or equivalently θ_o') is equal to zero. For $s_{33} = 1$, $F_1 = F_2 = 0$ implies either

(i) $\sin \theta_o' = 0$

or

(ii) $K_R\omega - 1 = 0$.

Under what circumstances can the latter condition hold? This condition can be put in the form:

$$\text{(ii)}' \quad K_R = \frac{1}{\sqrt{a^2 + (1 + k)^2\omega_s^2}} \tag{4.49}$$

Consider two cases. First, if K_R is greater than its critical value

$$K_R > \frac{1}{(1 + k)\omega_s} \geq \frac{1}{\sqrt{a^2 + (1 + k)^2\omega_s^2}} \tag{4.50}$$

Therefore, (ii) cannot be satisfied so that $\sin \theta_o' = 0$ as required for the equilibrium. Second, consider K_R less than its critical value. For satisfaction of (4.49)

$$\frac{1}{\sqrt{a^2 + (1 + k)^2\omega_s^2}} = K_R < \frac{1}{(1 + k)\omega_s} \tag{4.51}$$

and the equality will hold for some positive (nonzero) value of a. At first glance, this would appear to negate the possibility of showing instability of the origin. But this is not the case. If we restrict our attention (for proof of instability) to a region, $\mathcal{R}_\Sigma$, of the origin defined by $\|\bar{x}\| < a_o$, where a_o is the value of a satisfying the equality of (4.51) for the particular value of K_R in question, we have shown that within this region, no nontrivial solutions exist such that $\dot{V}$ is equal to zero for all time. There is, of course, no need to consider the entire state space to demonstrate instability of the origin.

To summarize, if we can show that expression (4.43) being zero for all time requires that all p_{ij} are equal to zero, we can conclude that the origin is asymptotically stable in-the-large for $K_R > 1/(1+k)\omega_s$ and that the origin is unstable for $K_R < 1/(1+k)\omega_s$.

1. Untilted Dipole

The untilted dipole model of the earth's magnetic field is given in (4.17). Expanding σ as in (4.43):

$$\sigma = -\frac{M_e}{2r_o^3}\{p_{23}\sin\theta_i - 2p_{33}\cos\theta_i + (3p_{13}\sin\theta_i)\sin 2\alpha$$

$$- (3p_{23}\sin\theta_i)\cos 2\alpha + (p_{21}\sin\theta_i - 2p_{31}\cos\theta_i)\sin \emptyset'$$

$$+ (p_{22}\sin\theta_i - 2p_{32}\cos\theta_i)\cos \emptyset'$$

$$+ \frac{3}{2}[(p_{11} - p_{22})\cos(\emptyset' - 2\alpha) - (p_{11} + p_{22})\cos(\emptyset' + 2\alpha)$$

$$- (p_{12} + p_{21})\sin(\emptyset' - 2\alpha)$$

$$+ (p_{12} - p_{21})\sin(\emptyset' + 2\alpha)]\sin\theta_i\} \qquad (4.52)$$

where $\dot{\emptyset}' = \omega = \sqrt{a^2 + (1+k)^2\omega_s^2} \geq (1+k)\omega_s$, and $\dot{\alpha} = \omega_o$. For spin-stabilized vehicles the spin speed is typically two or more orders of

magnitude greater than the orbit rate. Thus, if σ is to be zero for all t, each of the coefficients of (4.52) must be zero. These coefficients are:

constant:

$$p_{23} \sin \theta_i - 2p_{33} \cos \theta_i$$

$2\omega_o$:

$$p_{13} \sin \theta_i; \qquad p_{23} \sin \theta_i$$

ω:

$$p_{21} \sin \theta_i - 2p_{31} \cos \theta_i; \qquad p_{22} \sin \theta_i - 2p_{32} \cos \theta_i$$

$\omega - 2\omega_o$:

$$(p_{11} - p_{22}) \sin \theta_i; \qquad (p_{12} + p_{21}) \sin \theta_i$$

$\omega + 2\omega_o$:

$$(p_{11} + p_{22}) \sin \theta_i; \qquad (p_{12} - p_{21}) \sin \theta_i$$

Consider first the case $0 < \theta_i < 90°$ so that $\sin \theta_i$ and $\cos \theta_i$ are nonzero. It is trivial to show that all p_{ij} are zero and that the conclusion of ASIL for $K_R > 1/(1+k)\omega_s$ and instability for $K_R < 1/(1+k)\omega_s$ follows.

The remaining two cases are more involved; for $\theta_i = 0$, sufficient conditions for σ to be zero for all t are $p_{31} = p_{32} = p_{33} = 0$. From (4.43) we see that these conditions can be satisfied by choosing $a = 0$ (hence $\theta_o' = 0$) and, to make $p_{33} = 0$, either $v_{13} = 0$ (which will occur if $\emptyset$ is zero) or, more generally, $s_{32} = 0$. This does not constrain s_{33} to be unity so that for $\theta_i = 0$, the system is not asymptotically stable. Therefore, the vehicle can come to rest with $\omega_x = \omega_y = 0$ (no wobble), $a_{32} = 0$ and a_{31}, a_{33} constant. This corresponds to the spin axis being fixed in the reference coordinate frame with a steady attitude error.

If $\theta_i = 90°$, σ will be zero for all time if $p_{11} = p_{12} = p_{13} = p_{21} = p_{22} = p_{23} = 0$ with no restriction upon p_{31}, p_{32}, and p_{33}. Since $\cos \theta_o' \neq 0$, $p_{13} = p_{23} = 0$ implies:

$$\begin{bmatrix} v_{21} & -v_{11} \\ v_{22} & -v_{12} \end{bmatrix} \begin{bmatrix} s_{31} \\ s_{32} \end{bmatrix} = \begin{bmatrix} 0 \\ 0 \end{bmatrix} \tag{4.53}$$

This will be satisfied if:

(i) $v_{11}v_{22} - v_{12}v_{21} \neq 0$, $s_{31} = s_{32} = 0$

(ii) $v_{11}v_{22} - v_{12}v_{21} = 0$, s_{31} and s_{32} must be determined.

Assume that condition (i) holds; then the only question is whether θ_o' (and a) can be nonzero. Define two new functions

$$G_1 = p_{11}^2 + p_{12}^2 + p_{13}^2$$

$$G_2 = p_{21}^2 + p_{22}^2 + p_{23}^2 \tag{4.54}$$

Each of these functions is zero for $\theta_i = 90°$ and $\sigma = 0$. Expanding these functions with $s_{31} = s_{32} = s_{13} = s_{23} = 1 - s_{33} = 0$, they become

$$G_1 = (\sin \theta_o' - K_R a)^2 (v_{11}^2 + v_{21}^2)$$

$$G_2 = (\sin \theta_o' - K_R a)^2 (v_{12}^2 + v_{22}^2) \tag{4.55}$$

Thus either

$$v_{11} = v_{12} = v_{21} = v_{22} = 0 \tag{4.56}$$

or $a = \omega \sin \theta_o' = 0$. But (4.56) violates the assumed condition (i) above, so $\sigma = 0$ with $\theta_i = 90°$ and condition (i) requires the trivial solution and the system is ASIL. If condition (ii) pertains, $\emptyset$ must

be 90°, from the definition of the v_{ij} following expression (4.42). This immediately yields $v_{11} = v_{12} = v_{23} = v_{33} = 0$, $v_{13} = -1$, $v_{21} = -\sin\delta$, $v_{22} = \cos\delta$, $v_{31} = \cos\delta$, $v_{32} = \sin\delta$. Then (4.53) requires

$$-s_{31}\sin\delta = 0$$
$$s_{31}\cos\delta = 0 \qquad (4.57)$$

and $s_{31} = 0$ with s_{32} arbitrary will satisfy (4.57). Note that if we assume $a = \omega \sin\theta_o' = 0$, $s_{31} = 0$, and the v_{ij} values above, we have, from (4.43),

$$p_{11} = p_{12} = p_{21} = p_{22} = p_{31} = p_{32} = 0$$

by $a = 0$, and

$$p_{13} = p_{23} = 0$$

from $v_{11} = v_{12} = s_{31} = 0$. This satisfies the necessary conditions for $\sigma = 0$ for all time (with $\theta_i = 90°$) for a solution which is not the equilibrium solution; that is, the solution $\omega_x = \omega_y = 0$, $s_{31} = 0$, s_{32} arbitrary and $s_{33}^2 = 1 - s_{32}^2$.*

It is concluded that, as in the case of the simplified equations of motion with the untilted dipole magnetic field model, the system is ASIL (if $K_R > 1/(1+k)\omega_s$) unless $\theta_i = 0°$ or $\theta_i = 90°$ and $\phi = 90°$. If K_R is less than the critical value, we replace "ASIL" by "unstable" in the above statement.

---

* This corresponds to the vehicle spinning without wobble with $a_{31} = 0$ and a_{23}, a_{33} arbitrary and constant. Thus, the spin axis is fixed in (x_R, y_R, z_R) coordinates with a steady attitude error.

2. Tilted Dipole

The magnetic model of the tilted dipole is given in (4.21). With this model, σ, along unforced solutions of the system, becomes

$$\sigma = -\frac{M_e}{2r_o^3}\{p_{23}d_5 + p_{33}d_7 + p_{13}(d_1 - d_3)\sin\mu + [p_{23}(d_1 + d_3) + p_{33}d_8]\cos\mu$$

$$+ 3p_{13}d_1 \sin(2\alpha + \mu) + 3p_{13}d_3 \sin(2\alpha - \mu) + 3p_{13}d_5 \sin 2\alpha$$

$$- 3p_{23}d_1 \cos(2\alpha + \mu) - 3p_{23}d_3 \cos(2\alpha - \mu) - 3p_{23}d_5 \cos 2\alpha$$

$$+ (p_{21}d_5 + p_{31}d_7)\sin\phi' + (p_{22}d_5 + p_{32}d_7)\cos\phi'$$

$$+ \frac{1}{2}[p_{11}(d_1 - d_3) + p_{22}(d_1 + d_3) + p_{32}d_8]\cos(\mu - \phi')$$

$$- \frac{1}{2}[p_{11}(d_1 - d_3) - p_{22}(d_1 + d_3) - p_{32}d_8]\cos(\mu + \phi')$$

$$+ \frac{1}{2}[p_{12}(d_1 - d_3) + p_{21}(d_1 + d_3) + p_{31}d_8]\sin(\mu + \phi')$$

$$+ \frac{1}{2}[p_{12}(d_1 - d_3) - p_{21}(d_1 + d_3) - p_{31}d_8]\sin(\mu - \phi')$$

$$+ \frac{3}{2}(p_{11} + p_{22})d_1 \cos(2\alpha + \mu - \phi') - \frac{3}{2}(p_{11} - p_{22})d_1 \cos(2\alpha + \mu + \phi')$$

$$+ \frac{3}{2}(p_{12} - p_{21})d_1 \sin(2\alpha + \mu + \phi') + \frac{3}{2}(p_{12} + p_{21})d_1 \sin(2\alpha + \mu - \phi')$$

$$+ \frac{3}{2}(p_{11} - p_{22})d_3 \cos(2\alpha - \mu - \phi') - \frac{3}{2}(p_{11} + p_{22})d_3 \cos(2\alpha - \mu + \phi')$$

$$+ \frac{3}{2}(p_{12} - p_{21})d_3 \sin(2\alpha - \mu + \phi') + \frac{3}{2}(p_{12} + p_{21})d_3 \sin(2\alpha - \mu - \phi')$$

$$+ \frac{3}{2}(p_{11} - p_{22})d_5 \cos(2\alpha - \phi') - \frac{3}{2}(p_{11} + p_{22})d_5 \cos(2\alpha + \phi')$$

$$+ \frac{3}{2}(p_{12} - p_{21})d_5 \sin(2\alpha + \phi') + \frac{3}{2}(p_{12} + p_{21})d_5 \sin(2\alpha - \phi')\}. \quad (4.58)$$

With the assumption of a nonsynchronous orbit ($\omega_o > \omega_e$) and $\omega_s \gg \omega_o$, this yields 27 conditions to be satisfied by the nine p_{ij} coefficients so that $\sigma = 0$ for all time. It can be shown that simultaneous satisfaction of these 27 conditions requires that each p_{ij} is zero, so that the system is asymptotically stable in-the-large for all θ_i, ϕ and δ, if $K_R > 1/(1+k)\omega_s$. If K_R is less than this critical value, the system is unstable. This conclusion, as mentioned in Sec. A of this chapter, applies rigorously only for orbits such that ω_o/ω_e is a rational number.

D. SUMMARY OF STABILITY RESULTS

In the most realistic case considered, that of the tilted dipole magnetic field model, in-the-large asymptotic stability has been demonstrated, for $K_R > 1/(1+k)\omega_s$, in orbits such that ω_o/ω_e is rational, with any value of θ_i, ϕ and δ. Thus, this system has been shown to be capable of effecting acquisition for arbitrarily large initial attitude errors (up to 180 deg) and arbitrarily large initial transverse angular velocities. Moreover, the relationship $K_R > 1/(1+k)\omega_s$ has been shown to be both necessary and sufficient for asymptotic stability in-the-large. The stability properties of this nonlinear, time-varying system have been completely determined.

By demonstrating ASIL for this particular control law, the theoretical feasibility of magnetic control of any axially symmetric satellite in any circular earth orbit (rigorously, ω_o/ω_e must be rational), with any desired spin-axis direction, has been demonstrated. There is no assurance from this stability analysis that the system will be practically feasible; e.g., convergence times for reasonable torquing coils may be on the order of weeks. As will be demonstrated, this system is, in fact, useful in a significant number of applications.

This stability analysis has been performed for a very general control function (Fig. 3-1); the basic limitations are $\eta(\sigma)$ continuous (imposed by continuity of the $f_i(\bar{x}, t)$ as required by the stability theorems), $\eta(0) = 0$ and $\sigma\eta(\sigma) > 0$ for $\sigma \neq 0$. This explicitly excludes the signum function. This limitation poses no difficulty because the signum function can be approached arbitrarily closely by a continuous function.

Moreover, since a current is being controlled, rather than the rate of mass expulsion, there is no physical reason to exclude proportional control $[\eta(\sigma) = K\sigma]$, or saturating proportional control, or any other control characteristic which is found to be desirable. It may, in fact, be desirable to exclude signum control to avoid the possibility of chatter.

The major limitations of this stability analysis are the assumptions of a circular orbit and a dipole magnetic field model. However, even without these constraints the Lyapunov function developed here is sufficient to demonstrate stability (since $\dot{V} \leq 0$ regardless of the variation of B_{xR} and B_{yR}). We can conjecture (with some confidence) that asymptotic stability in-the-large exists for elliptical orbits and the exact environmental magnetic field. The obvious cases where asymptotic stability will not occur are those in which either B_{xR} or B_{yR} is zero for all time (e.g., the untilted dipole model with $\theta_i = 0$, or $\theta_i = \emptyset = 90°$, as shown above), or where $B_{xR}(t) = C_1 B_{yR}(t)$ with C_1 a constant. In either instance, considering the simplified equations of motion, σ_h can remain zero for constant values of h_x and h_y, with at least one of these variables nonzero. It is, of course, extremely unlikely that the environmental magnetic field will, for any mission, satisfy either of these conditions.

V. ESTIMATES OF SYSTEM RESPONSE

In this chapter expressions are derived which, while not giving an exact determination of system response, will yield estimates which are very useful for design purposes. The basis of these estimates is the averaging of the periodic coefficients in the differential equations over a period and thus deriving equations which are, heuristically, differential equations of the average motion. These estimates, unsupported, would be doubtful; however, the estimates derived in this study have been judiciously spot checked by numerical integration of the equations of motion and found to have sufficient accuracy for design purposes. Using these results, it is possible to determine quantitatively the effect of various parameters (e.g., θ_i, ϕ, δ, K_R) upon system performance.

Figure 5-1 is a comparison of the response of the exact model with that of the simplified model for a typical case with proportional control (i.e., $u = K\sigma$, where K is the gain) and an initial pointing error of 135 deg. The solid curves indicate the response of the simplified model while the circles and crosses are sample points from the response of the exact model for two damping levels. All three runs exhibit the same position response initially; however, as time passes, the transverse angular velocities are excited and the c_{3j} begin to show the presence of terms near spin frequency. With low damping ($K_R = 10$) the difference between the models is apparent, indicating that the transverse angular velocities were damped quite slowly; increasing K_R by a factor of five results, for practical purposes, in equivalence of the models. The increase in damping maintains ω_1 and ω_2 at much lower levels and, in view of the structural similarity between the simplified and exact momentum equations (Chapter II), the above results are to be expected.

The data from the above and other computer runs indicates that, with K_R sufficiently large, the solutions h_x, h_y, and h_z of the simplified equations give a good approximation of, respectively, c_{31}, c_{32}, and c_{33}, the attitude variables of the exact equations of motion, at least for large attitude errors. It is reasonable, in order to develop approximate relationships between the system parameters and the response

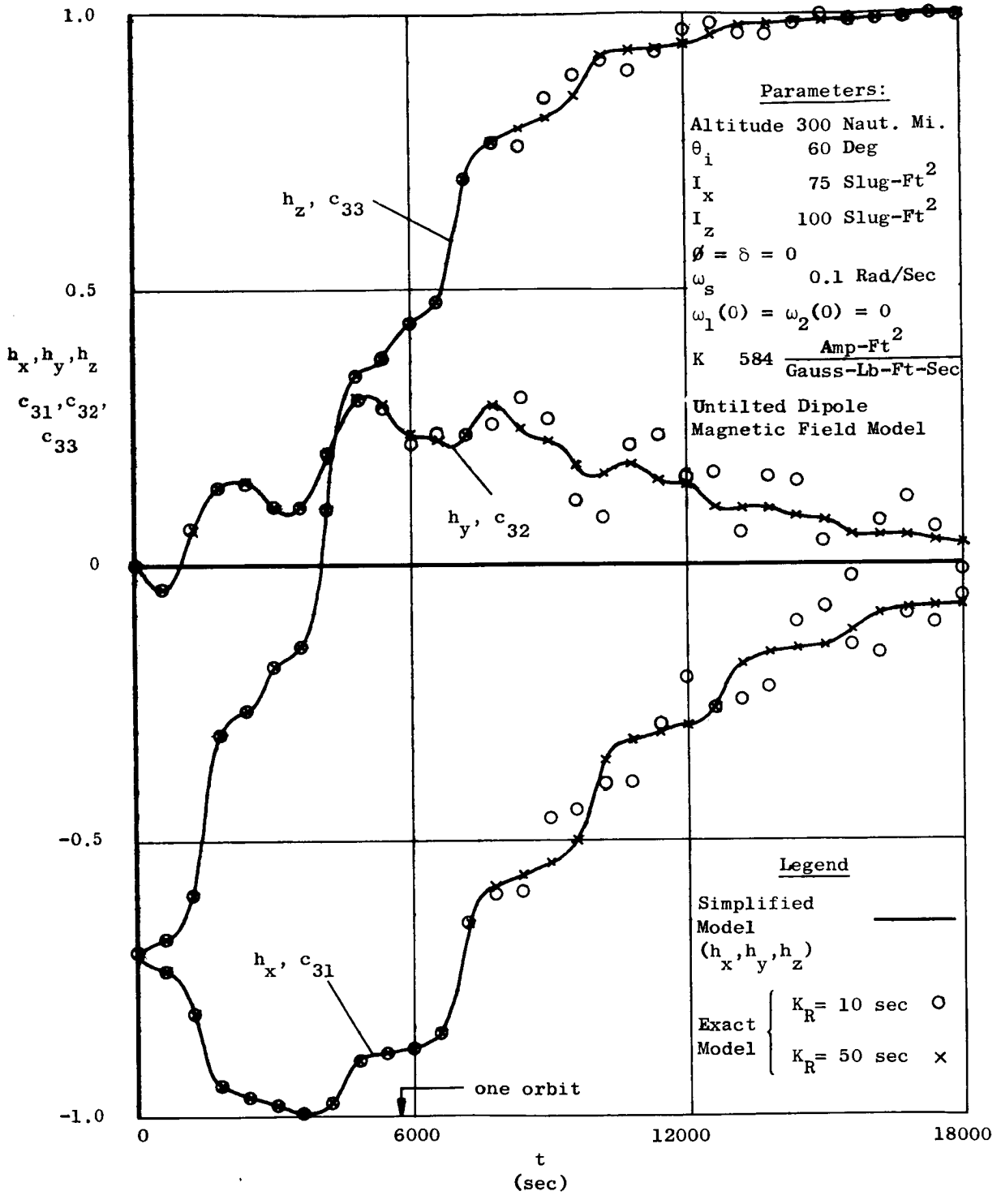

FIG. 5-1. RESPONSE COMPARISON WITH PROPORTIONAL CONTROL AND ZERO INITIAL TRANSVERSE ANGULAR VELOCITIES.

of the (exact) system, to assume that there is "sufficient damping" and deal with the simplified model in estimating system performance for large errors. On the other hand, in estimating small-error performance, the exact equations will be linearized.

Intuitively, a signum control of coil current will be preferred for rapid convergence; this conclusion will be given support by the optimal control investigations of the simplified model presented in the next chapter. However, to avoid chatter near the origin, $\eta(\sigma)$ will be assumed to have a small linear region for σ near zero, as shown in Fig. 5-2. Thus, for the large-error performance estimate a signum control will be used, with the assumption that the saturation level, σ_s,

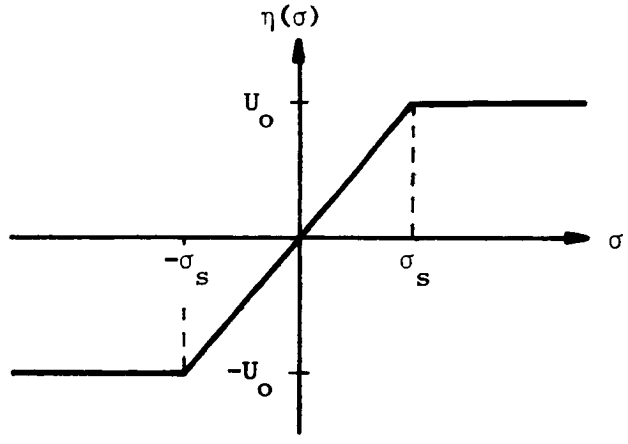

FIG. 5-2. THE SATURATING-PROPORTIONAL CONTROL FUNCTION.

is small enough that the current is essentially full on at all times. On the other hand, the small-error performance estimate will assume a linear control; i.e., that $\sigma < \sigma_s$ at all times. Clearly there is an intermediate region where neither approximation is valid, but this transition case will be neglected.

This chapter, it should be noted, is restricted to the case when the reference coordinates are inertial and there are no disturbance torques. The effect of certain of these disturbances will be discussed in a later

chapter. Furthermore, for simplicity, the untilted dipole magnetic field model is employed for all performance estimates.*

A. LARGE-ERROR PERFORMANCE ESTIMATE

The simplified equations of motion are:

$$\begin{aligned} \dot{h}_x &= (B_{zR}h_y - B_{yR}h_z)u \\ \dot{h}_y &= (B_{xR}h_z - B_{zR}h_x)u \\ \dot{h}_z &= (B_{yR}h_x - B_{xR}h_y)u \ . \end{aligned} \tag{5.1}$$

It will be convenient to define the position of $\bar{h}$ in polar form as in Fig. 5-3. In terms of these polar variables the normalized momentum

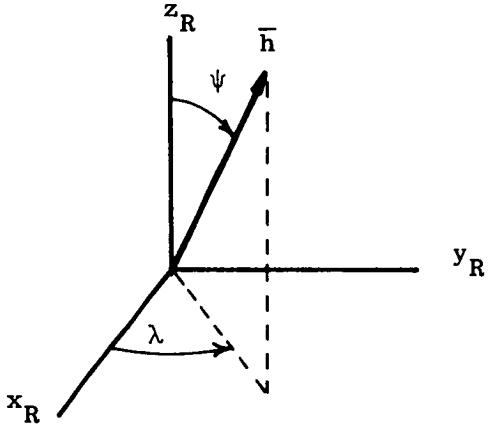

FIG. 5-3. POLAR ATTITUDE VARIABLES.

components are:**

---

* Appendix A includes a discussion of the effect of using the untilted (rather than the tilted) dipole model.

** ψ is restricted to the range $[0,\pi]$; the azmuthal angle λ is unrestricted.

$$h_x = \sin\psi \cos\lambda$$

$$h_y = \sin\psi \sin\lambda \tag{5.2}$$

$$h_z = \cos\psi \ .$$

The equations of motion in terms of ψ and λ are

$$\boxed{\begin{aligned} \dot{\psi} &= -(B_{yR} \cos\lambda - B_{xR} \sin\lambda)u \\ \dot{\lambda} \sin\psi &= [(B_{yR} \sin\lambda + B_{xR} \cos\lambda) \cos\psi - B_{zR} \sin\psi]u \end{aligned}} \tag{5.3}$$

Let

$$u = U_o \ \text{sgn}\ \sigma_h = U_o \ \text{sgn}\ (B_{yR} \cos\lambda - B_{xR} \sin\lambda) \tag{5.4}$$

With this control

$$\dot{\psi} = - U_o |B_{yR} \cos\lambda - B_{xR} \sin\lambda| \tag{5.5}$$

If a proportional control is employed, that is, $u = K\sigma$:

$$\dot{\psi} = - K(B_{yR} \cos\lambda - B_{xR} \sin\lambda)^2 \sin\psi \tag{5.6}$$

Notice that (5.5) and (5.6) are complicated by the presence of λ which, strictly speaking, can be determined only by solving the complete system of Eqs. (5.3).

It is useful at this point to examine the character of the solutions of the simplified equations of motion as revealed by analog simulation. These results are conveniently represented by plots of h_y vs. h_x as in Fig. 5-4. In this representation, the distance from the origin to the trajectory is $\sin\psi$ and λ is the polar angle (measured counterclockwise) from the h_x axis to the trajectory (Fig. 5-4). Because $\bar{h}$ is a unit vector, the trajectory must always lie within the unit circle (which corresponds to an error of 90 deg). There is a certain amount of

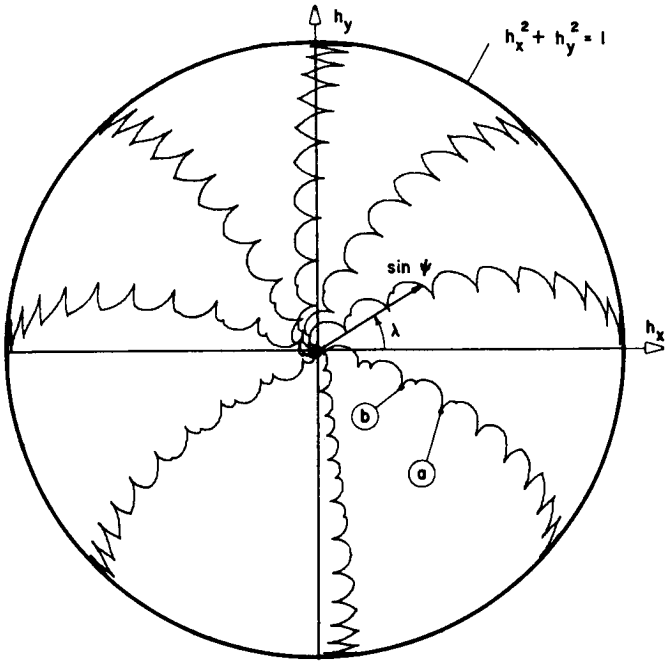

FIG. 5-4. TRAJECTORIES IN THE (h_x, h_y) PLANE FOR $\theta_i = 30°$, $\phi = 0°$, $\delta = 0°$.

ambiguity because the sign of h_z is not shown, so these plots do not show whether ψ is in the range $[0, 90°]$ or the range $[90°, 180°]$. For convenience, all runs presented here begin with $\psi = 90°$, and this value is, of course, never exceeded since $\dot{\psi} \leq 0$.

Figures 5-4 through 5-9 show the results of 48 "typical" analog runs with signum control and $U_o = 58.4$ for a vehicle at an altitude of 300 nautical miles. Each figure represents a different combination of θ_i (the orbital inclination), and ϕ and δ (which define the nominal pointing direction). In each instance, the partial trajectory between the points (a) and (b) corresponds to a time increment of approximately a half orbit (the period of B_{xR} and B_{yR}). At (a) and (b), as well as at a single intermediate point, the trajectory becomes tangent to a circle centered at the origin. This condition corresponds to $\dot{h}_z = 0$ and, therefore, the control changes sign at such points. We see that in no case does ψ ever increase along a trajectory. Since $h_z = \cos \psi$, this means $\dot{h}_z \geq 0$ at all times along every solution — which is the condition imposed in deriving the control law.

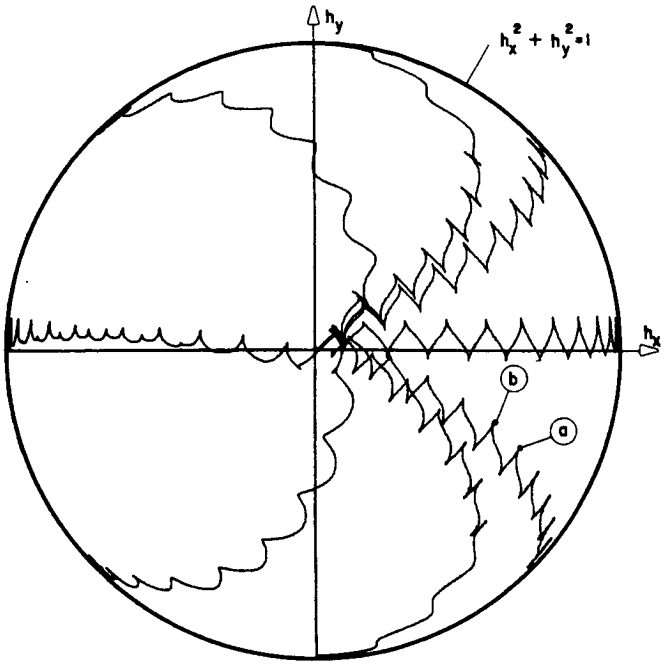

FIG. 5-5. TRAJECTORIES IN THE (h_x, h_y) PLANE FOR $\theta_i = 30°$, $\phi = 60°$, $\delta = -90°$.

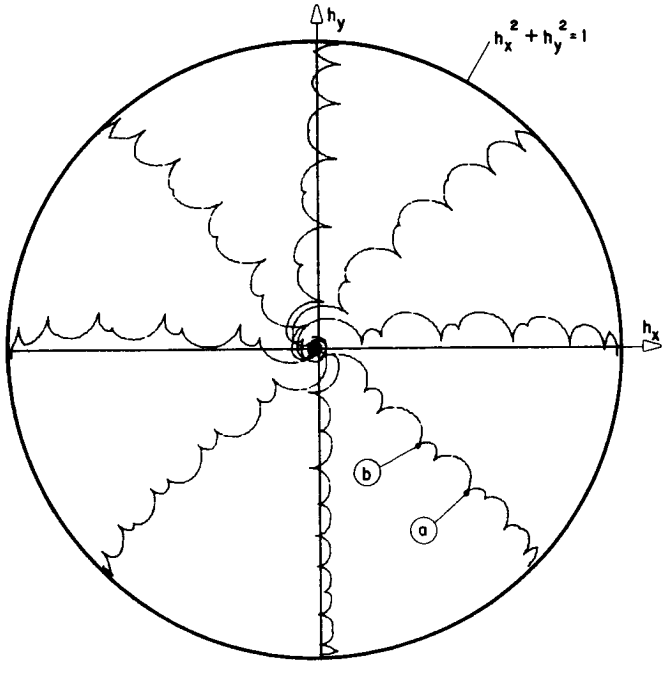

FIG. 5-6. TRAJECTORIES IN THE (h_x, h_y) PLANE FOR $\theta_i = 60°$, $\phi = 0°$, $\delta = 0°$.

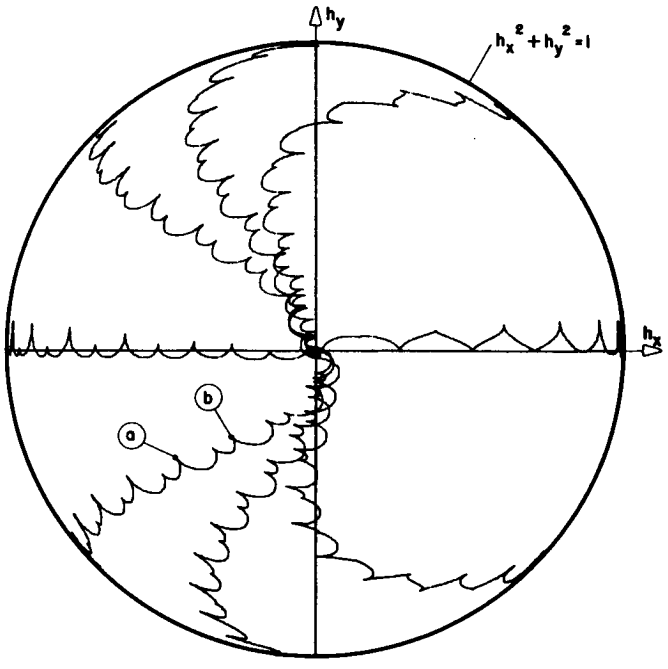

FIG. 5-7. TRAJECTORIES IN THE (h_x, h_y) PLANE FOR $\theta_i = 60°$, $\phi = 60°$, $\delta = -90°$.

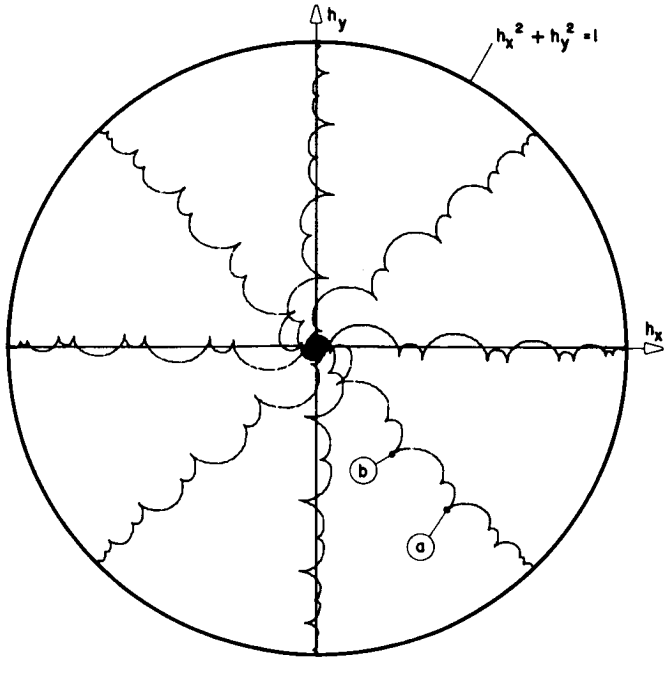

FIG. 5-8. TRAJECTORIES IN THE (h_x, h_y) PLANE FOR $\theta_i = 90°$, $\phi = 0°$, $\delta = 0°$.

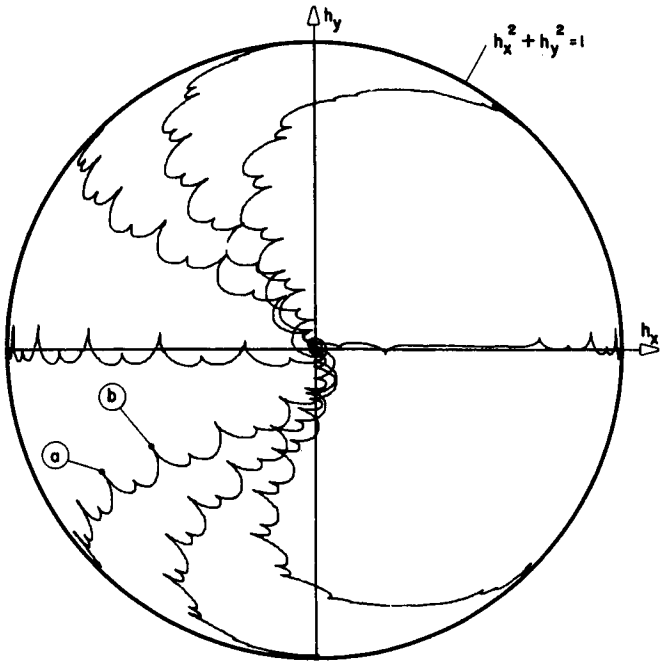

FIG. 5-9. TRAJECTORIES IN THE (h_x, h_y) PLANE FOR $\theta_i = 90°$, $\phi = 60°$, $\delta = -90°$.

Sequential examination of Figs. 5-4, 5-6, and 5-8, all of which correspond to a nominal spin-axis orientation which is normal to the orbit plane, shows that the distance between (a) and (b) increases (hence the speed of response increases) as the orbit becomes more nearly polar. This is expected because, for $\phi = \delta = 0$, the term $\sin\theta_i$ can be factored from both B_{xR} and B_{yR}, and hence from $\dot{\psi}$ in (5.3).

For other nominal spin-axis orientations such a factorization is not possible and, not unexpectedly, the relationship between the speed of response and the orbital inclination is not clear from examining Figs. 5-5, 5-7, and 5-9 (all of which correspond to $\phi = 60°$, $\delta = -90°$). As a matter of fact, as is shown later in this chapter, the speed of response is much more sensitive to the orbital inclination for $\phi = 0°$ than for $\phi = 90°$

As noted earlier, Eqs. (5.5) and (5.6) are complicated by the presence of λ which is, in general, time varying. However, examining Figs. 5-4 through 5-9 we see, in each case, that λ, during any half orbit with ψ sufficiently large, varies only through a small range. This variation

would be even less for smaller values of U_o. As a first approximation, then, we will assume in (5.5) and (5.6) that λ is constant, but arbitrary, over one period of the coefficients.

From this point the $\dot{\psi}$ Eqs. (5.5) and (5.6) could be solved over a half orbit starting with $\psi = \psi_o$ and $\lambda = \lambda_o$. Then the time variation of ψ (and λ_o) could be used in the $\dot{\lambda}$ equation from (5.3) to find a new starting value for $\lambda = \lambda_1$. The procedure would then be repeated starting with $\psi = \psi_1$ and $\lambda = \lambda_1$. This approach appears to be tedious and no more useful for design purposes than an exact numerical solution.

A more gross approach yields more useful (if less accurate) results. First, assuming that all values of λ are equally likely (in any case the initial value of λ would generally be unknown), average the right-hand sides of (5.5) and (5.6) over λ. Notice that

$$\left| B_{yR} \cos \lambda - B_{xR} \sin \lambda \right| = \sqrt{B_{xR}^2 + B_{yR}^2} \left| \cos (\lambda + \vartheta) \right|$$

where ϑ is a phase angle which need not be determined. As a second approximation, average the right-hand sides over one-half orbit. The result of this is an estimate of the average (in time) variation of ψ on the average (in λ). For signum control:

$$\boxed{\dot{\psi}_{AV} = - \frac{M_e}{2r_o^3} U_o G_{AV}}^{*} \qquad (5.7)$$

---

* As noted earlier these results assume MKS units. For English units (i.e., slug-ft^2, lb-ft-sec, amp-ft^2, gauss, ft-lb) the torque is

$$\bar{N} = 6.86 \times 10^{-6} \bar{M} \times \bar{B}$$

where $\bar{M}$ is in amp-ft^2, $\bar{B}$ is in gauss and $\bar{N}$ is in ft-lb. To use these units this additional factor must be included on the right-hand side of (5.7) and (5.8). U_o, in this case, is in units of amp-ft^2/lb-ft-sec while K is in units of amp-ft^2/lb-ft-sec per gauss. These units are used for all numerical computations in this dissertation.

where

$$G_{AV} = \underset{2\alpha}{\text{ave}} \left(\frac{2}{\pi} \sqrt{\beta_{xR}^2 + \beta_{yR}^2} \right)$$

and

$$\beta_{xR} = -\frac{B_{xR}}{M_e/2r_o^3}$$

$$\beta_{yR} = -\frac{B_{yR}}{M_e/2r_o^3}$$

With proportional control the approximate average motion is:

$$\boxed{\dot{\psi}_{AV} = -\left[\left(\frac{M_e}{2r_o^3}\right)^2 KF_{AV}\right] \sin \psi_{AV}} \quad * \qquad (5.8)$$

where

$$F_{AV} = \underset{2\alpha}{\text{ave}} \left[\frac{1}{2} (\beta_{xR}^2 + \beta_{yR}^2) \right]$$

As before the untilted dipole model is assumed. From Appendix A:

$$\beta_{xR} = [\sin \delta + 3 \sin (2\alpha - \delta)] \cos \phi \sin \theta_i + 2 \sin \phi \cos \theta_i$$

$$\beta_{yR} = [\cos \delta - 3 \cos (2\alpha - \delta)] \sin \theta_i \qquad (5.9)$$

Because G_{AV} involves the average of a square root of a periodic function, it is most easily evaluated (and has been) by numerical techniques. However, F_{AV} can be written in closed form:

$$F_{AV} = \left[\frac{5}{2} (1 + \cos^2 \phi) + \frac{1}{4} \sin \phi \cos 2\delta \right] \sin^2 \theta_i$$

$$+ 2 \sin^2 \phi \cos^2 \theta_i + 2 \sin \phi \cos \phi \sin \theta_i \cos \theta_i \sin \delta \, . \qquad (5.10)$$

---

* Ibid, page 74.

Figures 5-10 through 5-15 show contours of constant F_{AV} and G_{AV} in the (ϕ, δ) plane for several values of θ_i. As will be seen in a later chapter, these curves are very useful for design purposes.

It is important to determine the validity of the estimate of the response with signum control. For this purpose the equations were solved by simulation for $U_o = 58.4$ and all combinations of the following parameter values:

$$\theta_i = 30°, 60°, 90°$$

$$\phi = 0°, 30°, 60°, 90°$$

$$\delta = -90°, -60°, -30°, 0, 30°, 60°, 90°$$

$$\lambda(0) = 0, 45°, 90°, 135°, 180°, 225°, 270°, 315°.$$

(From investigation of Figs. 5-13, 5-14, and 5-15 we see that these values of ϕ are δ are, by symmetry, sufficient to sample the entire range of these parameters.) For each run the time required to reduce ψ from 90° to 10° was recorded. From this data the average rate of change of ψ was computed and from (5.7) an empirical value of G_{AV} was obtained. These results were then averaged over δ for each (θ_i, ϕ) combination and the results plotted in Fig. 5-16 were obtained. Also plotted in Fig. 5-16 are numerical computations of G_{AV} from the defining relationship (again these are averaged over δ). Figure 5-16 indicates a close correspondence between the empirical results and the response estimates, particularly for small values of ϕ. However, as ϕ approaches 90° a systematic error is exhibited. Examining the analog data (for example, Fig. 5-7) it is apparent that as ϕ approaches 90°, the system favors certain values of λ for convergence. Moreover, the rate of convergence for these preferred values of λ is apparently slower than the average (over λ) rate of convergence. Thus, the response estimate is slightly optimistic for the larger values of ϕ. On the whole, the estimate (5.7) is a good one.

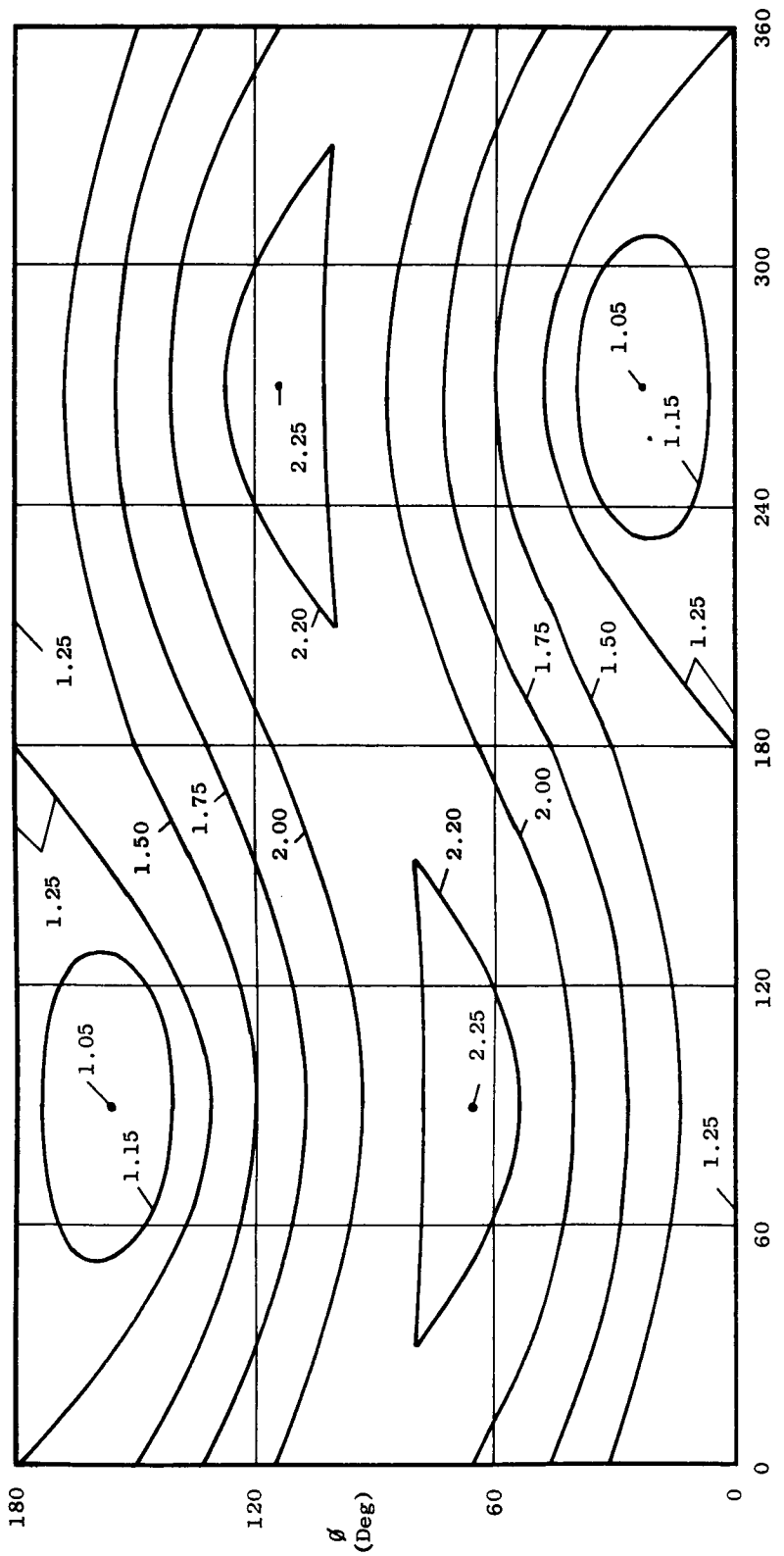

FIG. 5-10. CONTOURS OF CONSTANT F_{AV} FOR $\Theta_i = 30°$.

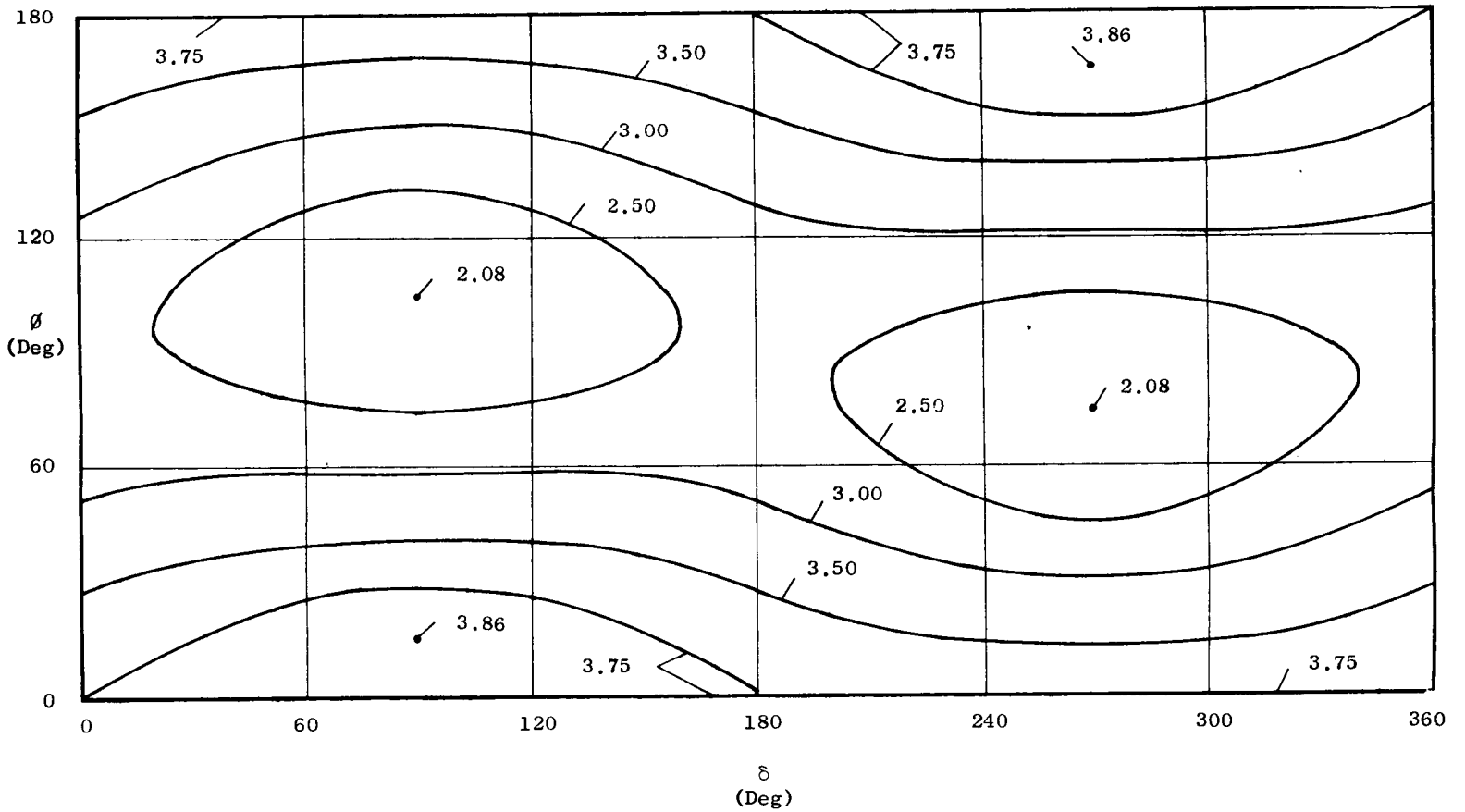

FIG. 5-11. CONTOURS OF CONSTANT F_{AV} FOR $\theta_i = 60°$.

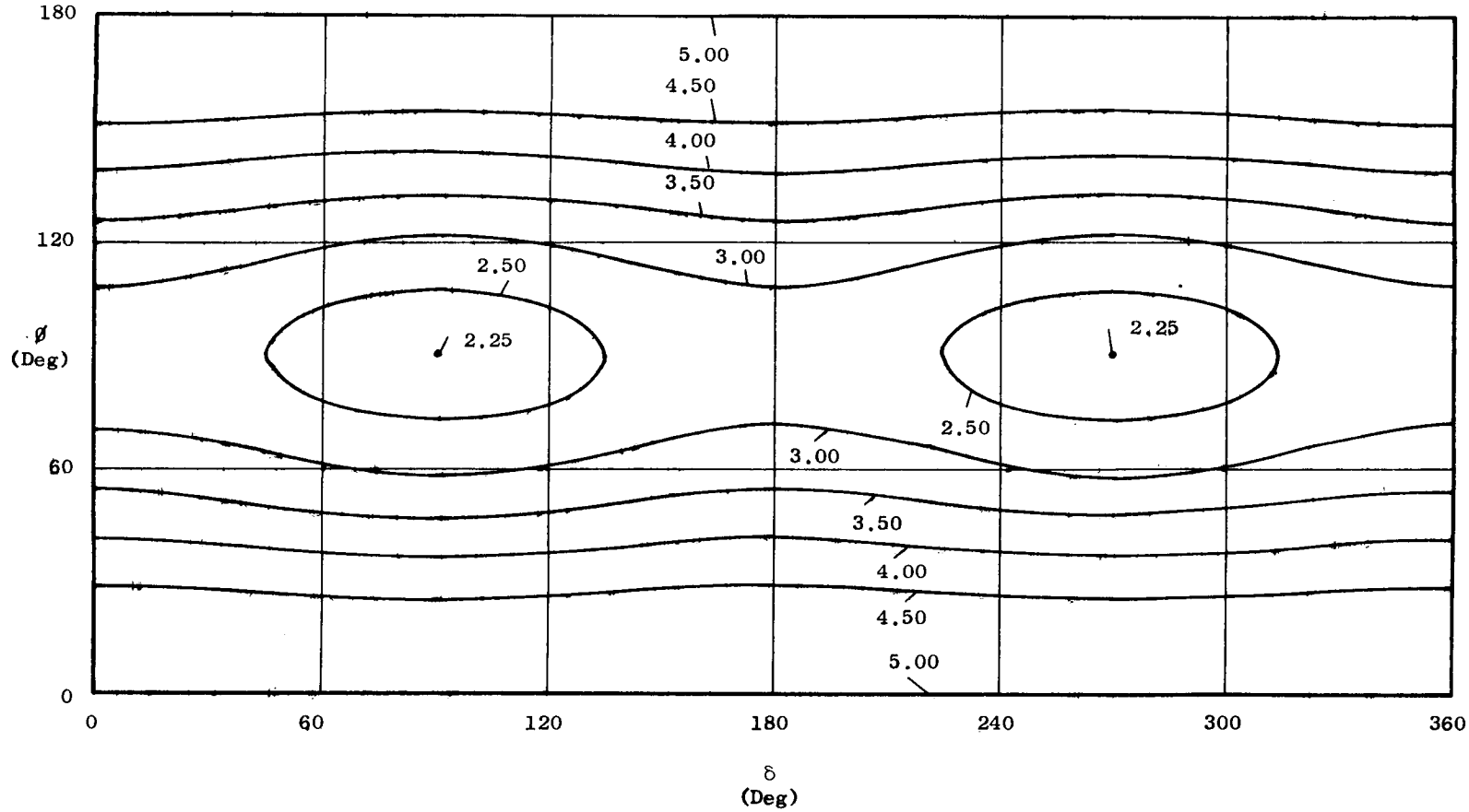

FIG. 5-12. CONTOURS OF CONSTANT F_{AV} FOR $\theta_i = 90°$.

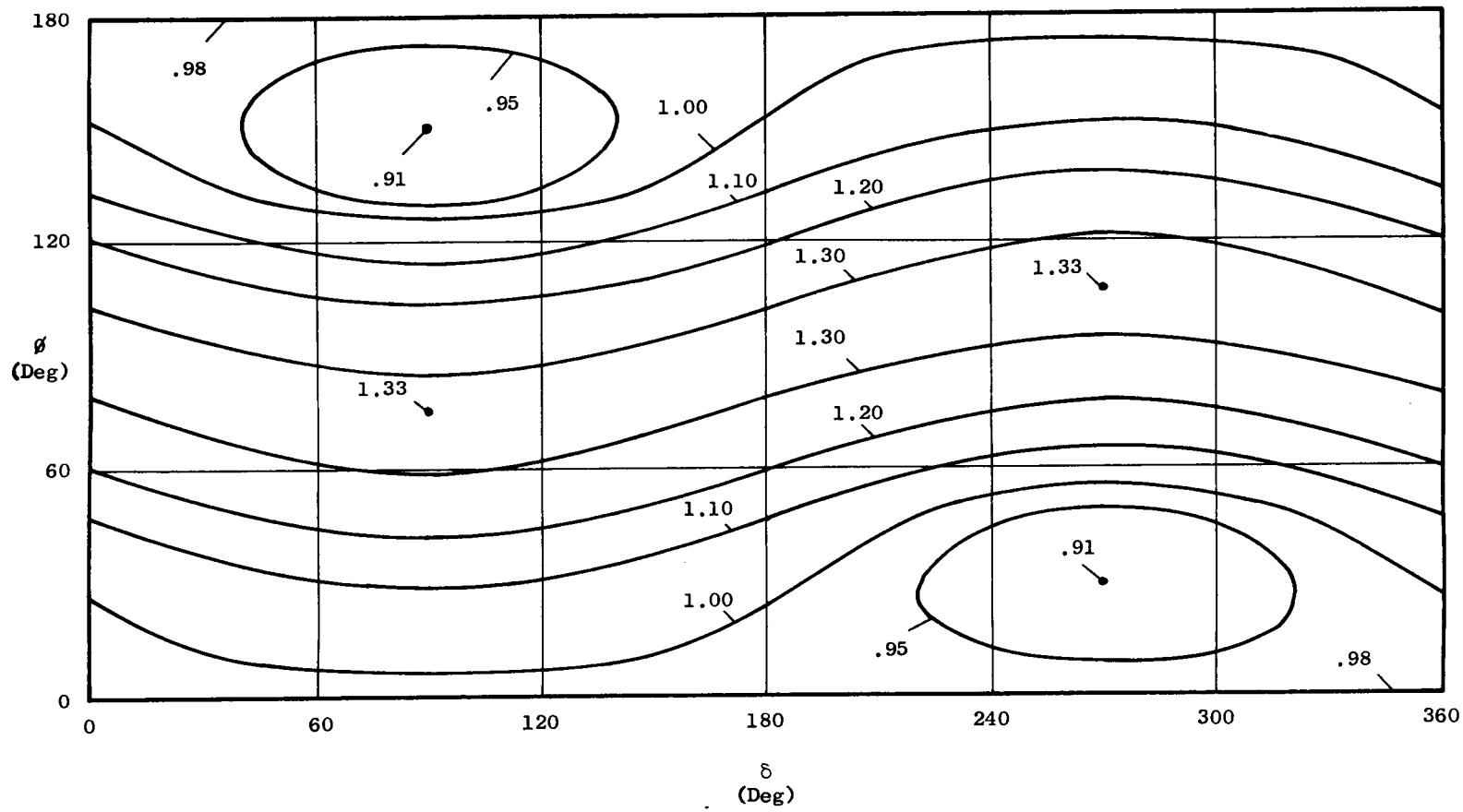

FIG. 5-13. CONTOURS OF CONSTANT G_{AV} FOR $\theta_i = 30°$.

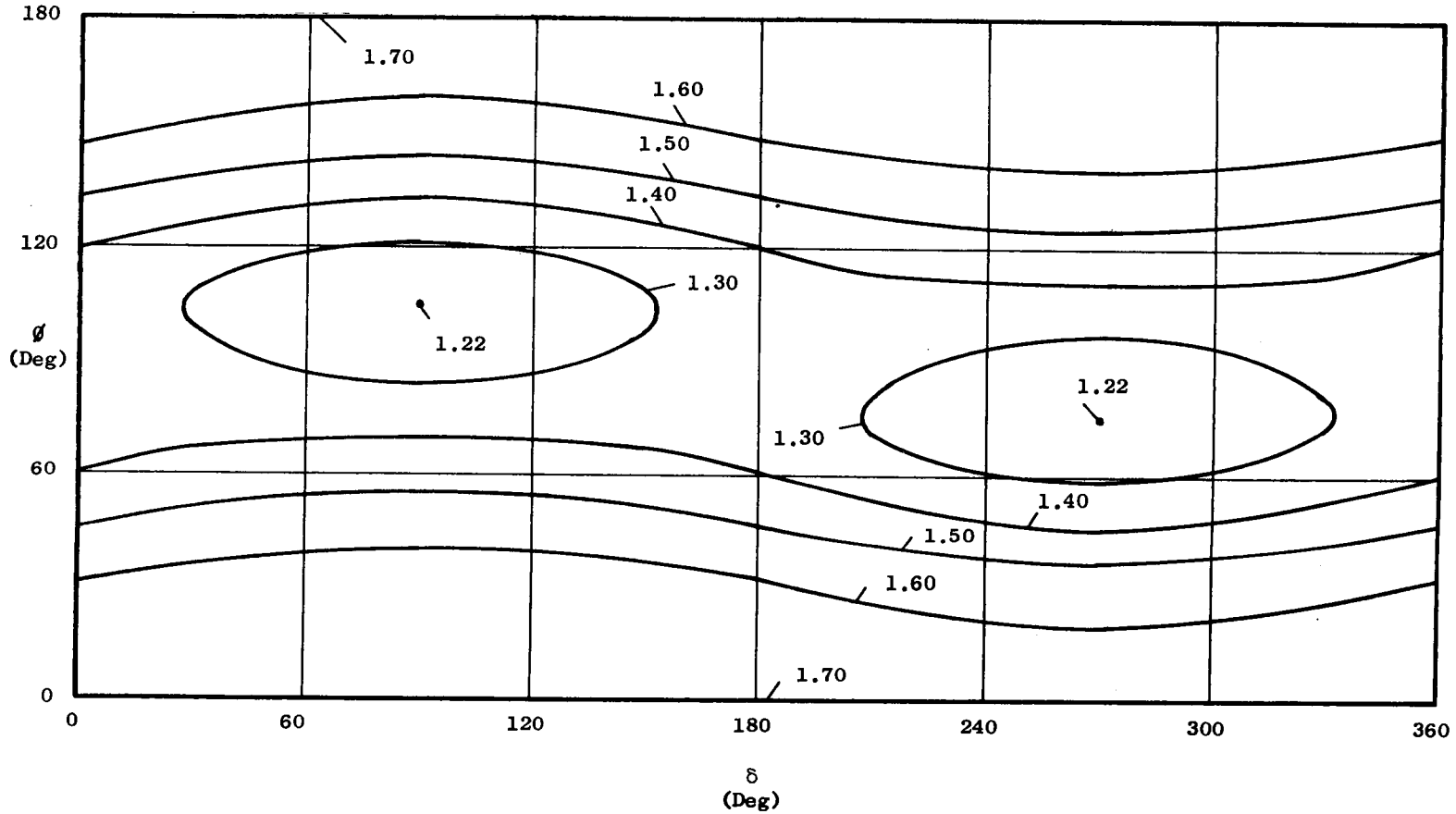

FIG. 5-14. CONTOURS OF CONSTANT G_{AV} FOR $\Theta_i = 60°$.

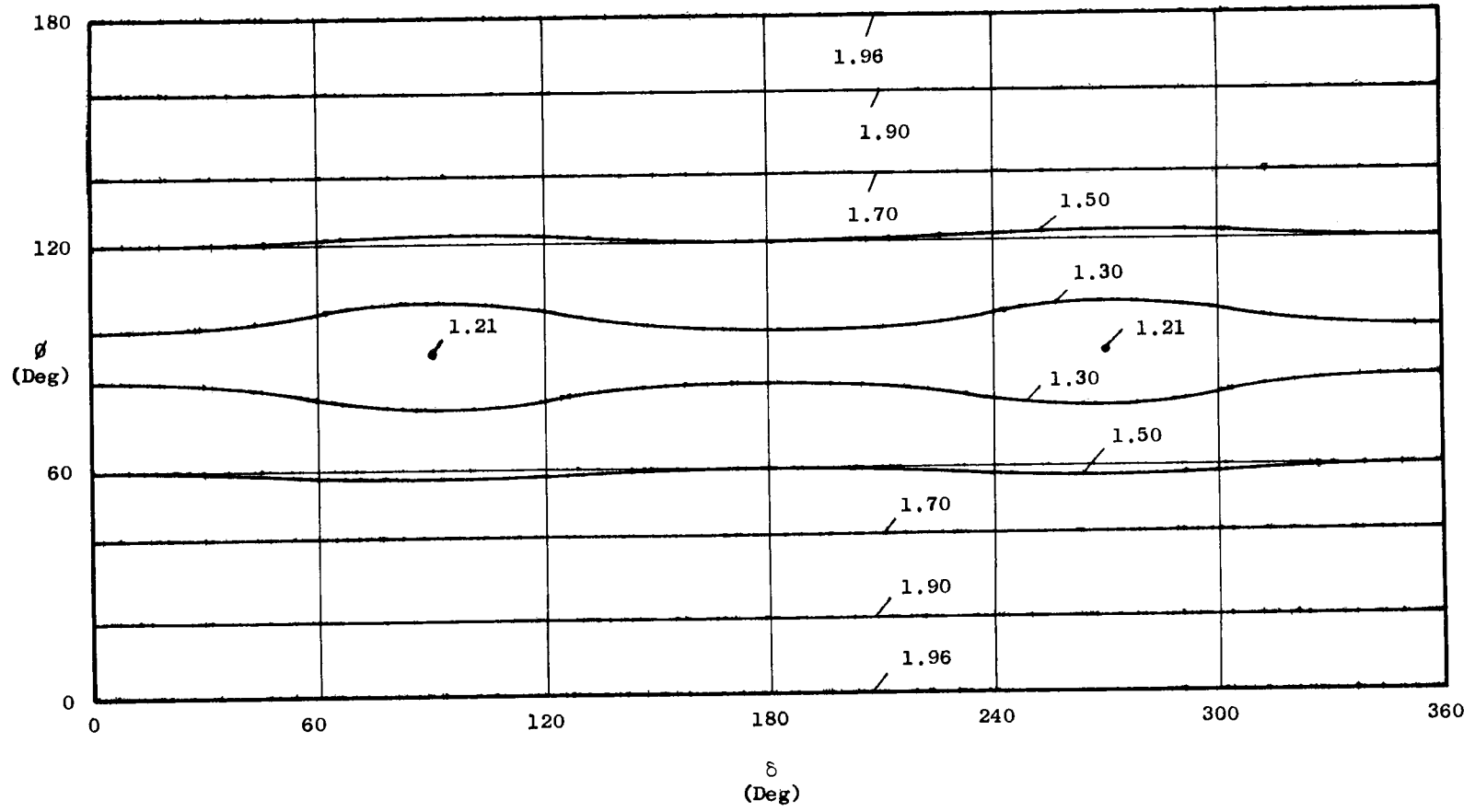

FIG. 5-15. CONTOURS OF CONSTANT G_{AV} FOR $\theta_i = 90°$.

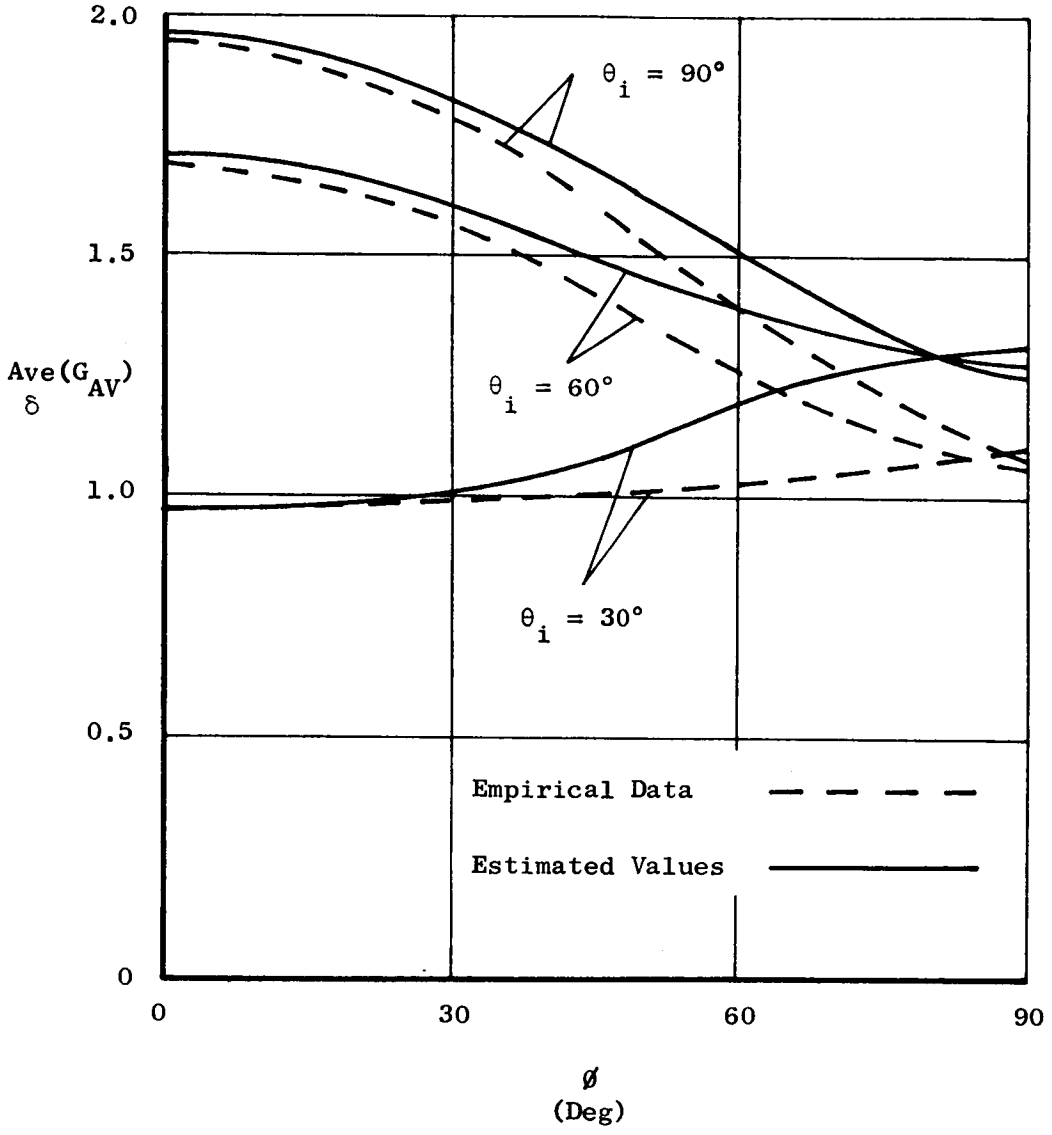

FIG. 5-16. COMPARISON OF LARGE-ERROR RESPONSE ESTIMATES WITH EMPIRICAL DATA.

B. SMALL-ERROR PERFORMANCE ESTIMATE

For estimation of small-error performance the linearized exact equations of motion will be used. Neglecting all disturbances and assuming the (x_R, y_R, z_R) coordinate frame to be inertially stationary, the linearized equations of motion with proportional control are:

$$\begin{aligned} \dot{\omega}_1 &= -\omega_n(\omega_2 + KB_{y1}\sigma) \\ \dot{\omega}_2 &= \omega_n(\omega_1 + KB_{x1}\sigma) \\ \dot{c}_{13} &= -\omega_2 \\ \dot{c}_{23} &= \omega_1 \end{aligned} \tag{5.11}$$

where $\omega_n = (1+k)\omega_s$ and, as before,

$$\sigma = B_{x1}c_{23} - B_{y1}c_{13} + K_R(B_{y1}\omega_1 - B_{x1}\omega_2) \ .$$

For small errors

$$\begin{aligned} B_{x1} &= B_{xR} + B_{zR}c_{13} \\ B_{y1} &= B_{yR} + B_{zR}c_{23} \end{aligned} \tag{5.12}$$

because, for $a_{33} = c_{33} \approx 1$, C can be assumed to be

$$C = \begin{bmatrix} 1 & 0 & c_{13} \\ 0 & 1 & c_{23} \\ -c_{13} & -c_{23} & 1 \end{bmatrix} \tag{5.13}$$

The uncontrolled solution to the set of Eqs. (5.11) is of the general form

$$\omega_1 = a \cos (\omega_n t + \theta)$$

$$\omega_2 = a \sin (\omega_n t + \theta)$$

$$c_{13} = \chi_1 + \frac{\omega_1}{\omega_n} \qquad (5.14)$$

$$c_{23} = \chi_2 + \frac{\omega_2}{\omega_n}$$

The constants a, θ, χ_1, and χ_2 are specified by the initial conditions. The character of this motion is shown in Fig. 5-17. Notice that the phase angle θ is not important; moreover, because only the total attitude error is significant, knowledge of ψ^a and a is sufficient to specify the essential properties of the motion.

In the presence of proportional magnetic control with sufficient damping ω_1, ω_2, c_{13}, and c_{23} will eventually be reduced to zero. However, since magnetic control results in a rather slow motion of the spin axis, the controlled response will appear very similar to that shown in Fig. 5-17 if viewed over a time equivalent to several cycles of the unforced oscillatory solution. It is reasonable, therefore, (in the style of Krylov and Bogoliubov [Ref. 5-1]) to regard the forced solution as being of the form (5.14) where χ_1, χ_2, a, and θ are, relative to the frequency ω_n, slowly varying parameters. If, under these assumptions, reasonable estimates can be developed for the variation of a and ψ^a, they can be used for design purposes.

1. Variation of a

Define $\xi \triangleq \omega_n t+\theta$. Then $\omega_1 = a \cos \xi$ and $\omega_2 = a \sin \xi$. Differentiating ω_1 and ω_2:

$$\dot{\omega}_1 = \dot{a} \cos \xi - a\dot{\xi} \sin \xi$$

$$\dot{\omega}_2 = \dot{a} \sin \xi + a\dot{\xi} \cos \xi \ . \qquad (5.15)$$

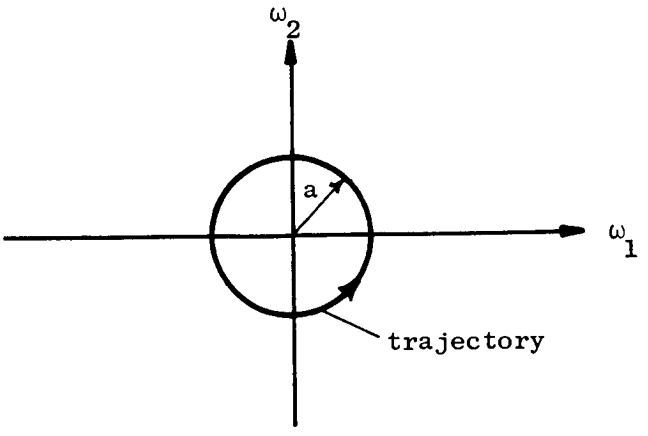

(a) Motion in the (ω_1, ω_2) Plane

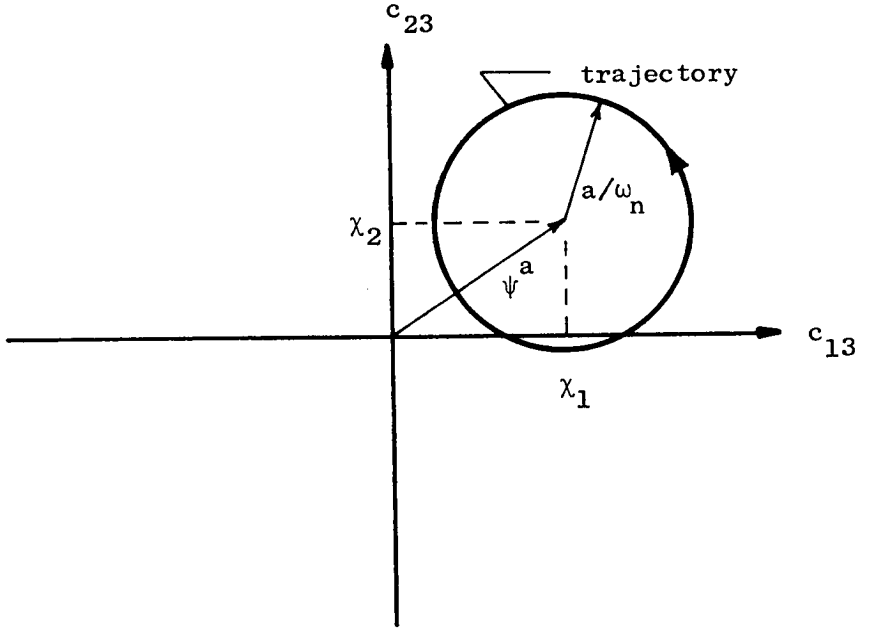

(b) Motion in the (c_{13}, c_{23}) Plane

FIG. 5-17. SMALL-ERROR UNFORCED RESPONSE.

By proper combination of these results

$$\dot{a} = \dot{\omega}_1 \cos \xi + \dot{\omega}_2 \sin \xi \ . \tag{5.16}$$

From (5.11) it follows that

$$\dot{a} = - K\omega_n(B_{y1} \cos \xi - B_{x1} \sin \xi)\sigma \ . \tag{5.17}$$

Employing the form of the solution specified in (5.14), σ can be written in terms of χ_1, χ_2, a and ξ:

$$\sigma = B_{x1}\left(\chi_2 - \frac{K_R\omega_n - 1}{\omega_n} a \sin \xi\right) - B_{y1}\left(\chi_1 - \frac{K_R\omega_n - 1}{\omega_n} a \cos \xi\right) \ . \tag{5.18}$$

If the foregoing two expressions are combined and expanded, there will be terms independent of ξ as well as those involving $\sin \xi$, $\cos \xi$, $\sin 2\xi$ and $\cos 2\xi$. Because we are assuming that a, χ_1, and χ_2 are constant over several cycles at the frequency ω_n, it is reasonable as a first approximation to neglect all but the terms not involving ξ (this is the "averaging principle" of Krylov and Bogoliubov [Ref. 5-1]). This step yields:

$$\dot{a} = - \frac{1}{2} K(K_R\omega_n - 1)(B_{x1}^2 + B_{y1}^2)a \tag{5.19}$$

Because c_{13}, c_{23}, ω_1, ω_2, a, χ_1, and χ_2 are all assumed to be small, expression of (5.19) in terms of B_{xR}, B_{yR}, and B_{zR} does not alter its form in the linear approximation:

$$\dot{a} = - \frac{1}{2} K(K_R\omega_n - 1)(B_{xR}^2 + B_{yR}^2)a \tag{5.20}$$

As in the case of the large-error estimate, it is convenient to average the effect over a half orbit to obtain a useful design approximation which does not involve time. Then, noting the definition of F_{AV} following (5.8):

$$\dot{a}_{AV} = -\left[\left(\frac{M_e}{2r_o^3}\right)^2 K(K_R\omega_n - 1)F_{AV}\right] a_{AV} \ . \qquad (5.21)$$

Observe that (5.21) is a first-order differential equation whose solution is a decaying exponential for $K_R > 1/(1+k)\omega_s$ and a growing exponential for $K_R < 1/(1+k)\omega_s$. This result is in complete agreement with the conclusions, regarding the effect of K_R upon stability, derived rigorously in Chapter IV.

The validity of this response estimate has been spot checked by means of several machine solutions of the small-error differential equations and found to be adequate for design purposes. A run indicating rather good agreement is shown in Fig. 5-18. The parameters of this run are: $\theta_i = 90°$, $\phi = \delta = 0$, altitude = 300 nautical miles, $K = 584$ amp-ft^2/gauss-lb-ft-sec, $I_x = 75$ slug-ft^2, $I_z = 100$ slug-ft^2, $\omega_s = 0.1$ rad/sec, $K_R = 20$ sec.

2. Variation of ψ^a

By virtue of (5.14), $\dot{\chi}_1$ and $\dot{\chi}_2$ are:

$$\dot{\chi}_1 = \dot{c}_{13} - \frac{\dot{\omega}_1}{\omega_n} = B_{y1}K\sigma$$
$$\dot{\chi}_2 = \dot{c}_{23} - \frac{\dot{\omega}_2}{\omega_n} = -B_{x1}K\sigma \ . \qquad (5.22)$$

Utilizing the "averaging principle" and the expression for σ developed in the foregoing section:

$$\dot{\chi}_1 = K(-B_{y1}^2\chi_1 + B_{x1}B_{y1}\chi_2)$$
$$\dot{\chi}_2 = K(-B_{x1}^2\chi_2 + B_{x1}B_{y1}\chi_1) \ . \qquad (5.23)$$

(As in the estimate for the variation of a, B_{x1} and B_{y1} in (5.23) can be replaced respectively by B_{xR} and B_{yR}.) Now define a new angle λ_a by the relationships $\chi_1 = \psi^a \cos\lambda_a$ and $\chi_2 = \psi^a \sin\lambda_a$. Then

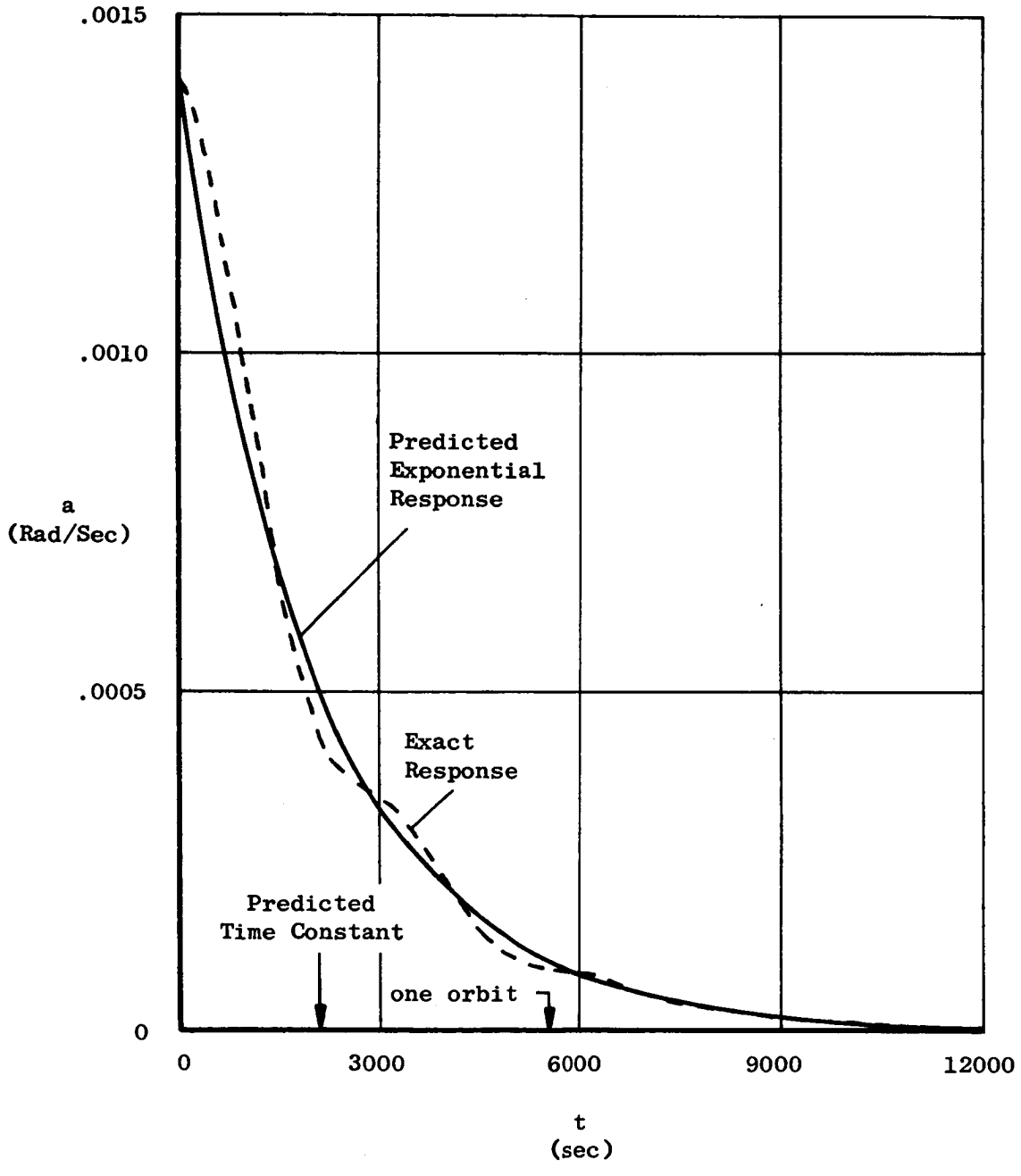

FIG. 5-18. DAMPING OF TRANSVERSE ANGULAR VELOCITIES.

$$\dot{\psi}^a = \dot{\chi}_1 \cos \lambda_a + \dot{\chi}_2 \sin \lambda_a \tag{5.24}$$

and

$$\dot{\psi}^a = - K(B_{yR} \cos \lambda_a - B_{xR} \sin \lambda_a)^2 \psi^a \ . \tag{5.25}$$

There is a clear similarity between (5.25) and (5.6); this is not unexpected because, with small errors, $\chi_1 = -h_x$ and $\chi_2 = -h_y$ as may be seen by comparing expressions (5.14) and (2.27), with $\Omega_x = \Omega_y = \Omega_z = 0$ and C as in (5.13). Averaging over time and over λ_a (as the large-error expressions (5.5) and (5.6) were averaged over λ):

$$\boxed{\dot{\psi}^a_{AV} = - \left[\left(\frac{M_e}{2r_o^3} \right)^2 KF_{AV} \right] \psi^a_{AV} \ .} \tag{5.26}$$

Figure 5-19 is a comparison of the exponential response estimate of (5.26) with the exact response for the run from which the data of Fig. 5-18 was taken. It is to be expected that the estimate for ψ^a will not be as accurate as that for a because of the additional approximation of averaging over λ_a.

These response estimates show clearly the dependence of the small-error system response upon K and K_R. Most interesting is the fact that the amount of effective damping does not depend linearly upon K_R but is, rather, proportional to $K_R\omega_n - 1$, where $K_R\omega_n$ is the ratio of K_R to its critical value. Thus, for the two runs of Fig. 5-1 the rate gains are in the ratio of 5 to 1, but the effective damping is in the ratio of 17 to 1. Another observation is that if K_R is twice its critical value the position and rate estimates exhibit the same time constant.

C. SUMMARY OF PERFORMANCE ESTIMATES

This chapter has developed performance estimates for both the large-error and small-error performance of a magnetic control system in which the coil current is a saturating-proportional function of the error signal. The primary importance of these estimates is that they separate the geometric effects, as characterized by $G_{AV}(\theta_i, \phi, \delta)$, $F_{AV}(\theta_i, \phi, \delta)$, and

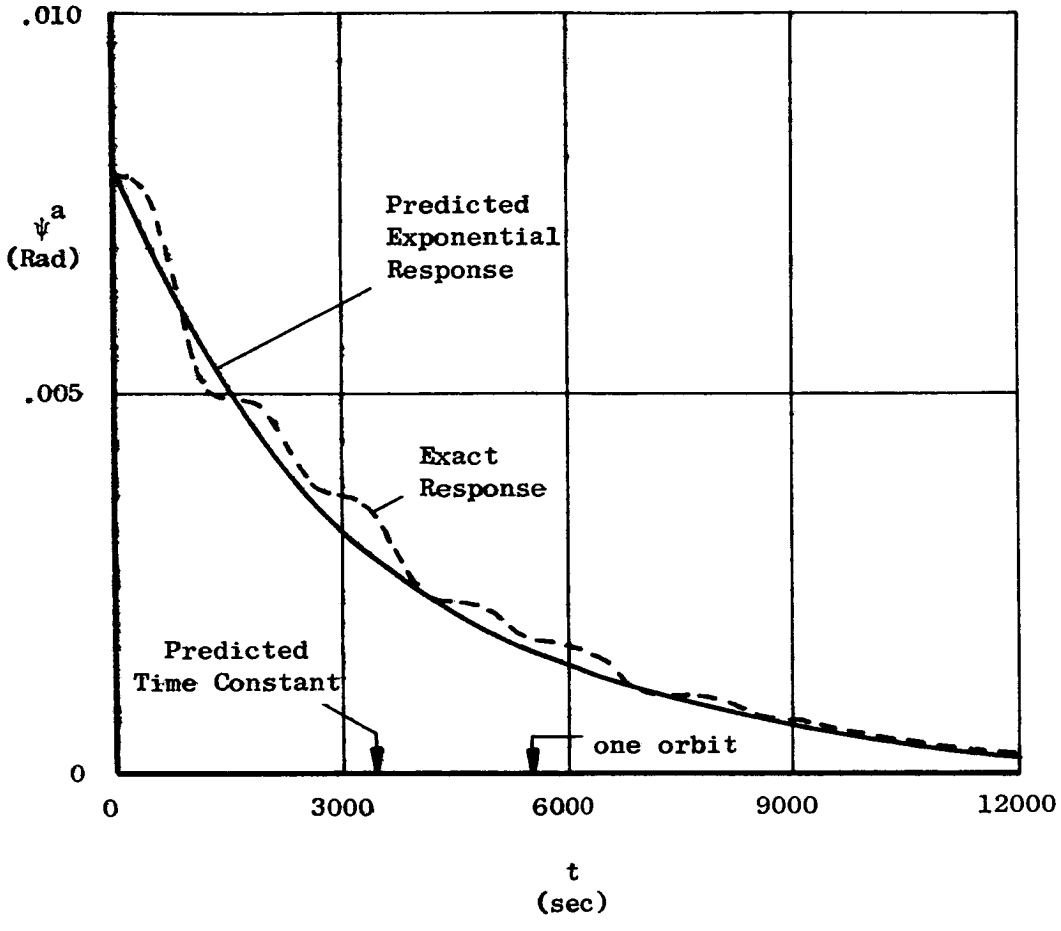

FIG. 5-19. REDUCTION OF AVERAGE ATTITUDE ERROR.

the altitude, from the parameters of control (i.e., U_o, K and K_R). It is possible to see, for example, that if the geometry is altered so that F_{AV} is reduced by a factor of two, increasing K by a factor of two will preserve, in essence, the same small-error performance.

In any particular orbit θ_i will be constant but ϕ and δ will, typically, vary slowly (a fact which has been neglected as a dynamic effect) in accordance with the first two parts of expression (2.3). In designing the control system developed here for any particular mission it is necessary, then, to evaluate the variation of ϕ and δ and, using contours such as those presented earlier in the chapter, to evaluate the range of variation of the geometrical gain factors. The control parameters can then be chosen appropriately, always bearing in mind that an improvement in performance will generally be accompanied by greater weight and/or power requirements. These aspects of the problem are discussed in Chapters VIII and IX.

In this chapter (indeed, in most chapters involving design) the tilt of the magnetic dipole has been neglected. We find, from the stability analyses, that this is probably a pessimistic view of the situation; for example, with the untilted dipole this system will not converge to the origin with the vehicle in an equatorial orbit, whereas with the tilted magnetic dipole model convergence will occur because the vehicle cannot remain in the magnetic equatorial plane (at nonsynchronous altitudes) due to the rotation of the earth and the inclination of the magnetic dipole to the geographical polar axis.*

Although the untilted dipole yields pessimistic stability results for $\theta_i = 0$, use of magnetic control in near-equatorial orbits is generally questionable; in any orbit inclined 11 deg or less the orbit plane will coincide closely, for several hours a day, with the magnetic equatorial plane, thus producing a situation in which convergence is, at

---

* Notice that for $\theta_i = 0$, F_{AV} and G_{AV} are misleading in that they are generally nonzero. The system actually does converge in this case, but not to the origin (see Chapter IV). The performance estimates are meaningless in cases for which asymptotic stability does not exist.

best, slow. On the other hand, for orbits of at least moderate inclination (say $30° \leq \theta_i \leq 150°$) the tilt of the magnetic dipole can be neglected for purposes of preliminary design.

We conclude that the estimates developed in this chapter are useful for most applications of magnetic control to a spinning vehicle. For orbits of very low inclination each mission should be studied in detail by simulation; this does not suggest that the control law is not applicable to such situations, but only that care must be taken in its application.

VI. MINIMUM-TIME CONTROL FOR THE SIMPLIFIED EQUATIONS OF MOTION

In preceding chapters a magnetic control law has been evolved and shown to be asymptotically stable in-the-large, and its performance has been estimated for the important case that the coil current is a saturating-proportional function of the error signal. Thus far, however, no evidence has been presented to show that there is not a much better control law available--for example, one which would reduce the initial error in much less time than the feedback control system developed in Chapter III. This chapter presents such evidence, derived by application of Pontryagin's maximum principle [Ref. 6-1].

Of primary importance is the quality of the feedback control law for large errors (the acquisition problem), because the small-error design will be affected significantly by such factors as the avoidance of chatter and the character of the disturbance environment. A reasonable design goal for in-the-large performance is the removal of the initial attitude error in the least time, consistent with constraints upon the weight and power consumption. For these reasons, and to reduce the order of the system of differential equations to be dealt with, we now consider minimum-time control of the simplified equations of motion.

The problem treated is that of finding the bounded control ($|u| \leq U_o$) which will take this third-order system from its initial state, $\underline{h}(t_o) = \underline{h}_o$, to its desired terminal state ($h_x = h_y = 0$, $h_z = 1$) in less time than any other bounded control. Using the maximum principle (which gives necessary conditions for the optimal control) a set of six differential equations and a control equation are developed which, when simulated in reverse time on an analog computer, produce trajectories which satisfy the necessary conditions for the motion of the optimally controlled system. These reverse-time trajectories are then compared qualitatively to the trajectories of the system with signum feedback control of the coil current.

A. THE MAXIMUM PRINCIPLE

The general problem of optimal control of a stationary continuous system can be stated as follows. Define the system by a set of n first-order ordinary differential equations of the form

$$\dot{x}_i = f_i(x_1,\ldots,x_n,\ u_1,\ldots,u_m) \tag{6.1}$$

where the m-dimensional vector with components $u_1,\ u_2,\ldots,u_m$ is the control vector, $\bar{u}$. In general, $\bar{u}$ is subject to a constraint (due, for example, to mechanization considerations) and we say that $\bar{u}$ must be in the class of admissible controls, Ω. A common constraint upon $\bar{u}$ is $|u_j| \leq U_o$ for all j. The cost of control is defined as

$$J = \int_{t_o}^{t_f} f_o(x_1,\ldots,x_n,\ u_1,\ldots,u_m)dt \tag{6.2}$$

where, for example, f_o is set equal to unity for minimum-time control and is chosen to be a quadratic function of the components of the control vector for minimum energy control [Ref. 6-2].

The optimal control is defined to be that vector time-function of class Ω which satisfies the specified boundary conditions of the system in such a way that the cost is less than or equal to the cost with any other control in Ω which matches the boundary conditions. The boundary conditions generally restrict $t,\ x_1,\ x_2,\ldots,x_n$ at the initial and final times. These restraints may take on many forms; for example, t and the state may be specified completely at both ends of the solution or, on the other hand, the motion could be constrained to begin at a specific point and terminate on a subspace of the n-dimensional state space at some unspecified time. In the minimum-time study to be pursued in the following section, the initial time and both the inital and final states are prescribed, but the final time is free (unspecified).

To apply the maximum principle to the above problem, we first introduce a new system variable x_o where

$$\dot{x}_o = f_o(x_1,\ldots,x_n,\ u_1,\ldots,u_m)$$

and $x_o(t_o) = 0$. The vector $\bar{x}$ will be the n+1 vector with components $x_o,\ x_1,\ldots,x_n$; the vector $\bar{\lambda}$ has components $\lambda_o,\ \lambda_1,\ldots,\lambda_n$. Define a scalar function, the Hamiltonian, by

$$\mathcal{H} = \sum_{i=0}^{n} \lambda_i f_i \tag{6.3}$$

where the adjoint functions $\lambda_o,\ldots,\lambda_n$ and the state variables satisfy Hamilton's differential equations:

$$\dot{\lambda}_i = -\frac{\partial \mathcal{H}}{\partial x_i}\ ; \qquad \dot{x}_i = \frac{\partial \mathcal{H}}{\partial \lambda_i} \tag{6.4}$$

for $i = 0,1,\ldots,n$. Notice that $\mathcal{H}$ is independent of x_o so that λ_o is constant; we will, as in Ref. 6-2, choose $\lambda_o = -1$. It should be noted that for the case where the initial and final position of the system is specified, the boundary conditions upon the λ_i are free. There are 2n differential equations (omitting λ_o and x_o) but only n boundary conditions.

The maximum principle states that if $\bar{u}^*(t)$ is the optimal control and $\bar{x}^*(t)$ is the corresponding solution, then there exists a vector function $\bar{\lambda}^*(t)$ such that $\mathcal{H}(x^*,\ \lambda^*,\ u^*) \geq \mathcal{H}(x^*,\ \lambda^*,\ u)$ for any u^* and u in Ω.

It is important to remember that this result gives only necessary conditions; there is, in general, no guarantee that the control and trajectory so derived will be optimal or, indeed, that an optimal control exists. The existence problem has been explored extensively [Refs. 6-3, 6-4], but the question of sufficiency is apparently more imposing. Indeed, several of the trajectories generated in the present study were found to be nonsufficient, even though they satisfied the necessary conditions of the maximum principle.

In the formulation above, the system considered is stationary; these results can be readily extended to nonstationary systems by introducing

yet another state variable and appropriately augmenting the Hamiltonian

$$\dot{x}_{n+1} = 1 \; ; \qquad x_{n+1}(0) = t_o \tag{6.5}$$

$$\mathcal{H}' = \mathcal{H} + \lambda_{n+1} \; ; \qquad \dot{\lambda}_{n+1} = \frac{\partial \mathcal{H}}{\partial x_{n+1}} \; . \tag{6.6}$$

The new state variable is, of course, time and allows an n-dimensional, time varying system to be represented as an n+1-dimensional stationary system. We see also, from (6.6), that maximizing $\mathcal{H}'$ relative to u is identical to maximizing $\mathcal{H}$ with respect to u. Thus the introduction of the additional state variable may be omitted in practice [Ref. 6-1].

B. FORMULATION FOR OPTIMAL MAGNETIC CONTROL

It will prove convenient to use classical vector notation in applying the maximum principle to optimal control of the simplified equations of motion. The (three-dimensional) system to be considered is

$$\dot{\bar{h}} = - (\bar{B} \times \bar{h})u \; ; \qquad |u| \leq U_o \; . \tag{6.7}$$

Now define a new 3-dimensional vector $\bar{p}$ with components $p_1 = \lambda_1$, $p_2 = \lambda_2$ and $p_3 = \lambda_3$. The Hamiltonian is

$$\mathcal{H} = - f_o(\bar{h},u) - [(\bar{B} \times \bar{h}) \cdot \bar{p}]u$$

or (6.8)

$$\mathcal{H} = - f_o(\bar{h},u) + [(\bar{B} \times \bar{p}) \cdot \bar{h}]u \; .$$

From (6.4)

$$\dot{\bar{p}} = - \bar{\nabla}_h \mathcal{H} = - (\bar{B} \times \bar{p})u \; . \tag{6.9}$$

Thus, for this problem, the adjoint equations (6.9) have exactly the same form as the system equations (6.7).

The optimal control* is found by maximizing, at each time, (6.8) with respect to u. For the minimum-time optimal control problem $f_o = 1$ and

$$u = U_o \text{ sgn } [\bar{B} \cdot (\bar{p} \times \bar{h})] \ . \tag{6.10}$$

Much insight can be gained by introducing the auxiliary vector

$$\bar{y} = \bar{p} \times \bar{h} \ . \tag{6.11}$$

A differential equation can be developed for $\bar{y}$ using the relationship $\dot{\bar{y}} = \dot{\bar{p}}\times\bar{h}+\bar{p}\times\dot{\bar{h}}$. The result is

$$\dot{\bar{y}} = - (\bar{B} \times \bar{y})u = - U_o(\bar{B} \times \bar{y}) \text{ sgn } (\bar{B} \cdot \bar{y}) \tag{6.12}$$

which is independent of $\bar{h}$ and $\bar{p}$. This equation can replace the $\bar{p}$ equation in the optimal control formulation.

A common method of generating optimal trajectories for a problem in which $\bar{h}(t_o)$ and $\bar{h}(t_f)$ are specified is to replace the initial boundary conditions on the system equations by (arbitrary) terminal conditions upon the adjoint equations. The 2n differential equations are then simulated in reverse time, using the fixed $\bar{h}(t_f)$ and the arbitrary $\bar{p}(t_f)$. By repeating this process for various choices of $\bar{p}(t_f)$ a family of (potentially) optimal trajectories will be generated. This procedure is followed in this study, with the exception that $\bar{y}$ rather than $\bar{p}$ is simulated.

A major problem is the choice of the final conditions upon $\bar{y}$. Notice first that $\bar{y}\cdot\bar{h} = 0$ so that $\bar{y}(t_f)$ must be in the plane normal to $\bar{h}(t_f)$. Thus $y_3(t_f) = 0$. From (6.12) it is clear that $\dot{\bar{y}}\cdot\bar{y} = 0$ so that the magnitude of $\bar{y}$ is invariant. Furthermore, if we define a new vector $\bar{y}' = K\bar{y}$ (K a positive constant), the form of (6.12) is unchanged. Thus the magnitude of $\bar{y}$ can be chosen arbitrarily without altering u(t). In this study $|\bar{y}| = 1$.

---

* For this problem the existence of an optimal control is insured by Theorem 1 of Ref. 6-3. For semantic convenience, we will refer to the control derived here as optimal even though sufficiency is not shown.

One advantage of introducing $\bar{y}$ is now apparent; although $\bar{y}$ is necessarily normal to $\bar{h}$, $\bar{p}$ may not be. Thus, it would seem at first glance that all possible final directions of $\bar{p}$ would have to be considered in the reverse time simulation. With hindsight, it is obvious that, without loss of generality, the constraints $p_3(t_f) = 0$, $|\bar{p}| = 1$ can be imposed to make $\bar{h}$, $\bar{y}$, and $\bar{p}$ an orthonormal set. This orthonormality is, of course, preserved for all time.

C. THE SIMULATION

1. Procedure

The six differential equations (in terms of $\bar{h}$ and $\bar{y}$) and the control equation were simulated in reverse time using two (slaved) TR-48 analog computers. For purposes of comparison with the feedback control runs reported in Chapter V, the vehicle altitude was 300 nautical miles, an untilted magnetic dipole model was used, and U_o was 58.4.* The terminal conditions upon $\bar{y}$ were

$$y_1(t_f) = \cos \theta_f \; ; \qquad y_2(t_f) = \sin \theta_f \; ; \qquad y_3(t_f) = 0 \; .$$

and the terminal state was $h_x(t_f) = h_y(t_f) = 0$, $h_z(t_f) = 1$. For each combination of θ_i, ϕ, and δ, eight values of θ_f were employed. The runs were allowed to proceed until the attitude error increased to 90 deg. The results, as in the feedback control runs, were plotted in the (h_x, h_y) plane. In addition, the time required to reach an error of 90 deg was recorded but has little meaning since at least a few of the trajectories generated were nonoptimal.

2. Simulation Results

Qualitatively, the trajectories generated in this study are very similar to those from the feedback control; moreover, the "speed" of response differs very little. For the special case of $\phi = 0$

---

* In the runs presented here α, the orbit position (Fig. 2-1) was zero at $t = t_f$; however, additional runs indicated that variation of $\alpha(t_f)$ altered the small-error optimum trajectories without materially affecting the motion for large errors.

(corresponding to orientation of the spin axis normal to the orbit plane), this similarity is very pronounced and the feedback control is an excellent approximation (except very near the origin) to the minimum-time control.

Figures 6-1, 6-2, and 6-3 are the optimal trajectories generated for $\phi = \delta = 0$; these runs are directly comparable to the feedback control results presented in Figs. 5-4, 5-6, and 5-8. The similarities

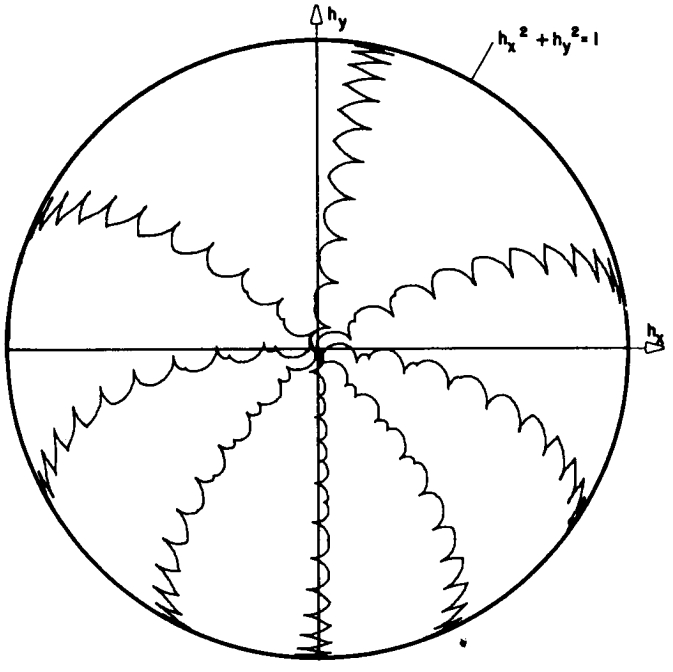

FIG. 6-1. MINIMAL-TIME (h_x, h_y) TRAJECTORIES FOR $\theta_i = 30°$, $\phi = 0°$, $\delta = 0°$.

are very striking, except near the origin where the feedback system chatters and, as a result, converges more slowly. It is interesting to observe that, whereas the feedback control switches by definition when $\dot{h}_z = 0$, this is not always so for the optimal solution; for example, at the switch point (a) of Fig. 6-3, $\dot{h}_z$ is nonzero.

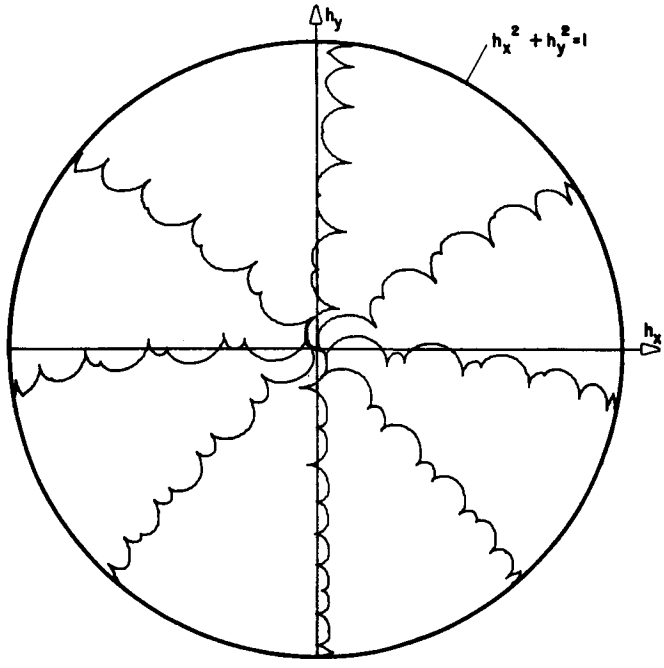

FIG. 6-2. MINIMAL-TIME (h_x, h_y) TRAJECTORIES FOR $\Theta_i = 60°$ $\emptyset = 0°$, $\delta = 0°$.

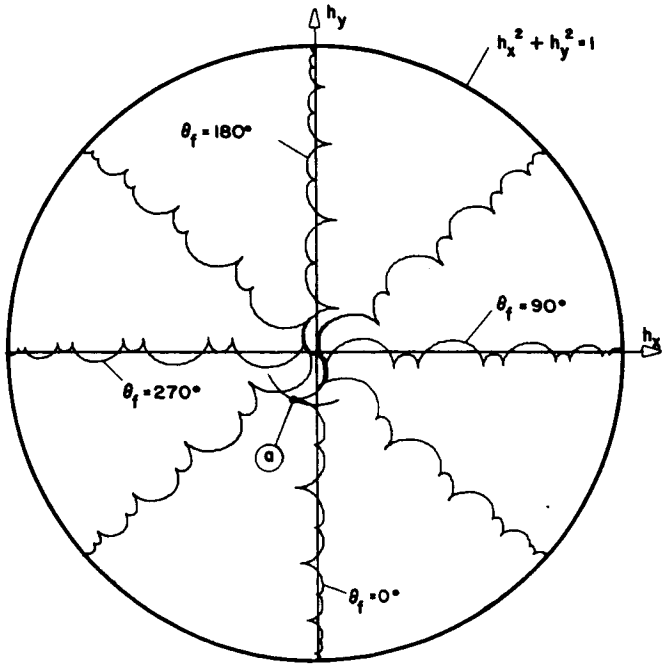

FIG. 6-3. MINIMAL-TIME (h_x, h_y) TRAJECTORIES FOR $\Theta_i = 90°$, $\emptyset = 0°$, $\delta = 0°$.

The cause of this similarity can be explained by examining the control equation and the auxiliary differential equation (concerning $\bar{y}$). The control equation is

$$u = U_o \text{ sgn } (\bar{B} \cdot \bar{y})$$

where the argument can be expanded to yield:

$$\bar{B} \cdot \bar{y} = B_{xR}(p_2 h_z - p_3 h_y) + B_{yR}(p_3 h_x - p_1 h_z) + B_{zR}(p_1 h_y - p_2 h_x) . \tag{6.13}$$

Consider the form of (6.13) if y_3 is assumed to remain zero all during the solution. Then

$$\bar{B} \cdot \bar{y} = B_{xR}(p_2 h_z - p_3 h_y) + B_{yR}(p_3 h_x - p_1 h_z) . \tag{6.14}$$

With $\bar{h}$, $\bar{p}$, and $\bar{y}$ comprising an orthonormal set

$$\bar{h} = \bar{y} \times \bar{p} . \tag{6.15}$$

Using the definition of y_1 and y_2, and assuming y_3 to be zero, (6.15) yields:

$$\begin{aligned} h_x &= p_3(p_3 h_x - p_1 h_z) \\ h_y &= - p_3(p_2 h_z - p_3 h_y) \end{aligned} \tag{6.16}$$

Combination with (6.14) gives

$$\bar{B} \cdot \bar{y} = \frac{1}{p_3} (B_{yR} h_x - B_{xR} h_y) \tag{6.17}$$

which, for $p_3 > 0$, is equivalent to the feedback control error function (3.2) for the simplified equations of motion. It remains to show that $p_3 > 0$. From (6.9)

$$\dot{p}_3 = - (B_{xR} p_2 - B_{yR} p_1) u \tag{6.18}$$

where $\dot{p}_3 = dp_3/dt = -dp_3/d\tau$ and τ is the reverse time. In a manner similar to the derivation of (6.17), we can show that

$$\bar{B} \cdot \bar{y} = \frac{B_{xR}p_2 - B_{yR}p_1}{h_z}$$

so that $dp_3/d\tau \geq 0$ throughout the reverse-time optimum trajectory. The overall situation is as pictured in Fig. 6-4. The reverse time motion begins as shown in (a) and proceeds to the state shown in (b), if y_3 remains near zero for the entire solution.

Examination of the variation of $\bar{y}$ for the cases with $\emptyset = 0$ indicates that y_3 does remain quite small (but not zero) throughout the runs, and, as has been shown, this accounts for the similarity between the minimum time and feedback controls.

Figure 6-5 involves a case for which $\emptyset$ is nonzero. The equivalent feedback run is presented in Fig. 5-7. Notice that all but two of the trajectories of Fig. 6-5 (those with $h_y \approx 0$) are plainly dissimilar to the feedback trajectories. However, the convergence speeds do not differ by much, and the performance of the feedback system compares favorably to that of the minimum-time system. Notice that in two cases the trajectories cross. This does not necessarily mean that one of the trajectories is not optimum because, unless when they cross the periodic coefficients are identical (at times differing by an integral number of half orbits), the runs are not directly comparable.

Figure 6-6 is particularly interesting because it shows a clear case of a trajectory which is not optimum, even though it satisfies the necessary conditions. Trajectory ① begins (in forward time) at point $(t_o)_1$, moves counterclockwise through point $(t_o)_2$, reverses itself and continues to the origin, requiring a total time corresponding to 6.7 orbits. Now the time required to move from point $(t_o)_1$ to point $(t_o)_2$ is much less than an orbit. So if instead of following ①, the control were removed at point $(t_o)_2$ and reapplied to follow trajectory ② at the first time when $(t_o)_1+t = (t_o)_2+nT$, where T is the period of the periodic coefficients (one-half orbit), an upper

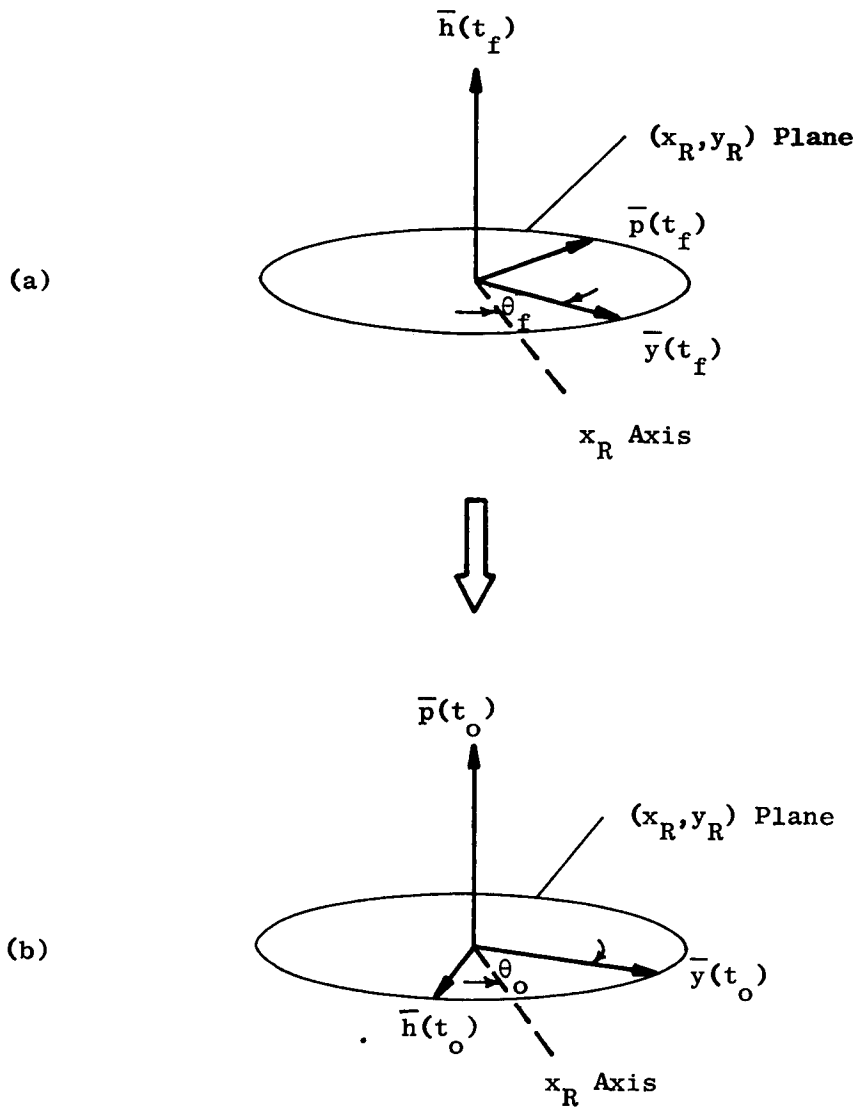

FIG. 6-4. REVERSE-TIME MOTION OF $\bar{h}$, $\bar{p}$, AND $\bar{y}$ FOR $y_3(t) \approx 0$.

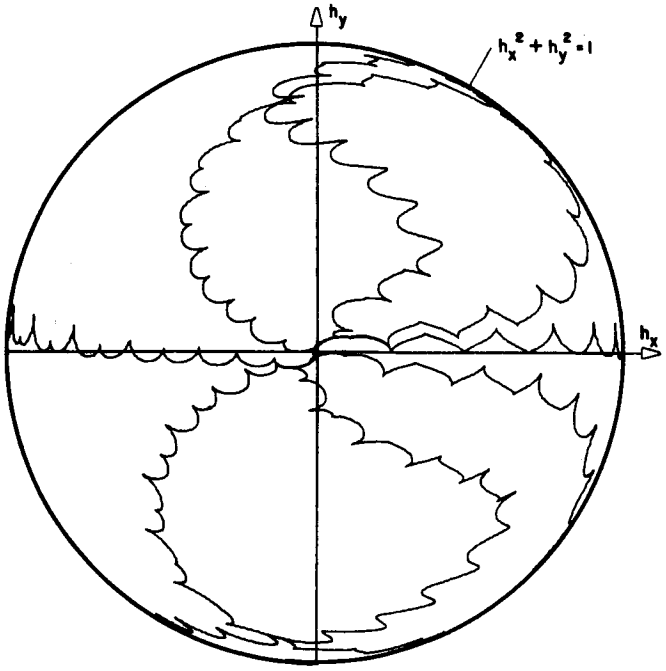

FIG. 6-5. MINIMAL-TIME (h_x, h_y) TRAJECTORIES FOR $\theta_i = 60°$, $\phi = 60°$, $\delta = -90°$.

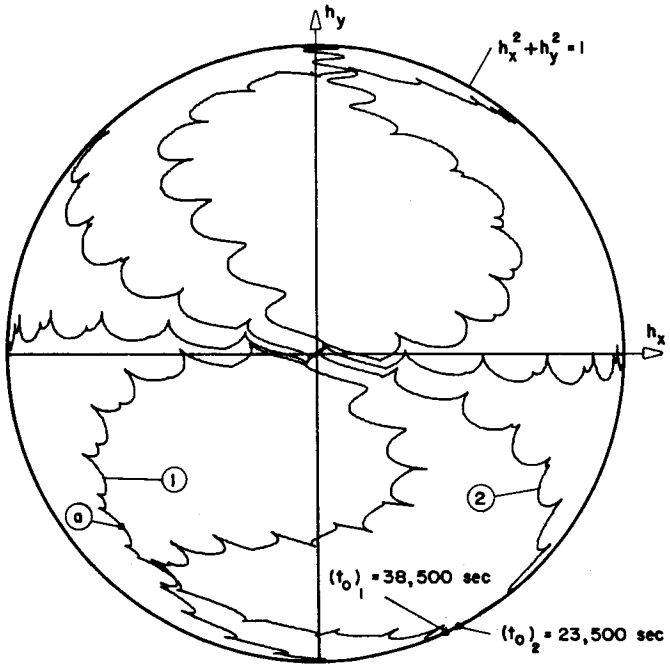

FIG. 6-6. MINIMAL-TIME (h_x, h_y) TRAJECTORIES FOR $\theta_i = 60°$, $\phi = 90°$, $\delta = 0°$.

limit on the total time would be $(t_o)_2+3T$ or 5.6 orbits. Furthermore, this solution also is not the optimum since the minimum-time control must be a signum control and therefore cannot be deactivated. Hence, although ① may represent a minimum-time path to the origin for some points on it (for example, ⓐ), it is not an optimum trajectory along its entire length.

As a final specific case, consider Figs. 6-7 and 6-8. Figure 6-7 represents the effect of feedback control for $\theta_i = \emptyset = 90°$ and $\delta = 0$.

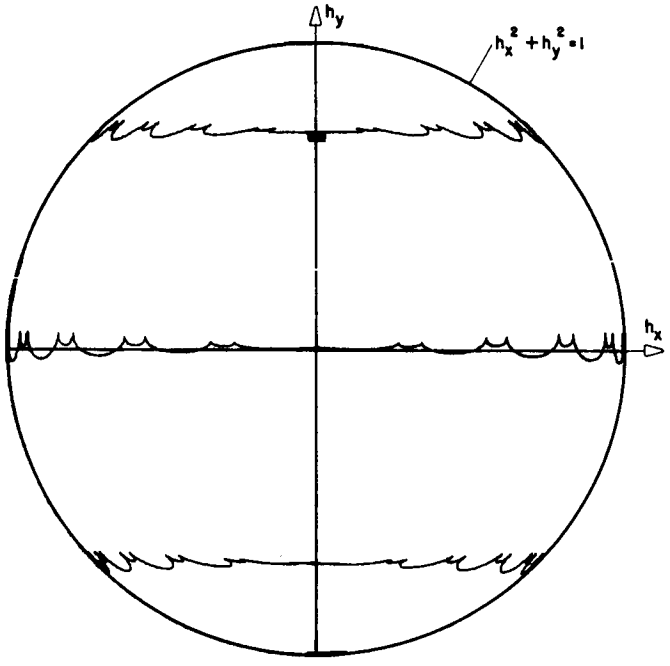

FIG. 6-7. FEEDBACK CONTROL (h_x, h_y) TRAJECTORIES FOR $\theta_i = 90°$, $\emptyset = 90°$, $\delta = 0°$.

Notice that all motions terminate (neglecting terminal chatter) on the line $h_x = 0$ as predicted in the stability analysis for the simplified model with the untilted dipole. Figure 6-8 shows the minimum time trajectories for the same case (the very slow trajectories marked by an asterisk were not run to completion). These results are of interest primarily because they show that even though the feedback control does

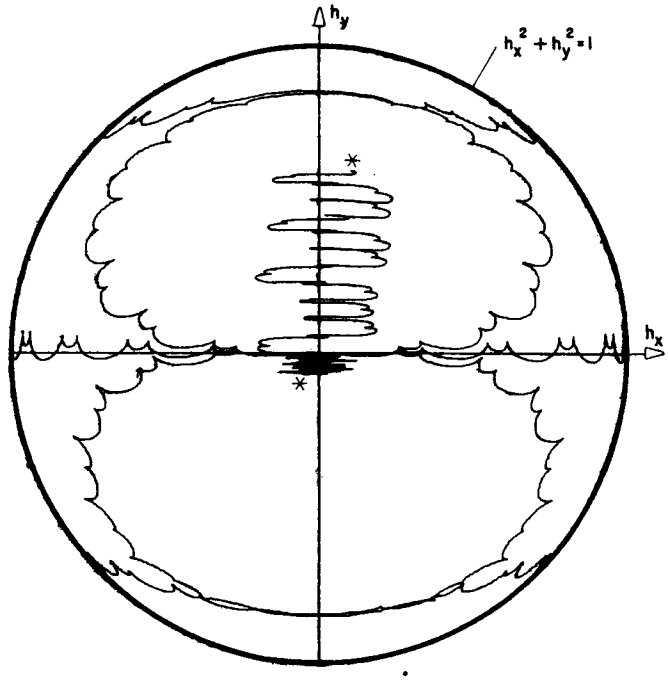

FIG. 6-8. MINIMAL-TIME (h_x, h_y) TRAJECTORIES FOR $\theta_i = 90°$, $\phi = 90°$, $\delta = 0°$.

not give asymptotic stability in this case, there is a control program which will produce convergence. It must be recalled, however, that this case is of academic interest only, because with the more realistic tilted dipole model of the earth's magnetic field the feedback control system is asymptotically stable in-the-large for all cases.

D. SUMMARY

The feedback control system developed in Chapter III has been shown to compare very favorably with minimum-time control of the simplified equations of motion, except very near the origin. This small-error dissimilarity is not considered important because:

1. Signum control is probably not desirable near the origin, due to the possibility of chatter.

2. In many applications intermittent (rather than continuous) control may be preferred for small-error control. The role of the continuous

control scheme developed here would be the reduction of the initial errors to the point where the intermittent control scheme could maintain control.

3. The primary criterion for small-error control is the maintenance of the specified attitude accuracy, in the presence of external disturbances, with the minimum possible energy expenditure.

VII. MAGNETIC CONTROL WITH DISTURBANCES

The lifetime of a satellite is typically composed of a short interval (a day or less) during which the nominal attitude orientation is initially acquired and a longer period (a month or more) during which the attitude control system must maintain the required orientation accuracy in the face of disturbances. Although the initial transient (acquisition) mode of operation is important, the steady-state mode of operation will be the primary factor in determining the total fuel (or energy) consumed by the control system.

Current design practice is to require of the acquisition mode only that the nominal orientation be attained successfully within a specified time following separation of the satellite from the booster. The criterion for operation in the steady-state mode is the maintenance of the specified control accuracy with the least control effort.

In this chapter the forced response of the magnetically controlled spinning satellite is discussed, using techniques analogous to those employed in Chapter V to analyze the unforced small-error motion with the exact equations of motion. The disturbances considered are of two types: (i) motion of the reference frame (x_R, y_R, z_R) in inertial space (kinematic disturbances), and (ii) environmental torques upon the vehicle (dynamic disturbances). Of the latter, this discussion is restricted to aerodynamic pressure torques, solar radiation torques, gravity-gradient torques, and torques due to residual magnetic moments in the vehicle. For the pressure torques, the outer structure of the vehicle will be assumed spherically shaped.

Notably absent from this list is the torque due to eddy currents induced in the satellite. Although they are not always negligible, it is not unrealistic to restrict this discussion to cases in which they are. For example, the eddy current torque on a homogeneous, spherical, thin-walled, spinning shell has been shown by Vinti [Ref. 7-1] to be approximately proportional to $(\bar{\omega}\times\bar{B})\times\bar{B}$, where $\bar{\omega}$ is the total angular velocity of the shell and $\bar{B}$ is the environmental magnetic field. Put in the form of a cross-product of a magnetic moment $\bar{\omega}\times\bar{B}$ with a magnetic field vector $\bar{B}$, it can be seen that, for a vehicle spinning about its

nominal spin axis, the eddy currents produce a magnetic moment normal to the spin axis, z_b. The lines of current flow are circles about the transverse diameter of the satellite defined by $\bar{e}_{zb} \times \bar{B}$, and each current path traverses parts of both the upper and lower hemispheres of the spherical shell. It is clear, then, that this current distribution will be completely disrupted (and the magnitude of the eddy current torques greatly reduced) if the satellite is assembled from two hemispheres with an insulating layer between the half-shells. The plane of joining must, of course, be normal to the nominal spin axis. This scheme of lamination can be extended to more realistic satellite configurations for which, owing to their shape and/or their lack of conductive homogeneity, the eddy currents cannot be readily evaluated.

One parameter which is not often at the disposal of the designer of the control system is ω_s, the spin speed. As will be seen, the attitude drift rate due to disturbance torques is inversely proportional to the spin rate. The level of control torque required to alter the attitude at a given rate is similarly related to the spin speed. On the other hand, the kinematic error buildup due to motion of the reference frame is unaffected by ω_s. Thus, from the attitude control viewpoint, the spin rate should be large enough to provide the vehicle with short-term gyroscopic stability without being so large that the cost of tracking the moving reference axes becomes prohibitive.* Clearly this is a tradeoff which involves the relative amplitudes of the kinematic and dynamic disturbances, and is, therefore, a function of each particular application.

A. DISTURBANCES

1. Motion of the Reference Coordinate Frame

The components in reference coordinates of the inertial angular velocity, $\bar{\Omega}^R$, of the reference axes are Ω_x, Ω_y, and Ω_z. These components are

---

* This is the reason that spin stabilization is impractical if the axis of desired orientation, z_R, is moving rapidly in inertial space. We would not, for example, attempt to align a spinning satellite with the vehicle-earth line (local vertical).

mission dependent; for example, if the spin axis is to be pointed at a star, $\bar{\Omega}^R$ is essentially zero, while if the vehicle is sun oriented, the magnitude of $\bar{\Omega}^R$ is approximately one deg per day.

One other example of special interest is that in which the spin axis is aligned normal to the orbit plane. In this case, $\phi = \delta = 0$ and the (x_R, y_R, z_R) coordinate frame is aligned with the (x_n, y_n, z_n) axes (see Fig. 2-1). The total angular rate $\bar{\Omega}^R$ is

$$\bar{\Omega}^R = \dot{\beta}\bar{e}_{za} \tag{7.1}$$

Resolution into reference coordinates yields:

$$\begin{aligned} \Omega_x &= 0 \\ \Omega_y &= \dot{\beta} \sin \theta_i \\ \Omega_z &= \dot{\beta} \cos \theta_i \end{aligned} \tag{7.2}$$

where $\dot{\beta}$ is given in Chapter II.

2. Disturbance Torques

a. Aerodynamic Pressure

For altitudes in excess of 100 nautical miles it is reasonable to consider the atmosphere as an aggregation of stationary molecules through which the vehicle is moving at a high speed.* Each molecule which impacts with the vehicle has a certain probability of "sticking" to (being accommodated by) the satellite (and imparting all of its relative momentum to the vehicle), or of being reemitted from the satellite (in this case a nondissipative collision will be assumed). Under these circumstances, the pressure and shear on the differential area of Fig. 7-1 are [Ref. 7-2]:

---

* The vehicle velocity is much greater than the RMS molecular velocity of the atmosphere.

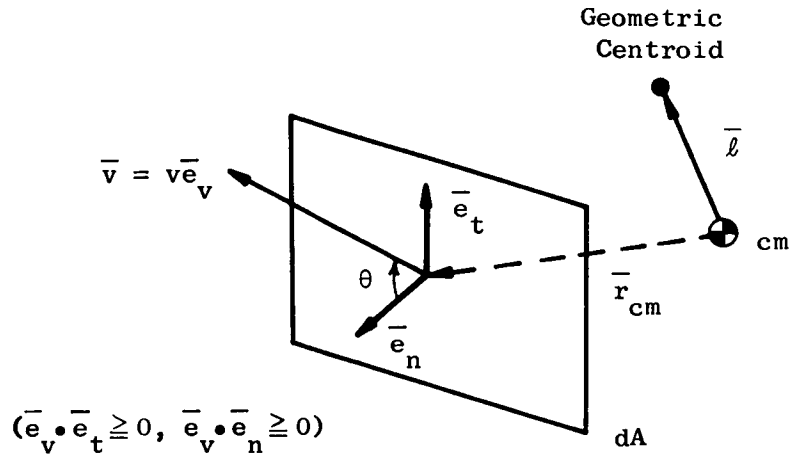

FIG. 7-1. AERODYNAMIC FORCES ON A DIFFERENTIAL AREA.

$$p_a = (2 - f_n)\rho_a v^2 \cos^2 \theta \quad \text{lb/ft}^2$$

$$\tau_a = f_t \rho_a v^2 \sin \theta \cos \theta \quad \text{lb/ft}^2$$

where $\bar{v} = v\bar{e}_v$ is the vehicle velocity (for circular orbits $\bar{e}_v = \bar{e}_{yo}$ as defined in Fig. 2-1), $\bar{e}_n$ is the outward unit vector normal to dA, ρ_a is the atmospheric density, f_t is the tangential accommodation coefficient, and f_n is the normal accommodation coefficient (see Ref. 7-2). The total incremental force, resolved along the orthogonal unit vectors $\bar{e}_t$ and $\bar{e}_n$ is

$$d\bar{F}_a = -\rho_a v^2 \{(2 - f_n)(\bar{e}_v \cdot \bar{e}_n)^2 \bar{e}_n + f_t(\bar{e}_v \cdot \bar{e}_n)[\bar{e}_n \times (\bar{e}_v \times \bar{e}_n)]\} dA \tag{7.3}$$

The force may also be resolved with respect to the nonorthogonal directions $\bar{e}_v$ and $\bar{e}_n$:

$$d\bar{F}_a = -2q^*\left[(2 - f_n - f_t)(\bar{e}_v \cdot \bar{e}_n)^2 \bar{e}_n + f_t(\bar{e}_v \cdot \bar{e}_n)\bar{e}_v\right] dA \tag{7.4}$$

where q^* is the dynamic pressure (see Fig. 7-2).

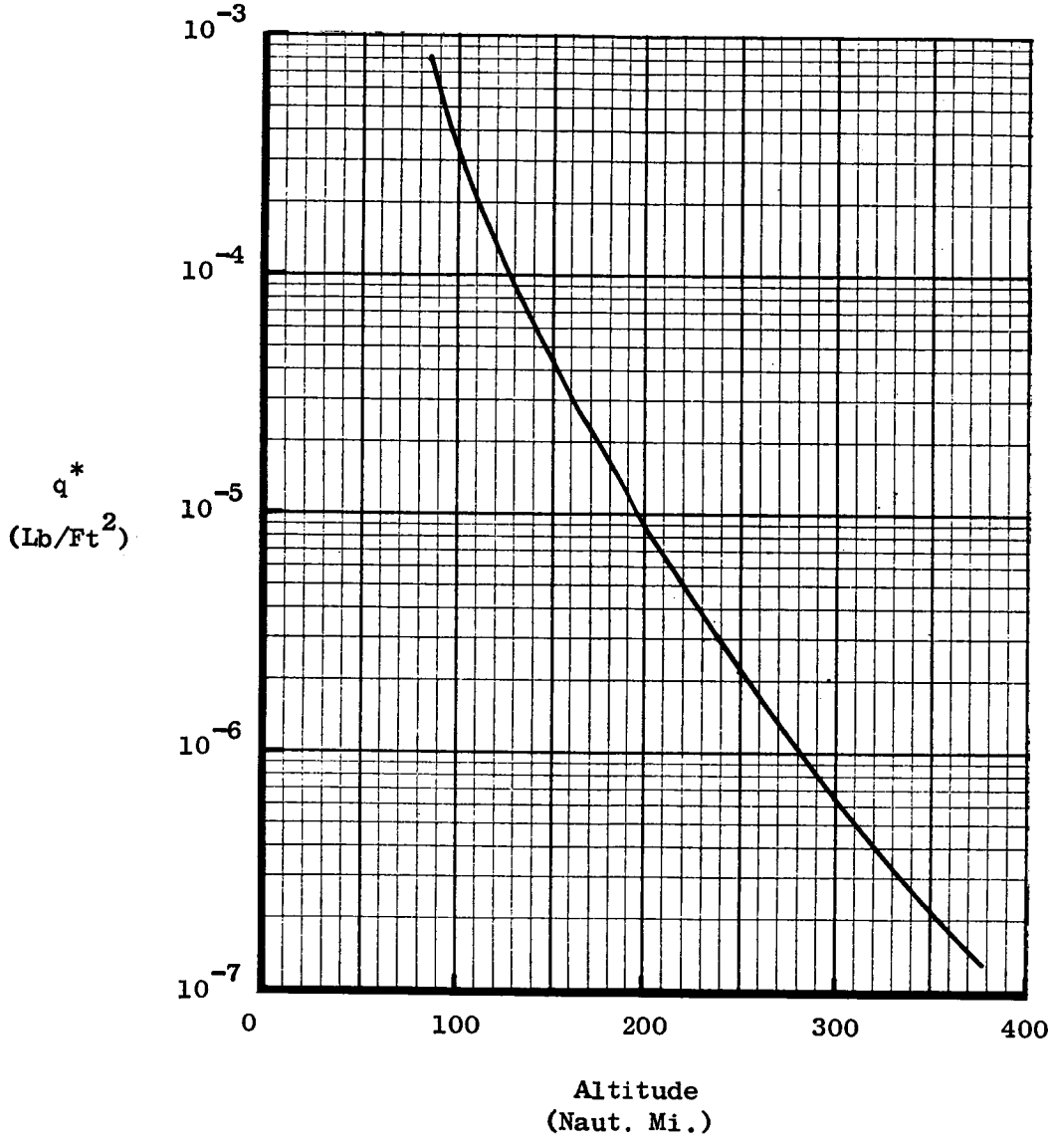

FIG. 7-2. DYNAMIC PRESSURE FOR LOW ALTITUDE CIRCULAR ORBITS (ARDC 1959 ATMOSPHERE).

The incremental torque upon the vehicle is

$$d\bar{N} = \bar{r}_{cm} \times d\bar{F}_a \tag{7.5}$$

where, of course, $d\bar{F}_a$ is taken to be zero if the differential area is shaded from the air stream by some other portion of the vehicle.

For a vehicle with a spherical outer structure, the total force acts through the geometrical centroid in the direction $-\bar{e}_v$. If $\bar{\ell}$ is the vector from the center of mass to the geometric centroid, the aerodynamic torque is:

$$\bar{N}_a = \bar{\ell} \times \bar{F}_a \tag{7.6}$$

The total aerodynamic force is, by integration of (7.4) over one hemisphere, found to be:

$$\bar{F}_a = -(2 + f_t - f_n)\pi R_b^2 q^* \bar{e}_v \quad \text{lb} \tag{7.7}$$

where the quantity in parenthesis is the drag coefficient, C_D, and R_b is the radius of the vehicle. According to Schamberg [Ref. 7-3] the drag coefficient is approximately 2.63 for spherical satellites.

As in Chapter V, the equations of motion in the "despun" coordinate system (x_1, y_1, z_1) will be used. After expressing $\bar{F}_a$ and $\bar{\ell}$ in this coordinate system, formation of the indicated cross-product gives:

$$\begin{bmatrix} n_{a1} \\ \\ n_{a2} \end{bmatrix} = D_a \begin{bmatrix} -\ell_3 v_{a2} + \ell_2 v_{a3} - \ell_2 v_{a1} c_{13} - (\ell_3 v_{a3} + \ell_2 v_{a2}) c_{23} \\ \\ \ell_3 v_{a1} - \ell_1 v_{a3} + (\ell_3 v_{a3} + \ell_1 v_{a1}) c_{13} + \ell_1 v_{a2} c_{23} \end{bmatrix} \tag{7.8}$$

where:

$$D_a = - \frac{C_D \pi R_b^2 q^*}{I_x}$$

$$v_{a1} = \bar{e}_{yo} \cdot \bar{e}_{xR} = - \cos \phi \sin (\alpha - \delta)$$

$$v_{a2} = \bar{e}_{yo} \cdot \bar{e}_{yR} = \cos (\alpha - \delta)$$

$$v_{a3} = \bar{e}_{yo} \cdot \bar{e}_{zR} = - \sin \phi \sin (\alpha - \delta)$$

$$\ell_1 = \bar{\ell} \cdot \bar{e}_{x1} = \ell_x \cos \gamma - \ell_y \sin \gamma$$

$$\ell_2 = \bar{\ell} \cdot \bar{e}_{y1} = \ell_x \sin \gamma + \ell_y \cos \gamma$$

$$\ell_3 = \bar{\ell} \cdot \bar{e}_{z1} = \ell_z .$$

The components of the geometric centroid--center of mass offset in the body-fixed (x_b, y_b, z_b) coordinate system are ℓ_x, ℓ_y, and ℓ_z. The angle γ, defined in expression (2.4), varies at spin rate $(\dot{\gamma} = \omega_s)$. The aerodynamic torque is seen, from expression (7.8), to contain no terms which have a nonzero average over an orbit.

b. Solar Radiation Pressure

The solar radiation pressure torque upon a satellite can be determined using a momentum interchange model analogous to the one for aerodynamic torques, where, in this case, the vehicle velocity is negligible with respect to the particle velocity. Using such a model (and assuming that the probability of reflection of tangentially incident photons is the same as that of normally incident photons) the following result is presented in Ref. 7-4:

$$d\bar{F}_s = - V_s \{(1 + \nu)(\bar{e}_{xs} \cdot \bar{e}_n)^2 \bar{e}_n + (1 - \nu)(\bar{e}_{xs} \cdot \bar{e}_n)[\bar{e}_n \times (\bar{e}_{xs} \times \bar{e}_n)]\} dA \tag{7.9}$$

where ν is the solar reflectivity $(0 \leq \nu \leq 1)$, $\bar{e}_{xs}$ is the unit vector from the vehicle to the sun, and V_s is the solar radiation pressure

constant. (V_s varies as the inverse of the square of the distance from the vehicle to the sun, and is approximately 0.94×10^{-7} lb/ft^2 in the vicinity of the earth's orbit.) Notice that expression (7.3) yields expression (7.9) if the following replacements are made:

$$\rho_a v^2 \longrightarrow V_s$$

$$f_n \longrightarrow 1 - \nu$$

$$f_t \longrightarrow 1 - \nu$$

$$\bar{e}_v \longrightarrow \bar{e}_{xs} .$$

By analogy with (7.8), the accelerations due to solar radiation pressure are:

$$\begin{bmatrix} n_{s1} \\ \\ n_{s2} \end{bmatrix} = D_s \begin{bmatrix} -\ell_3 v_{s2} + \ell_2 v_{s3} - \ell_2 v_{s1} c_{13} - (\ell_3 v_{s3} + \ell_2 v_{s2}) c_{23} \\ \\ \ell_3 v_{s1} - \ell_1 v_{s3} + (\ell_3 v_{s3} + \ell_1 v_{s1}) c_{13} + \ell_1 v_{s2} c_{23} \end{bmatrix} \qquad (7.10)$$

where

$$D_s = - \frac{\pi R_b^2 V_s}{I_x}$$

$$v_{s1} = \bar{e}_{xs} \cdot \bar{e}_{xR}$$

$$v_{s2} = \bar{e}_{xs} \cdot \bar{e}_{yR}$$

$$v_{s3} = \bar{e}_{xs} \cdot \bar{e}_{zR}$$

and ℓ_1, ℓ_2, and ℓ_3 are defined as before. (Occultation of the sun by the earth is neglected.)

In order to determine the components of $\bar{e}_{xs}$ in reference coordinates, $\bar{e}_{xs}$ is assumed equivalent to the earth-sun line (for earth satellites this is a good approximation). In this case, $\bar{e}_{xs}$, which moves in the ecliptic plane, can be referenced to the inertial (x_e, y_e, z_e) coordinate system as shown in Fig. 7-3. The angle S is zero at the Vernal Equinox. Applying the transformations indicated by Figs. 2-1, 2-3, and 7-3:

$$
\begin{aligned}
v_{s1} &= -\cos\phi\cos\delta(\cos\beta\cos S + \cos\zeta\sin\beta\sin S) \\
&\quad + \cos\phi\sin\delta[\cos\theta_i(\sin\beta\cos S - \cos\zeta\cos\beta\sin S) + \sin\theta_i\sin\zeta\sin S] \\
&\quad + \sin\phi[\sin\theta_i(\sin\beta\cos S - \cos\zeta\cos\beta\sin S) - \cos\theta_i\sin\zeta\sin S] \\
v_{s2} &= \sin\delta(\cos\beta\cos S + \cos\zeta\sin\beta\sin S) \\
&\quad + \cos\delta[\cos\theta_i(\sin\beta\cos S - \cos\zeta\cos\beta\sin S) + \sin\theta_i\sin\zeta\sin S] \\
v_{s3} &= -\sin\phi\cos\delta(\cos\beta\cos S + \cos\zeta\sin\beta\sin S) \\
&\quad + \sin\phi\sin\delta[\cos\theta_i(\sin\beta\cos S - \cos\zeta\cos\beta\sin S) + \sin\theta_i\sin\zeta\sin S] \\
&\quad - \sin\delta[\sin\theta_i(\sin\beta\cos S - \cos\zeta\cos\beta\sin S) - \cos\theta_i\sin\zeta\sin S] .
\end{aligned}
\tag{7.11}
$$

These coefficients are essentially constant over an interval of a day; thus, the terms $\ell_3 v_{s2}$ and $\ell_3 v_{s1}$ in expression (7.10) will be considered as constant forcing torques for evaluation of the steady-state response.

c. Gravity Gradient

As shown in Ref. 7-5, the gravity gradient torque upon a satellite in a circular orbit is, in body-fixed coordinates:

$$
\begin{bmatrix} N_{xb} \\ N_{yb} \\ N_{zb} \end{bmatrix} = 3\omega_o^2 \begin{bmatrix} (I_z - I_y)(\bar{e}_{xo}\cdot\bar{e}_{yb})(\bar{e}_{xo}\cdot\bar{e}_{zb}) \\ (I_x - I_z)(\bar{e}_{xo}\cdot\bar{e}_{xb})(\bar{e}_{xo}\cdot\bar{e}_{zb}) \\ (I_y - I_x)(\bar{e}_{xo}\cdot\bar{e}_{xb})(\bar{e}_{xo}\cdot\bar{e}_{yb}) \end{bmatrix} \tag{7.12}
$$

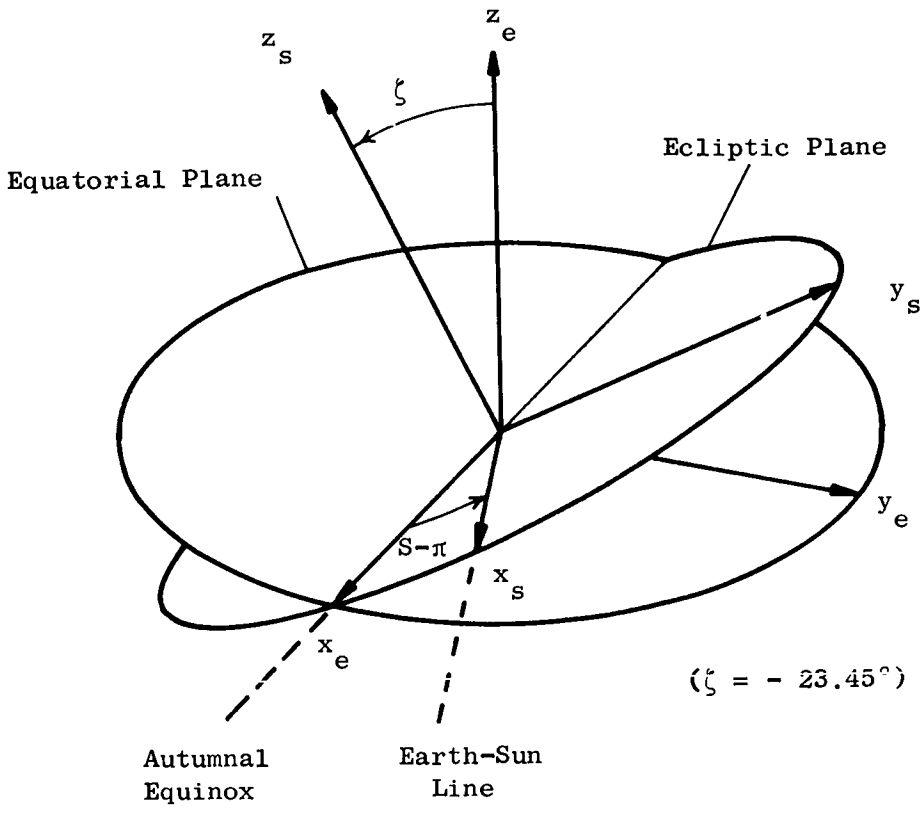

FIG. 7-3. MOTION OF THE EARTH-SUN LINE IN EQUATORIAL COORDINATES.

By suitable transformation the components of gravity gradient acceleration along the x_1 and y_1 axes are determined to be, for an axially symmetric vehicle:

$$\begin{bmatrix} n_{g1} \\ \\ n_{g2} \end{bmatrix} = 3k\omega_o^2 \begin{bmatrix} (\bar{e}_{xo} \cdot \bar{e}_{y1})(\bar{e}_{xo} \cdot \bar{e}_{z1}) \\ \\ -(\bar{e}_{xo} \cdot \bar{e}_{x1})(\bar{e}_{xo} \cdot \bar{e}_{z1}) \end{bmatrix} \tag{7.13}$$

In terms of the attitude variables and the components of the unit local vertical vector $(\bar{e}_{xo})$ in reference coordinates:

$$\begin{bmatrix} n_{g1} \\ \\ n_{g2} \end{bmatrix} = D_g \begin{bmatrix} v_{g2}v_{g3} - v_{g1}v_{g2}c_{13} + (v_{g3}^2 - v_{g2}^2)c_{23} \\ \\ -v_{g1}v_{g3} - (v_{g3}^2 - v_{g1}^2)c_{13} + v_{g1}v_{g2}c_{23} \end{bmatrix} \tag{7.14}$$

where

$$D_g = 3k\omega_o^2$$

$$v_{g1} = \bar{e}_{xo} \cdot \bar{e}_{xR} = \cos \phi \cos (\alpha - \delta)$$

$$v_{g2} = \bar{e}_{xo} \cdot \bar{e}_{yR} = \sin (\alpha - \delta)$$

$$v_{g3} = \bar{e}_{xo} \cdot \bar{e}_{zR} = \sin \phi \cos (\alpha - \delta) \ .$$

It is particularly interesting to examine the character of the attitude-independent terms in (7.14). Forming the indicated products:

$$\begin{aligned} v_{g2}v_{g3} &= \frac{1}{2} \sin \phi \sin 2(\alpha - \delta) \\ v_{g1}v_{g3} &= \frac{1}{2} \sin \phi \cos \phi [1 + \cos 2(\alpha - \delta)] \ . \end{aligned} \tag{7.15}$$

Thus, unless ϕ is 0 deg, 90 deg, or 180 deg, gravity gradient will produce a constant forcing term.

d. Residual Magnetic Moment

In any satellite there will be an undesirable magnetic moment made up of a residual component (essentially constant) due to magnetization of various parts of the vehicle, and a time-varying component caused by currents flowing in the vehicle (e.g., current flowing to or from the battery). Considering only the residual magnetic moment, the torque is

$$\bar{N} = 6.86 \times 10^{-6} \bar{m} \times \bar{B} \tag{7.16}$$

where $\bar{m}$ is measured in amp-ft^2 and $\bar{B}$ is in gauss. The components of acceleration due to this effect are:

$$\begin{bmatrix} n_{m1} \\ \\ n_{m2} \end{bmatrix} = D_m \begin{bmatrix} -B_{yR}m_3 + B_{zR}m_2 - B_{xR}m_2c_{13} - (B_{zR}m_3 + B_{yR}m_2)c_{23} \\ \\ B_{xR}m_3 - B_{zR}m_1 + (B_{zR}m_3 + B_{xR}m_1)c_{13} + B_{yR}m_1c_{23} \end{bmatrix} \quad (7.17)$$

where

$$D_m = \frac{6.86 \times 10^{-6}}{I_x}$$

$$B_{xR} = -\frac{M_e}{2r_o^3}\{[\sin\delta + 3\sin(2\alpha - \delta)]\cos\phi\sin\theta_i + 2\sin\phi\cos\theta_i\}$$

$$B_{yR} = -\frac{M_e}{2r_o^3}\{[\cos\delta - 3\cos(2\alpha - \delta)]\sin\theta_i\}$$

$$B_{zR} = -\frac{M_e}{2r_o^3}\{[\sin\delta + 3\sin(2\alpha - \delta)]\sin\phi\sin\theta_i - 2\cos\phi\cos\theta_i\}$$

$$m_1 = m_x\cos\gamma - m_y\sin\gamma$$

$$m_2 = m_x\sin\gamma + m_y\cos\gamma$$

$$m_3 = m_z$$

and m_x, m_y, m_z are the body-fixed constant components of residual magnetic moment.

The magnetic field components B_{xR} and B_{yR} can have an average value. Therefore, if m_z is nonzero, a steady forcing torque will be produced. It is interesting that such a residual magnetic moment along the spin axis is equivalent to a bias in the control magnetic moment; with proportional control m_z will amount to an offset of the null point in the control characteristic as shown in Fig. 7-4.

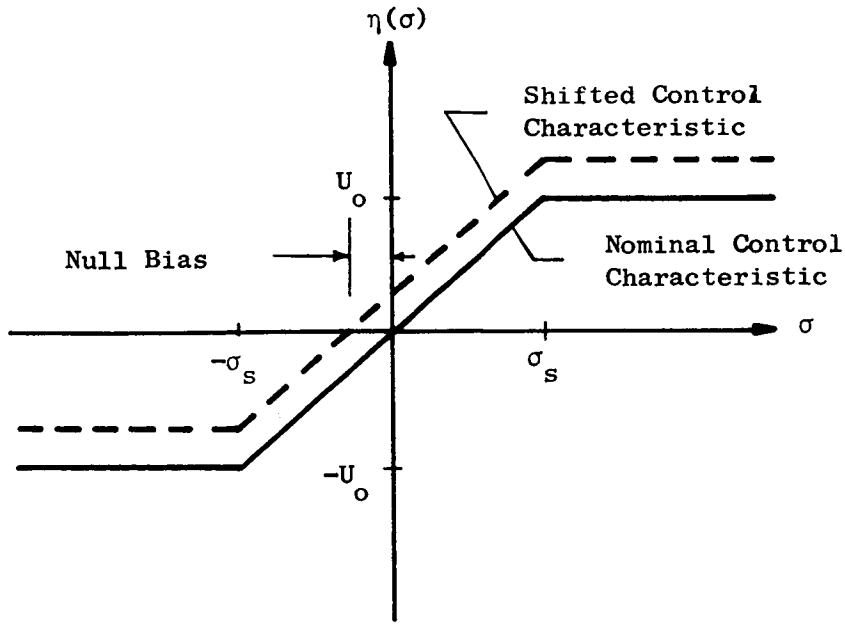

FIG. 7-4. SHIFT OF THE CONTROL CHARACTERISTIC BY A RESIDUAL SPIN AXIS MAGNETIC MOMENT (EXAGGERATED).

B. SYSTEM RESPONSE TO DISTURBANCES

Assuming proportional control, the small-error equations of motion with disturbances (see Chapter II) are, neglecting second-order terms of the type $c_{13}\Omega_y$, etc:

$$\begin{aligned}
\dot{\omega}_1 &= -\omega_n(\omega_2 + KB_{yR}\sigma) + n_1 \\
\dot{\omega}_2 &= \omega_n(\omega_1 + KB_{xR}\sigma) + n_2 \\
\dot{c}_{13} &= -\omega_2 + \Omega_y \\
\dot{c}_{23} &= \omega_1 - \Omega_x
\end{aligned} \tag{7.18}$$

where

$$\sigma = B_{xR}(c_{23} - K_R\omega_2) - B_{yR}(c_{13} - K_R\omega_1)$$

$$\omega_n = (1 + k)\omega_s \ .$$

Examination of the torque equations derived above shows that n_1 and n_2 can be written in the general form:

$$\begin{aligned} n_1 &= n_{10} + n_{11} \cos\gamma + n_{12} \sin\gamma \\ n_2 &= n_{20} + n_{21} \cos\gamma + n_{22} \sin\gamma \end{aligned} \tag{7.19}$$

where the n_{ij} (neglecting torque terms which are attitude dependent) are:

$$\begin{aligned} n_{10} &= D_g v_{g2} v_{g3} - D_s \ell_z v_{s2} - D_a \ell_z v_{a2} - D_m m_z B_{yR} \\ n_{20} &= -D_g v_{g1} v_{g3} + D_s \ell_z v_{s1} + D_a \ell_z v_{a1} + D_m m_z B_{xR} \\ n_{11} &= n_{22} = D_s \ell_y v_{s3} + D_a \ell_y v_{a3} + D_m m_y B_{zR} \\ n_{12} &= -n_{21} = D_s \ell_x v_{s3} + D_a \ell_x v_{a3} + D_m m_x B_{zR} \ . \end{aligned} \tag{7.20}$$

The parameters in (7.20) are defined in expressions (7.8), (7.10), (7.14), and (7.17).

The disturbance accelerations, as well as the control terms, are so small that the variables χ_1, χ_2, and a (see Chapter V) defined by

$$\begin{aligned} \omega_1 &= a \cos\xi \\ \omega_2 &= a \sin\xi \\ c_{13} &= \chi_1 + \frac{\omega_1}{\omega_n} \\ c_{23} &= \chi_2 + \frac{\omega_2}{\omega_n} \end{aligned} \tag{7.21}$$

are slowly varying to a good approximation. Let a_o, χ_{10}, and χ_{20} be the slowly varying solutions to the first approximation of Krylov and Bogoliubov [Ref. 5-1]. Following the procedure used in Chapter V:

$$\dot{a}_o = -\left[K(K_R\omega_n - 1)\frac{B_{xR}^2 + B_{yR}^2}{2}\right]a_o + \underset{\xi}{\text{ave}}\{n_1 \cos\xi + n_2 \sin\xi\}$$

$$\dot{\chi}_{10} = \Omega_y - \frac{n_{10}}{\omega_n} + K(-B_{yR}^2\chi_{10} + B_{xR}B_{yR}\chi_{20}) \tag{7.22}$$

$$\chi_{20} = -\Omega_x - \frac{n_{20}}{\omega_n} + K(-B_{xR}^2\chi_{20} + B_{xR}B_{yR}\chi_{10})$$

Since $\dot{\xi}$ is very nearly equal to $\omega_n = (1+k)\omega_s$ and, for $k \neq 0$, this frequency does not appear in the disturbance acceleration components, the disturbance-dependent part of $\dot{a}_o$ is zero. Thus, in order to estimate the forced response of a, the first approximation must be refined as in Ref. 5-1. Noting that

$$\dot{a} = \dot{\omega}_1 \cos\xi + \dot{\omega}_2 \sin\xi \tag{7.23}$$

the time derivative of a can be written in the form:

$$\dot{a} = \dot{a}_o + A_1 \cos\xi + A_2 \sin\xi + A_3 \cos 2\xi + A_4 \sin 2\xi$$

$$+ n_{11} \cos(\xi - \gamma) - n_{12} \sin(\xi - \gamma) \tag{7.24}$$

where:

$$A_1 = n_{10} + K\omega_n(B_{yR}^2\chi_{10} - B_{xR}B_{yR}\chi_{20})$$

$$A_2 = n_{20} + K\omega_n(B_{xR}^2\chi_{20} - B_{xR}B_{yR}\chi_{10})$$

$$A_3 = K(1 - K_R\omega_n)\frac{B_{yR}^2 - B_{xR}^2}{2}a_o$$

$$A_4 = -K(1 - K_R\omega_n)B_{xR}B_{yR}a_o .$$

These coefficients are slowly varying so that a can be found by taking the indefinite integral of (7.24) with the coefficients assumed constant. This yields a refinement of the first approximation:

$$a = a_o + \frac{A_1}{\omega_n}\sin\xi - \frac{A_2}{\omega_n}\cos\xi + \frac{A_3}{2\omega_n}\sin 2\xi$$

$$- \frac{A_4}{2\omega_n}\cos 2\xi + \frac{n_{11}}{k\omega_s}\sin(\xi - \gamma) + \frac{n_{12}}{k\omega_s}\cos(\xi - \gamma) . \qquad (7.25)$$

In the steady state a_o is zero, by solution of the differential equation for a_o. Thus, in determining the steady-state response, the terms concerning a_o, A_3, and A_4 may be neglected. Using this result, upper bounds may be derived for the angular velocities ω_1 and ω_2:

$$|\omega_1| \le \frac{1}{2}\left\{\left|\frac{A_2}{\omega_n}\right| + \frac{\sqrt{A_1^2 + A_2^2}}{\omega_n} + \frac{2\sqrt{n_{11}^2 + n_{12}^2}}{k\omega_s}\right\}$$

$$|\omega_2| \le \frac{1}{2}\left\{\left|\frac{A_1}{\omega_n}\right| + \frac{\sqrt{A_1^2 + A_2^2}}{\omega_n} + \frac{2\sqrt{n_{11}^2 + n_{12}^2}}{k\omega_s}\right\} \qquad (7.26)$$

This indicates that the effect of the disturbances is inversely proportional to the spin rate; moreover, the amplitude of the response excited by the forcing terms at spin frequency is inversely proportional to k (these results assume $k \neq 0$).

Examination of (7.26) shows that, for most applications, the transverse angular velocities are negligible, owing to the small magnitude of A_1,

A_2, n_{11}, and n_{22}. Typically, $|\omega_1|$ and $|\omega_2|$ will be no more than 10^{-4} rad/sec.

Refinement of the first approximation in (7.22) for the average attitude variables χ_1 and χ_2 yields terms which are proportional to a_o. Since a_o is zero in the steady-state motion, the Eqs. (7.22) of the first approximation are sufficient to describe the steady-state motion. Furthermore, if the steady-state pointing accuracy is not required to be extremely high, the contribution of ω_1 and ω_2 to c_{13} and c_{23} may be neglected. In such cases, the steady-state attitude motion can be estimated to good accuracy by solving the following linear, time-varying differential equations:

$$\begin{bmatrix} \dot{\chi}_1 \\ \dot{\chi}_2 \end{bmatrix} = K \begin{bmatrix} -B_{yR}^2 & B_{xR}B_{yR} \\ B_{xR}B_{yR} & -B_{xR}^2 \end{bmatrix} \begin{bmatrix} \chi_1 \\ \chi_2 \end{bmatrix} + \begin{bmatrix} \Omega_y - n_{10}/\omega_n \\ -\Omega_x - n_{20}/\omega_n \end{bmatrix} . \qquad (7.27)$$

Analytically, these equations are no easier to solve than the nonaveraged equations (7.18), because both sets are nonstationary. However, machine solution of the averaged equations proceeds much more rapidly than numerical integration of the nonaveraged equations because in the latter case the speed of solution must be scaled to accommodate the rapidly varying components (which have been averaged out in deriving the equations of the first approximation).

Figure 7-5 exhibits comparative solutions for the exact small-error equations of motion and the averaged equations of motion with forcing from gravity-gradient, solar radiation, and aerodynamic disturbance torques as well as motion of the reference coordinate axes. System parameters for this data are:

$$\omega_1(0) = \omega_2(0) = c_{13}(0) = c_{23}(0) = \alpha(0) = 0$$

$$I_x = 75 \text{ slug-ft}^2$$

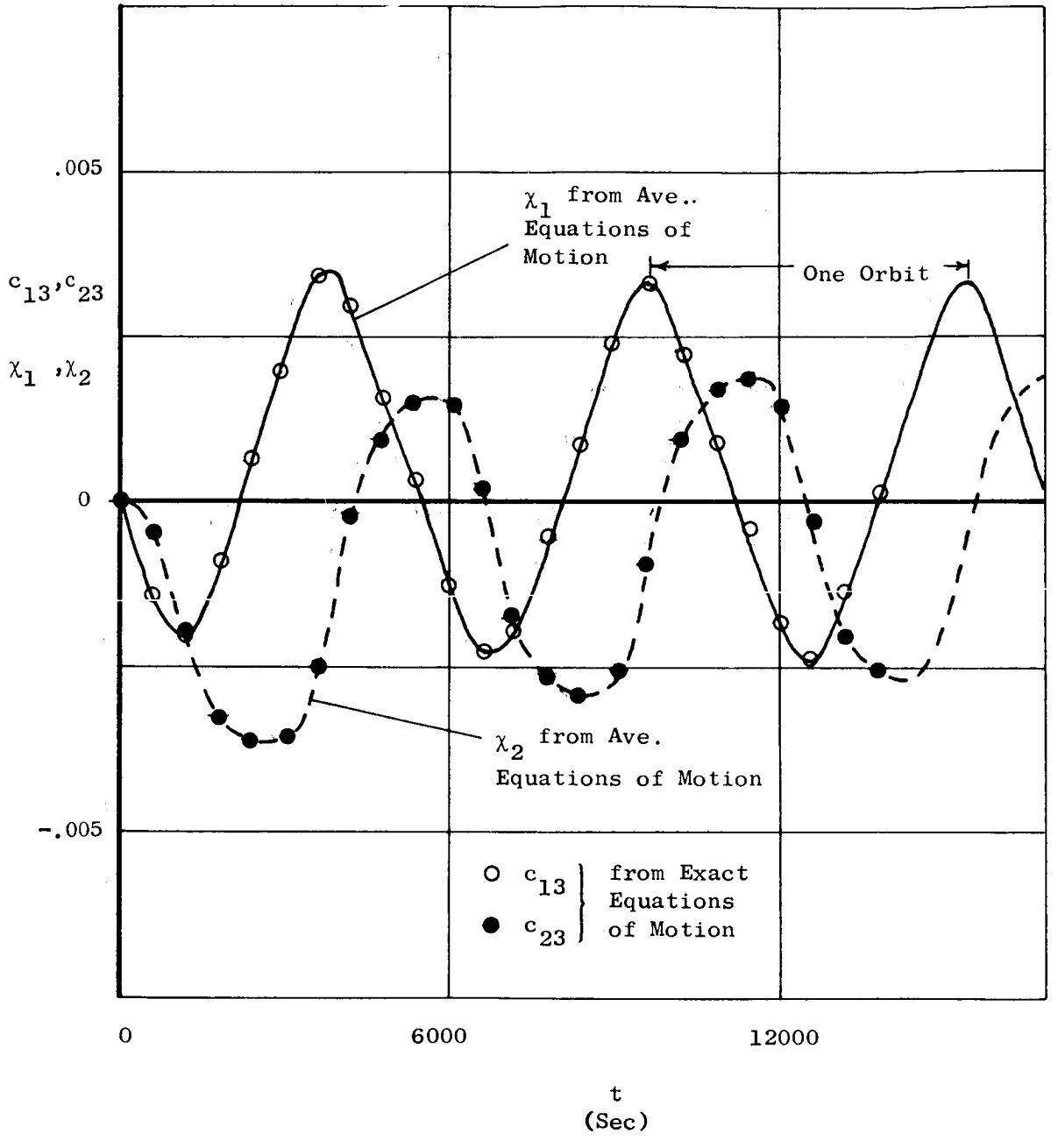

FIG. 7-5. COMPARISON OF SOLUTIONS TO EXACT AND AVERAGED EQUATIONS OF MOTION WITH DISTURBANCES.

$I_z = 100$ slug-ft^2

$\omega_s = 0.1$ rad/sec

Altitude = 300 naut. mi.

$\theta_i = 90°$

$\phi = \delta = 0$

$K_R = 20$ sec

$K = 584$ amp-ft^2/gauss-lb-ft-sec*

$\Omega_x = 2 \times 10^{-7}$ rad/sec

$\Omega_y = 10^{-7}$ rad/sec

$R_b = 5$ ft

$v_{s1} = .7071$

$v_{s2} = 0$

$v_{s3} = .7071$

$c_D = 2.6$

$\ell_x = \ell_y = \ell_z = 0.2$ ft .

As always in these performance studies, the untilted dipole model of the earth's magnetic field is used.

---

* As mentioned before, with K specified in these units, the equations of motion must be modified everywhere, replacing K by 6.86×10^{-6}K.

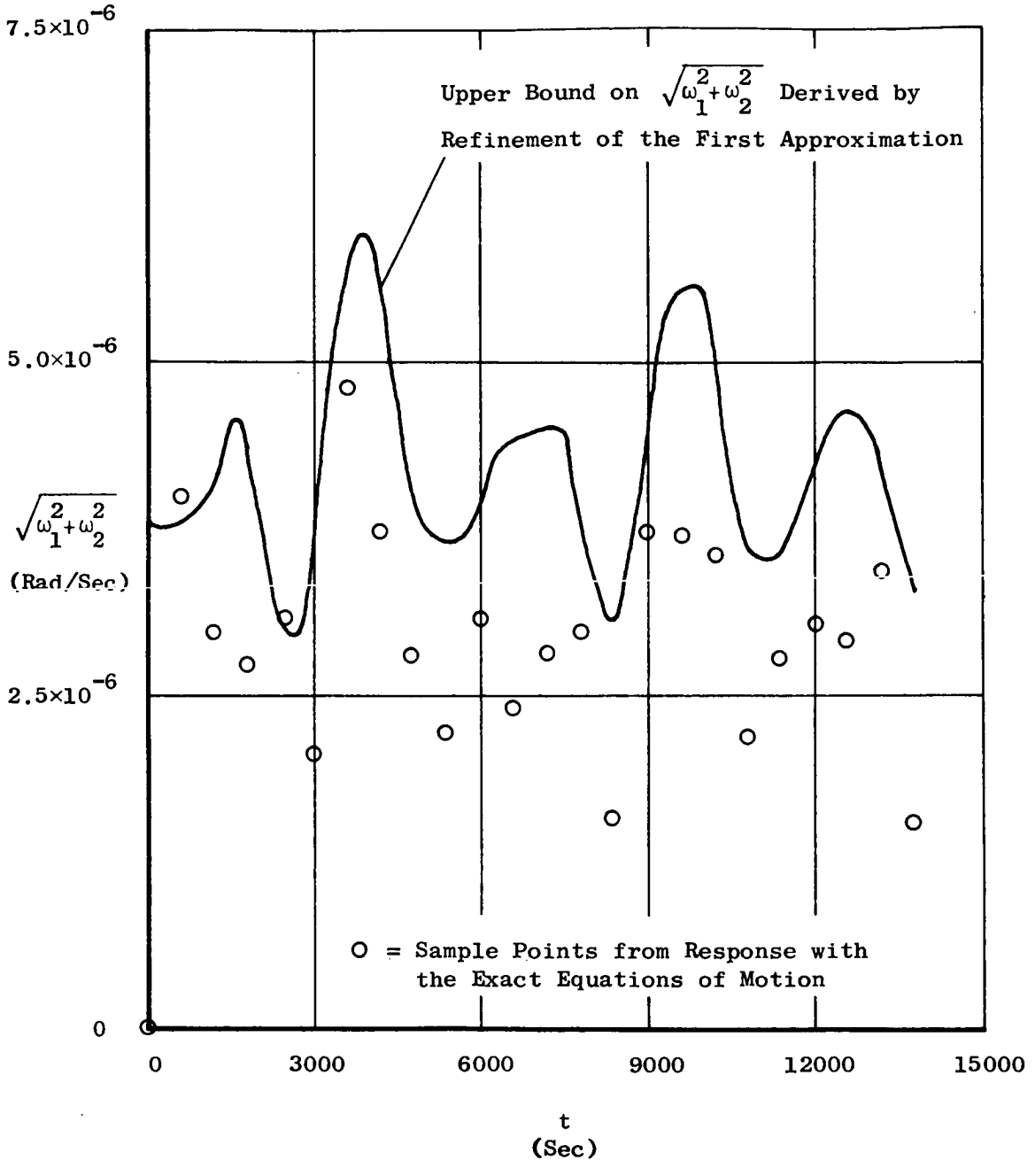

FIG. 7-6. COMPARISON OF EXACT SOLUTION FOR THE TOTAL TRANSVERSE ANGULAR VELOCITY WITH THE APPROXIMATE UPPER BOUND IN THE PRESENCE OF DISTURBANCES.

Solution of the exact equations required, in this case, five minutes on the B5000 digital computer, while solution of the averaged equations of motion for the same amount of orbital motion (2.4 orbits) required a computation time of only 16 sec. Thus the averaged equations were solved, in this case, at a cost of approximately one twentieth the cost of obtaining the same solution by means of the exact small-error equations of motion.

Notice that the motion, as we might expect from the character of the forcing terms (and the periodic coefficients in the differential equations), exhibits both constant components and terms at frequencies related to the orbital motion of the vehicle. The effectiveness of the active damping law is shown by the close correspondence between the solutions to the averaged equations and the exact solutions. From (7.21), this indicates that ω_1 and ω_2 are maintained at levels which, in this case, contribute negligibly (when compared with χ_1 and χ_2) to c_{13} and c_{23}.

From (7.26) an upper bound on the total transverse angular velocity, $\sqrt{\omega_1^2+\omega_2^2}$, can be computed. Figure 7-6 shows this bound and sample points from solution of the exact equations for the preceding case. The bound gives a good estimate of the behavior of the total transverse angular velocity. The small discrepancy at the beginning of the data occurs because a_o is not quite zero initially, although it was assumed to be so in deriving the upper bound.

C. SUMMARY

In this chapter, averaged equations of motion for the disturbed system have been developed. Although these equations still require numerical solution, their solution can be obtained much more economically than the solution of the exact small-error equations. Using a refinement technique of Krylov and Bogoliubov, it is seen that in many applications, the attitude errors c_{13} and c_{23} are accurately represented by χ_1 and χ_2. In situations for which ω_1 and ω_2 contribute significantly to c_{13} and c_{23}, the attitude errors are bounded by:

$$|c_{13}| \leq |\chi_1| + \frac{|\omega_1|}{\omega_n}$$

$$|c_{23}| \leq |\chi_2| + \frac{|\omega_2|}{\omega_n} \qquad (7.28)$$

As mentioned above, the averaged equations (7.27) are not amenable to closed-form solution. For this reason, and because the disturbances depend strongly upon the vehicle configuration, it is difficult to make any precise statement regarding the relative significance of various disturbances. Because the coefficients of χ_1 and χ_2 in the differential equations (7.27) depend parametrically upon θ_i, ϕ, and δ, and since the coefficients of the forcing terms n_{10}/ω_n and n_{20}/ω_n are functions of these parameters as well, the manner in which the accuracy of control depends upon θ_i, ϕ, and δ is impossible to ascertain without an exhaustive (and prohibitively expensive) simulation study.

It is, however, possible to make qualitative statements regarding the effect of altitude upon the relative importance of the various disturbance torques considered in this chapter. At extremely low altitudes, atmospheric pressure can be expected to be the dominant disturbance with solar radiation pressure much less important, and gravity gradient and residual magnetic disturbances somewhere in between. As the altitude increases (say to 500 nautical miles) the dynamic pressure decreases sharply (Fig. 7-2), and the effects of gravity-gradient and residual magnetism become relatively more significant, since these latter effects are inversely proportional to the cube of the orbital radius. At very high altitudes (for example, 10,000 nautical miles), solar radiation pressure can be expected to dominate, since the magnitude of this effect is dependent upon the distance of the vehicle from the sun and, therefore, essentially independent of the orbital altitude.

The magnitudes of the coefficients of χ_1 and χ_2 in (7.27) are inversely proportional to the sixth power of the orbital radius; however, this effective decrease in control gain as the altitude increases can be compensated, to a point, by increasing the control gain K.

The logical approach is to treat each design problem individually by simulation. The averaged equations of motion (7.27) developed in this chapter greatly facilitate such studies. A particular mission is treated by these techniques in Chapter IX.

VIII. MECHANIZATION CONSIDERATIONS

The magnetic control system developed and analyzed in preceding chapters requires, in addition to a torquing coil, knowledge of certain attitude variables and magnetic field components. In order to realize a completely self-contained system, the variables present in the error function, σ, must be determined by on-board measurements. This chapter deals with the implementation of the actuator (torquing coil) and discusses the problem of sensing the necessary attitude variables and magnetic field components.

A. ACTUATOR DESIGN

Magnetic moments can be generated either by air-core coils or solenoids with ferromagnetic cores. In the former case, the area of the coil is made as large as is compatible with the structure of the vehicle. Ferromagnetic actuators are generally made in the form of long, slender rods and offer the advantages of reduced size and weight. A disadvantage of using a ferromagnetic torquer is the presence of residual flux in the core which may result in a residual magnetic moment of from one to ten percent of the maximum available control moment [Ref. 8-1]. For our purposes, it is sufficient to consider only air-core coils.*

The control law developed in this study requires the generation of a magnetic moment aligned with the spin axis of the vehicle. This requirement can be satisfied by passing current through a planar coil normal to the spin axis. For an N_c-turn circular coil of radius R_c, and winding thickness much less than R_c, the magnetic moment will be:

$$m = \pi R_c^2 N_c i \tag{8.1}$$

---

* Reference 8-2 includes a thorough discussion of the design of ferromagnetic actuators for satellite attitude control, with experimental data. Reference 8-1 is an abbreviated version of the actuator design study presented in Ref. 8-2.

where i is the current through the coil and the direction of the magnetic moment is as shown in Fig. 8-1.

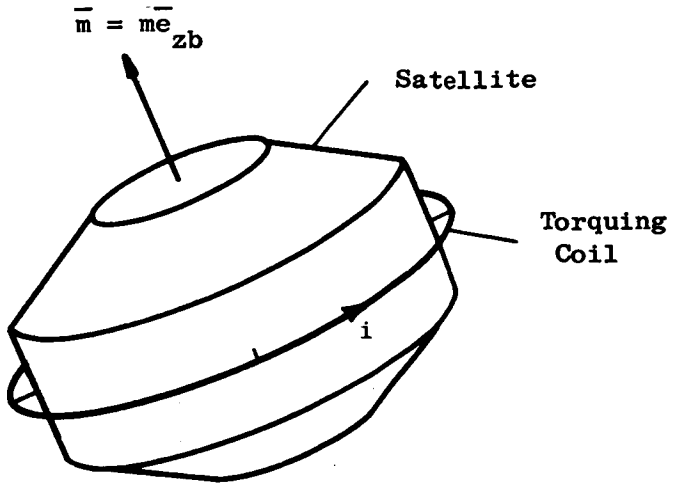

FIG. 8-1. MAGNETIC MOMENT PRODUCED BY A CIRCULAR TORQUING COIL.

One approach to the coil design problem is to regard the maximum available voltage (v_m), the coil radius and the maximum required magnetic moment (m_m) as specified quantities [Ref. 8-3]. If ρ is the resistance per unit length of the wire, the magnetic moment depends upon the applied voltage in the following way:

$$m = \frac{R_c v}{2\rho} . \tag{8.2}$$

This immediately specifies ρ as:

$$\rho = \frac{R_c v_m}{2m_m} . \tag{8.3}$$

The power consumed is

$$P = \frac{v^2}{2\pi R_c N_c \rho} \tag{8.4}$$

With ρ specified as in (8.3), the maximum power (corresponding to $v = v_m$) is:

$$P_m = \frac{m_m v_m}{\pi R_c^2 N_c} . \tag{8.5}$$

The coil weight is

$$W = 2\pi R_c N_c w \tag{8.6}$$

where w is the mass per unit length of the wire.* Notice that ρw is equal to the product of the mass density and the resistivity of the material used in the actuator. Values of $K_w = \rho w$ are tabulated below for several metallic conductors.

TABLE 8-1. THE PARAMETER $K_w = \rho w$ FOR SEVERAL CONDUCTORS (TEMPERATURE = 20° C.)

	Resistivity (Ω - ft)	Density (lb/ft^3)	10^5 ρw (lb - Ω/m^2)
Aluminum	9.28×10^{-8}	$.554 \times 10^3$	1.57
Copper (annealed)	5.64×10^{-8}	1.82×10^3	3.14
Copper (hard-drawn)	5.80×10^{-8}	1.83×10^3	3.24
Gold	7.27×10^{-8}	3.96×10^3	8.77
Magnesium	15.1×10^{-8}	$.356 \times 10^3$	1.64
Silver	5.35×10^{-8}	2.15×10^3	3.50
Zinc	19.4×10^{-8}	1.46×10^3	8.66

The product of the coil weight and the maximum power consumption is, for any particular coil material, independent of the coil parameters:

---

* The total system weight, including the power supply, will depend upon the maximum power as well as upon the coil weight. This factor is not considered here, but it is discussed in Ref. 8-1.

$$P_m W = \frac{K_w}{\rho^2} v_m^2 \quad . \tag{8.7}$$

For ρ chosen as in (8.3):

$$P_m W = \frac{4K_w m_m^2}{R_c^2} \quad . \tag{8.8}$$

Assuming that the coil temperature is controlled to a specified value, specification of ρ and the material will dictate the wire size. From the preceding table, aluminum is the material giving the smallest coil weight for any ρ. The remaining parameter to be specified is N_c, the number of turns in the coil; its choice is equivalent to specifying the weight-power trade-off for the coil. However, the choice of N_c is limited by either the current which may safely pass through the wire or the current available from the power source. If i_R is the current limit:

$$N_c \geq \frac{m_m}{\pi R_c^2 i_R} \tag{8.9}$$

Determination of the current limitation for the wire is not easy. It depends upon the temperature at which the wire may safely be operated and the thermal environment of the coil, which may or may not be the same as that of the interior of the satellite. With an effective thermal control system it is likely that the primary limitation upon N_c will result from the current available from the power source.

B. SENSOR REQUIREMENTS

Implementation of the control law evolved in Chapter III requires the formation of the error function

$$\sigma = B_{xb}(a_{23} - K_R\omega_y) - B_{yb}(a_{13} - K_R\omega_x) \tag{8.10}$$

where B_{xb} and B_{yb} are the magnetic field components along the transverse vehicle axes, and ω_x and ω_y are the transverse angular velocities.* The attitude variables, a_{13} and a_{23}, are the components of the $\bar{e}_{zR}$ vector (which defines the desired spin-axis orientation) measured along the body-fixed transverse axes. Each of these variables must be measured, or calculated from measurements of other variables, to mechanize the control law.

1. Magnetic Field Measurements

Several devices have been developed for making magnetic field measurements in space [Ref. 8-4]. Of these, the fluxgate magnetometer appears most useful for measurement of the components of the earth's magnetic field in the vehicle [Refs. 8-4 and 8-5]. According to Cahill [Ref. 8-4] fluxgate magnetometers are capable of a measurement accuracy of 0.1% of full scale with a full-scale range of from $\pm$ 0.0002 gauss to $\pm$ 0.50000 gauss. The frequency range of this sensor is approximately zero to 100 cps, giving a cutoff frequency well in excess of the spin frequency of any conceivable spinning satellite. Such a magnetometer (capable of measurements along three orthogonal axes) has a weight of one to two lbs and a power requirement of about 0.3 watts. The other types of magnetometers thus far employed in outer space have better absolute accuracies (for example, the rubidium vapor magnetometer has a sensitivity of 10^{-7} gauss, 25 times better than that of the fluxgate magnetometer), but in general, they weigh more, consume more power, and have a much smaller frequency range. The loss in sensitivity is acceptable because magnetic control will be practical only in regions of space where the maximum magnetic field is much larger than 0.0000025 gauss, the null sensitivity of the fluxgate magnetometer.

A major limitation in measurement of the transverse components of the earth's magnetic field is interference with the measurement by the magnetic field generated by the torquing coil. Theoretically, the

---

* If, instead of active magnetic damping, another form of damping is employed, the rate-dependent terms are omitted from (8.10).

magnetometers can be located so that the magnetic field from the actuator is normal to the sensitive axis. Another approach, often employed on scientific satellites, is the placement of the magnetometers on long booms extending away from the vehicle. Still another technique, suggested in Ref. 8-2, is the creation of a compensatory field in the region of the magnetometers by means of small coils connected in series with the torquing coil. Such a system must be calibrated prior to launch.

2. Attitude and Rate Measurements

Measurement of the transverse angular velocities can be accomplished by using two rate-sensing gyroscopes. Of course, these gyroscopes must be carefully aligned to minimize the interference caused by any component of spin rate along the gyro input axis.

Another source of rate information, often used in controlling fully stabilized vehicles, is provided by observing the rate of change of the attitude variables. From the kinematic equations of (4.3)

$$\begin{aligned} \dot{a}_{13} &= a_{23}\omega_s - a_{33}\omega_y \\ \dot{a}_{23} &= a_{33}\omega_x - a_{13}\omega_s \end{aligned} \tag{8.11}$$

For small errors, $a_{33} \approx 1$ and (approximately)

$$\begin{aligned} \omega_x &= a_{23} + \omega_s a_{13} \\ \omega_y &= -a_{13} + \omega_s a_{23} \end{aligned} \tag{8.12}$$

These equations can be mechanized as shown in Fig. 8-2. The differentiation is mechanized approximately to reduce the noise problem introduced by differentiation of sensor outputs. The cutoff frequency of the differentiation filter, $1/\tau$, should be somewhat greater than the spin frequency for accurate differentiation at the frequencies of interest. Of course, since this technique is based upon the assumption that a_{33} is unity, it is accurate only when the attitude errors are small.

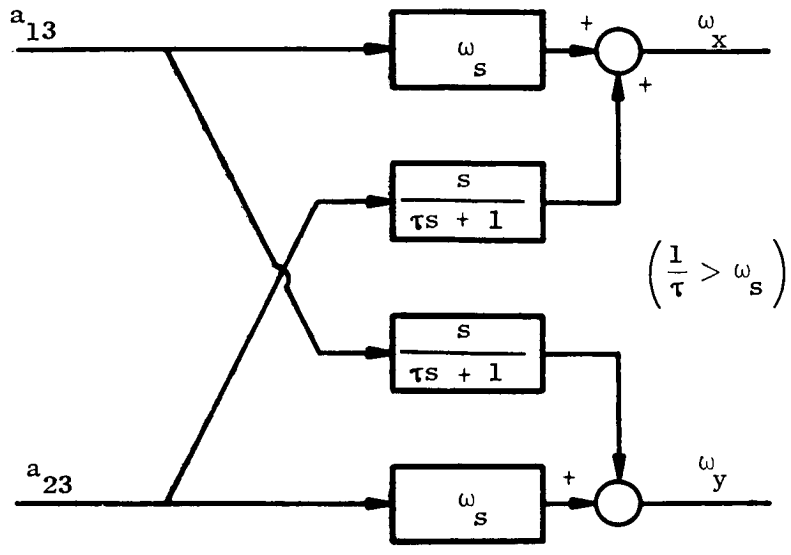

FIG. 8-2. ESTIMATION OF THE TRANSVERSE ANGULAR VELOCITIES FROM THE ATTITUDE VARIABLES.

The necessary magnetic field and angular velocity measurements can be made by using magnetometers and gyroscopes as outlined above, independent of the desired spin-axis direction. In contrast, the ease with which a_{13} and a_{23} can be measured (or estimated) is very dependent upon the mission. To illustrate this fact, three specific examples will be discussed.

a. Solar Pointing

First, consider the problem of orienting the spin axis of a spinning vehicle toward the center of the sun for solar experimentation or to provide efficient solar-to-electrical energy conversion in a case where the spin-axis attitude need not be otherwise constrained (a detailed design for an application of this type is exhibited in Chapter IX). A simple sensing element which can be used in this case is the silicon solar cell, the output voltage of which is very nearly proportional to the cosine of the angle of incidence of the solar radiation upon its surface [Ref. 8-6]; that is, the output is, to a good approximation, proportional to the projection of the vehicle-sun line (which is z_R in this case) upon the axis normal to the surface. Figure 8-3 shows a view in the transverse plane of a satellite with the shape shown in

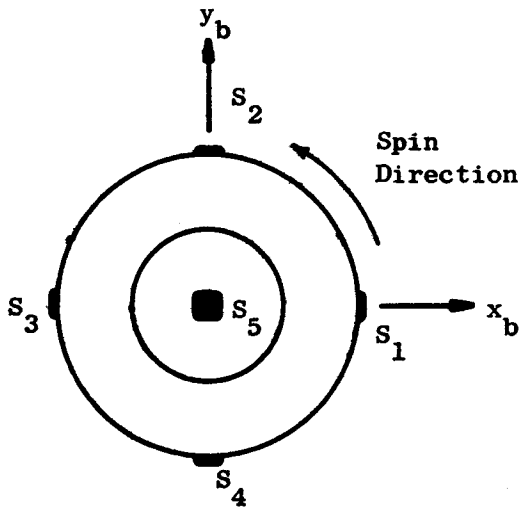

FIG. 8-3. SENSOR CONFIGURATION FOR SOLAR POINTING.

Fig. 8-1. Each of the sensors S_1, S_2, S_3 and S_4 is positioned with its sensitive surface outward and normal to the axis along which it is located. Denoting the output voltage of S_i as $\bar{S}_i$, and assuming each cell to have the same gain factor, K_s, it is clear that

$$\begin{aligned} \bar{S}_1 - \bar{S}_3 &= K_s a_{13} \\ \bar{S}_2 - \bar{S}_4 &= K_s a_{23} \end{aligned} \tag{8.13}$$

In most applications, an additional fine sensor, S_5, will be included to provide a high degree of null accuracy. One such fine sensor is described in Ref. 8-6.

It is clear that the required attitude variables may be readily measured for the solar pointing application; moreover, the ability to measure these variables is not a function of the pointing error because the sensors, if they are not shaded, provide all-attitude information.

b. Stellar Pointing

Next, consider a mission for which the spin axis is to be pointed toward a specific star. A null-seeking star tracker is generally used for such an application. This device consists of a photoelectric sensor and associated optics mounted on a platform which is coupled to the body by means of gimbals (for example, as in Fig. 8-4). Using the sensor outputs, the gimbal control system attempts to track

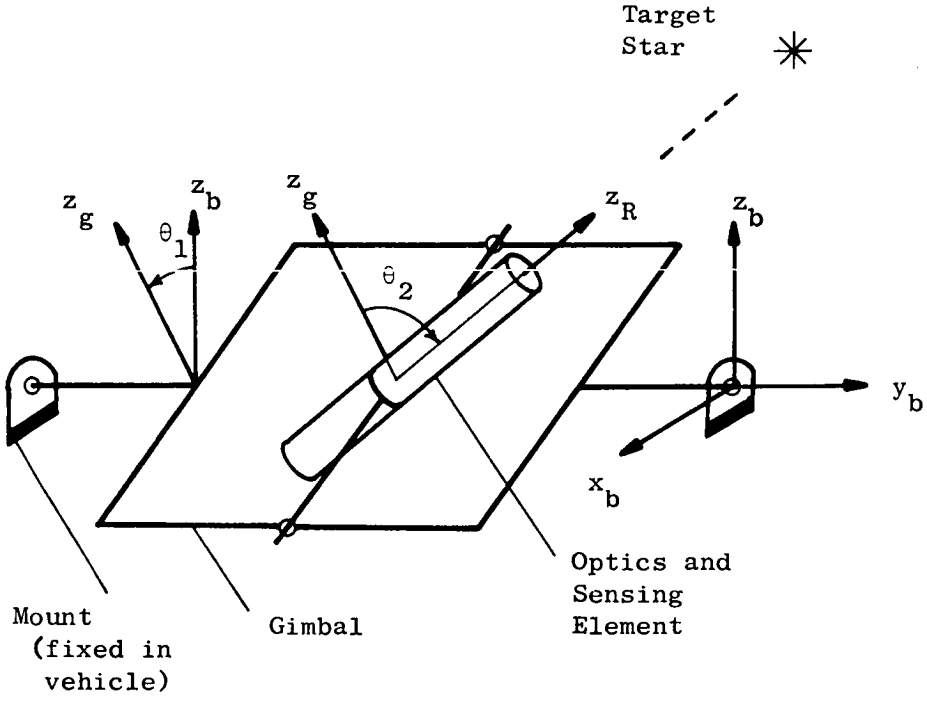

FIG. 8-4. A STAR TRACKER CONFIGURATION.

the star so that, statically, the sensor outputs are zero. The attitude variables a_{13} and a_{23} can be computed directly from the gimbal angles to an accuracy dependent upon the tracking error and the quality of the pickoffs:

$$a_{13} = \bar{e}_{zR} \cdot \bar{e}_{xb} = \sin \theta_1 \cos \theta_2$$
$$a_{23} = \bar{e}_{zR} \cdot \bar{e}_{yb} = \sin \theta_2 \,. \tag{8.14}$$

The star tracker presents several problems not encountered with sun sensors. One of these concerns the gimbal control system; its response must be "fast" relative to the motion of the vehicle; otherwise the gimbal control loop and the attitude control system will be coupled. Still more disastrous is the possibility that a rapid vehicle motion could take the star line-of-sight out of the field of view of the optics (which is usually on the order of 1 deg).

A second difficulty is that the star tracker is generally enclosed in the vehicle and must "see" through a window of limited dimensions. This factor limits θ_1 and θ_2 and, therefore, attitude control can be maintained only for a restricted range of a_{13} and a_{23}.

Yet another problem associated with the use of a star tracker in a spinning vehicle is that of assuring that the correct star is tracked. The target star must be found initially by some sort of pre-programmed search. Since such a search will be difficult from a rapidly spinning vehicle, the search will probably be performed prior to separation of the satellite from the final stage of the booster (which must be attitude controlled as is, for example, the AGENA). If, due to a subsequent malfunction, the target star is lost, its relocation may be a major problem.

c. Orbit-Plane-Normal Pointing

An application which has received considerable attention in the past is alignment of the spin axis normal to the plane of the orbit of the satellite [Refs. 1-9, 1-11, and 8-7]. In this case there is no object (i.e., source of radiation) toward which the spin axis is pointed and, as might be expected, the required attitude information is relatively difficult to obtain.

Figure 8-5 shows a sensor configuration useful for such a vehicle. S_1 and S_2 are infrared sensors which are fixed in the vehicle and inclined equally to the plane normal to the spin axis. As the spin of the vehicle causes a sensor line-of-sight to intersect the earth, the sensor emits a pulse. Comparison of the pulses from the two sensors gives an indication of the angle (the bank angle) by which the spin axis is inclined to the horizontal plane; if the bank angle is zero,

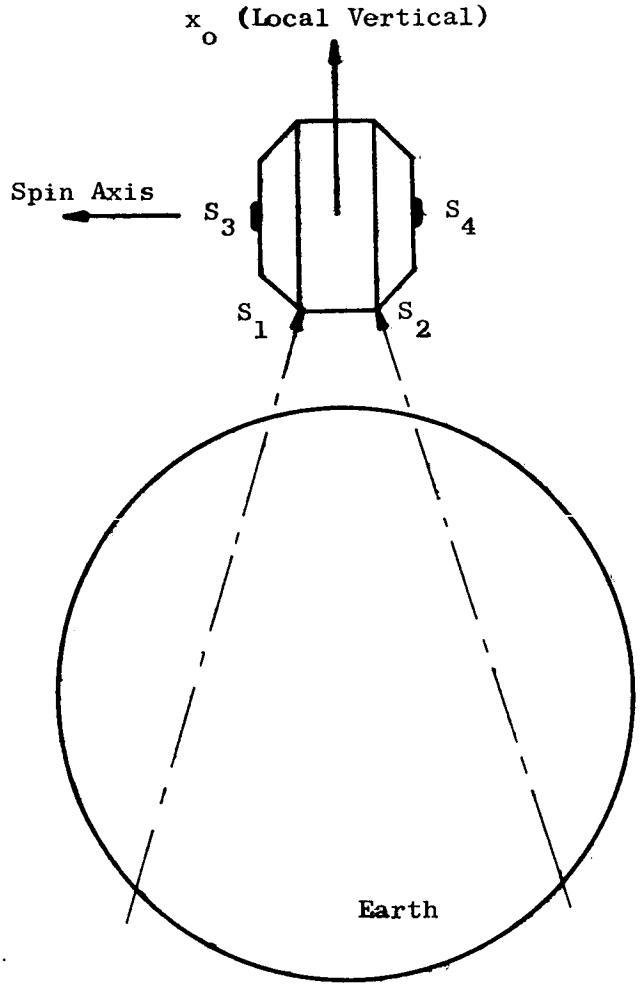

FIG. 8-5. SENSOR CONFIGURATION FOR BANK ANGLE MEASUREMENT.

the sensor outputs will (ideally) be equal. Notice that this measurement is not sufficient to establish the spin-axis attitude because these sensors are insensitive to rotation of the vehicle about the x_o axis.

Figure 8-6 defines the satellite axes in terms of θ_1, θ_2, and θ_3, where θ_2 is the bank angle and θ_1 will be referred to as

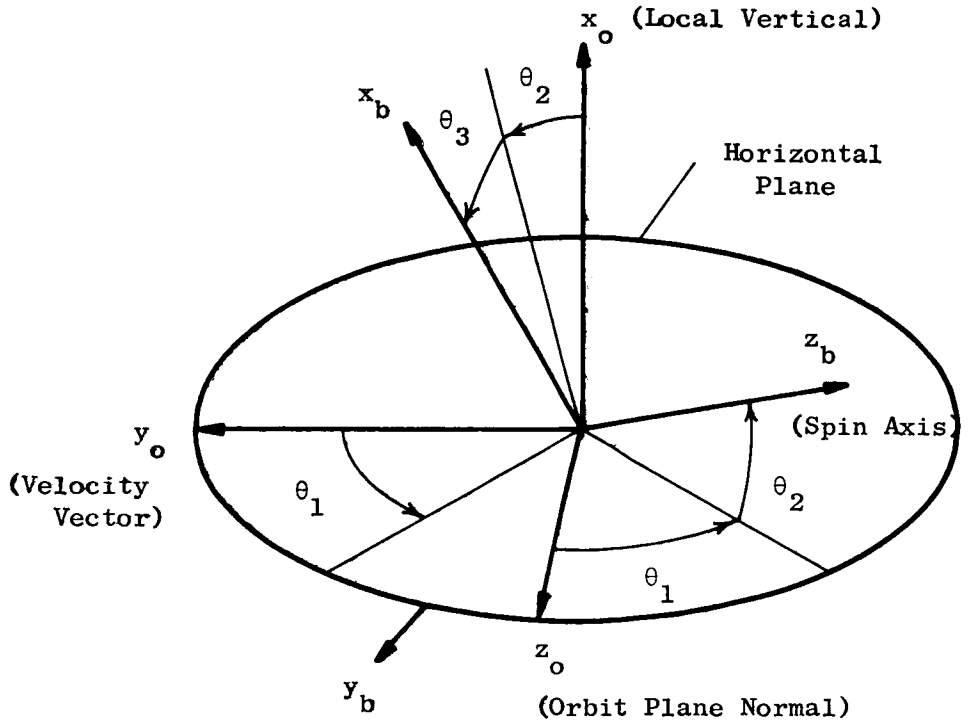

FIG. 8-6. DEFINITION OF SATELLITE ATTITUDE IN TERMS OF THE BANK ANGLE θ_2.

the yaw angle because it is a rotation about local vertical. In terms of these angles:

$$a_{13} = -\cos\theta_3 \sin\theta_2 \cos\theta_1 + \sin\theta_3 \sin\theta_1$$

$$a_{23} = \sin\theta_3 \sin\theta_2 \cos\theta_1 + \cos\theta_3 \sin\theta_1 .$$

Of these angles only θ_2 can be measured directly. However, if the sensors S_1 and S_2 are positioned along the $-x_b$ axis, the center

of the output pulses will occur when θ_3 is zero. Furthermore, to a very good approximation, $\dot{\theta}_3 = \omega_s$. Therefore, $\sin \theta_3$ and $\cos \theta_3$ can be generated by an on-board sine-cosine generator synchronized by the outputs of the infrared sensors.

The problem of estimating θ_1 still remains; this might be accomplished by adding solar cells to detect the component of solar radiation along the spin axis (S_3 and S_4 of Fig. 8-5). Combination of this data with knowledge of the position of the sun in (x_o, y_o, z_o) coordinates (as provided by computations based upon orbital data and the known motion of the sun in the ecliptic plane) will allow computation of θ_1. However, this approach results in a very complicated system.

Another method which may be used to measure θ_1 is the use of aerodynamic pressure sensors in the positions S_3 and S_4 of Fig. 8-5 [Ref. 8-8]. In theory, this is an ideal technique because it affords a direct measurement of θ_1. However, there are several practical difficulties. For example, the altitude at which such devices may be used is limited by the rapid decrease in dynamic pressure as the altitude increases (see Fig. 7-2). In addition, crosswinds can be a significant source of measurement error.

This particular application is one in which an intermittent control technique is probably preferable to one which operates continuously. For intermittent control the bank angle sensor is sufficient because the variation of the yaw angle can be predicted from that of the bank angle by using the kinematic relationships which apply to the attitude variables during the control-free periods. A detailed discussion of small-error intermittent magnetic control for this problem is presented in Ref. 1-9.

C. SUMMARY

Realization of the magnetic control law requires an actuator and appropriate measurements of the magnetic field, the transverse angular velocities of the vehicle and the attitude errors. Of these factors, measurement of the attitude errors is the most critical because the character of the available attitude data depends strongly upon the

desired orientation of the spin axis. The greatest difficulties arise when the spin axis is to be directed toward a point not occupied by a source of detectable radiation. In such cases a possible source of attitude information is a strapped-down inertial reference system [Ref. 8-9]. In theory this technique will, through integration of the appropriate kinematic differential equations (Chapter II), provide the necessary attitude data from knowledge of the components of vehicle angular velocity and of the initial attitude. However, this scheme can result in a complex mechanization (particularly in the case of large attitude errors and a noninertial reference frame) and, because it involves an open-loop system which is subject to many sources of inaccuracy (e.g., integrator drift), this attitude reference system must be periodically reset from some independent source of attitude information.

IX. DESIGN CONSIDERATIONS

The first problem generally encountered in designing an attitude control system for a spinning vehicle is that of selecting a control configuration. Assuming that magnetic torquing has been chosen as the means of modifying the total momentum of the vehicle, there is still a wide choice of damping mechanisms ranging from passive mechanical dampers and active magnetic damping to gimbaled rotors which store the component of momentum in the transverse plane of the vehicle [Refs. 9-1 and 9-2].

This discussion will be limited to the design of the continuous magnetic control law (with active magnetic damping) which was developed in Chapter III. First a design procedure, based upon the performance analyses of Chapters V and VII, will be presented. A magnetic control system is then designed for a specific application.

A. A DESIGN PROCEDURE

The large-error and small-error attitude control requirements for a satellite are often unrelated; that is, large-error performance is usually constrained by an upper limit upon the time required to remove the initial attitude errors following separation from the booster, whereas the small-error specification involves the maintenance of long-term accuracy in opposition to disturbances.

For small values of σ_s (the error saturation level of the control characteristic), the saturating-proportional control characteristic can be assumed to be a signum function for convergence from large errors. As shown in Chapter V, the rate of error reduction with a signum control characteristic is approximated by

$$\dot{\psi}_{AV} = -\frac{M_e}{2r_o^3} U_o G_{AV} . \qquad (9.1)$$

The coefficient $M_e/2r_o^3$ is readily determined from the satellite altitude (see Fig. A-3). Assuming that the orbital inclination is specified,

G_{AV} contours such as those shown in Chapter V can be plotted. As a first approximation, the minimum possible value of G_{AV} for this particular inclination can be used; as an alternative the variation of ϕ and δ can be determined from kinematical considerations and, plotting ϕ vs. δ on the contour chart, a more realistic estimate of the smallest possible G_{AV} can be derived. With the above information, as well as knowledge of the initial attitude error, U_o can be selected to remove this error within the specified time.

Selecting U_o in the manner above, the parameters σ_s (the linear range of the control characteristic) and K_R (which must be greater than $1/(1+k)\omega_s$ for stability) are determined by small-error performance requirements. If the rate gain is selected as

$$K_R = \frac{2}{(1 + k)\omega_s} \tag{9.2}$$

the attitude error and transverse angular velocity will decay at approximately the same speed, as shown in the small-error performance analysis of Chapter V.

The gain in the linear control region $(K = U_o/\sigma_s)$ is selected to give the required long-term orientation accuracy. The minimum allowable gain is determined by simulation of the averaged small-error equations of motion (developed in Chapter VII) with the appropriate disturbances.

Finally, the large-error performance of the system can be verified by simulation of the simplified equations of motion (see Chapter V).

B. AN EXAMPLE

As an illustrative example, a solar-pointing satellite in a circular orbit will be considered. The vehicle will be assumed to have a spherical outer structure with a radius of three feet and the following moments of inertia:*

---

* The largest possible moment of inertia ratio is, of course,

$$\frac{I_z}{I_x} = 2 .$$

$$I_x = I_y = 75 \text{ slug-ft}^2$$

$$I_z = 100 \text{ slug-ft}^2 .$$

The spin rate is 0.1 rad/sec.

The attitude control system will be required to reduce an initial attitude error of 90 deg to 5 deg within 9 hours after separation from the final stage, with acquisition assumed to begin with zero transverse angular velocities.* The small-error long-term accuracy requirement is 0.1°.

An additional constraint is that during its lifetime (assumed to be in excess of one year) the satellite will never enter the shadow of the earth; that is, the orbit is to be fully sunlit for the entire year. This somewhat arbitrary requirement restricts both the altitude and inclination of the orbit.

1. Orbit Selection

The requirement for a full-year fully sunlit orbit will place upper and lower bounds upon both the orbital inclination and the altitude.

The possibility of the satellite passing through the earth's shadow during any one orbit is determined by the position of the earth-sun line relative to the orbit plane. For example, if the sun is in the orbit plane it will certainly be occulted by the earth, whereas if the sun is normal to the orbit plane no occultation can occur. Since the reference axis z_R is, in this problem, the earth-sun line, the first of the above cases corresponds to $\phi = 90°$, and the latter to $\phi = 0$ or 180°.

---

* For an application of this sort, the primary acquisition constraint is usually dictated by the requirements of the power system (charged by solar cells) and/or thermal control considerations. Thus (for the example considered here), there is no penalty placed upon the time required to reduce the error from 5° to 0.1° because, with errors of 5° or less, the power system and thermal control system will operate normally.

The position of the sun relative to the orbit plane will vary during the year as a function of β (the displacement of the line of nodes from Autumnal Equinox) and S (an angular measure of the time of year). This relative motion is completely specified by the variation of ϕ and δ. From Figs. 2-1, 2-3, and 7-3 the following relationships can be derived:

$$\frac{\sin \delta}{\cos \delta} = \frac{(\sin \beta \cos S - \cos \zeta \cos \beta \sin S) \cos \theta_i - \sin \theta_i \sin \zeta \sin S}{-(\cos \beta \cos S + \cos \zeta \sin \beta \sin S)} \tag{9.3}$$

$$\cos \phi = -[(\sin \beta \cos S - \cos \zeta \cos \beta \sin S) \sin \theta_i + \cos \theta_i \sin \zeta \sin S]$$

where $\zeta = -23.45°$ and $\dot{\beta}$ is a constant determined by the altitude and inclination of the orbit (see Chapter II):

$$\dot{\beta} \approx -0.00164 \left(\frac{R_e}{r_o}\right)^2 \omega_o \cos \theta_i . \tag{9.4}$$

Figure 9-1 illustrates the conditions under which the vehicle

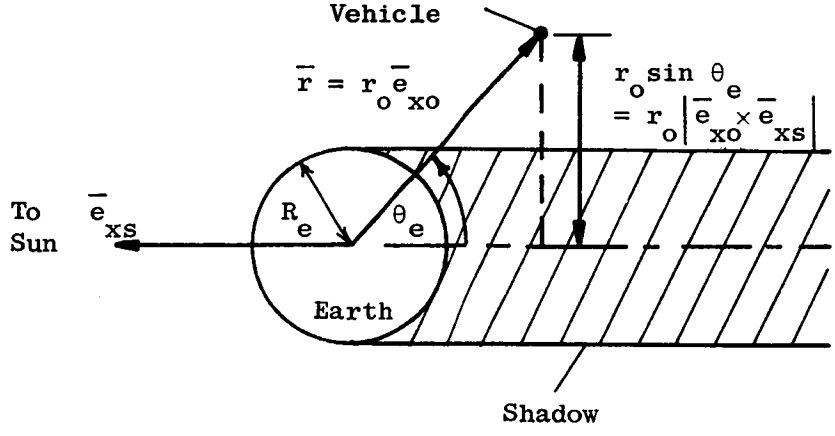

FIG. 9-1. OCCULT GEOMETRY IN THE SUN-EARTH-VEHICLE PLANE.

will be in the shadow of the earth. The plane of the page corresponds to the instantaneous sun-earth-vehicle plane. Assuming a cylindrical shadow, the occult condition is seen to be:

$$|\bar{e}_{xo} \times \bar{e}_{xs}| \leq \frac{R_e}{r_o} \quad \text{and} \quad \bar{e}_{xo} \cdot \bar{e}_{xs} < 0 \tag{9.5}$$

or, equivalently:

$$\bar{e}_{xo} \cdot \bar{e}_{xs} \leq -\sqrt{1 - \left(\frac{R_e}{r_o}\right)^2} \quad . \tag{9.6}$$

With $\bar{e}_{zR} = \bar{e}_{xs}$ as required for sun orientation, the components of $\bar{e}_{xs}$ in the (x_o, y_o, z_o) coordinate frame can be expressed in terms of $\emptyset$, δ and the orbital position α:

$$\begin{aligned} \bar{e}_{xs} \cdot \bar{e}_{xo} &= \sin \emptyset \cos (\alpha - \delta) \\ \bar{e}_{xs} \cdot \bar{e}_{yo} &= -\sin \emptyset \sin (\alpha - \delta) \\ \bar{e}_{xs} \cdot \bar{e}_{zo} &= \cos \emptyset \ . \end{aligned} \tag{9.7}$$

In terms of $\emptyset$, δ, and α the occult condition is

$$\sin \emptyset \cos (\alpha - \delta) \leq -\sqrt{1 - \left(\frac{R_e}{r_o}\right)^2} \quad . \tag{9.8}$$

From this result it is seen that the condition for no occultation during an orbit is

$$\sin \emptyset < \sqrt{1 - \left(\frac{R_e}{r_o}\right)^2} \tag{9.9}$$

where $\sin \emptyset$ is always positive with $\emptyset$ as defined in Chapter II. This condition upon $\emptyset$ must be maintained throughout the year (i.e., for all values of S) if full-year fully sunlit operation is desired.

The range of $\emptyset$ can be restricted by constraining the motion of β. In particular, if $\beta = S - \pi/2$, the relationships of (9.3) become:*

---

* The alternate condition $\beta = S + \pi/2$ will give completely equivalent results.

$$\cos \phi = [\cos \zeta + (1 - \cos \zeta)\cos^2 S]\sin \theta_i - \cos \theta_i \sin \zeta \sin S$$

$$\frac{\sin \delta}{\cos \delta} = \frac{-[\cos \zeta + (1 - \cos \zeta)\cos^2 S]\cos \theta_i - \sin \theta_i \sin \zeta \sin S}{-(1 - \cos \zeta) \sin S \cos S} \quad (9.10)$$

With this constraint upon β:

$$\min_S(\cos^2 \phi) = \begin{cases} \cos^2\left(\zeta - \theta_i + \frac{\pi}{2}\right), & \zeta \leq \theta_i \leq \frac{\pi}{2} \\ 0, & \theta_i < \zeta \text{ or } \theta_i > \pi - \zeta \\ \cos^2\left(\zeta + \theta_i - \frac{\pi}{2}\right), & \frac{\pi}{2} \leq \theta_i \leq \pi - \zeta . \end{cases} \quad (9.11)$$

Condition (9.9) can be rewritten as

$$\cos^2 \phi \geq \left(\frac{R_e}{r_o}\right)^2 \quad (9.12)$$

for comparison with (9.11).

The imposition of $\beta = S - \pi/2$ requires that r_o and θ_i be so related that $\dot{\beta} = \dot{S}$ [see expression (9.4)].* Since $\dot{S}$ is a constant, the required inclination is given by:

$$\cos \theta_i = - \frac{\dot{S}}{0.00164\,(R_e/r_o)^2 \omega_o} \quad (9.13)$$

Notice that $\pi/2 \leq \theta_i \leq \pi$ is required so that the line of nodes will advance in the orbit plane.

---

* Maintenance of $\beta = S - \pi/2$ will probably require active control of the satellite altitude to correct for launch errors and perturbations of the orbit.

From (9.11) and (9.12), θ_i is further restricted by the relationship:

$$\cos^2\left(\zeta + \theta_i - \frac{\pi}{2}\right) > \left(\frac{R_e}{r_o}\right)^2 . \qquad (9.14)$$

These conditions are shown graphically in Fig. 9-2. For year-long fully sunlit operation the orbit parameters must lie on the solid curve ($\dot{\beta} = \dot{S}$) and be above the dashed curve. Thus, the range of orbits is bounded as indicated.

For the design example treated here, the orbit will have an altitude of 1000 nautical miles with an inclination of 103.9 deg to the equatorial plane. The corresponding variation of ϕ and δ is shown in Figs. 9-3 and 9-4. The maximum value of ϕ is approximately 37.5 deg whereas the minimum value for which occultation can occur at this altitude is 39.2 deg.

2. Preliminary Control System Design

The maximum control level, U_o, is specified by the large-error convergence requirement. At an altitude of 1000 nautical miles, $M_e/2r_o^3 = .075$ gauss. Reduction of the attitude error by 85 deg in nine hours requires an average convergence rate of $\dot{\psi}_{AV} = -4.58\times10^{-5}$ rad/sec.

Figure 9-5 shows contours of G_{AV} for $\theta_i = 103.9$ deg upon which is superimposed the variation of ϕ and δ for $\beta = S-\pi/2$. G_{AV} is clearly always greater than 1.6. Using expression (9.1) and the above data (and the conversion factor 6.86×10^{-6} mentioned in earlier chapters):

$$U_o \geq 55.7 \text{ amp-ft}^2/\text{lb-ft-sec} .$$

Since this result is based upon an estimate of the average convergence speed (not the worst case), $U_o = 100$ amp-ft^2/lb-ft-sec will be chosen as a trial design value.

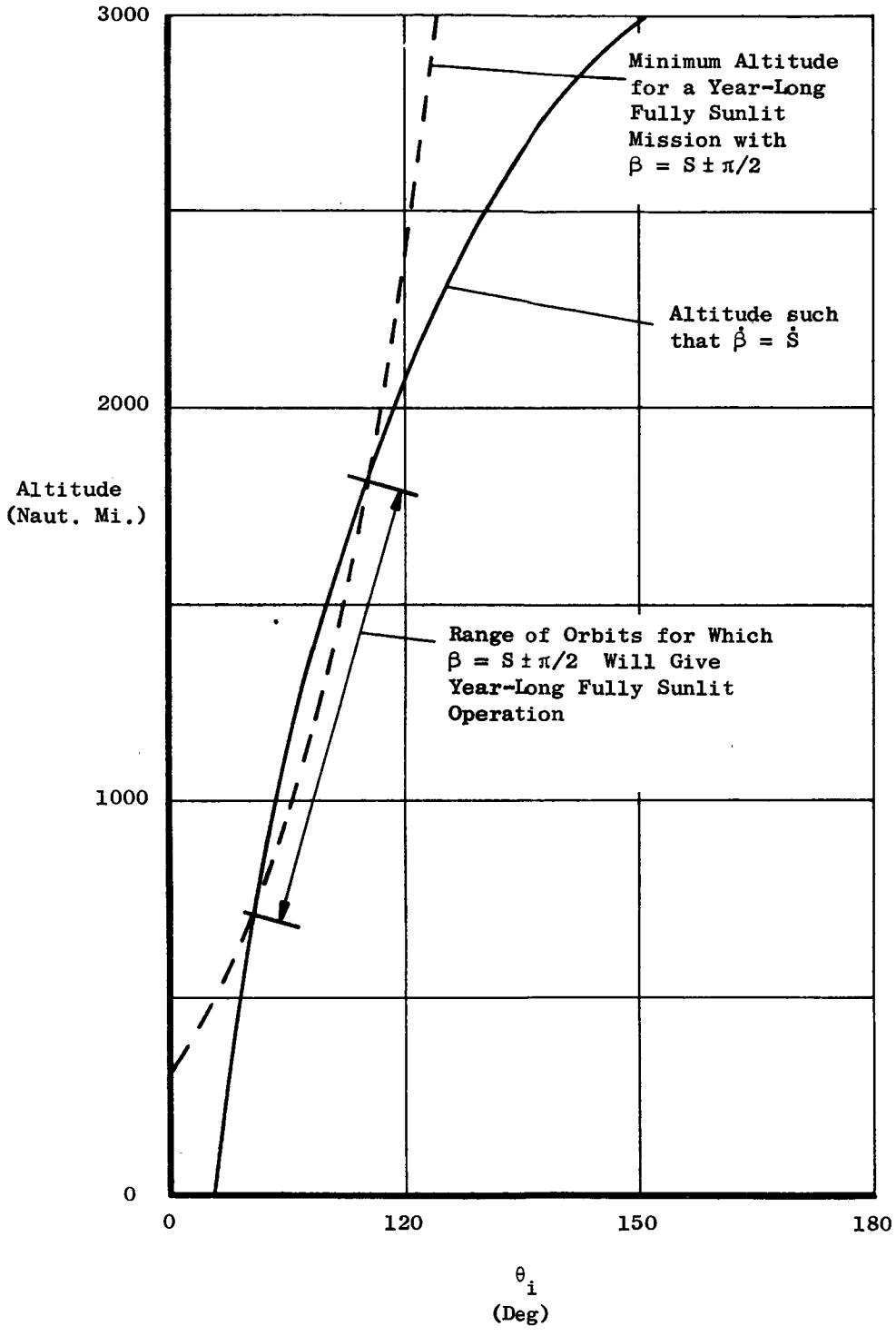

FIG. 9-2. ALTITUDE AND INCLINATION FOR YEAR-LONG FULLY SUNLIT OPERATION.

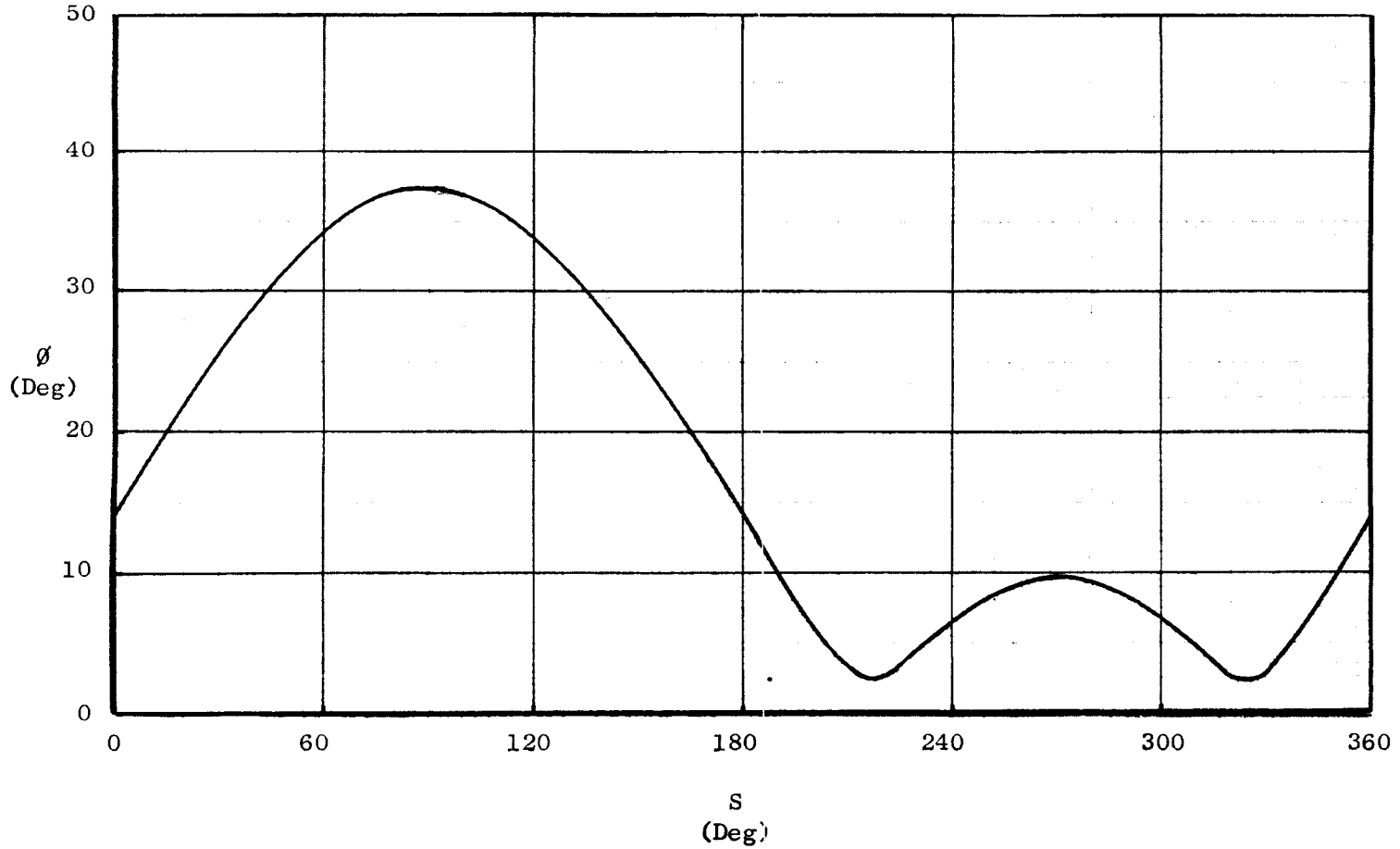

FIG. 9-3. TIME VARIATION OF ϕ FOR $\beta = S-\pi/2$ AND $\theta_i = 103.9°$.

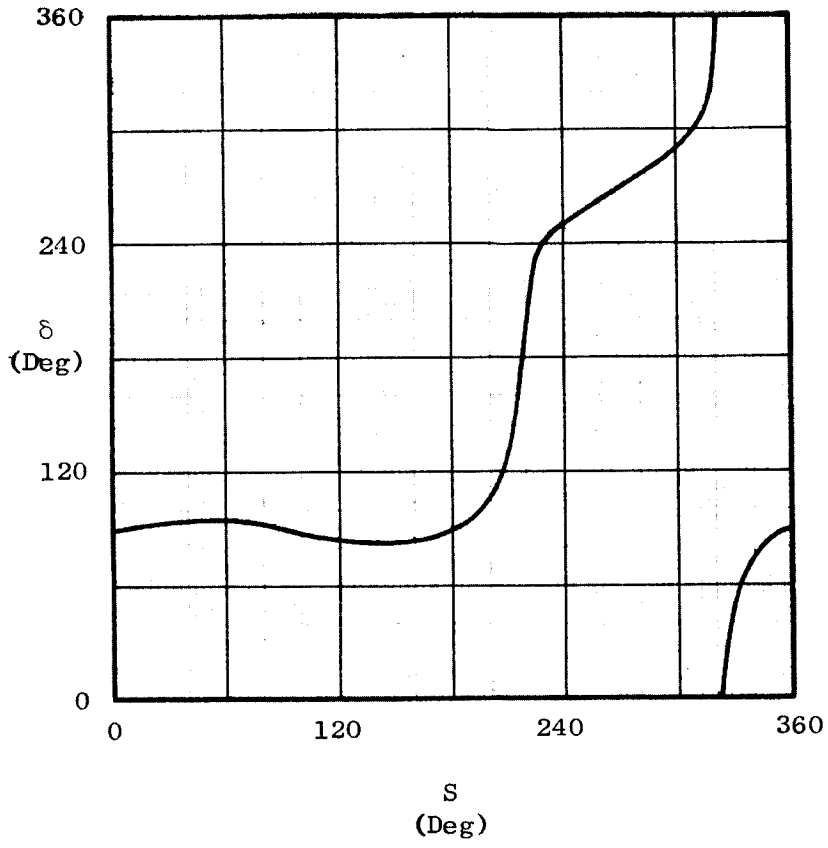

FIG. 9-4. TIME VARIATION OF δ FOR $\beta = S-\pi/2$ AND $\theta_i = 103.9°$.

Selection of σ_s will be based upon keeping the steady-state error of the disturbed system less than 0.1 deg. However, it is desired to have σ_s large enough that control saturation cannot occur during steady-state operation, but not so large that the large-error performance deviates noticeably from that with a signum control characteristic. This rule of thumb can be used to choose a preliminary trial value of σ_s. Neglecting the rate-dependent terms in σ (which will usually be quite small during steady-state operation)

$$|\sigma| \leq |B_{xR}c_{23}| + |B_{yR}c_{13}| \tag{9.15}$$

for small errors. Setting c_{13} and c_{23} equal to the steady-state accuracy requirement (ψ_e) and B_{xR} and B_{yR} equal to $2M_e/r_o^3$:

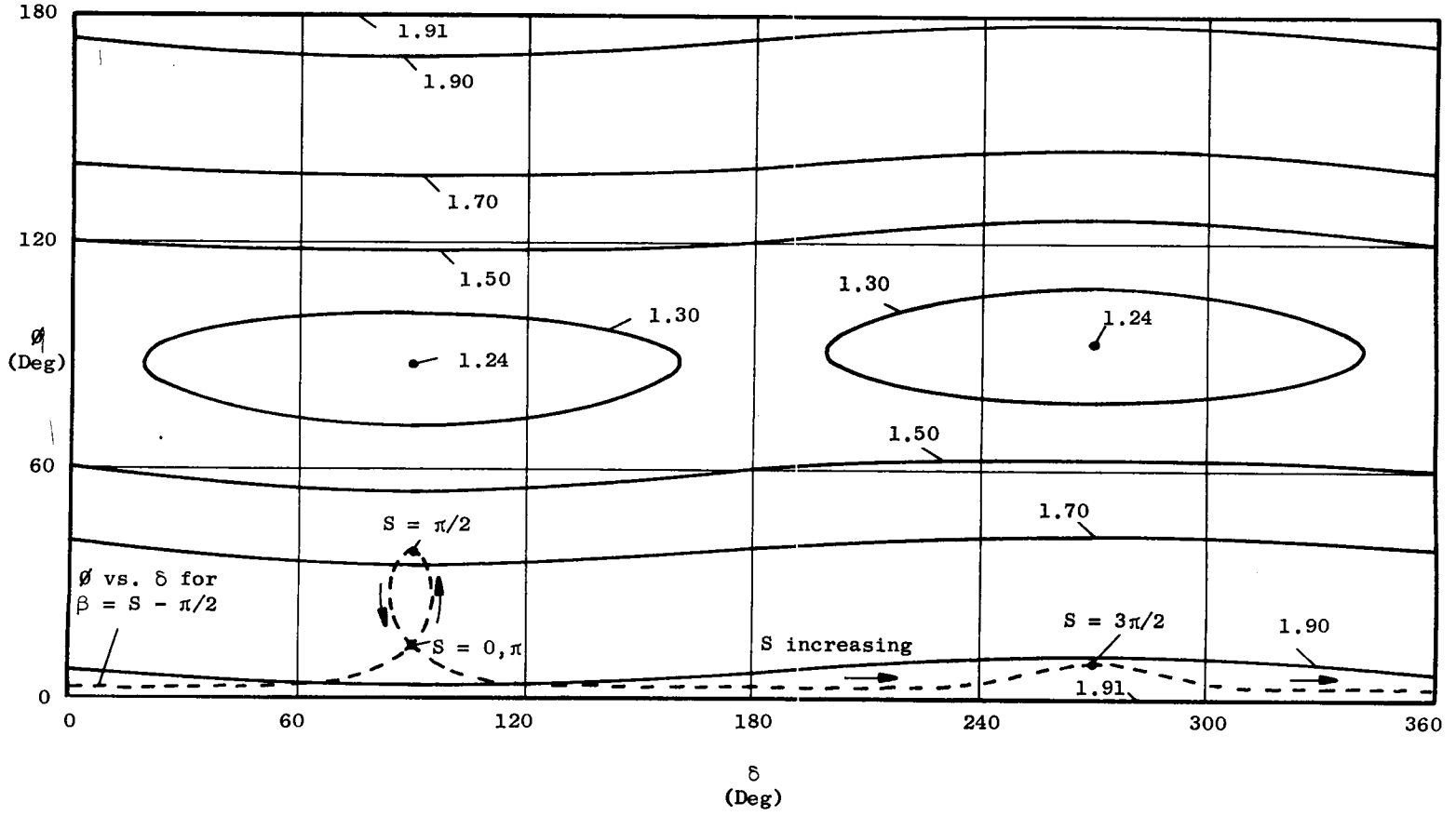

FIG. 9-5. CONTOURS OF CONSTANT G_{AV} FOR $\theta_i = 103.9°$.

$$|\sigma| \leq 4\left(\frac{M_e}{r_o^3}\right)\psi_e \text{ gauss} . \qquad (9.16)$$

In this case the bound is .001 gauss. For the preliminary design σ_s = .01 gauss will be selected, giving a linear range (in attitude error) of at most one deg.

With the inertias and spin speed specified above, the rate gain (K_R) must be greater than 7.5 sec . In accordance with the discussion of the previous section K_R = 15 sec will be chosen.

These preliminary control system parameters may be acceptable, or it may be necessary to modify them based upon simulation results.

3. Simulation Results

Before evaluating the disturbed motion, realistic values must be selected for the components of center-of-mass — geometric-centroid offset and the components of residual magnetic moment. In addition, the components Ω_x and Ω_y of the inertial rate of the (x_R, y_R, z_R) coordinate frame must be found.* It should be noted that at this altitude aerodynamic torques are negligible.

A reasonable choice for ℓ_x, ℓ_y, and ℓ_z is two inches. According to Bandeen and Manger [Ref. 9-3], TIROS I had a residual magnetic moment along the spin axis on the order of one amp-m^2. For this discussion m_x, m_y, and m_z will be assumed to be 3.28 amp-ft^2 approximately one-third of the level reported in Ref. 9-3.

The required components of $\bar{\Omega}^R$, Ω_x, and Ω_y, can be computed as a function of S by noting that the only contribution to these two rates is $\dot{S}\bar{e}_{zi}$ where z_i is the axis normal to the ecliptic plane;

---

* For small errors the only effect of a nonzero Ω_z is to limit the time for which c_{12} and c_{21} can be assumed to be zero (see the kinematic equations of Chapter II). Assumption of $c_{12} = c_{21} = 0$ means, in this case, that the inertial spin rate is modified by Ω_z, since the spin rate has been assumed to be ω_s relative to the (x_1, y_1, z_1) coordinate system. This effect is negligible because $\omega_s \gg \Omega_z$.

since $\bar{e}_{zi}$ is normal to $\bar{e}_{xs} = \bar{e}_{zR}$, the z_i axis lies in the (x_R, y_R) plane. However, it is convenient, in this case, to assume (pessimistically) that $\Omega_x = \Omega_y = \dot{S} = 2\times10^{-7}$ rad/sec.

Using the above data, and $\sigma_s = .01$ gauss as specified by the preliminary design, the small error averaged equations of motion (see Chapter VII) were simulated digitally to evaluate system performance. Figure 9-6 shows the steady-state forced response in this case.* Clearly more gain is required in the linear region. Figure 9-7 presents the steady-state response for $\sigma_s = .005$ gauss. It should be noted that in all cases the total transverse angular velocity was no more than 5×10^{-6} rad/sec and, therefore, contributes negligibly to the total attitude error; that is, $c_{13} \approx \chi_1$ and $c_{23} \approx \chi_2$ are extremely good approximations.

The foregoing results indicate that the steady-state peak error amplitude is very dependent upon the time of year. This fact is further illustrated by Fig. 9-8. It is particularly interesting that for $S = 75$ deg ($\emptyset = 37.0°$, $\delta = 88.0°$) the peak amplitude is 0.00170 radians, while for $S = 105$ deg ($\emptyset = 37.0°$, $\delta = 92.0°$) the peak amplitude is .00153 radians. This high sensitivity to the value of δ can be explained by observing that both the magnetic field components (upon which the coefficients of the differential equations depend) and the gravity gradient torques involve terms at twice orbital frequency with phasing which is dependent upon δ. It is not unexpected that the relative phasing of the periodic coefficients and the (synchronous) periodic forcing terms will affect the amplitude of the response.

Based as they are upon the untilted dipole model of the magnetic field, these results may be slightly optimistic. For example, at $S = 75°$ a tilted dipole model could result in errors slightly in excess of 0.1° at times when the magnetic dipole is, due to rotation of the earth, tilted away from the earth-sun line. This would signal a further decrease in σ_s.

---

* As usual, the untilted dipole model of the earth's magnetic field is employed.

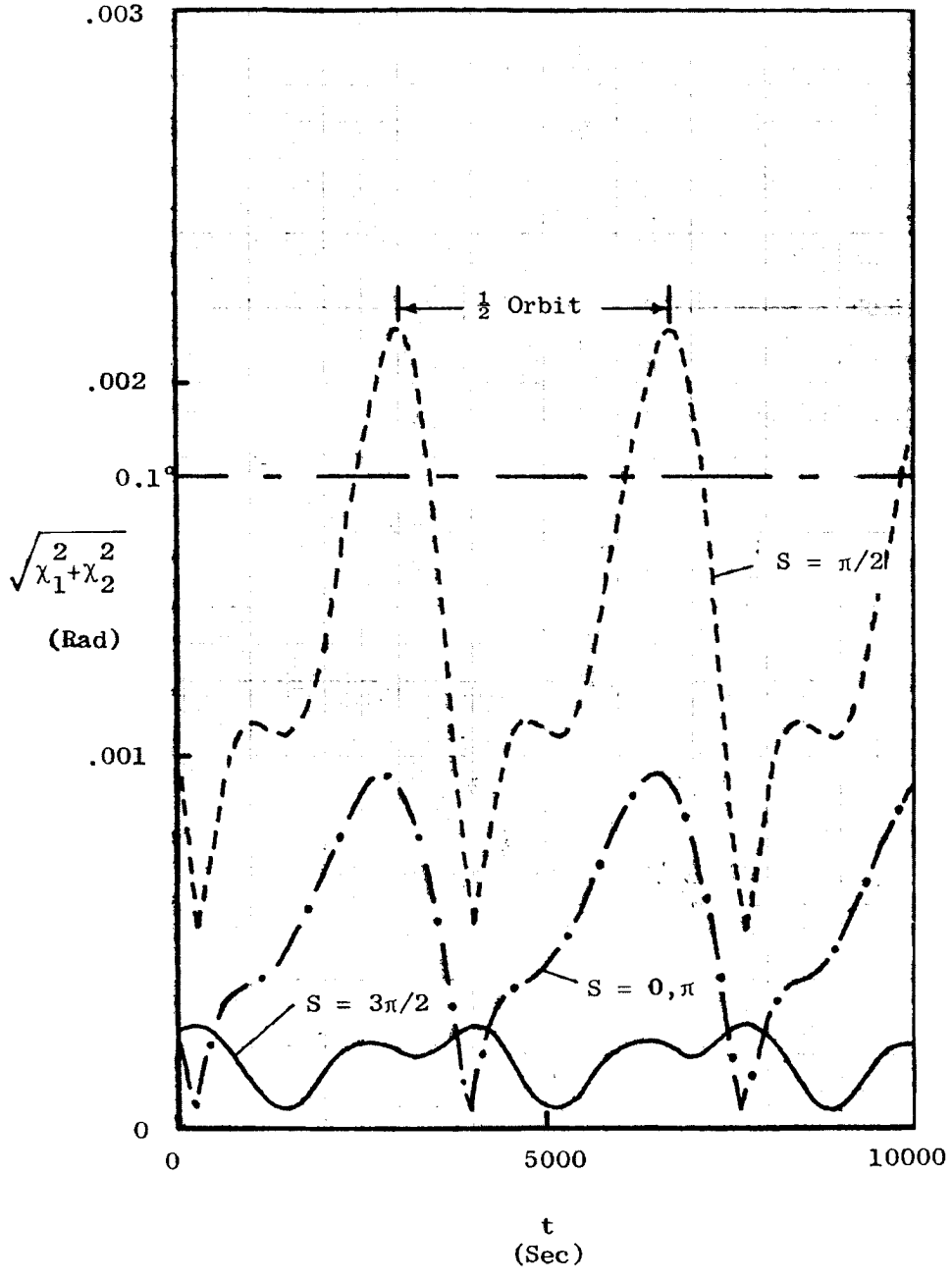

FIG. 9-6. SMALL-ERROR FORCED RESPONSE WITH $\sigma_s = 0.01$.

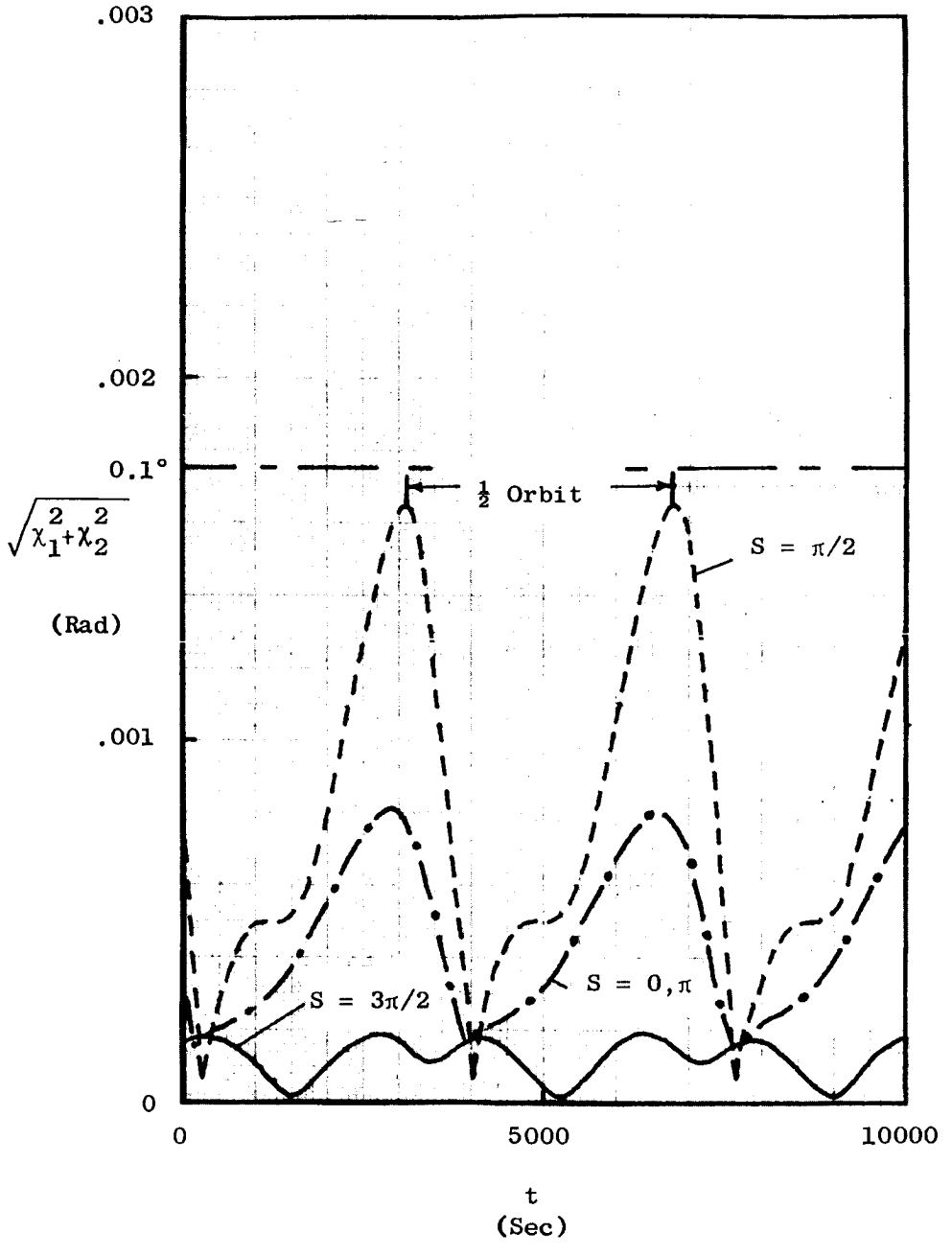

FIG. 9-7. SMALL-ERROR FORCED RESPONSE WITH $\sigma_s = 0.005$.

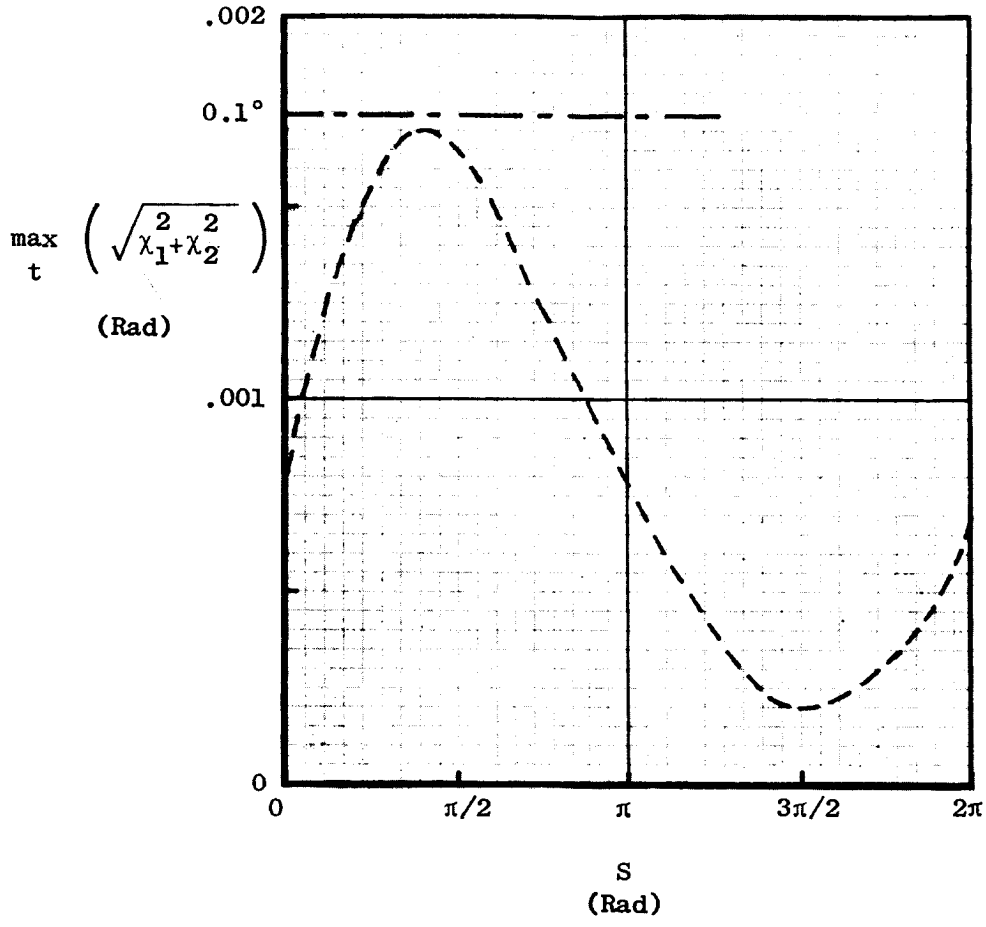

FIG. 9-8. MAXIMUM ATTITUDE ERROR VS. S WITH $\sigma_s = 0.005$.

On the other hand, at times when the magnetic dipole is tilted toward the earth-sun line these results may be somewhat pessimistic.

Figures 9-9, 9-10, and 9-11 show the large-error response based upon signum control of the simplified equations of motion. On each figure the time required to move from point (a) to point (b) is approximately one-half orbit period (about one hour). Reduction of the attitude error from 90 deg $(h_x^2+h_y^2 = 1)$ to 5 deg is easily accomplished within the allowed nine hours. The slowest of these cases is $S = \pi/2$, as predicted by Fig. 9-5.

4. Actuator Design

Chapter VIII presents a design procedure for air-cored actuators based upon specified values for the maximum available voltage (v_m), the

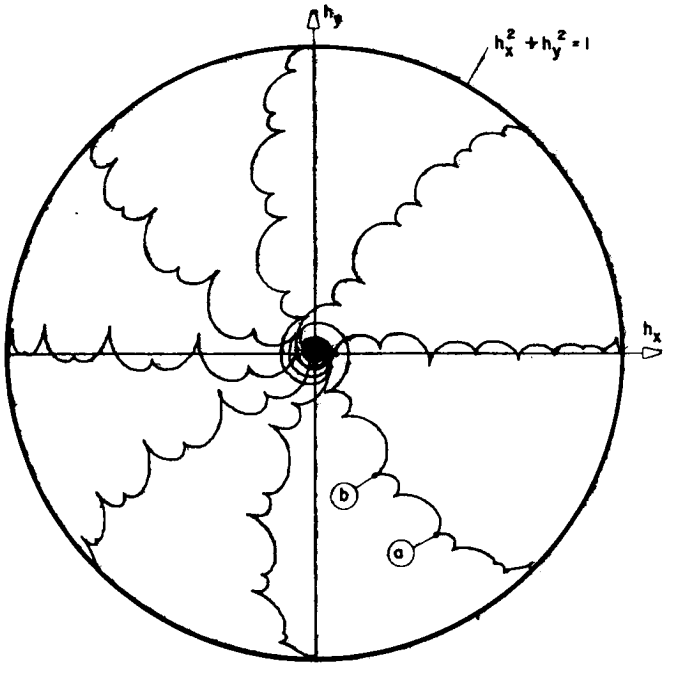

FIG. 9-9. LARGE-ERROR TRAJECTORIES FOR S = 0 AND S = π.

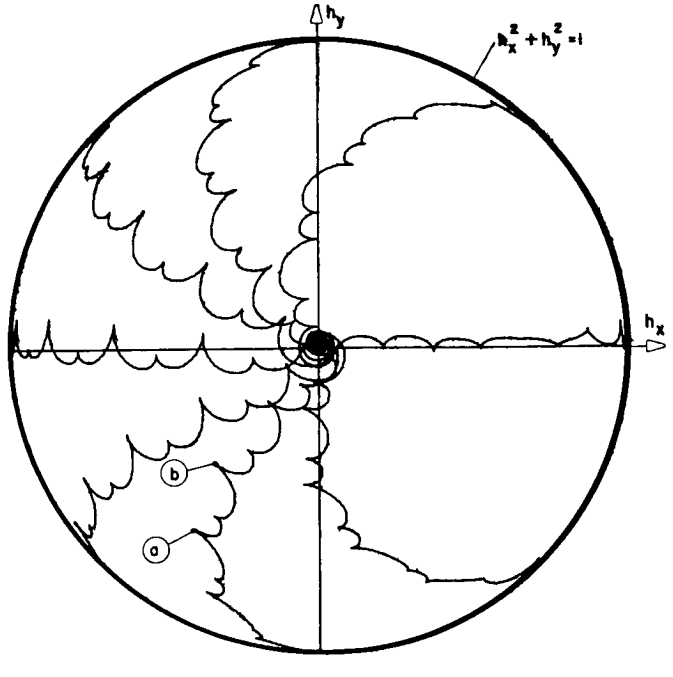

FIG. 9-10. LARGE-ERROR TRAJECTORIES FOR S = $\pi/2$.

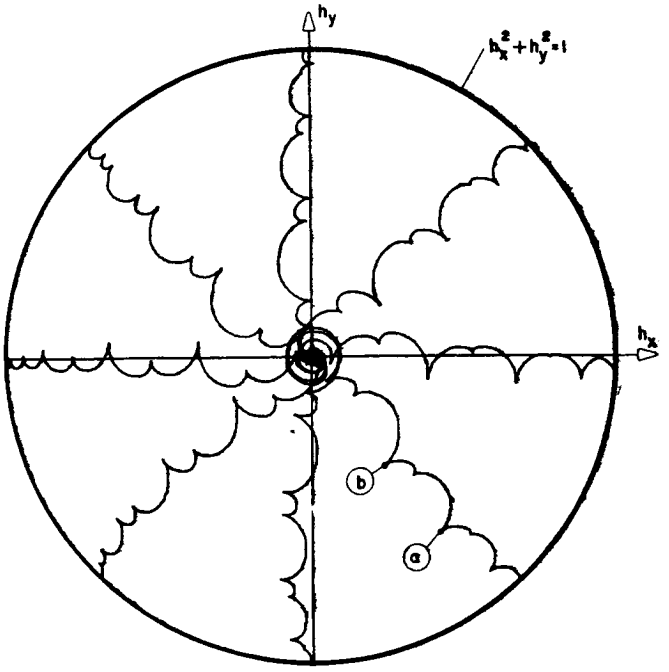

FIG. 9-11. LARGE-ERROR TRAJECTORIES FOR $S = 3\pi/2$.

coil radius (R_c), and the maximum required magnetic moment (m_m). The maximum required magnetic moment is the product of U_o and the spin momentum, H_s. For this problem

$$m_m = 1000 \text{ amp-ft}^2$$

$$R_c = 3 \text{ ft}$$

$$v_m = 28 \text{ volts} .$$

The value chosen for v_m is typical of many satellite power systems.

From expression (8.3) the resistance per unit length of the wire will be

$$\rho = \frac{R_c v_m}{2m_m} = 0.042 \text{ ohms/ft} .$$

Using AWG-24 aluminum wire, $\rho = .041$ ohms/ft which is close enough to the design value. The weight per unit length is, from the table of

Chapter VIII, 3.83×10^{-4} lbs/ft. From the above data, and expressions (8.5) and (8.6), the weight and maximum power are:

$$W = 0.00720 \cdot N_c \text{ lbs}$$

$$P_m = .992 \times \frac{10^3}{N_c} \text{ watts} .$$

The current through the wire is limited to i_R, by either power or thermal considerations. Then

$$N_c \geq \frac{m_m}{\pi R_c^2 i_R} = \frac{35.4}{i_R} .$$

The fusing current the wire in question is approximately 20 amperes. We may certainly consider 0.1 amperes as a safe value for i_R. Choosing $N_c = 354$ turns:

$$W = 2.55 \text{ lb}$$

$$P_m = 2.80 \text{ watts} .$$

It is of interest to consider the power drain during steady-state operation. Figure 9-12 shows $u(t)$ and $u^2(t)$ for $\sigma_s = .005$ gauss and $S = 75°$. From expressions (8.2) and (8.4) the power, as a function of u $(= m_c/H_s)$ is:

$$P = P_m\left(\frac{u}{U_o}\right)^2 . \qquad (9.17)$$

For this design the peak power drain in steady-state operation is 18.2×10^{-4} watts and the average power drain is 6.3×10^{-4} watts. Clearly the steady-state power drain is negligible. In many cases even the relatively large acquisition power drain will not add to the required capacity of the power supply because many power-consuming devices (e.g., the experiments) may not be activated until acquisition is complete.

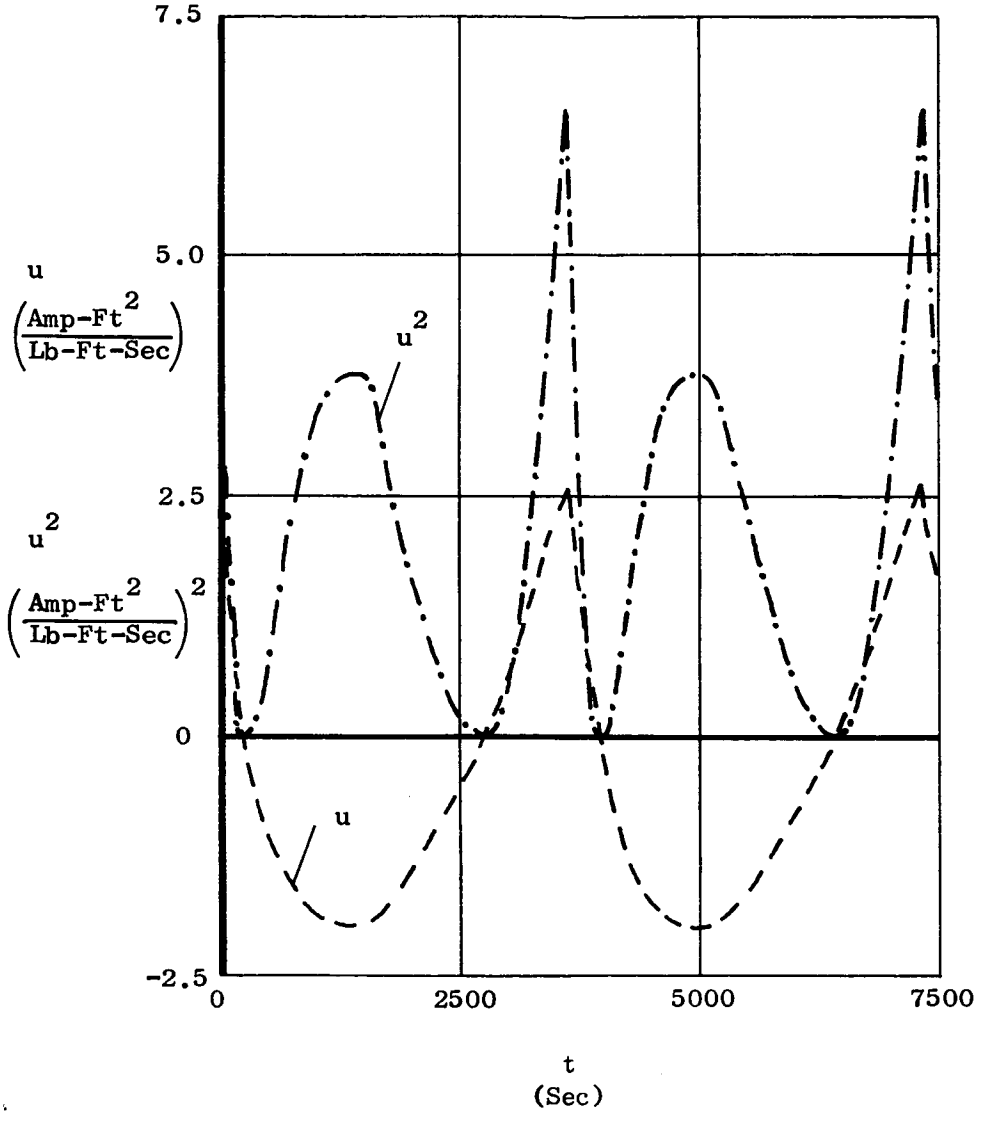

FIG. 9-12. u AND u^2 FOR $\sigma_s = 0.005$ AND S = 75°.

The same required peak magnetic moment could be generated using a ferromagnetic torquer. However, a residual magnetic moment of even one percent of the peak magnetic moment will in this case be quite significant, corresponding to 40 percent of the maximum value of u occurring during steady-state operation.

C. SUMMARY

This chapter has presented a design procedure for continuous magnetic attitude control of spinning satellites. This approach has been demonstrated by designing such a control system for a realistic application. For this example, the primary power and weight requirements are imposed by acquisition constraints; the power required for steady-state operation is negligible. If, for instance, the satellite can be separated from the booster in such a way that the initial attitude error is significantly less than the value (90°) assumed here, the weight of the coil can be reduced considerably, without affecting the small-error performance.

The results of this chapter also give a strong indication of the practical feasibility of controlling the attitude of a general spinning vehicle, in an orbit "sufficiently near" the earth, by means of the control law developed in this study.* Although the application considered in this chapter was not chosen as a critical test of the magnetic control scheme, neither was it selected to show magnetic control in a favorable light, except perhaps from the point of view of mechanization as indicated in Chapter VIII. Indeed, it is reasonable to conjecture that the orbital parameters of this mission could have been changed markedly without affecting our ability to choose control system

---

* In this context "sufficiently near" orbits are those for which (1) the dipole magnetic field model is a reasonable approximation (Appendix A) and, (2) the magnetic field is intense enough to provide sufficient control authority to satisfy the requirements of the specified mission. The results presented in this dissertation indicate that it is reasonable to consider attitude control for spinning satellites at altitudes as great as 10,000 nautical miles. At higher altitudes simulation studies using a more realistic magnetic field model are advisable.

parameters to achieve the required control accuracy. Of course, the cost of control would, in this event, be altered.

This is not to say that cases cannot be found for which the feasibility of magnetic control would be doubtful. We might, for instance, alter the example of this chapter by making the orbit equatorial. With the untilted dipole model, the system would be uncontrolled as established by the stability analyses of Chapter IV; even with the tilted dipole model control authority would be limited.

In spite of the existence of cases for which magnetic control is impractical, the results of this and preceding chapters indicate strongly that this magnetic control system is worth considering for a wide variety of missions.

X. CONCLUSIONS

A. SUMMARY OF IMPORTANT RESULTS

1. Theoretical Feasibility of Magnetic Attitude Control of Spinning Vehicles

The primary goal of this study was the demonstration of the theoretical feasibility of control of the attitude of a general spinning satellite using control torques generated by the interaction of a current-carrying coil with the earth's magnetic field. This phase of the study was based upon the following major assumptions:

1. The vehicle was assumed inertially symmetric with respect to the spin axis ($I_z > I_x = I_y$).

2. The orbit was assumed to be circular.

3. Nodal regression was neglected (this is equivalent to assuming a spherical earth).

4. The desired spin-axis direction was assumed to be fixed in inertial space.

5. The magnetic field was approximated by a dipole model (Appendix A).

Under these conditions, and with a specific control law developed in this dissertation (Chapter III), theoretical feasibility has been demonstrated for any orbit parameters (altitude and inclination) and desired pointing direction, for the tilted dipole model of the earth's magnetic field. The control law has, moreover, been shown to be asymptotically stable for arbitrarily large initial errors and transverse angular velocities. These results were obtained by using Lyapunov's second method and represent one of the few instances in which this technique has been successfully applied to nonlinear, time-varying differential equations.

It is particularly interesting that use of the untilted dipole model of the earth's magnetic field (which assumes the geomagnetic and geographic polar axes to be aligned and is, therefore, much simpler than the tilted dipole model), yields pessimistic stability results as a direct

result of the simplification of the magnetic field components. For example, with the untilted dipole, B_{yR} (one of the two magnetic field components normal to the desired pointing direction, z_R) is zero for all time if the orbit is equatorial. With this field model, the feedback control law is ineffective in such orbits, and the system is not asymptotically stable. However, with the tilted dipole model, the geomagnetic and geographic equatorial planes are not coincident, and the vehicle cannot remain for all time in the geomagnetic equatorial plane (except for synchronous orbits--which occur at altitudes where the dipole models of the earth's magnetic field are invalid) so that B_{yR} cannot be always zero.

Major limitations of this stability analysis are the assumptions of a circular orbit and a dipole magnetic field model. However, the results of the stability analysis and the character of the Lyapunov function employed allow us to conjecture with a high degree of confidence that asymptotic stability in-the-large exists for elliptical orbits and the exact environmental magnetic field.

2. Control Law

A major contribution of this thesis is the development of a new and practical feedback control law for magnetic attitude control of spinning spacecraft. This control law specifies a control of the form $u = \eta(\sigma)$ (hence, a coil current proportional to $\eta(\sigma)$) where $\sigma = \sigma_p + K_R\sigma_R$, σ_p being a function of the attitude error and σ_R depending only upon the transverse components of the total angular velocity of the vehicle. (Both terms have coefficients depending upon the measured environmental magnetic field.) Thus, this control law provides active magnetic damping as well as position control. As a result of the stability analysis, the amount of damping (as characterized by the gain K_R) required for asymptotic stability has been determined as a function of the vehicle moments of inertia and its spin rate, ω_s:

$$K_R > \frac{1}{(1 + k)\omega_s}$$

with k defined by

$$k = \frac{I_z - I_x}{I_x}$$

where I_z is the moment of inertia about the nominal spin axis, and I_x is the moment of inertia about any transverse axis of the axially symmetric vehicle.

A major unanswered question is that of the feasibility of combining a magnetic control of the form $u = \eta(\sigma_p)$, for attitude control, with a passive mechanical damper for damping of the transverse angular velocities. Intuitively such a combination is practical if the damper has sufficient authority.

3. Performance Evaluation

Using a combination of Krylov-Bogoliubov averaging techniques and other heuristic approaches, estimates have been developed for both the large-error and small-error undisturbed performance of the magnetic control law. These estimates show explicitly the influence of the altitude, the orbital inclination, and the nominal pointing direction upon the response of the undisturbed system. These results are very useful for preliminary selection of the free parameters in the magnetic control system.

In order to evaluate the effects of disturbances upon the performance of the magnetic control law, similar techniques have been applied. Disturbances considered are inertial motion of the axis defining the desired spin-axis direction (a kinematic effect), and external torques due to aerodynamic pressure, solar radiation pressure, gravity gradient, and residual vehicle magnetic moments. In this case, no closed form result was obtained; however, the resulting small-error averaged equations of motion can be integrated numerically in a time much shorter than that required to integrate the exact equations of motion. This results in a considerable saving, both by reducing the magnitude of the simulation required and by reducing the computer time required for each solution. The validity of these averaged equations of motion (as well as that of the

estimates of the undisturbed motion) has been confirmed by extensive analog and digital simulation.

A reasonable performance criterion for the large-error (acquisition) performance of an attitude control system is the speed of response. The large-error performance of the feedback control law developed in this dissertation has been shown (with $u = U_o \text{ sgn } \sigma$) to compare favorably in this respect with minimal-time control programs derived by applying Pontryagin's maximum principle.

4. Practical Feasibility of Magnetic Attitude Control of Spinning Vehicles

Practical feasibility involves both considerations of mechanization and the ability of the control system to maintain the required steady-state accuracy in the face of environmental disturbances. In each of these areas, practical feasibility depends strongly upon the specific requirements of a particular vehicle, including the orbital altitude, the orbital inclination, the required pointing direction, and the level of accuracy required.

The most critical mechanization problem is that of measuring the spin-axis attitude, the greatest difficulties arising when the spin axis is to be directed toward a point not occupied by a source of detectable radiation.

Aside from sensor considerations, the major limitation upon the applicability of this control system occurs when the coil weight and/or power required to achieve the specified performance become unacceptable. The cases where this problem is most likely to occur are those in which the control torque available is severely limited throughout the orbit by either the magnitude of the magnetic field (due to high altitudes--10,000 nautical miles or more) or its direction (due to low orbital inclinations--30 deg or less). It should be noted that the altitude limitation concerns the magnitude of the field, rather than deviations of the field from that of a magnetic dipole (due, for example, to the effect of the solar wind). Indeed, as was seen in comparing the stability properties derived using a tilted dipole model with those obtained using an untilted dipole model, additional frequencies in the magnetic field

model (which can be present at both low and high altitudes--see Appendix A) can be expected to improve the stability properties of the control system.

Other factors which potentially limit the applicability of this control law are the level of accuracy required and the character of the disturbances (which, for missions requiring extremely high accuracy, include such effects as sensor misalignments and magnetometer interference). Unfortunately, owing to the time-varying coefficients in the equations of motion, it has not been possible to establish general conclusions regarding the attainable accuracy. In the final analysis, each case must be treated individually, using simulation techniques, as has been done for a specific application in Chapter IX.

B. RECOMMENDATIONS FOR FUTURE STUDIES

1. Extensions of this Study

There are several directions in which the results of this study may be extended. Among these are consideration of vehicles in elliptic orbits, extension to vehicles which do not possess axial inertial symmetry, and use of the position control law developed here in combination with various mechanical dampers. In each of these cases, the critical problem is that of demonstrating stability. These extensions are definitely nontrivial. However, it appears, intuitively, that these suggested studies would not yield negative results.

2. Fully Stabilized Vehicles

Although magnetic attitude control of fully stabilized vehicles has received considerable attention, most of the published results are based upon simulation studies and intuitive arguments. The problems of large-error convergence and small-error stability have not been treated rigorously. The problems appear to be even more formidable than those associated with magnetic control of spinning vehicles, and the magnetic control of fully stabilized satellites offers a fertile area for future investigations.

APPENDIX A. DIPOLE MODELS OF THE EARTH'S MAGNETIC FIELD

The analytic developments of this study are based upon dipole models (tilted and untilted) of the earth's magnetic field. The magnetic field is assumed to be produced by a single magnetic dipole located at the geographical center of the earth. Although more accurate models are available, they are generally not employed in analysis owing to their complex nature.

The appendix derives a dipole model for the earth's magnetic field in terms of the geometry defined in Chapter II. Following the derivation is a qualitative discussion of the degree to which the actual magnetic field departs from the dipole model.

A. DERIVATION OF DIPOLE MODELS

In the (x_m, y_m, z_m) coordinate frame of Fig. A-1 the dipole moment of the earth is [Ref. A-1]

$$\bar{M}_e = - M_e \bar{e}_{zm}$$

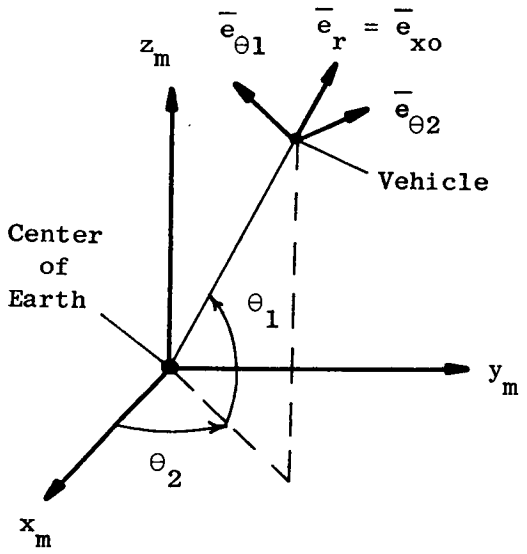

FIG. A-1. SPHERICAL COORDINATE AXES.

where $M_e = 2.845 \times 10^{21}$ gauss-ft^3. In the spherical coordinate frame of Fig. A-1 the magnetic field is [Ref. A-1]:

$$\bar{B} = -\left(\frac{M_e}{r_o^3}\right)[(2 \sin \theta_1)\bar{e}_r - (\cos \theta_1)\bar{e}_{\theta 1}] . \qquad \text{(A.1)}$$

The (x_m, y_m, z_m) coordinates of the figure are defined with the z_m axis along the effective north magnetic pole and the x_m axis in the geographic equatorial plane, as shown in Fig. A-2. The transformation from the spherical set to (x_m, y_m, z_m) is:

$$\begin{bmatrix} \bar{e}_{xm} \\ \bar{e}_{ym} \\ \bar{e}_{zm} \end{bmatrix} = \begin{bmatrix} -\sin \theta_2 & -\cos \theta_2 \sin \theta_1 & \cos \theta_2 \cos \theta_1 \\ \cos \theta_2 & -\sin \theta_2 \sin \theta_1 & \sin \theta_2 \cos \theta_1 \\ 0 & \cos \theta_1 & \sin \theta_1 \end{bmatrix} \begin{bmatrix} \bar{e}_{\theta 2} \\ \bar{e}_{\theta 1} \\ \bar{e}_r \end{bmatrix} \qquad \text{(A.2)}$$

The components of the magnetic field in the (x_m, y_m, z_m) coordinate frame are, then:

$$\begin{bmatrix} B_{xm} \\ B_{ym} \\ B_{zm} \end{bmatrix} = -\frac{M_e}{r_o^3} \begin{bmatrix} 3 \cos \theta_2 \sin \theta_1 \cos \theta_1 \\ 3 \sin \theta_2 \sin \theta_1 \cos \theta_1 \\ 3 \sin^2 \theta_1 - 1 \end{bmatrix} \qquad \text{(A.3)}$$

which may also be written:

$$\begin{bmatrix} B_{xm} \\ B_{ym} \\ B_{zm} \end{bmatrix} = -\frac{M_e}{r_o^3} \begin{bmatrix} 3(\bar{e}_{xm} \cdot \bar{e}_r)(\bar{e}_{zm} \cdot \bar{e}_r) \\ 3(\bar{e}_{ym} \cdot \bar{e}_r)(\bar{e}_{zm} \cdot \bar{e}_r) \\ 3(\bar{e}_{zm} \cdot \bar{e}_r)^2 - 1 \end{bmatrix} . \qquad \text{(A.4)}$$

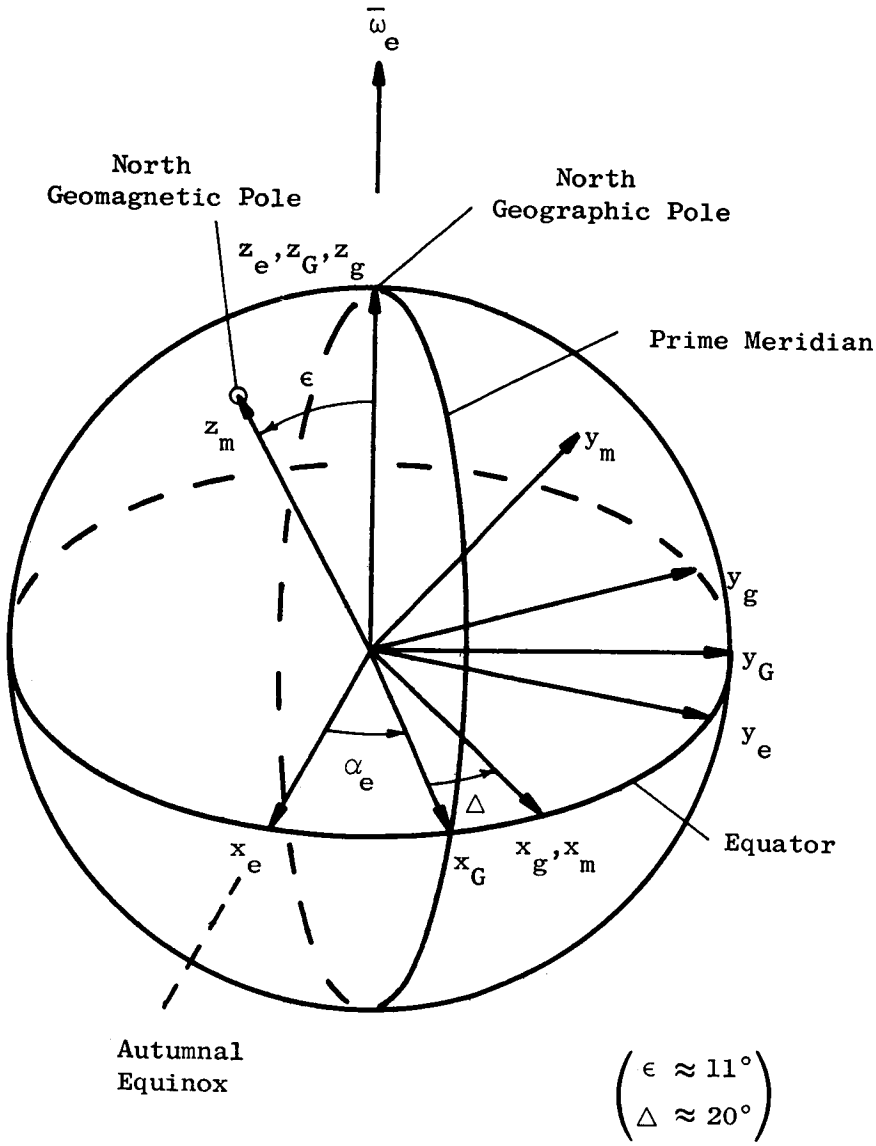

FIG. A-2. MAGNETIC DIPOLE COORDINATES.

The transformation of these components into the (x_o, y_o, z_o) frame of Fig. 2-1 proceeds through the coordinate frames of Fig. 2-1 and Fig. A-2. Notice that the rotations α_e, Δ, and β are about the same axis (z_e). Therefore, with

$$\mu \triangleq \alpha_e + \Delta - \beta \tag{A.5}$$

the field components in (x_o, y_o, z_o) coordinates are

$$\begin{bmatrix} B_{xo} \\ B_{yo} \\ B_{zo} \end{bmatrix} = \begin{bmatrix} \cos\alpha & \sin\alpha & 0 \\ -\sin\alpha & \cos\alpha & 0 \\ 0 & 0 & 1 \end{bmatrix} \begin{bmatrix} A_{11} & A_{12} & A_{13} \\ A_{21} & A_{22} & A_{23} \\ A_{31} & A_{32} & A_{33} \end{bmatrix} \begin{bmatrix} B_{xm} \\ B_{ym} \\ B_{zm} \end{bmatrix} \tag{A.6}$$

where

$$A_{11} = \cos\mu$$

$$A_{12} = -\cos\epsilon \sin\mu$$

$$A_{13} = \sin\epsilon \sin\mu$$

$$A_{21} = \cos\theta_i \sin\mu$$

$$A_{22} = \cos\epsilon \cos\theta_i \cos\mu + \sin\epsilon \sin\theta_i$$

$$A_{23} = -\sin\epsilon \cos\theta_i \cos\mu + \cos\epsilon \sin\theta_i$$

$$A_{31} = -\sin\theta_i \sin\mu$$

$$A_{32} = -\cos\epsilon \sin\theta_i \cos\mu + \sin\epsilon \cos\theta_i$$

$$A_{33} = \sin\epsilon \sin\theta_i \cos\mu + \cos\epsilon \cos\theta_i$$

Note that $\bar{e}_{xo} = \bar{e}_r$. Then, if

$$\begin{bmatrix} B_{xo} \\ B_{yo} \\ B_{zo} \end{bmatrix} = \begin{bmatrix} C_{11} & C_{12} & C_{13} \\ C_{21} & C_{22} & C_{23} \\ C_{31} & C_{32} & C_{33} \end{bmatrix} \begin{bmatrix} B_{xm} \\ B_{ym} \\ B_{zm} \end{bmatrix} = \approx{C} \begin{bmatrix} B_{xm} \\ B_{ym} \\ B_{zm} \end{bmatrix} \tag{A.7}$$

it is clear from (A.4) that:

$$\begin{bmatrix} B_{xm} \\ B_{ym} \\ B_{zm} \end{bmatrix} = -\frac{M_e}{r_o^3} \begin{bmatrix} 3C_{11} & C_{13} \\ 3C_{12} & C_{13} \\ 3C_{13}^2 & -1 \end{bmatrix} . \tag{A.8}$$

Therefore:

$$\begin{bmatrix} B_{xo} \\ B_{yo} \\ B_{zo} \end{bmatrix} = -\frac{M_e}{r_o^3} \left\{ 3C_{13} \begin{bmatrix} C_{11} & C_{12} & C_{13} \\ C_{21} & C_{22} & C_{23} \\ C_{31} & C_{32} & C_{33} \end{bmatrix} \begin{bmatrix} C_{11} \\ C_{12} \\ C_{13} \end{bmatrix} - \begin{bmatrix} C_{13} \\ C_{23} \\ C_{33} \end{bmatrix} \right\} . \tag{A.9}$$

However, the matrix $\approx{C}$ is an orthogonal transformation matrix with the property

$$C_{il}C_{jl} + C_{i2j2} + C_{i3}C_{j3} = \begin{cases} 1, & i = j \\ 0, & i \neq j \end{cases} . \tag{A.10}$$

The components of $\bar{B}$ in (x_o, y_o, z_o) coordinates are simply:

$$\begin{bmatrix} B_{xo} \\ B_{yo} \\ B_{zo} \end{bmatrix} = -\frac{M_e}{r_o^3} \begin{bmatrix} 2C_{13} \\ -C_{23} \\ -C_{33} \end{bmatrix} . \qquad \text{(A.11)}$$

Forming C_{13}, C_{23}, and C_{33} from expression (A.6) and using the appropriate trigonometric identities:

$$B_{xo} = -\frac{M_e}{r_o^3}\left\{2\cos\epsilon \sin\theta_i \sin\alpha - [(1+\cos\theta_i)\sin(\alpha-\mu) - (1-\cos\theta_i)\sin(\alpha+\mu)]\sin\epsilon\right\}$$

$$B_{yo} = -\frac{M_e}{r_o^3}\left\{-\cos\epsilon \sin\theta_i \cos\alpha + \frac{1}{2}[(1+\cos\theta_i)\cos(\alpha-\mu) - (1-\cos\theta_i)\cos(\alpha+\mu)]\sin\epsilon\right\}$$

$$B_{zo} = -\frac{M_e}{r_o^3}\left\{-\cos\epsilon \cos\theta_i - \sin\epsilon \sin\theta_i \cos\mu\right\} . \qquad \text{(A.12)}$$

The coefficient M_e/r_o^3 varies with altitude as shown in Fig. A-3.

The magnetic field can be expressed in the nodal coordinate frame (x_n, y_n, z_n) of Fig. 2-1 as:

$$B_{xn} = -\left(\frac{M_e}{2r_o^3}\right)[(d_1 - d_3)\sin\mu + 3d_1\sin(2\alpha+\mu) + 3d_3\sin(2\alpha-\mu) + 3d_5\sin2\alpha]$$

$$B_{yn} = -\left(\frac{M_e}{2r_o^3}\right)[(d_1 + d_3)\cos\mu - 3d_1\cos(2\alpha+\mu) - 3d_3\cos(2\alpha-\mu) + d_5 - 3d_5\cos2\alpha]$$

$$B_{zn} = -\left(\frac{M_e}{2r_o^3}\right)(d_7 + d_8\cos\mu) \qquad \text{(A.13)}$$

where

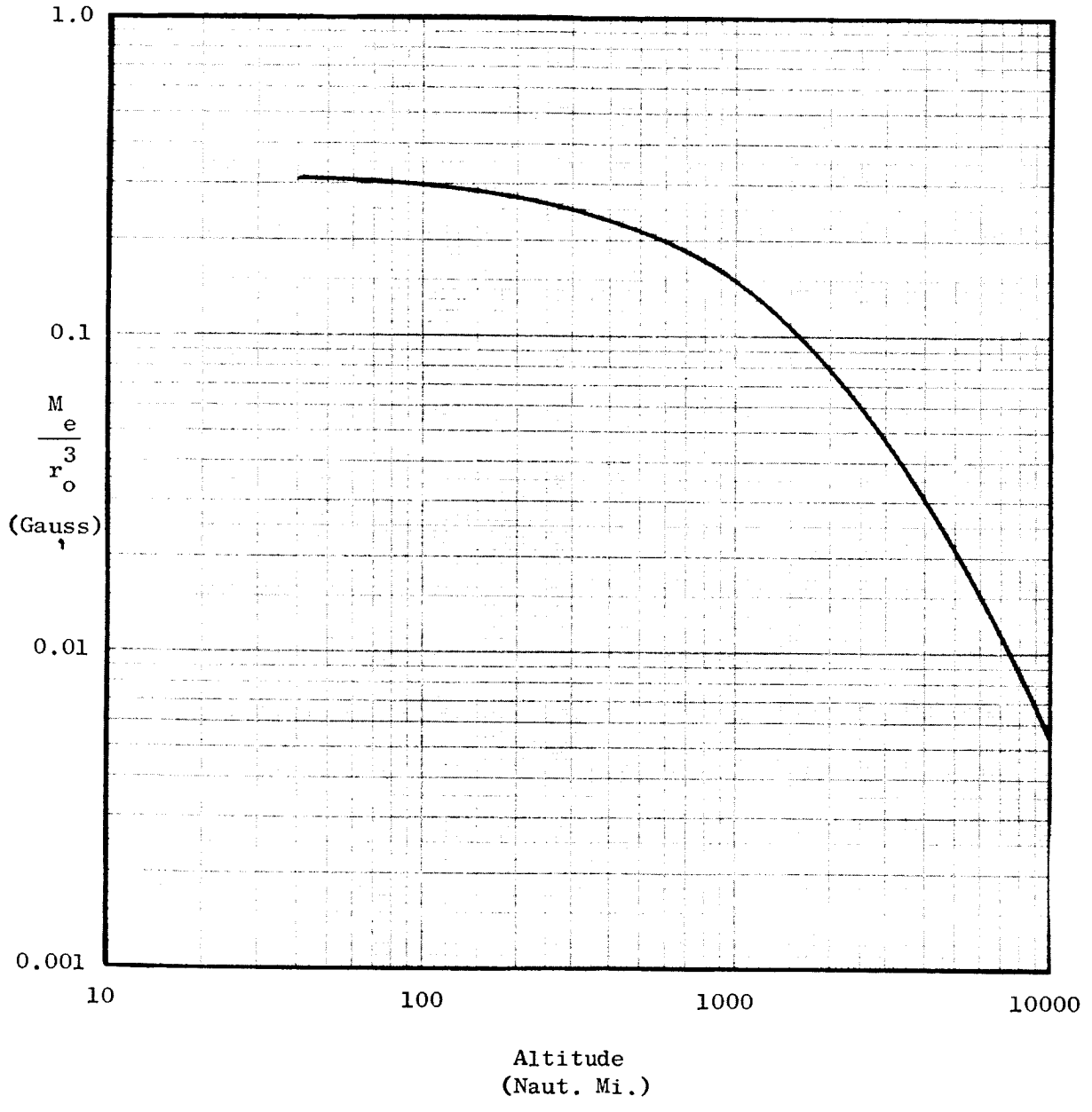

FIG. A-3. MAGNITUDE OF M_e/r_o^3 AS A FUNCTION OF SATELLITE ALTITUDE.

$$d_1 = \sin \epsilon \sin^2 \frac{1}{2} \theta_i$$

$$d_3 = -\sin \epsilon \cos^2 \frac{1}{2} \theta_i$$

$$d_5 = \cos \epsilon \sin \theta_i$$

$$d_7 = -2 \cos \epsilon \cos \theta_i$$

$$d_8 = -2 \sin \epsilon \sin \theta_i \ .$$

Notice that, since $\epsilon \approx 11°$, the dominant time-varying terms in (A.13) are those at twice orbital frequency. Since the secondary terms vary at frequencies whose ratio to the orbital rate can be irrational, the magnetic field components are, in general, almost periodic functions.

In many cases useful results can be obtained by employing the less refined dipole model which results from considering the earth's magnetic dipole to be aligned with the spin axis of the earth ($\epsilon = 0$). For the untilted dipole model, (A.13) reduces to:

$$\begin{bmatrix} B_{xn} \\ B_{yn} \\ B_{zn} \end{bmatrix} = -\left(\frac{M_e}{2r_o^3}\right) \begin{bmatrix} 3 \sin 2\alpha \sin \theta_i \\ (1 - 3 \cos 2\alpha) \sin \theta_i \\ -2 \cos \theta_i \end{bmatrix} \ . \qquad \text{(A.14)}$$

In the (x_R, y_R, z_R) coordinate frame of Fig. 2-3 (with $\xi' = 0$), the untilted dipole model yields

$$B_{xR} = -\left(\frac{M_e}{2r_o^3}\right)\left\{[\sin \delta + 3 \sin (2\alpha - \delta)]\cos \phi \sin \theta_i + 2 \sin \phi \cos \theta_i\right\}$$

$$B_{yR} = -\left(\frac{M_e}{2r_o^3}\right)\left\{[\cos \delta - 3 \cos (2\alpha - \delta)]\sin \theta_i\right\} \qquad \text{(A.15)}$$

$$B_{zR} = -\left(\frac{M_e}{2r_o^3}\right)\left\{[\sin \delta + 3 \sin (2\alpha - \delta)]\sin \phi \sin \theta_i - 2 \cos \phi \cos \theta_i\right\} \ .$$

The angles α_e, β, and α, all of which appear in the tilted dipole model, are time varying. For circular orbits

$$\alpha = \omega_o t + \alpha_o \tag{A.16}$$

and

$$\beta = \dot{\beta} t + \beta_o \tag{A.17}$$

where $\dot{\beta}$ is given in expression (2.1).

The angle α_e is the angular displacement from the Autumnal Equinox of the intersection of the prime meridian with the equatorial plane. In terms of T_s, the apparent solar time at Greenwich (in hours),

$$\alpha_e(T) = \omega_e T_s + \alpha_{eo}$$

where $\omega_e = 15$ deg/hour and α_{eo} is the value of α_e at $T_s = 0$ (midnight). Because at midnight the sun must be over the meridian 180° from the prime meridian, it can be shown that

$$\alpha_{eo} = \arctan(\cos \zeta \tan S)$$

where $\zeta = -23.45°$ and S is the displacement of the sun in the ecliptic plane from Vernal Equinox (see Fig. 7-3). The angles α_{eo} and S must be in the same quadrant.

B. VALIDITY OF DIPOLE MODELS

We may regard the magnetic field at any point in space as being composed of a stationary term (one which depends only upon the location of the point in question in geomagnetic coordinates) and a nonstationary term (one which depends upon time as well as upon the geometry).

The stationary field is that part of the magnetic field which we have attempted to represent by a magnetic dipole located at the center of the earth. The model derived above is, at best, a first approximation. According to Bartels, the horizontal field component measured in some regions on the surface of the earth differs by as much as 0.1 gauss

(approximately 30%) from the values given by the centered dipole model [Ref. A-2]. A somewhat better approximation is given by the eccentric dipole model, a model which assumes the source of the magnetic field to be a single dipole displaced from the geometric center of the earth [see Ref. A-3]. The most exact model for the stationary component of the earth's magnetic field is based upon matching the gradient of a high-order potential function to the magnetic field. The results of a 48-term harmonic analysis of the earth's magnetic field are discussed briefly in Ref. A-3. Even this model fails at high altitudes (5 to 10 earth radii) due to distortion of the geomagnetic field by the solar wind [Ref. A-4].

The nonstationary field, which is not represented in the dipole model of the preceding section, is composed of secular terms which require many years to produce a noticeable change, and more significant terms which have periods ranging from less than a second to several years. Most of the short-term variations arise from interactions of the geomagnetic field with the solar wind. A typical level for this disturbance field (observed at the surface of the earth) is several milligauss; hence, in near-earth orbits, these transient variations are much smaller than the main field.

C. USE OF THE UNTILTED DIPOLE MODEL FOR ANALYTICAL STUDIES

The primary motivation for using the untilted dipole model of the earth's magnetic field rather than the more accurate tilted dipole model is convenience of analysis [compare, for example, expressions (A.13) and (A.14)]. But the existence of this very strong motive does not, of course, mean that the results obtained with this approximation will be valid.

The stability analyses presented in this dissertation (Chapter IV) employ both the untilted and tilted dipole models. It is particularly interesting that the untilted model gives pessimistic stability results, and that this pessimism is directly due to the simplification of the expressions for the magnetic field components.

The effect of employing the untilted dipole model in the performance estimates is another matter. To consider this problem it is useful to cast the tilted dipole model in a form comparable to the untilted model of expression (A.14). Define θ_m as the (time-varying) inclination of the orbit plane to the geomagnetic equatorial plane and the α_m as the angle from the orbi plane--geographic equatorial plane line of nodes to the orbit plane--geomagnetic equatorial plane line of nodes, as shown in Fig. A-4. The tilted dipole model, defined here relative to the

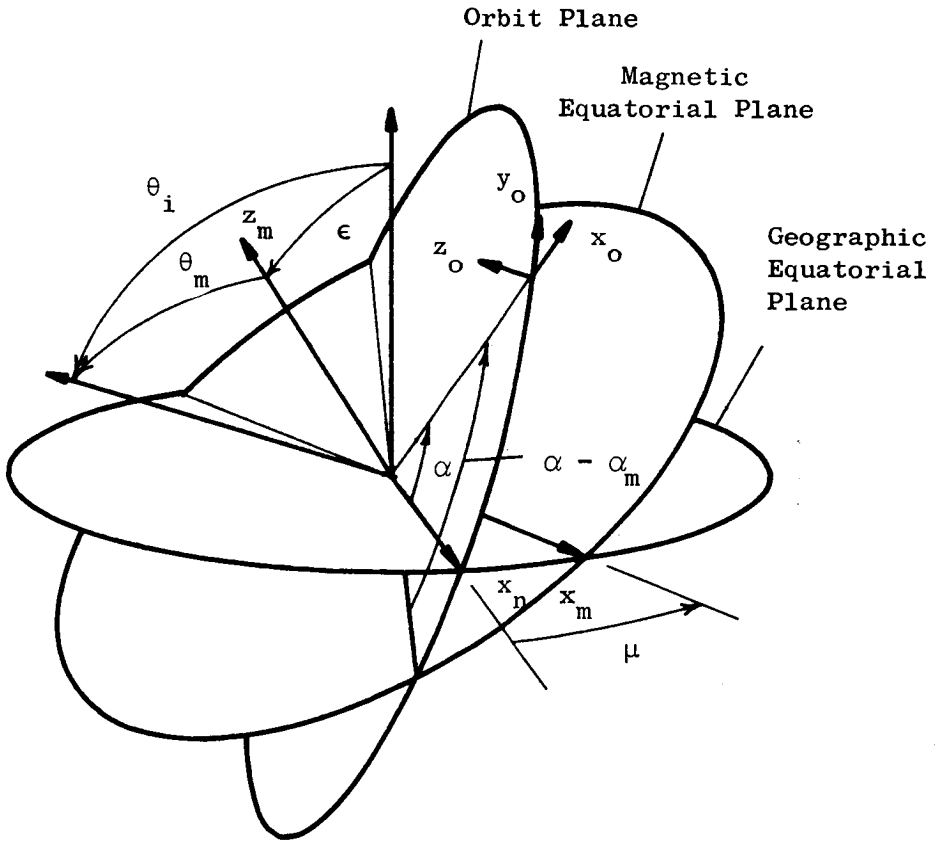

FIG. A-4. DEFINITION OF θ_m AND α_m.

geomagnetic equator, takes the same form as the untilted dipole defined relative to the geographic equator, when resolved in the (x_o, y_o, z_o) coordinate frame. That is:

$$\begin{bmatrix} B_{xo} \\ B_{yo} \\ B_{zo} \end{bmatrix} = -\frac{M_e}{r_o^3} \begin{bmatrix} 2\sin\theta_m \sin(\alpha - \alpha_m) \\ -\sin\theta_m \cos(\alpha - \alpha_m) \\ -\cos\theta_m \end{bmatrix} \qquad \text{(A.18)}$$

which can be derived from (A.12) by letting ϵ be zero, and making the substitutions $\theta_i \to \theta_m$ and $\alpha \to \alpha - \alpha_m$. Since (A.18) and (A.12) must be identical, the following identities must apply:

$$\begin{aligned} \sin\theta_m \sin\alpha_m &\equiv -\sin\epsilon \sin\mu \\ \sin\theta_m \cos\alpha_m &\equiv -\sin\epsilon \cos\theta_i \cos\mu + \cos\epsilon \sin\theta_i \\ \cos\theta_m &\equiv \cos\epsilon \cos\theta_i + \sin\epsilon \sin\hat{\theta}_i \cos\mu \ . \end{aligned} \qquad \text{(A.19)}$$

In the (x_n, y_n, z_n) coordinate frame:

$$\begin{bmatrix} B_{xn} \\ B_{yn} \\ B_{zn} \end{bmatrix} = -\frac{M_e}{2r_o^3} \begin{bmatrix} [-\sin\alpha_m + 3\sin(2\alpha - \alpha_m)]\sin\theta_m \\ [\cos\alpha_m - 3\cos(2\alpha - \alpha_m)]\sin\theta_m \\ -2\cos\theta_m \end{bmatrix} \qquad \text{(A.20)}$$

which reduces to expression (A.14) if $\alpha_m = 0$ and $\theta_m = \theta_i$, as is the case for $\epsilon = 0$. This result can be put into a form which is more useful for our purposes:

$$\begin{bmatrix} B_{xn} \\ B_{yn} \\ B_{zn} \end{bmatrix} = -\frac{M_e}{2r_o^3} \begin{bmatrix} (\sin\theta_m \cos\alpha_m)(3\sin 2\alpha) - (\sin\theta_m \sin\alpha_m)(1 + 3\cos 2\alpha) \\ (\sin\theta_m \cos\alpha_m)(1 - 3\cos 2\alpha) - (\sin\theta_m \sin\alpha_m)(3\sin 2\alpha) \\ -2\cos\theta_m \end{bmatrix} \qquad \text{(A.21)}$$

These magnetic field components depend on time due to orbital motion of the vehicle as well as through the variation of μ, where $\mu = \alpha_e + \Delta - \beta$. Since $\dot{\beta} \ll \dot{\alpha}_e$, the coefficients given in (A.19) vary with a period very close to one day. The terms concerning 2α vary, of course, at twice orbital frequency.

To evaluate precisely the performance of a magnetic attitude control system with this tilted dipole model we must have knowledge of not only the initial orbital position of the vehicle, but the values of the coefficients $\sin\theta_m \sin\alpha_m$, $\sin\theta_m \cos\alpha_m$, and $\cos\theta_m$ as well. As shown earlier, to specify these coefficients explicitly we must know the initial value of β, the time of year (i.e., the angle S) and the initial apparent solar time at Greenwich. This is reasonable for a specific mission because values for these parameters may be available.

For a general study, these coefficients must be assumed to be arbitrary (within their allowable range of variation as defined by (A.19) with $\epsilon \approx 11°$). Using simulation techniques it is possible (albeit prohibitively time consuming and expensive in some cases) to evaluate the performance for all possible values of α_m and θ_m.

Another approach for general performance studies, such as the estimates developed in Chapter V, is to consider, at least for low orbits, replacing the coefficients of (A.21) by their average value (over a day). This will (heuristically) give an estimate of the "average" performance. Then

$$\underset{\mu}{\text{ave}}(\sin\theta_m \sin\alpha_m) = 0$$

$$\underset{\mu}{\text{ave}}(\sin\theta_m \cos\alpha_m) = \cos\epsilon \sin\theta_i$$

$$\underset{\mu}{\text{ave}}(\cos\theta_m) = \cos\epsilon \cos\theta_i$$

and

$$\begin{bmatrix} B_{xn} \\ B_{yn} \\ B_{zn} \end{bmatrix}_{AV} = -\frac{M_e \cos \epsilon}{2r_o^3} \begin{bmatrix} 3 \sin 2\alpha \sin \theta_i \\ (1 - 3 \cos 2\alpha) \sin \theta_i \\ -2 \cos \theta_i \end{bmatrix} . \qquad (A.22)$$

Notice that this agrees with expression (A.14) except that all components are attenuated by $\cos \epsilon \approx .982$. It appears, then, that using the untilted dipole model yields, to a good approximation, the "average" (over a day) performance of the magnetic control system. Of course, during any day there will probably be orbits for which the performance is better and other orbits for which the performance will be worse. However, owing to the small angle (approximately 11°) between the geographic and geomagnetic polar axes, these performance extremes can be expected to depart only slightly from the "average" performance.

APPENDIX B. INTERMITTENT MAGNETIC ATTITUDE CONTROL OF SPINNING VEHICLES

The study presented in the body of this report is concerned with continuous magnetic control of the attitude of a spinning satellite. For small errors, intermittent control is an alternative. The primary advantage of intermittent control is that continuous measurement of the attitude and magnetic field variables is not required. Furthermore, it is sometimes possible to mechanize an intermittent control law with less attitude information than is required for continuous control, because the motion of the spin axis between attitude corrections admits to kinematic constraints [Refs. 1-9, 1-11]. A major limitation of intermittent control is the difficulty in maintaining a high degree of accuracy.

The discussion of intermittent magnetic control which follows is an adaptation of the results presented in Ref. 1-9. The attention of Ref. 1-9 is limited to a specific mission--that of orienting the spin axis normal to the orbit plane. However, Ref. 1-9 includes a detailed discussion of mechanization for this specific application. The following development generalizes the control law development of the reference to arbitrary missions, but implementation is not considered. It is assumed (as in Ref. 1-9) that the satellite contains a passive damper of sufficient authority that the simplified equations of motion (Chapter II) can be employed.

The simplified equations of motion are presented in polar form (for inertial reference axes) in expression (5.3) of Chapter V. For small attitude errors:

$$\begin{aligned} \dot{\psi} &= -(B_{yR} \cos \lambda - B_{xR} \sin \lambda)u \\ \dot{\lambda\psi} &= (B_{yR} \sin \lambda + B_{xR} \cos \lambda - B_{zR}\psi)u \ . \end{aligned} \tag{B.1}$$

Let $\bar{h}_{xy}$ be the projection of the normalized momentum vector in the (x_R, y_R) plane of Fig. 5-3. With small attitude errors

$$\begin{aligned} h_x &\approx \psi \cos \lambda \\ h_y &\approx \psi \sin \lambda \\ h_z &\approx 1 \end{aligned} \tag{B.2}$$

and

$$|\bar{h}_{xy}| \approx \psi \ .$$

Figure B-1 shows the geometrical situation prior to an attitude

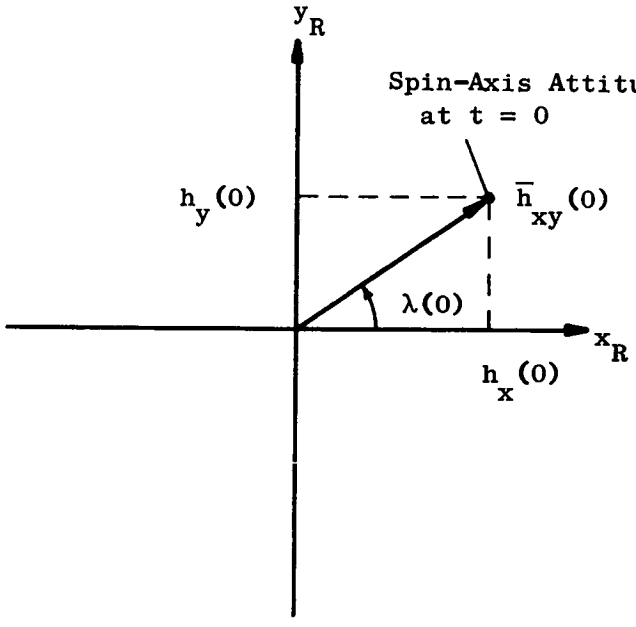

FIG. B-1. INTERMITTENT CONTROL GEOMETRY.

correction. Neglecting motion of the reference frame and disturbance torques over a half orbit (the primary period of the magnetic field components), h_x and h_y will be constant.

Attitude corrections will be made by application of $u = \pm U_o$ for a short period of time (for example, in Ref. 1-9 each correction must be accomplished during no more than nine deg of the vehicle's orbital motion). The need for an attitude correction is indicated when the attitude error ψ exceeds a preassigned threshold.

Assuming that a correction is required, it is necessary to decide when during the subsequent half orbit to initiate the correction, and to select the level and direction of u. The last two questions are the easiest to answer. The control level, U_o, is specified by the attitude

increment desired. This increment must be greater than the maximum increase in ψ (due to disturbances) which can occur during a half orbit, and less than the threshold level (to avoid overcorrection). The sign of u is specified by the obvious requirement that $\dot{\psi}$ must be negative at the beginning of a correction.

One method of selecting the time of correction initiation is that of detecting the time at which $|B_y(t)h_x(0)-B_x(t)h_y(0)|$ is a maximum. Application of u at this time will maximize the initial rate of decrease of the attitude error.

Another technique, probably more easy to implement, is based upon requiring that the initial motion of the spin axis be toward the origin--that is, $\dot{\lambda}(0) = 0$. Imposing this constraint yields, from (B.1):

$$B_{yR}(0) \sin \lambda(0) + B_{xR}(0) \cos \lambda(0) - B_{zR}(0)\psi(0) = 0 . \qquad (B.3)$$

Or, in terms of $h_x(0)$ and $h_y(0)$:

$$B_{yR}(0)h_y(0) + B_{xR}(0)h_x(0) - B_{zR}(0)[h_x^2(0) + h_y^2(0)] = 0 . \qquad (B.4)$$

To summarize, if ψ is greater than the threshold level and condition (B.4) is satisfied, apply a control

$$u = U_o \text{ sgn } [B_{yR}(0)h_x(0) - B_{xR}(0)h_y(0)] \qquad (B.5)$$

for a period of time short enough that the time variation of B_{xR} and B_{yR} does not cause $\dot{\psi}$ to change sign.

Obviously, showing that condition (B.4) will always be satisfied at some point in orbit for a given application is a matter of some importance. For very small errors, (B.4) can be replaced by

$$B_{yR}(0)h_y(0) + B_{xR}(0)h_x(0) = 0 . \qquad (B.6)$$

Using the untilted dipole magnetic field model of Appendix A, and factoring out the coefficient $-M_e/2r_o^3$, (B.6) becomes:

$$(\sin\delta\cos\phi\sin\theta_i + 2\sin\phi\cos\theta_i)h_x(0) + (\cos\delta\sin\theta_i)h_y(0)$$

$$+ 3\sin\theta_i \cdot \{h_x(0)\cos\phi\sin[2\alpha(0) - \delta] - h_y(0)\cos[2\alpha(0) - \delta]\} = 0. \tag{B.7}$$

The last term is periodic in $\alpha(0)$. This result may be rewritten as:

$$(\sin\delta\cos\phi\sin\theta_i + 2\sin\phi\cos\theta_i)h_x(0) + (\cos\delta\sin\theta_i)h_y(0)$$

$$+ 3\sin\theta_i \cdot \sqrt{h_x^2(0)\cos^2\phi + h_y^2(0)}\cos[2\alpha(0) - \delta + \vartheta] = 0\ . \tag{B.8}$$

For satisfaction of this condition at some value of $\alpha(0)$, the amplitude of the periodic part must be greater than the constant term for all small values of h_x and h_y. As an example, consider pointing the spin axis normal to the orbit plane ($\phi = \delta = 0$). The required condition is

$$3\sin\theta_i\sqrt{h_x^2(0) + h_y^2(0)} > h_y(0)\sin\theta_i \tag{B.9}$$

which is clearly satisfied for nonzero orbital inclinations.

APPENDIX C. LYAPUNOV'S SECOND METHOD

The second (or direct) method of Lyapunov is a powerful technique for the study of the stability properties of systems of differential equations. It is most valuable in those cases for which such techniques as the Routh-Hurwitz test (applicable to linear stationary systems) and the Floquet theory (applicable to linear systems with periodic coefficients) fail [Ref. C-1]. This appendix presents a brief summary of the basic concepts of Lyapunov's second method. The primary source upon which this discussion is based is Ref. 4-4.

A. PRELIMINARY CONCEPTS

Assume that we are concerned with a physical system which can be adequately described by the vector differential equation

$$\dot{\bar{z}} = \bar{g}(\bar{z},t) \tag{C.1}$$

where $\bar{z}$ is an n-dimensional vector with real components and t is time. If $\bar{z} = \bar{z}_o(t)$ is a solution (an unperturbed motion) of the system (C.1), a new n-vector $\bar{x} = \bar{z}-\bar{z}_o(t)$ can be defined. From (C.1), this new vector must satisfy the following equations of the perturbed motion:

$$\dot{\bar{x}} = \bar{f}(\bar{x},t) \tag{C.2}$$

where

$$\bar{f}(\bar{x},t) = \bar{g}(\bar{x}+\bar{z}_o,t) - \bar{g}(\bar{z}_o,t)$$

If, as is often the case, the unperturbed solution is $\bar{z}_o(t) = \bar{0}$, the equations of the perturbed motion are the same as the original equations of motion (C.1).

It is common practice to assume that the components of $\bar{f}(\bar{x},t)$ are continuous functions of t and the components of $\bar{x}$ in some open region G containing the origin $(\bar{x} = \bar{0})$ for all $t \geq 0$. A further restriction

upon the right-hand side of (C.2) is that in every bounded closed subregion of G, the functions $f_i(\bar{x},t)$ satisfy a Lipschitz condition with respect to $\bar{x}$. That is,

$$\left|f_i(\bar{x}',t) - f_i(\bar{x}'',t)\right| \leq M_o \sup_j \left\{\left|x_j' - x_j''\right|\right\} \qquad (C.3)$$

where M_o is a positive constant.

Following are two stability definitions quoted (in essence) from Krasovskii (Ref. 4-4):

Definition 1: Stability*

The null solution $\bar{x} = \bar{0}$ of the system (C.2) is said to be stable (at $t = t_o$), provided that for arbitrary $\epsilon > 0$ there is a $\delta(\epsilon,t_o)$ such that, whenever $\|\bar{x}_o\| < \delta$, the inequality $\|\bar{\varphi}(t;\bar{x}_o,t_o)\| < \epsilon$ is satisfied for all $t \geq t_o$.

Definition 2: Asymptotic Stability

The null solution $\bar{x} = \bar{0}$ of the system (C.2) is called asymptotically stable and the region G_δ of $\bar{x}$ space is said to lie in the region of attraction of the point $\bar{x} = \bar{0}$ (at $t = t_o$), provided that the conditions of Definition 1 are satisfied, and provided further that $\bar{\varphi}(t;\bar{x}_o,t_o) \to \bar{0}$ as $t \to \infty$ and $\bar{\varphi}(t;\bar{x}_o,t_o) \cdot \epsilon \cdot \Gamma$ for all $t \geq t_o$ and for $\bar{x}_o \cdot \epsilon \cdot G_\delta$. Here Γ is some subregion of G which is given in advance and with which the physical problem is intrinsically concerned.

If the null solution is asymptotically stable for all points $\bar{x}_o$ <u>from which motions originate</u>, the equilibrium is said to be asymptotically stable in-the-large (ASIL). If the region of attraction of $\bar{x} = \bar{0}$ is the entire $\bar{x}$ space, the origin is said to possess global asymptotic stability.

---

* In the following discussion $\bar{\varphi}(t;\bar{x}_o,t_o)$ is the trajectory of (C.2) which takes on the value $\bar{x}_o$ at $t = t_o$; that is, $\bar{\varphi}(t_o;\bar{x}_o,t_o) = \bar{x}_o$.

Definition 3: Instability

Any motion which is not stable (Definition 1) is said to be unstable.

B. LYAPUNOV'S THEOREMS

Lyapunov's second method is based upon a real scalar (Lyapunov) function $V(\bar{x},t)$ which is defined and continuous for all $t > 0$ in some region Γ of the n-dimensional state space. It is assumed that $V(\bar{0},t) = 0$ for all $t > 0$. The following definitions and theorems are again quoted in essence from Krasovskii [Ref. 4-4].

Definition 4: Semidefinite Function

If the inequality

$$V(\bar{x},t) \geq 0 \qquad [\text{or} \quad V(\bar{x},t) \leq 0]$$

holds for all $\bar{x}$ in Γ and for all $t > 0$, the function $V(\bar{x},t)$ is said to be semidefinite in the region Γ.

Definition 5: Definite Function

Let $V(\bar{x})$ be a function which does not depend explicitly on the time t. The function $V(\bar{x})$ is called definite in the region Γ if it is positive definite (or negative definite) in the region Γ; that is, if for all $\bar{x}$ in Γ $(\bar{x} \neq \bar{0})$, the inequality

$$V(\bar{x}) > 0 \qquad [\text{or} \quad V(\bar{x}) < 0]$$

holds. The time dependent function $V(\bar{x},t)$ is called positive definite (negative definite) if

$$V(\bar{x},t) \geq U(\bar{x})[V(\bar{x},t) \leq - U(\bar{x},t)] \qquad \text{for} \quad \bar{x} \in \Gamma , \qquad t > 0$$

holds for some positive definite function $U(\bar{x})$.

Definition 6: Infinitely Small Upper Bound

A function $V(\bar{x},t)$ admits an infinitely small upper bound in the region Γ, provided there is a continuous function $W(\bar{x})$ such that $W(\bar{0}) = 0$ and

$$|V(\bar{x},t)| \leq W(\bar{x})$$

holds for all $\bar{x}$ in Γ, $t > 0$.

Lyapunov's Theorem on Stability

Suppose there exists a function V which is definite along every trajectory of (C.2) and is such that the total time derivative $\dot{V}$ is semidefinite of opposite sign (or identically zero) along every trajectory of (C.2). Then the perturbed motion is stable. If a function V exists with these properties and admits to an infinitely small upper bound, and if $\dot{V}$ is definite (with sign opposite to that of V), it can be shown further that every perturbed trajectory which is sufficiently close to the unperturbed motion $\bar{x} = \bar{0}$ approaches the latter asymptotically.

Lyapunov's First Theorem on Instability

Suppose a function V exists for which the total derivative is definite along every trajectory of (C.2); suppose V admits an infinitely small upper bound; and suppose that for all values of t above a certain bound there are arbitrarily small values $\bar{x}_s$ of $\bar{x}$ for which V has the same sign as its derivative. Then the perturbed motion is unstable.

C. APPLICATION OF LYAPUNOV'S SECOND METHOD

The key to application of the second method lies in finding a Lyapunov function V with the required properties.* There are formalized

* Modern authors have developed theorems which relax the constraints upon V. See, for example, the theorems of Krasovskii in Chapter IV of this report, which allow the demonstration of asymptotic stability and instability with $\dot{V}$ semidefinite.

procedures for generating Lyapunov functions which are sometimes useful [Refs. C-2, C-3, and C-4]. Often, candidates for Lyapunov functions are suggested by physical considerations; for example, Pringle has shown that the Hamiltonian function is an ideal Lyapunov function for mechanical systems [Ref. C-5]. The Lyapunov functions presented in Chapter IV of this study were also suggested by physical considerations. Reference 4-1 devotes a chapter to application of the second method.

REFERENCES

1-1. R. E. Fischell and F. F. Mobley, "A System for Passive Gravity-Gradient Stabilization of Earth Satellites," Guidance and Control - II (Progress in Aeronautics and Astronautics, vol. 13), Academic Press, New York, 1964.

1-2. L. H. Grasshoff, "A Method of Controlling the Attitude of a Spin-Stabilized Satellite," ARS J., 31, 5, May 1961.

1-3. D. R. Corson and P. Lorrain, Introduction to Electromagnetic Fields and Waves, W. H. Freeman and Co., San Francisco and London, 1962.

1-4. L. J. Kamm, "Magnetorquer--A Satellite Orientation Device," ARS J., 31, 6, Jun 1961.

1-5. J. S. White, F. H. Shigemoto and K. Bourquin, "Satellite Attitude Control Utilizing the Earth's Magnetic Field," NASA TN D-1068, National Aeronautics and Space Administration, Washington, D. C., Aug 1961.

1-6. A. G. Buckingham, "A New Method of Attitude Control Utilizing the Earth's Magnetic Field for Long Life Space Vehicles," ARS Paper No. 1915-61 (presented at the ARS Guidance and Control Conference at Stanford University, Aug 1961).

1-7. R. J. McElvain, "Satellite Angular Momentum Removal Utilizing the Earth's Magnetic Field," AAS Paper No. 62-53 (presented at the Goddard Memorial Symposium in Washington, D. C., Mar 1962).

1-8. D. J. Blakemore, "Magnetic Torquing Scheme," AIAA J., 1, 8, Aug 1963.

1-9. E. I. Ergin and P. C. Wheeler, "Magnetic Attitude Control of a Spinning Satellite," AIAA Paper No. 64-235 (presented at the First AIAA Annual Meeting in Washington, D. C., Jun 1964).

1-10. P. G. Bhuta and L. R. Koval, "Decay Rates of Passive Precession Dampers and their Bounds," AIAA Paper No. 64-658 (presented at the AIAA/ION Astrodynamics Guidance and Control Conference, Los Angeles, Calif., Aug 1964).

1-11. P. C. Wheeler, "Two-Pulse Attitude Control of an Asymmetric Spinning Satellite," Guidance and Control - II (Progress in Aeronautics and Astronautics, vol. 13), Academic Press, New York, 1964.

2-1. L. Blitzer, "On the Motion of a Satellite in the Gravitational Field of the Oblate Earth," GM-TM-0165-00279, Space Technology Laboratories, Los Angeles, Calif., 5 Sep 1958.

2-2. H. Goldstein, Classical Mechanics, Addison-Wesley Press, Inc., Cambridge, Mass., 1950.

2-3. E. T. Whittaker, A Treatise on the Analytical Dynamics of Particles and Rigid Bodies (Fourth Edition), Cambridge University Press, London, 1964.

2-4. E. I. Ergin, V. D. Norum and T. G. Windeknecht, "Techniques for Analyzing Nonlinear Control Systems for Space Vehicles," (vol. 1), Rept. No. 8982-6-001-RU-000, Space Technology Laboratories, Inc., Los Angeles, Calif., 15 Dec 1961.

3-1. G. F. Carrier and J. W. Miles, "On the Annular Damper for a Freely-Precessing Gyroscope," STL/TN-59-0000-00239, Space Technology Laboratories, Inc., Los Angeles, Calif., 29 Jan 1959.

3-2. P. C. Wheeler, "A Note on the Feasibility of Wobble Damping via Eddy Currents," STL Internal Memorandum 9352.8-174, Space Technology Laboratories, Inc., Redondo Beach, Calif., 25 Mar 1963.

4-1. W. Hahn, Theory and Application of Lyapunov's Direct Method, Prentice-Hall, Inc., Englewood Cliffs, N. J., 1963.

4-2. R. E. Kalman and J. E. Bertram, "Control System Analysis and Design via the 'Second Method' of Lyapunov - Part 1," ASME J. of Basic Engrg., 82, 2, Jun 1960.

4-3. T. G. Windeknecht, "On Design of In-the-Large Stability in Space-craft Attitude Control," Rept. No. 9344-6001-KU000, Space Technology Laboratories, Inc., Redondo Beach, Calif., 24 July 1962.

4-4. N. N. Krasovskii, Stability of Motion, Stanford University Press, Stanford, Calif., 1963.

4-5. S. W. McCuskey, An Introduction to Advanced Dynamics, Addison-Wesley Publishing Co., Inc., Reading, Mass., 1959.

5-1. N. Krylov and N. Bogoliubov, Introduction to Non-Linear Mechanics, Annals of Mathematics Studies, No. 11, Princeton University Press, 1947.

6-1. L. S. Pontryagin, V. G. Boltyanskii, R. V. Gamkrelidze, and E. F. Mishchenko, The Mathematical Theory of Optimal Processes, Interscience Publishers, New York, 1962.

6-2. I. Flügge-Lotz and H. Marbach, "The Optimal Control of Some Attitude Control Systems for Different Performance Criteria," ASME J. of Basic Engrg., 85, 2, Jun 1963.

6-3. E. B. Lee and L. Markus, "Optimal Control for Nonlinear Processes," Archive of Rational Mechanics and Analysis, vol. 8, 1961.

6-4. E. Roxin, "On the Existence of Optimal Controls," Michigan Mathematical J., vol. 9, 1962.

7-1. J. P. Vinti, "Theory of the Spin of a Conducting Satellite in the Magnetic Field of the Earth," Rept. No. 1020, Ballistic Research Laboratory, Aberdeen Proving Ground, Maryland, Jul 1957.

7-2. W. D. Hayes and R. F. Probstein, Hypersonic Flow Theory, Academic Press, New York, 1959.

7-3. R. Schamberg, "A New Analytical Representation of Surface Interaction for Hyperthermal Free Molecule Flow with Application to Neutral-Particle Drag Estimates of Satellites, Research Memorandum RM-2213 (ASTIA Document No. AD215301), The Rand Corp., Santa Monica, Calif., 8 Jan 1959.

7-4. R. J. McElvain, "Effects of Solar Radiation Pressure on Satellite Attitude Control," Guidance and Control (Progress in Aeronautics and Astronautics, vol. 8), Academic Press, New York, 1962.

7-5. R. H. Frick and T. B. Garber, "General Equations of Motion of a Satellite in a Gravitational Gradient Field," Research Memorandum RM-2527, The Rand Corp., Santa Monica, Calif., 9 Dec 1959.

8-1. G. E. Lynn, J. G. Hurt and K. A. Harriger," Magnetic Control of Satellite Attitude," IEEE Trans. on Comm. and Electronics, 83, 74, Sep 1964.

8-2. "Electromagnetic Attitude Control System Study," NASA CR-24 (prepared by Westinghouse Electric Corp.), National Aeronautics and Space Administration, Washington, D. C., Mar 1964.

8-3. T. Bernstein, "Air Core Coil Calculations--Project Relay," STL Internal Memorandum No. 9352.2-78, Space Technology Laboratories, Inc., Redondo Beach, Calif., 16 Mar 1962.

8-4. L. J. Cahill, Jr., "Magnetic Field Measurements in Space," Space Science Reviews, vol. 1, 1962-1963.

8-5. S. C. Ling, "Fluxgate Magnetometer for Space Application," AIAA J. of Spacecraft and Rockets, 1, 2, Mar-Apr 1964.

8-6. P. R. Spencer, "Study of a Solar Sensor for Use in Space-Vehicle Orientation Control Systems," NASA TN D-885, National Aeronautics and Space Administration, Washington, D. C., Jun 1961.

8-7. H. Patapoff, "Bank Angle Control System for a Spinning Satellite," Guidance and Control - II (Progress in Aeronautics and Astronautics, vol. 13), Academic Press, New York, 1964.

8-8. R. E. Roberson, "Methods for the Control of Satellites and Space Vehicles: Vol. 1 Sensing and Actuating Methods," WADD Tech. Rept. 60-643, Wright Air Development Division, Wright-Patterson Air Force Base, Ohio, 31 Jul 1960.

8-9. B. O. Lange, "The Control and Use of Drag-Free Satellites," SUDAER No. 194, Department of Aeronautics and Astronautics, Stanford University, Stanford, Calif., Jun 1964.

9-1. J. J. Adams, "Study of an Active Control System for a Spinning Body," NASA TN D-905, National Aeronautics and Space Administration, Washington, D. C., Jun 1961.

9-2. J. H. Suddath, "Use of an Inertia Sphere to Damp the Angular Motions of Spinning Space Vehicles," NASA TR R-137, National Aeronautics and Space Administration, Washington, D. C., 1962.

9-3. W. R. Bandeen and W. P. Manger, "Angular Motion of the Spin Axis of the Tiros I Meteorological Satellite Due to Magnetic and Gravitational Torques," J. of Geophysical Res., 65, 9, Sep 1960.

A-1. W. F. Hodge and W. T. Blackshear, "An Analytical Study of the Magnetic Field Encountered by Artificial Earth Satellites in Circular Orbits," NASA TN D-2041, National Aeronautics and Space Administration, Washington, D. C., Feb 1964.

A-2. J. Bartels, "Some Problems of Terrestrial Magnetism and Electricity," Terrestrial Magnetism and Electricity, (edited by J. A. Fleming), Dover Publications, New York, 1949.

A-3. A. J. Dessler, "Geomagnetism," Satellite Environment Handbook, (edited by F. S. Johnson), Stanford University Press, Stanford, Calif., 1961.

A-4. L. J. Cahill, Jr., "The Magnetosphere," Scientific American, 212, 3, Mar 1965.

C-1. L. Cesari, Asymptotic Behavior and Stability Problems in Ordinary Differential Equations (Second Edition), Academic Press, Inc., New York, 1963.

C-2. D. R. Ingwerson, "A Modified Lyapunov Method for Nonlinear Stability Analysis," IRE Trans. on Automatic Control, AC-6, 2, May 1961.

C-3. D. G. Schultz and J. E. Gibson, "The Variable Gradient Method for Generating Lyapunov Functions," AIAA Trans. Paper No. 62-81, American Institute of Electrical Engineers, New York, 3 Jan 1962.

C-4. S. G. Margolis and W. G. Vogt, "Control Engineering Application of V. I. Zubov's Construction Procedure for Lyapunov Functions," IEEE Trans. on Automatic Control, AC-8, 2, Apr 1963.

C-5. R. Pringle, "On the Capture, Stability, and Passive Damping of Artificial Satellites," SUDAER No. 181, Department of Aeronautics and Astronautics, Stanford University, Stanford, Calif., Apr 1964.